

UNIVERSIDAD COMPLUTENSE DE MADRID
FACULTAD DE CIENCIAS QUÍMICAS



TESIS DOCTORAL

Entendiendo la reactividad de pares de Lewis frustrados

Understanding the reactivity of frustrated Lewis pairs

MEMORIA PARA OPTAR AL GRADO DE DOCTOR

PRESENTADA POR

Jorge Juan Cabrera Trujillo

Director

Israel Fernández López

Madrid

UNIVERSIDAD COMPLUTENSE DE MADRID
FACULTAD DE CIENCIAS QUÍMICAS



TESIS DOCTORAL
ENTENDIENDO LA REACTIVIDAD DE PARES
DE LEWIS FRUSTRADOS

UNDERSTANDING THE REACTIVITY OF
FRUSTRATED LEWIS PAIRS

MEMORIA PARA OPTAR AL GRADO DE DOCTOR

PRESENTADA POR

Jorge Juan Cabrera Trujillo

DIRECTOR

Israel Fernández López

Madrid, 2021

UNIVERSIDAD COMPLUTENSE DE MADRID

FACULTAD DE CIENCIAS QUÍMICAS

Departamento de Química Orgánica

Madrid, 2021



**UNIVERSIDAD
COMPLUTENSE
MADRID**

**ENTENDIENDO LA REACTIVIDAD DE PARES
DE LEWIS FRUSTRADOS**

**UNDERSTANDING THE REACTIVITY OF
FRUSTRATED LEWIS PAIRS**

TESIS DOCTORAL

JORGE JUAN CABRERA TRUJILLO

Director: Israel Fernández López

D. Israel Fernández López, Profesor Titular de Universidad en el Departamento de Química Orgánica de la Facultad de Ciencias Químicas de la Universidad Complutense de Madrid,

CERTIFICA:

Que la presente Memoria, titulada **ENTENDIENDO LA REACTIVIDAD DE PARES DE LEWIS FRUSTRADOS – UNDERSTANDING THE REACTIVITY OF FRUSTRATED LEWIS PAIRS**, ha sido realizada bajo su dirección en el Departamento de Química Orgánica de la Universidad Complutense de Madrid, por el graduado en Química **D. Jorge Juan Cabrera Trujillo**, y autoriza su presentación para ser calificada como Tesis Doctoral.

En Madrid, a 27 de mayo de 2021

Fdo. Prof. Israel Fernández López

*A mi familia,
especialmente a mis padres.
Sin ellos, nada de esto sería posible.*

Agradecimientos/Acknowledgments

La presente tesis doctoral se ha realizado en el Departamento de Química Orgánica de la Universidad Complutense de Madrid. El trabajo recogido en esta memoria ha sido financiado por los proyectos de investigación del Ministerio de Economía y Competitividad (CTQ2016-78205-P), y del Ministerio de Ciencia e Innovación (RED2018-102387-T y PID2019-106184GB-I00). Asimismo, Jorge Juan Cabrera Trujillo agradece al Ministerio de Economía y Competitividad por la concesión de un contrato predoctoral para la formación de doctores (Referencia: BES-2017-079626).

Todas las líneas de agradecimiento que pudiera escribir me parecerían insuficientes para expresar mi gratitud y admiración hacia mi director de tesis, Israel Fernández. En primer lugar, me gustaría agradecerle la oportunidad que me ha brindado de aprender y de trabajar junto a él, su pasión por la Química me resulta extraordinariamente contagiosa. También quisiera destacar que siempre se ha preocupado por mi formación académica, no sólo resolviéndome una infinidad de dudas, sino también facilitándome y animándome a participar en congresos, cursos y seminarios de Química. Para mí ha sido un auténtico privilegio contar con la supervisión de Israel Fernández durante estos años. Por todo, infinitas gracias Isra.

Cuando conseguí el título de Maestro Internacional de ajedrez, tuve que tomar una difícil decisión: dedicarme plenamente a conseguir el título de Gran Maestro o adentrarme en el mundo universitario para estudiar Química. La decisión que tomé en gran medida se la debo a mis padres. Ellos siempre me aconsejaron que por mucho que me apasionara el ajedrez, nunca debería descuidar mi formación académica. Creo que jamás hubiera llegado tan lejos sino fuera por ellos. Para mi madre y para mi padre, esta Tesis Doctoral va especialmente dedicada. También quiero agradecer todo el apoyo de mi hermana, Natalia, y de mi hermano, Gerson, de ambos me siento enormemente orgulloso.

Por méritos propios, mi grupo de amigos de Tenerife, “Los Trozados”, se merecen mi más profundo agradecimiento. Creo que ellos desconocen toda la energía positiva que me transmiten, la cual me he permitido el lujo de utilizar como combustible para el día a día. Ellos son, por siempre, parte de mi familia.

Especialmente quiero agradecer a todos los amigos que he conocido en la universidad durante mi etapa en Madrid. Sin ningún orden en particular, ellos/as son: Elena, Andrea, Jorge, Matías, Mayka, Paloma, Sara, Sergio, Paula, Dani, Yago y Cristina. Gracias por ayudarme a afrontar mi miedo a las rotondas de 7 carriles. Gracias por ese humor que tenéis que alegra a cualquier alma en pena. Gracias por las tardes de paraninfo tomando alguna que otra cerveza, por las casas rurales, las cenas, las rutas patentadas, y muchas cosas más. A pesar del hecho de encontrarme a muchos kilómetros de distancia de mi tierra natal, me habéis hecho sentir que ahora tengo dos hogares. P.D.: Quiero dejar constancia de que el testigo del “*me odiáis porque no soy doctor*” espero poder entregárselo pronto a Andrea.

I would like to thank Prof. Maria J. Ramos and Pedro A. Fernandes for hosting me for a 3-months internship at their research group in the *Faculdade de Ciências da Universidade do Porto*. My gratitude is also extended to all the members of the group, especially to Dr. Rui Neves, Dr. João Coimbra, Matilde Viegas, and Filipa Lopes de Mendonça. Despite the global sanitary emergency (lockdown included), they managed to make my stay more pleasant and teach me the “ins and outs” of molecular dynamics, QM/MM, and force field parameterization. I will never forget your hospitality. Muito obrigado!

Por último, quiero agradecer a la persona de la que estoy profundamente enamorado por dejarme ser parte de su vida. Junto a ella, me imagino fingiendo una bajada de azúcar con la única y pícara intención de que nuestros nietos nos traigan dulcitos. Siento mucho haberme perdido tu cumpleaños por encontrarme redactando la presente memoria. Espero que pronto podamos estar juntos paseando a la orilla del mar. Te amo Alba.

Parte de los resultados obtenidos durante la elaboración de la presente memoria han dado lugar a las siguientes publicaciones:

1. J. J. Cabrera-Trujillo, I. Fernández,
“Influence of the Lewis acid/base pairs on the reactivity of geminal E-CH₂-E' frustrated Lewis pairs”
Chem. Eur. J. **2018**, *24*, 17823-17831.
2. J. J. Cabrera-Trujillo, I. Fernández,
“Understanding the reactivity of neutral geminal Group 14 element/phosphorus frustrated Lewis pairs”
J. Phys. Chem. A **2019**, *123*, 10095-10101.
3. J. J. Cabrera-Trujillo, I. Fernández,
“Aromaticity can enhance the reactivity of P-donor/borole frustrated Lewis pairs”
Chem. Commun. **2019**, *55*, 675-678.
4. J. J. Cabrera-Trujillo, I. Fernández,
“Carbones and heavier ylidenes (EL₂) in frustrated Lewis pair chemistry: Influence of the nature of EL₂ on dihydrogen activation”
Inorg. Chem. **2019**, *58*, 7828-7836.
5. J. J. Cabrera-Trujillo, I. Fernández,
“Understanding the role of frustrated Lewis pairs as ligands in transition metal-catalyzed reactions”
Dalton Trans. **2020**, *49*, 3129-3137.
6. J. J. Cabrera-Trujillo, I. Fernández,
“Understanding the C-F bond activation mediated by frustrated Lewis pairs: Crucial role of non-covalent interactions”
Chem. Eur. J. **2021**, *27*, 3823-3831.

Lista de publicaciones no incluídas en la presente memoria:

7. J. J. Cabrera-Trujillo, I. Fernández,
“Understanding the Diels-Alder reactivity of 1,2-azaborine analogues”
Tetrahedron **2018**, *74*, 4289-4294.
8. J. J. Cabrera-Trujillo, I. Fernández,
“Understanding exo-selective Diels-Alder reactions involving Fischer-type carbene complexes”
Org. Biomol. Chem. **2019**, *17*, 2985-2991.
9. J. J. Cabrera-Trujillo, I. Fernández,
“Rationalizing the Al(I)-promoted oxidative addition of C–C versus C–H bonds in arenes”
Chem. Eur. J. **2020**, *26*, 11806-11813.
10. A. V. Pinto, A. N. L. Oliveira, C. Jerves, F. Lopes de Mendonça, I. F. M. Coutinho, J. T. S. Coimbra, J. P. M. Sousa, J. J. Cabrera-Trujillo, L. Teixeira, M. F. Viegas, P. Ferreira, P. Paiva, R. Fonseca, R. P. P. Neves, A. L. Magalhães, P. A. Fernandes, M. J. Ramos,
“Proteínas virais no Protein Data Bank”
Rev. Ciência Elem. **2020**, DOI: 10.24927/rce2020.022.
11. S. Portela, J. J. Cabrera-Trujillo, I. Fernández,
“Catalysis by bidentate iodine(III)-based halogen donors: Surpassing the activity of strong Lewis acids”
J. Org. Chem. **2021**, *86*, 5317-5326.
12. P. García-Arroyo, P. Navalpotro, M. J. Mancheño, E. Salagre, J. J. Cabrera-Trujillo, E. G. Michel, J. L. Segura, J. Carretero-González,
“Acidic triggering of reversible electrochemical activity in a pyrenetetraone-based 2D polymer”
Polymer **2021**, *212*, 123273.

La presente memoria de la Tesis Doctoral se ha escrito siguiendo el formato de publicaciones. Incluye una introducción general detallada sobre el estado actual del área de investigación en la que se enmarca este trabajo y una discusión integradora de los resultados obtenidos. Los capítulos se han dividido según las distintas publicaciones. Con el fin de respetar al máximo las diferentes publicaciones, se ha mantenido la numeración original de las moléculas, aunque se ha modificado la numeración referente a las gráficas, figuras, esquemas y tablas para su concordancia respecto al capítulo al que pertenecen. Al final de la presente memoria se incluye un resumen en inglés y otro en español de acuerdo con la normativa actual de tesis doctorales en la UCM.

INDEX

| | | |
|-------------|---|-----|
| I. | INTRODUCTION | |
| 1.1. | The concept of Frustrated Lewis Pairs (FLPs) | 1 |
| 1.2. | Reactivity of FLPs | 9 |
| 1.2.1. | <i>Dihydrogen activation and hydrogenation reactions</i> | 9 |
| 1.2.2. | <i>Activation of other small molecules</i> | 19 |
| 1.2.3. | <i>Activation of C–F Bonds</i> | 26 |
| 1.2.4. | <i>FLPs as ligands in transition metal chemistry</i> | 30 |
| 1.3. | Mechanisms of small molecule activations mediated by FLPs | 35 |
| 1.4. | Activation Strain Model (ASM) of reactivity | 50 |
| 1.5. | Energy Decomposition Analysis (EDA) method | 56 |
| II. | OBJECTIVES | 61 |
| III. | CHAPTER 1: <i>Influence of the Lewis acid/base pairs on the reactivity of geminal E–CH₂–E' frustrated Lewis pairs</i> | 67 |
| 3.1. | Introduction | 68 |
| 3.2. | Theoretical Methods and Computational Details | 69 |
| 3.3. | Results and Discussion | 71 |
| 3.4. | Conclusion | 83 |
| 3.5. | References | 85 |
| 3.6. | Supporting Information | 88 |
| IV. | CHAPTER 2: <i>Understanding the reactivity of neutral geminal Group 14 element/phosphorus frustrated Lewis Pairs</i> | 91 |
| 4.1. | Introduction | 92 |
| 4.2. | Theoretical Methods and Computational Details | 94 |
| 4.3. | Results and Discussion | 96 |
| 4.4. | Conclusion | 104 |
| 4.5. | References | 105 |
| 4.6. | Supporting Information | 107 |
| V. | CHAPTER 3: <i>Aromaticity can enhance the reactivity of P-donor/borole frustrated Lewis pairs</i> | 109 |
| 5.1. | References | 118 |
| 5.2. | Supporting Information | 120 |

| | | |
|--------------|--|-----|
| VI. | CHAPTER 4: <i>Carbones and heavier ylidones (EL₂) in frustrated Lewis pair chemistry: Influence of the nature of EL₂ on dihydrogen activation</i> | 123 |
| 6.1. | Introduction | 124 |
| 6.2. | Theoretical Methods and Computational Details | 126 |
| 6.3. | Results and Discussion | 128 |
| 6.4. | Conclusion | 140 |
| 6.5. | References | 142 |
| 6.6. | Supporting Information | 145 |
| VII. | CHAPTER 5: <i>Understanding the role of frustrated Lewis pairs as ligands in transition metal-catalyzed reactions</i> | 147 |
| 7.1. | Introduction | 148 |
| 7.2. | Theoretical Methods and Computational Details | 150 |
| 7.3. | Results and Discussion | 152 |
| 7.4. | Conclusion | 162 |
| 7.5. | References | 163 |
| 7.6. | Supporting Information | 166 |
| VIII. | CHAPTER 6: <i>Understanding the C–F bond activation mediated by frustrated Lewis pairs: Crucial role of non-covalent interactions</i> | 169 |
| 8.1. | Introduction | 170 |
| 8.2. | Computational Details | 171 |
| 8.3. | Results and Discussion | 173 |
| 8.4. | Conclusion | 186 |
| 8.5. | References | 188 |
| 8.6. | Supporting Information | 192 |
| IX. | DISCUSSION | |
| 9.1. | Influence of the Lewis acid/base pairs on the reactivity of geminal E–CH ₂ –E' frustrated Lewis pairs | 197 |
| 9.2. | Understanding the reactivity of neutral geminal Group 14 element/phosphorus frustrated Lewis pairs | 202 |
| 9.3. | Aromaticity can enhance the reactivity of P-donor/borole frustrated Lewis pairs | 205 |
| 9.4. | Carbones and heavier ylidones (EL ₂) in frustrated Lewis pair chemistry: Influence of the nature of EL ₂ on dihydrogen activation | 208 |

| | |
|--|-----|
| 9.5. Understanding the role of frustrated Lewis pairs as ligands in transition metal-catalyzed reactions | 212 |
| 9.6. Understanding the C–F bond activation mediated by frustrated Lewis pairs: Crucial role of non-covalent interactions | 217 |
| X. CONCLUSIONS | 227 |
| XI. SUMMARY | 233 |
| XII. RESUMEN | 239 |
| XIII. ANNEXES | 243 |

I. INTRODUCTION

*“Nearly everything is really interesting if
you go into it deeply enough.”*

Richard P. Feynman

1.1. The concept of Frustrated Lewis Pairs (FLPs)

In 1923, Gilbert Newton Lewis broadened the acid/base theory establishing a new way to classify acids and bases as nonbonding electron pair acceptors and donors, respectively.¹ This description has become a primary axiom in chemistry to understand not only the formation of classical Lewis acid/base adducts but also a wide range of organic transformations, main group chemistry, as well as the bonding in transition metal complexes.^{2,3,4}

In 1942, H. C. Brown and co-workers reported the relative stability of some coordination compounds.⁵ In this study, it was confirmed that 2,6-lutidine was a stronger base than pyridine and, as a consequence, pyridine was displaced by lutidine in a competitive reaction with hydrogen chloride (Scheme 1.1A). However, when the analogous reaction with the Lewis acid BF_3 was carried out, the opposite result was observed, *i.e.* the equilibrium was displaced towards the pyridine adduct (Scheme 1.1B). Furthermore, the acceptor BMe_3 did not react at all with lutidine, even at low temperatures (Scheme 1.1C). These observations were ascribed to the considerably higher steric hindrance in 2,6-lutidine compared to pyridine. This work is currently recognized as the first report where the formation of a classical Lewis acid-base adduct is hampered, or *frustrated*, due to the steric congestion produced by the groups surrounding the coordinating central atoms.

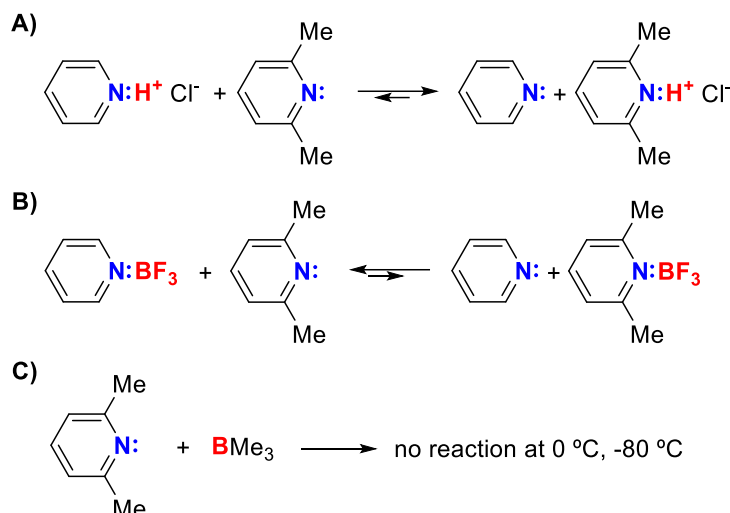
¹ (a) G. N. Lewis, *Valence and the Structure of Atoms and Molecules*, The Chemical Catalog Company, New York, 1923; (b) G. N. Lewis, *J. Franklin Inst.*, **1938**, *226*, 293-313.

² A. Corma, H. García, *Chem. Rev.*, **2003**, *103*, 4307-4366.

³ (a) T. Stahl, F. T. Klare, M. Oestreich, *ACS Catal.*, **2013**, *3*, 1578-1587; (b) M. Hong, J. Chen, E. Y.-X. Chen, *Chem. Rev.*, **2018**, *118*, 10551-10616.

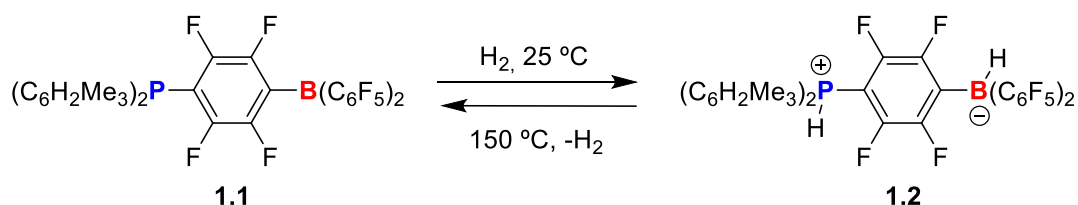
⁴ For a recent review on the Lewis electron-pair bonding model, see: L. Zhao, W. H. E. Schwarz, G. Frenking, *Nat. Rev. Chem.*, **2019**, *3*, 35-47, and references therein.

⁵ H. C. Brown, H. I. Schlesinger, S. Z. Cardon. *J. Am. Chem. Soc.*, **1942**, *64*, 325-329.



Scheme 1.1. Competitive reactions between pyridine and 2,6-lutidine with A) hydrogen chloride and B) BF_3 . C) 2,6-lutidine with BMe_3 led to the first reported frustration of an acid-base adduct.

Almost a century after the Lewis theory was brought forth, Douglas W. Stephan and co-workers uncovered the first reversible metal-free activation of dihydrogen mediated by **1.1** under remarkably mild reaction conditions (Scheme 1.2).⁶ This work, published in 2006, was fascinating for several reasons. Firstly, compound **1.1** was able to heterolytically split the rather strong bond present in the H_2 molecule at only $25\text{ }^\circ\text{C}$. This leads to the formation of the phosphonium boronate zwitterionic species **1.2**, where the Lewis base (LB) was protonated and a hydride was attached to the Lewis acid (LA). Secondly, the transformation was found to be reversible. Indeed, the initial reactants (**1.1** and H_2) were regenerated upon heating species **1.2** at $150\text{ }^\circ\text{C}$. Finally, the formation of the corresponding classical acid-base adduct was not observed either in solution or the solid-state due to steric hindrance of the substituents directly attached to both the LB and LA centers.



Scheme 1.2. Reversible dihydrogen splitting reaction reported by Stephan and co-workers (see reference 6).

⁶ G. C. Welch, R. R. San Juan, J. D. Masuda, D. W. Stephan, *Science*, **2006**, *314*, 1124-1126.

This seminal finding led to the formulation of the “*Frustrated Lewis Pair*” concept, coined to refer to a combination of a Lewis acid and a Lewis base where the dative bond is precluded by steric demands therefore preventing the formation of a classical LA-LB adduct (Figure 1.1).⁷ This special bonding situation results in a unique and unprecedented rich reactivity, where the cooperative action of the donor and acceptor sites is crucial. Although the importance of “frustration” was initially postulated, subsequent reports have demonstrated that even in some cases where a classical acid-base adduct is formed, the “FLP reactivity” remains. This typically occurs when the donor-acceptor interaction is relatively weak, *i.e.*, the formation of the classical adduct is reversible thus allowing the dissociation of the adduct and preserving the donor and acceptor functionalities (Figure 1.1).⁸

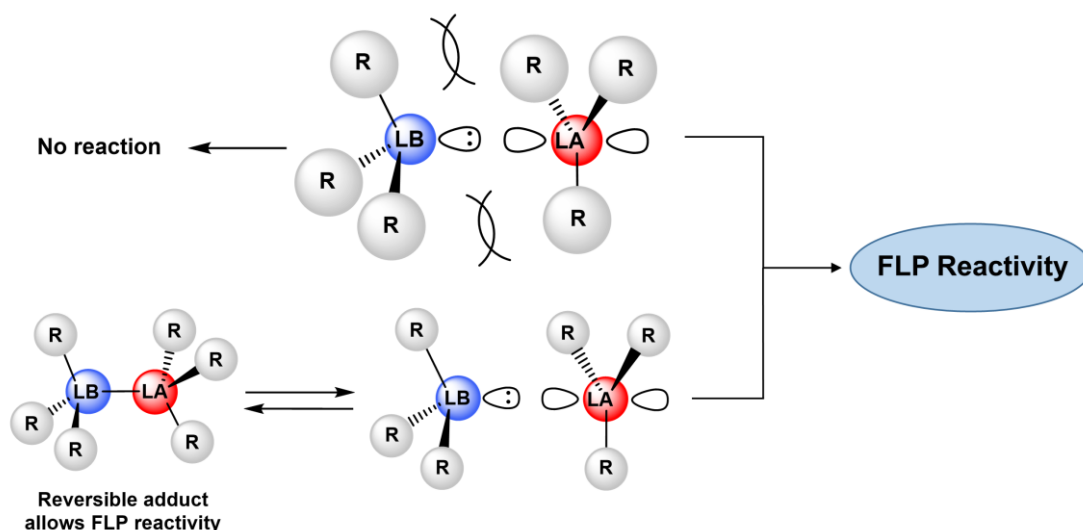
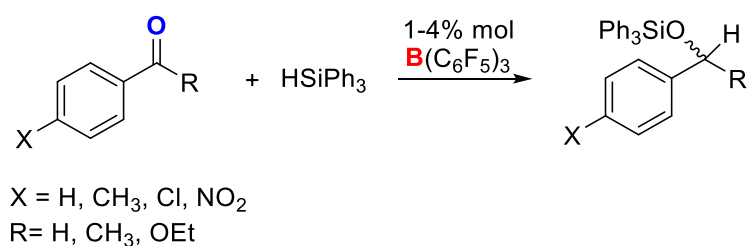


Figure 1.1. Combinations of Lewis base (LB, blue circles) and Lewis acid (LA, red circles), both surrounded by bulky substituents (R, grey circles) that sterically preclude the formation of a dative bond and therefore showing FLP reactivity. In the reversible adduct formation reactions, the FLP reactivity remains.

⁷ J. S. J. McCahill, G. C. Welch, D. W. Stephan, *Angew. Chem. Int. Ed.*, **2007**, *46*, 4968-4971.

⁸ (a) L. J. Hounjet, C. Bannwarth, C. N. Garon, C. B. Caputo, S. Grimme, D. W. Stephan, *Angew. Chem. Int. Ed.*, **2013**, *52*, 7492-7495; (b) R. Dobrovetsky, D. W. Stephan, *J. Am. Chem. Soc.*, **2013**, *135*, 4974-4977; (c) D. J. Scott, M. J. Fuchter, A. E. Ashley, *Angew. Chem. Int. Ed.*, **2014**, *53*, 10218-10222; (d) R. Dobrovetsky, K. Takeuchi, D. W. Stephan, *Chem. Commun.*, **2015**, *51*, 2396-2398; (e) L. Wu, S. S. Chitnis, H. Jiao, V. T. Annibale, I. Manners, *J. Am. Chem. Soc.*, **2017**, *139*, 16780-16790.

In this context, the pioneering work by Piers and Parks a decade before the articulation of the FLP concept must be especially highlighted.⁹ In this report, the authors described a mild methodology to selectively reduce aromatic aldehydes, ketones, and esters using silanes and the tris(pentafluorophenyl)boron (BCF) Lewis acid as a catalyst (Scheme 1.3). In a subsequent work, it was proposed that, contrary to expectation, the BCF does not facilitate the transformation by binding to the carbonyl group. Instead, the reaction proceeds through a mechanism where the Si–H bond is first activated by BCF and followed by a nucleophilic attack of the carbonyl group to the silicon center.¹⁰ Further evidence to support this mechanism was reported later by Oestreich and Rendler.¹¹ In this work, a S_N2 mechanism was confirmed in view of the inversion of the configuration of the silicon stereocenter observed in the final product. Hence, the carbonyl species and the BCF acts as a LB/LA combination which reacts in a concerted manner to activate the Si–H bond. This work is nowadays recognized as the first transformation involving a FLP in its reaction mechanism.¹²



Scheme 1.3. BCF-catalyzed reduction of aromatic aldehydes, ketones, and esters with silanes.

At present, the vast majority of the reported FLP systems are composed of bases derived from tertiary phosphines and boron-based acids. However, the range of basic and acid functionalities has been (and still is) widely extended to other

⁹ D. J. Parks, W. E. Piers, *J. Am. Chem. Soc.*, **1996**, *118*, 9440-9441.

¹⁰ D. J. Parks, J. M. Blackwell, W. E. Piers, *J. Org. Chem.*, **2000**, *65*, 3090-3098.

¹¹ S. Rendler, M. Oestreich, *Angew. Chem. Int. Ed.*, **2008**, *47*, 5997-6000.

¹² F.-G. Fontaine, D. W. Stephan, *Phil. Trans. R. Soc. A*, **2017**, *375*, 20170004.

LBs and LAs. Indeed, a good number of Al/P-based¹³ and Al/N-based¹⁴ (albeit to a lesser extent) FLPs have been reported. Furthermore, Uhl and co-workers have recently reported the modulated properties of FLPs based on Ga/P and In/P.¹⁵ On the other hand, Erker and co-workers reported a series of substituted alkenyl-bridged frustrated N/B Lewis pairs.¹⁶ The variety of bases and acids used in FLP chemistry has been even extended beyond Group 13/15 combinations. For instance, the Stephan group described FLPs formed by the combination of *N*-heterocyclic carbenes¹⁷ or ethers^{8a} with BCF, and Ashley and co-workers reported that solutions of 1,4-dioxane and BCF also exhibit FLP reactivity.¹⁸ In 2010, Alcarazo and co-workers explored the use of carbon(0)/borane-based FLPs. The two available lone-pairs at the carbon(0) atom of carbodiphosphanes are so basic that, after a first alkylation step, the resulting protonated species is still able to act as a LB showing FLP reactivity.¹⁹ In a related effort, the same group demonstrated that an electron-poor allene can be used as a LA to form an entirely carbon-based FLP together with a bulky carbene as the basic counterpart.²⁰ Also, a silylene/silylium FLP has been successfully employed to activate dihydrogen.²¹ In addition, the Mitzel group has reported neutral FLP systems based on Si/P,²²

¹³ (a) G. Ménard, D. W. Stephan, *J. Am. Chem. Soc.*, **2010**, *132*, 1796-1797; (b) C. Appelt, H. Westenberg, F. Bertini, A. W. Ehlers, J. C. Slootweg, K. Lammertsma, W. Uhl, *Angew. Chem. Int. Ed.*, **2011**, *50*, 3925-3928; (c) G. Ménard, D. W. Stephan, *Angew. Chem. Int. Ed.*, **2011**, *50*, 8396-8399; (d) G. Ménard, D. W. Stephan, *Angew. Chem. Int. Ed.*, **2012**, *51*, 4409-4412; (e) L. Keweloh, H. Klöcker, E.-U. Würthwein, W. Uhl, *Angew. Chem. Int. Ed.*, **2016**, *55*, 3212-3215; (f) M. Devillard, R. Declercq, E. Nicolas, A. W. Ehlers, J. Backs, N. Saffon-Merceron, G. Bouhadir, J. C. Slootweg, W. Uhl, D. Bourissou, *J. Am. Chem. Soc.*, **2016**, *138*, 4917-4926; (g) S. Styra, M. Radius, E. Moos, A. Bihlmeier, F. Breher, *Chem. Eur. J.*, **2016**, *22*, 9508-9512.

¹⁴ For a recent review, see: A. Bodach, N. Nöthling, M. Felderhoff, *Eur. J. Inorg. Chem.*, **2021**, 1240-1243.

¹⁵ J. Backs, M. Lange, J. Possart, A. Wollschläger, C. Mück-Lichtenfeld, W. Uhl, *Angew. Chem. Int. Ed.*, **2017**, *56*, 3094-3097.

¹⁶ T. Wang, C. G. Daniliuc, C. Mück-Lichtenfeld, G. Kehr, G. Erker, *J. Am. Chem. Soc.*, **2018**, *140*, 3635-3643.

¹⁷ P. A. Chase, A. L. Gille, T. M. Gilbert, D. W. Stephan, *Dalton Trans.*, **2009**, 7179-7188.

¹⁸ D. J. Scott, M. J. Fuchter, A. E. Ashley, *J. Am. Chem. Soc.*, **2014**, *136*, 15813-15816.

¹⁹ M. Alcarazo, C. Gomez, S. Holle, R. Goddard, *Angew. Chem. Int. Ed.*, **2010**, *49*, 5788-5791.

²⁰ B. Inés, S. Holle, R. Goddard, M. Alcarazo, *Angew. Chem. Int. Ed.*, **2010**, *49*, 8389-8391.

²¹ A. Schäfer, M. Reißmann, A. Schäfer, M. Schmidtman, T. Müller, *Chem. Eur. J.*, **2014**, *20*, 9381-9386.

²² B. Waerder, M. Pieper, L. A. Körte, T. A. Kinder, A. Mix, B. Neumann, H.-G. Stämmler, N. W. Mitzel, *Angew. Chem. Int. Ed.*, **2015**, *54*, 13416-13419.

Ge/P,²³ and Sn/P.²⁴ Even though these pioneering FLP reports highlighted their metal-free feature, transition metal complexes can be also used to produce highly active FLPs. Thus, FLPs composed of Zr,²⁵ Ti,²⁶ Hf,²⁷ or Au²⁸ as acid partners have been reported. In addition, Campos communicated in 2017 the synthesis of an electrophilic Au(I) and a nucleophilic Pt(0)-based FLP.^{29a} This work constituted the first FLP entirely based on transition metal functionalities and, for this reason, the term “*Transition Metal Only FLP*” (TMOFLP) was coined to describe these species.²⁹ Moreover, several rare-earth complexes, which can efficiently act as acid partners, have been also reported to exhibit FLP reactivity.³⁰ As a very recent example, Xu and co-workers described the dihydrogen activation by a FLP composed of an intermolecular rare-earth aryloxide and a *N*-heterocyclic carbene FLP.³¹ These examples clearly illustrate that the FLP chemistry is not limited to combinations of Group 13/15 elements but is extended to practically the entire Periodic Table.

Although most of the FLPs commented above are intermolecular systems, *i.e.* the LA and LB antagonists belong to different molecules, many intramolecular

²³ T. A. Kinder, R. Pior, S. Blomeyer, B. Neumann, H.-G. Stammler, N. W. Mitzel, *Chem. Eur. J.*, **2019**, *25*, 5899-5903.

²⁴ P. Holtkamp, F. Friedrich, E. Stratmann, A. Mix, B. Neumann, H.-G. Stammler, N. W. Mitzel, *Angew. Chem. Int. Ed.*, **2019**, *58*, 5114-5118.

²⁵ (a) A. M. Chapman, M. F. Haddow, D. F. Wass, *J. Am. Chem. Soc.*, **2011**, *133*, 18463-18478; (b) X. Xu, G. Kehr, C. G. Daniliuc, G. Erker, *J. Am. Chem. Soc.*, **2015**, *137*, 4550-4557; (c) H. B. Hamilton, A. M. King, H. A. Sparkes, N. E. Pridmore, D. F. Wass, *Inorg. Chem.*, **2019**, *58*, 6399-6409.

²⁶ A. M. Chapman, D. F. Wass, *Dalton Trans.*, **2012**, *41*, 9067-9072.

²⁷ M. J. Sgro, D. W. Stephan, *Chem. Commun.*, **2013**, *49*, 2610-2612.

²⁸ G. Lu, P. Zhang, D. Sun, L. Wang, K. Zhou, Z.-X. Wang, G.-C Guo, *Chem. Sci.*, **2014**, *5*, 1082-1090.

²⁹ (a) J. Campos, *J. Am. Chem. Soc.*, **2017**, *139*, 2944-2947. See also: (b) N. Hidalgo, S. Bajo, J. J. Moreno, C. Navarro-Gilabert, B. Q. Mercado, J. Campos, *Dalton Trans.*, **2019**, *48*, 9127-9138; (c) N. Hidalgo, J. J. Moreno, M. Pérez-Jiménez, C. Maya, J. López-Serrano, J. Campos, *Chem. Eur. J.*, **2020**, *26*, 5915; (d) N. Hidalgo, J. J. Moreno, M. Pérez-Jiménez, C. Maya, J. López-Serrano, J. Campos, *Chem. Eur. J.*, **2020**, *26*, 5982-5993; (e) N. Hidalgo, J. J. Moreno, M. Pérez-Jiménez, C. Maya, J. López-Serrano, J. Campos, *Organometallics*, **2020**, *39*, 2534-2544.

³⁰ (a) A. Berkefeld, W. E. Piers, M. Parvez, L. Castro, L. Maron, O. Eisenstein, *J. Am. Chem. Soc.*, **2012**, *134*, 10843-10851; (b) A. Berkefeld, W. E. Piers, M. Parvez, L. Castro, L. Maron, O. Eisenstein, *Chem. Sci.*, **2013**, *4*, 2152-2162; (c) P. Xu, Y. Yao, X. Xu, *Chem. Eur. J.*, **2017**, *23*, 1263-1267; (d) P. Xu, X. Xu, *ACS Catal.*, **2018**, *8*, 198-202; (e) P. Xu, L. Wu, L. Dong, X. Xu, *Molecules*, **2018**, *23*, 360-368; (f) K. Chang, X. Wang, Z. Fan, X. Xu, *Inorg. Chem.*, **2018**, *57*, 8568-8580.

³¹ K. Chang, Y. Dong, X. Xu, *Chem. Commun.*, **2019**, *55*, 12777-12780.

FLPs have been described as well. For instance, Erker and co-workers showed that ethylene-bridged phosphane-borane FLPs rapidly split dihydrogen³² and Stephan and co-workers employed $R_2P-B(C_6F_5)_2$ ($R = Cy$ or tBu) phosphinoboranes to achieve the same reactivity.³³ In 2008, Repo and co-workers reported a benzylene-bridged aminoborane able to quantitatively split H_2 in toluene solution at only 20 °C.³⁴ Similarly, Lammertsma and co-workers underscored the enhanced reactivity that can be achieved with a series of geminal phosphinoboranes as preorganized FLPs where the donor and acceptor sites are perfectly aligned.³⁵ Also, the use of a phenylene-bridged intramolecular B/N FLP to transform carbon dioxide into formyl, acetal and methoxy derivatives was reported by Fontaine and co-workers.³⁶ Figure 1.2 gathers several representative examples of intra- and intermolecular FLPs.

³² P. Spies, G. Erker, G. Kehr, K. Bergander, R. Fröhlich, S. Grimme, D. W. Douglas, *Chem. Commun.*, **2007**, 5072-5074.

³³ S. J. Geier, T. M. Gilbert, D. W. Stephan, *J. Am. Chem. Soc.*, **2008**, *130*, 12632-12633.

³⁴ V. Sumerin, F. Schulz, M. Atsumi, C. Wang, M. Nieger, M. Leskelä, T. Repo, P. Pyykkö, B. Rieger, *J. Am. Chem. Soc.*, **2008**, *130*, 14117-14119.

³⁵ F. Bertini, V. Lyaskovskyy, B. J. J. Timmer, F. J. J. de Kanter, M. Lutz, A. W. Ehlers, J. C. Slootweg, K. Lammertsma, *J. Am. Chem. Soc.*, **2012**, *134*, 201-204.

³⁶ M.-A. Courtemanche, A. P. Pulis, E. Rochette, M.-A. Légaré, D. W. Stephan, F.-G. Fontaine, *Chem. Commun.*, **2015**, *51*, 9797-9800.

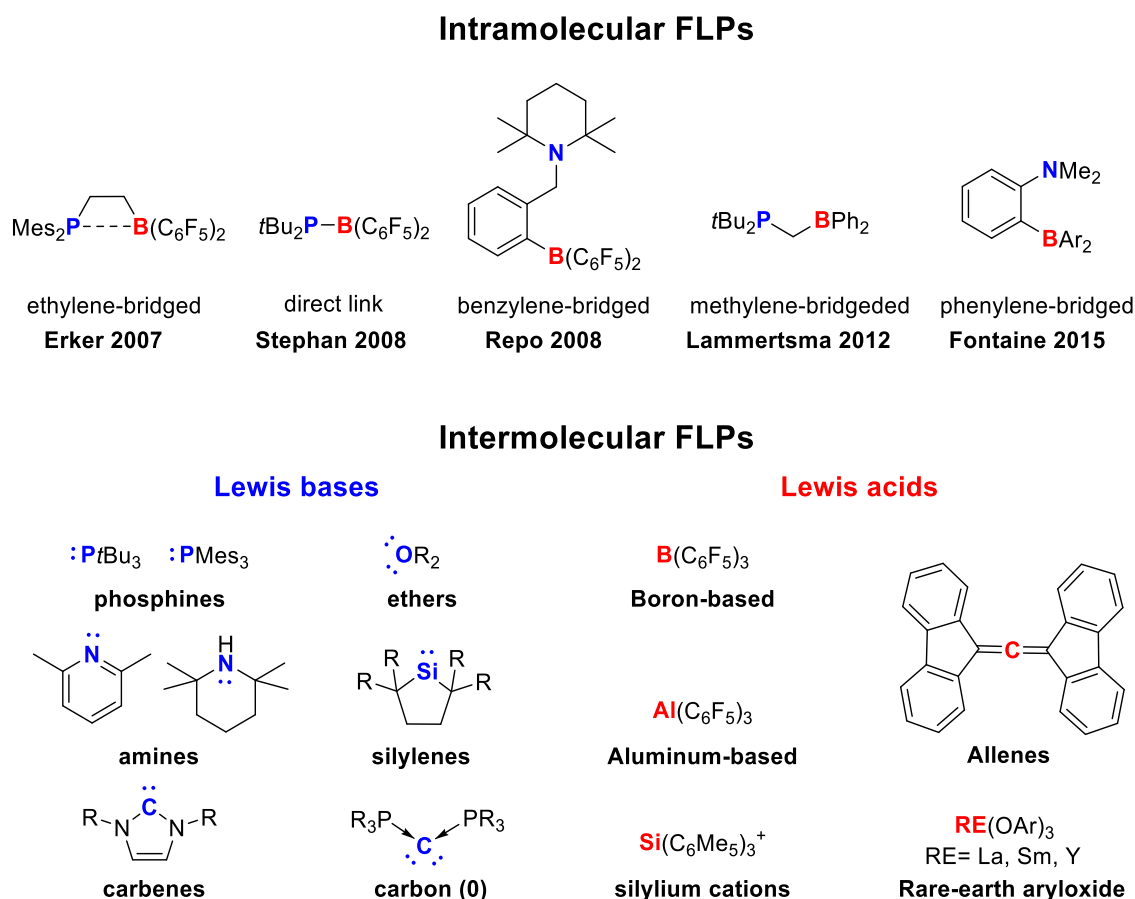


Figure 1.2. Selected examples of intra- and intermolecular FLPs.

The vast number of FLP systems reported so far and their unique and rich reactivity (see section 1.2) confirm the generality of the concept. This topic has been the focus of several recent books³⁷ and reviews,³⁸ to which we refer the

³⁷ (a) G. Erker, D. W. Stephan, *Frustrated Lewis Pairs I: uncovering and understanding*, *Topics in Current Chemistry*, 2013, vol. 332, Springer Berlin Heidelberg, Berlin/Heidelberg; (b) G. Erker, D. W. Stephan, *Frustrated Lewis Pairs II: expanding the scope*, *Topics in Current Chemistry*, 2013, vol. 334, Springer Berlin Heidelberg, Berlin/Heidelberg; (c) C. B. Caputo, D. W. Stephan, *Non-conventional Lewis Acids and Bases in Frustrated Lewis Pair Chemistry*, in: *The Chemical Bond III, Structure and Bonding*, D. Mingo (Ed.) 2015, vol. 171, Springer International Publishing. (d) J. C. Sloatweg, A. Jupp, *Frustrated Lewis Pairs*, 2021, Vol. 2, Springer International Publishing.

³⁸ For selected recent reviews, see: (a) T. Wiegand, M. Siedow, H. Eckert, G. Kehr, G. Erker, *Isr. J. Chem.*, **2015**, *55*, 150-178; (b) S. A. Weicker, D. W. Stephan, *Bull. Chem. Soc. Jpn.*, **2015**, *88*, 1003-1016; (c) D. W. Stephan, G. Erker, *Angew. Chem. Int. Ed.*, **2015**, *54*, 6400-6441; (d) D. W. Stephan, *Acc. Chem. Res.*, **2015**, *48*, 306-316; (e) L. Rocchigiani, *Isr. J. Chem.*, **2015**, *55*, 134-149; (f) M. Pu, T. Privalov, *Isr. J. Chem.*, **2015**, *55*, 179-195; (g) D. W. Stephan, *Science*, **2016**, *354*, aaf7229; (h) A. J. P. Cardenas, Y. Hasegawa, G. Kehr, T. H. Warren, G. Erker, *Coord. Chem. Rev.*, **2016**, *306*, 468-482; (i) J. M. Bayne, D. W. Stephan, *Chem. Soc. Rev.*, **2016**, *45*, 765-774; (j) F.-G. Fontaine, M.-A. Courtemanche, M.-A. Légaré, E. Rochette, *Coord. Chem. Rev.*, **2017**, *334*, 124-135; (k) W. Hui, Z. Yi, P. Zhentao, F. Hongliang, L. Fei, Z. Weihui, *Chinese J.*

interested reader for further details. The growing interest that FLPs have caused in the scientific community is clearly illustrated by the increasing number of annual publications and the high number of citations (~69000) since the 2006 seminal report by Stephan and co-workers (Figure 1.3).

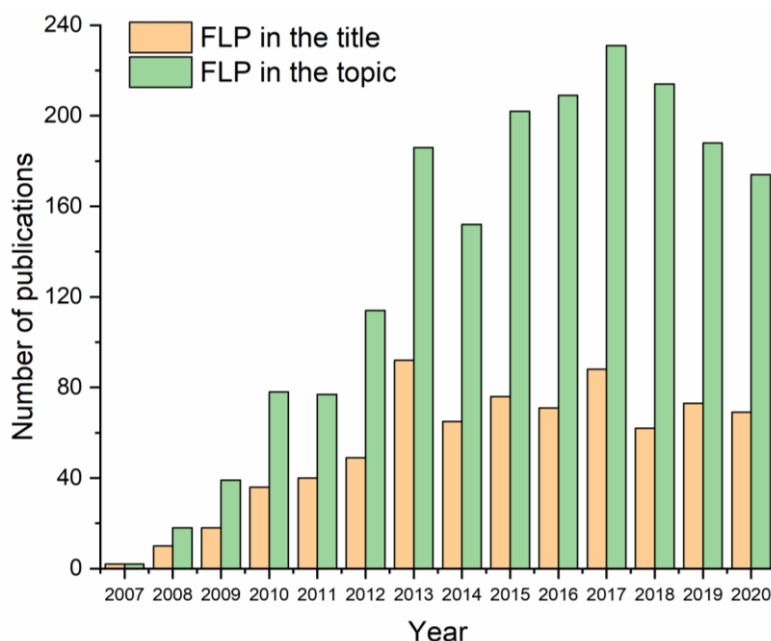


Figure 1.3. Publications per year containing “Frustrated Lewis Pairs” in the title (orange bars) or in the topic (green bars) according to the Web of Science database.

1.2. Reactivity of FLPs

1.2.1. Dihydrogen activation and hydrogenation reactions

By far, the heterolytic cleavage of the strong H–H bond (104 kcal/mol)³⁹ in the H₂ molecule is the most representative reaction in the FLP chemistry. Please note that neither LAs nor LBs alone are able to split dihydrogen. At variance, the cooperative action of LA/LB combinations makes this reaction feasible. This

Org. Chem., **2017**, *37*, 301-313; (l) S. Arndt, M. Rudolph, A. S. K. Hashmi, *Gold Bull.*, **2017**, *50*, 267-282; (m) D. J. Scott, M. J. Fuchter, A. E. Ashley, *Chem. Soc. Rev.*, **2017**, *46*, 5689-5700; (n) Z. Zhenbei, S. Wei, C. Zhishan, *Chinese J. Org. Chem.*, **2018**, *38*, 1292-1318; (o) Y. Ma, S. Zhang, C.-R. Chang, Z.-Q. Huang, J. C. Ho, Y. Qu, *Chem. Soc. Rev.*, **2018**, *47*, 5541-5553; (p) L. L. Liu, D. W. Stephan, *Chem. Soc. Rev.*, **2019**, *48*, 3454-3463; (q) L. Liu, B. Lukose, P. Jaque, B. Ensing, *Green Energy Environ.*, **2019**, *4*, 20-28; (r) J. Paradies, *Eur. J. Org. Chem.*, **2019**, 283-294; (s) A. R. Jupp, D. W. Stephan, *Trends Chem.*, **2019**, *1*, 35-38; (t) D. W. Stephan, *Chem.*, **2020**, *6*, 1520-1526; (u) N. Li, W.-X. Zhang, *Chin. J. Chem.*, **2020**, *38*, 1360-1370; (v) G. Sharma, P. D. Newman, J. A. Platts, *J. Mol. Graph. Model.*, **2021**, *105*, 107846.

³⁹ M. L. Huggins, *J. Am. Chem. Soc.*, **1953**, *75*, 4123-4126.

process, which typically proceeds in a smooth and reversible manner, can be subsequently used to carry out hydrogenation reactions of different unsaturated organic substrates, such as imines, aziridines, *N*-protected nitriles,⁴⁰ alkenes,^{41,42} alkynes,⁴³ silyl enol ethers,⁴⁴ aldehydes,¹⁸ ketones^{18,45} or polyaromatic hydrocarbons⁴⁶ (Figure 1.4). Both transformations, *i.e.* H₂ splitting and hydrogenation reactions, were traditionally mediated by transition metal complexes.⁴⁷ Therefore, a prominent aspect of the FLP chemistry is the possibility to achieve dihydrogen activation and hydrogenation reactions by employing main group species, in many instances in a catalytic manner. In this sense, FLPs constitute a metal-free alternative to the widely extended use of transition metal complexes, which in most cases are scarce, expensive, or toxic.

⁴⁰ P. A. Chase, G. C. Welch, T. Jurca, D. W. Stephan, *Angew. Chem. Int. Ed.*, **2007**, *46*, 8050-8053.

⁴¹ J. Paradies, *Angew. Chem. Int. Ed.*, **2014**, *53*, 3552-3557.

⁴² L. Greb, P. Oña-Burgos, B. Schirmer, S. Grimme, D. W. Stephan, J. Paradies, *Angew. Chem. Int. Ed.*, **2012**, *51*, 10164-10168.

⁴³ K. Chernichenko, Á. Madarász, I. Pápai, M. Nieger, M. Leskelä, T. Repo, *Nat. Chem.*, **2013**, *5*, 718-723.

⁴⁴ H. Wang, R. Fröhlich, G. Kehr, G. Erker, *Chem. Commun.*, **2008**, 5966-5968.

⁴⁵ T. Mahdi, D. W. Stephan, *J. Am. Chem. Soc.*, **2014**, *136*, 15809-15812.

⁴⁶ Y. Segawa, D. W. Stephan, *Chem. Commun.*, **2012**, *48*, 11963-11965.

⁴⁷ (a) R. L. Augustine, *Heterogeneous Catalysis for the Synthetic Chemist*, 1996, Dekker, New York; (b) Á. Molnár, A. Sárkány, M. Varga, *J. Mol. Catal. A: Chem.*, **2001**, *173*, 185-221; (c) S. Nishimura, *Handbook of Heterogeneous Catalytic Hydrogenation for Organic Synthesis*, 2001, Wiley, New York; (d) H.-U. Blaser, C. Malan, B. Pugin, F. Spindler, H. Steiner, M. Studer, *Adv. Synth. Catal.*, **2003**, *345*, 103-151; (e) G. J. Kubas, *J. Organomet. Chem.*, **2014**, *751*, 33-49.

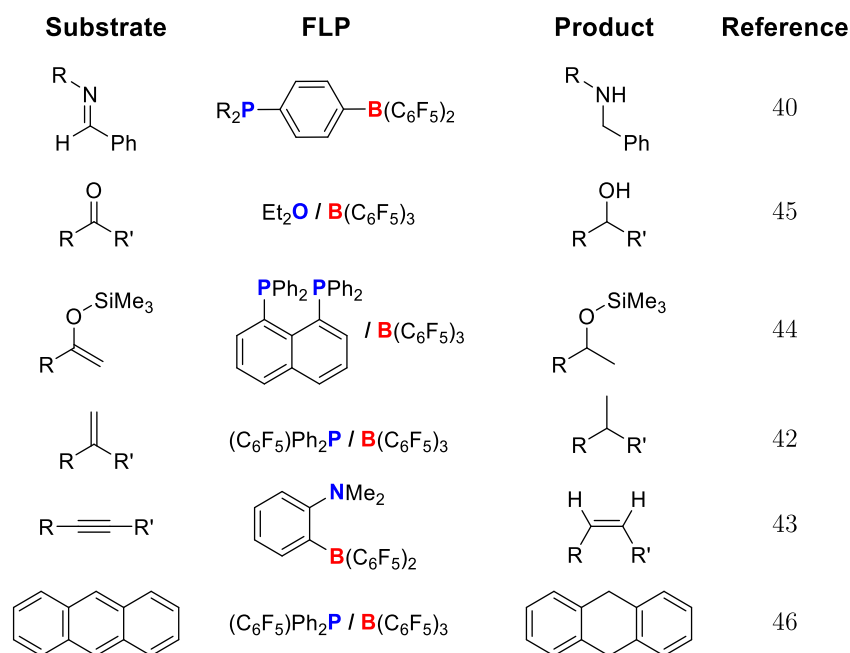


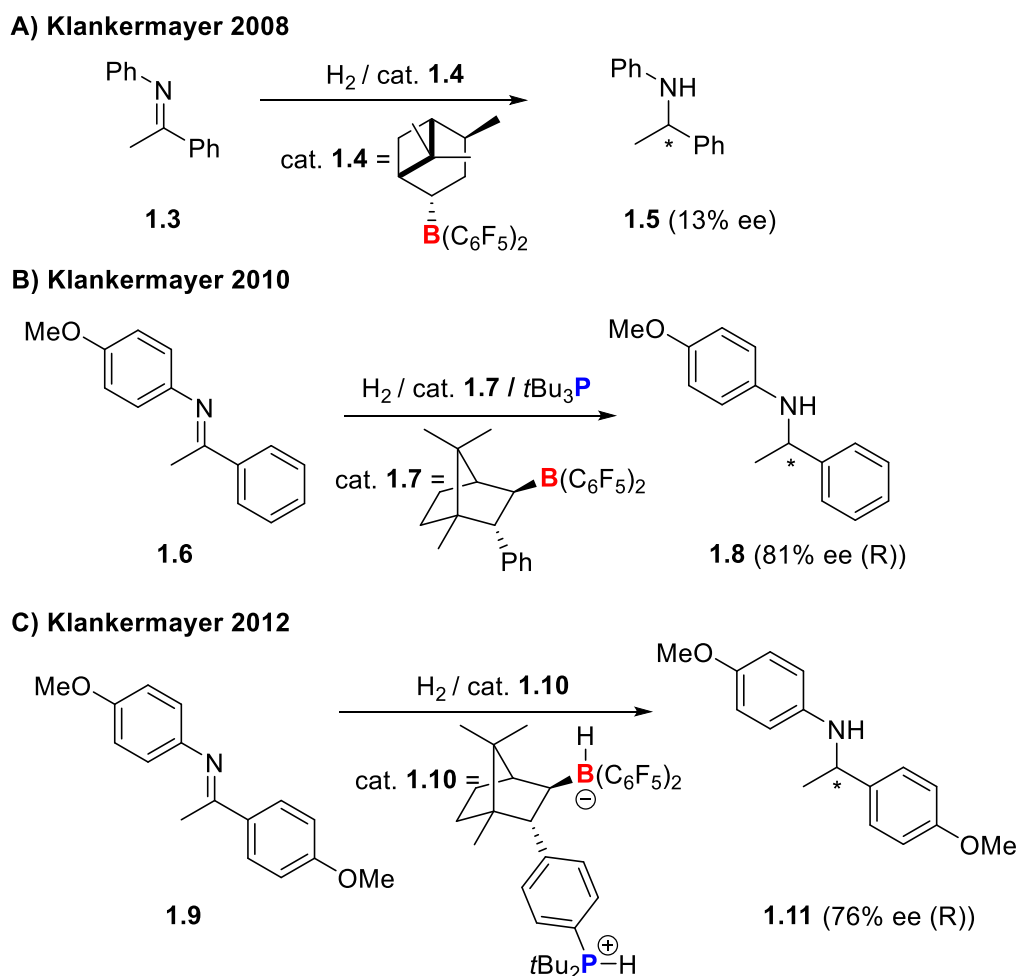
Figure 1.4. Selected examples of hydrogenation reactions mediated by FLPs.

Strikingly, these FLP mediated, metal-free, hydrogenation reactions can be also performed in an asymmetric manner. For instance, Klankermeyer and Chen initially reported that ketimine **1.3** can be quantitatively reduced to **1.5** by means of chiral borane **1.4** (Scheme 1.4A).⁴⁸ Although the observed enantiomeric excess (ee) was poor (13%), this initial report paved the way to further developments. Indeed, the same group developed a much more efficient catalyst based on the FLP composed of the chiral bicyclic borane **1.7** and *t*Bu₃P. This species was able to asymmetrically reduce several ketimines with ee's up to 81% (Scheme 1.4B).⁴⁹ In a further effort, the same group employed the chiral FLP catalyst **1.10** to reduce the imine **1.9** with an ee of 76% and using a rather low catalyst loading of only 2.0 mol% (Scheme 1.4C).⁵⁰

⁴⁸ D. Chen, J. Klankermeyer, *Chem. Commun.*, **2008**, 2130-2131.

⁴⁹ D. Chen, Y. Wang, J. Klankermeyer, *Angew. Chem. Int. Ed.*, **2010**, *49*, 9475-9478.

⁵⁰ G. Ghattas, D. Chen, F. Pan, J. Klankermeyer, *Dalton Trans.*, **2012**, *41*, 9026-9028.

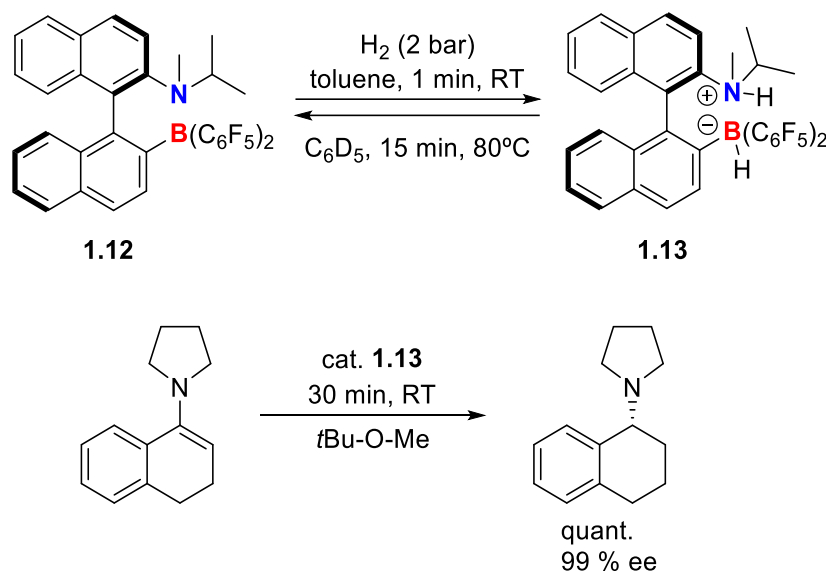


Scheme 1.4. FLP-catalyzed asymmetric reductions of ketimines reported by the Klankermayer group.

After these seminal reports by Klankermayer and co-workers, many groups have focused on broadening the substrate scope, enhancing the catalyst activity, and adapting FLP chemistry to design more effective catalysts for asymmetric reductions. Most of this research has been recently gathered in several review articles.^{37d,38m,51} Although the description of all these FLP applications is far beyond the scope of this introduction, we would like to highlight some representative examples reporting high reaction yields and/or enantiomeric excesses. For instance, Repo and co-workers described the synthetic route to the enantiopure aminoborane catalyst **1.12**, which could not be isolated due to its high moisture and air sensitivity. However, after a very fast (< 1 min) heterolytic splitting of H₂, it was possible to isolate and fully characterize the resulting ammonium borohydride salt

⁵¹ (a) W. Meng, X. Feng, H. Du, *Acc. Chem. Res.*, **2018**, *51*, 191-201; (b) J. Lam, K. M. Szkop, E. Mosafari, D. W. Stephan, *Chem. Soc. Rev.*, **2019**, *48*, 3592-3612.

1.13 (Scheme 1.5). This zwitterionic salt successfully catalyzes the asymmetric hydrogenation of enamines and unhindered imines with ee up to 99%.⁵²



Scheme 1.5. Reversible dihydrogen activation reaction mediated by aminoborane **1.12** (top) and asymmetric reduction of an enamine catalyzed by the zwitterionic salt **1.13** (bottom) reported by Repo and co-workers (see reference 52).

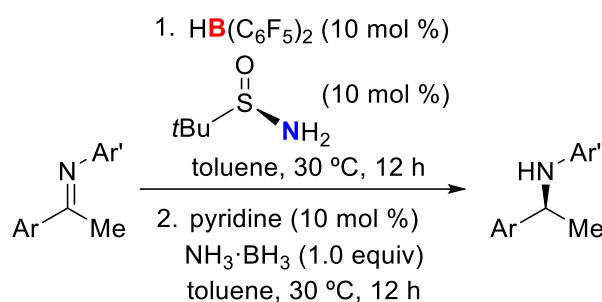
In 2016, Du and co-workers reported the catalytic asymmetric reduction of imines (84-95% ee) using a combination of the Piers' borane, $\text{HB}(\text{C}_6\text{F}_5)_2$, and chiral *tert*-butylsulfonamide as FLP partners (Scheme 1.6A).⁵³ Curiously, in this work the hydrogen source was ammonia borane ($\text{NH}_3 \cdot \text{BH}_3$) which afforded better results than H_2 . Only one year later, the same group reported, using a similar strategy, the metal-free asymmetric transfer hydrogenation of 2,3-disubstituted quinoxalines with excellent ee's as high as 99%.⁵⁴ (Scheme 1.6B).

⁵² M. Lindqvist, K. Borre, K. Axenov, B. Kótai, M. Nieger, M. Leskelä, I. Pápai, T. Repo, *J. Am. Chem. Soc.*, **2015**, *137*, 4038-4041.

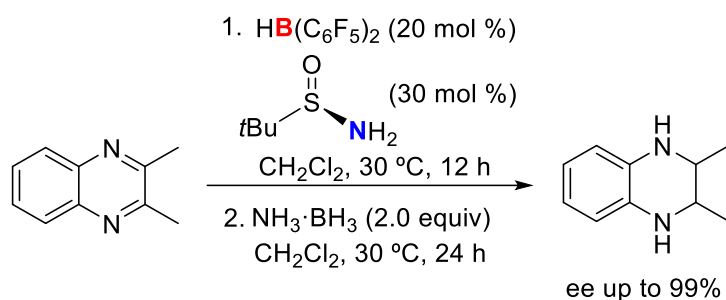
⁵³ S. Li, G. Li, W. Meng, H. Du, *J. Am. Chem. Soc.*, **2016**, *138*, 12956-12962.

⁵⁴ S. Li, W. Meng, H. Du, *Org. Lett.*, **2017**, *19*, 2604-2606.

A) Du 2016



B) Du 2017



Scheme 1.6. Catalytic asymmetric reductions of A) imines and B) disubstituted quinoxalines employing the FLP system $\text{HB}(\text{C}_6\text{F}_5)_2$ /chiral *tert*-butylsulfinamide.

Interestingly, the reversible cleavage of the hydrogen molecule mediated by FLPs has envisioned a potential application of the FLP chemistry within the field of renewable energies. In this regard, dihydrogen is a promising energy source that has gained much attention in the last years due to its advantages over the existing energy supplies, namely:

- i. The exothermic reaction of dihydrogen with oxygen or air generates harmless water as the only product.
- ii. It is environmentally clean and can be a good alternative for the widely extended use of fossil fuels which are scarce, expensive, and often produce greenhouse gases and other pollutants.
- iii. Hydrogen possesses a high energy storage capacity. It has been estimated that the energy contained in 1 kg of hydrogen is about 33.3 kWh (120 MJ/kg),⁵⁵ which exceeds double of most conventional fuels.

⁵⁵ D. Teichmann, W. Arlt, P. Wasserscheid, *Int. J. Hydrogen Energy*, **2012**, *37*, 18118-18132.

Despite that, there are some limitations to overcome in the use of the energy derived from dihydrogen. For example, its storage remains the major challenge due to its extremely low density (0.0898 g/L at 0 °C and 1 bar).⁵⁶ The existing storage methods usually require high-pressure technologies or harsh cryogenic conditions.⁵⁷ For this reason, much research is being done on low-cost materials that can easily sequester and release large amounts of dihydrogen as potential dihydrogen storage materials. In this regard, boron-nitrogen compounds have been proposed as an attractive alternative.⁵⁸ For instance, ammonia-borane (AB) is a promising hydrogen storage material because it is stable at room temperature, quite soluble in water and can sequester a high weight percentage of dihydrogen (19.6%).⁵⁹ However, the required H₂ release process from B–N compounds still constitutes the major limitation of this alternative. To overcome this drawback, several authors have reported different strategies based on FLPs to perform dehydrogenation reactions with concomitant regeneration of the starting amino-borane compounds.

For instance, Miller and Bercaw reported the stoichiometric dehydrogenation reaction of dimethylamine-borane (DMAB) using the FLP PtBu₃/B(C₆F₅)₃ under mild conditions to produce the corresponding phosphonium borohydride salt and the dimeric (R₂NBH₂)₂ with a high conversion rate of 95% (Scheme 1.7A).⁶⁰ The dehydrogenation of AB under the same conditions was also reported, albeit with lower conversion rates (80-85%), affording polyaminoboranes (NH₂BH₂)_n. Almost simultaneously, Manner and co-workers reported the ability of several FLPs based on Group 14 triflates and bulky nitrogen bases to stoichiometrically dehydrogenate amine- and phosphane-borane adducts.⁶¹ As a representative example of this work, the FLP constituted by *n*Bu₃SnOTf and 2,2,6,6-tetramethylpiperidine (TMP) was found to cleanly and rapidly dehydrogenate DMAB yielding [Me₂N–BH₂]₂ with 86%

⁵⁶ M. Feller, *Phys. Sci. Rev.*, **2018**, *4*, 20180033.

⁵⁷ A. Züttel, *Naturwissenschaften*, **2004**, *91*, 157-172.

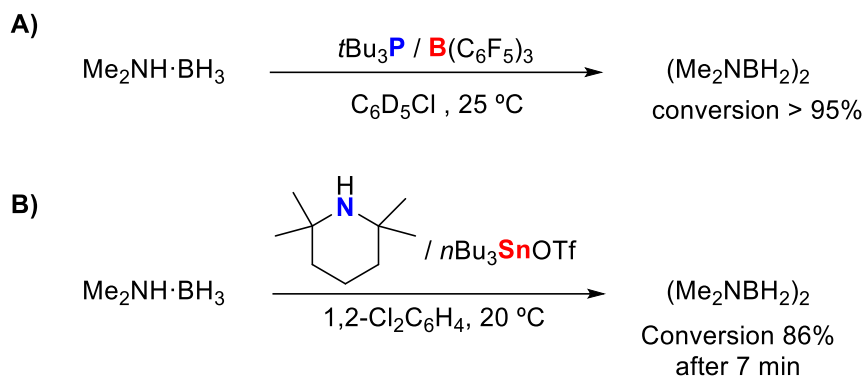
⁵⁸ For reviews on ammonia–borane as dihydrogen source, see: (a) T. B. Marder, *Angew. Chem. Int. Ed.*, **2007**, *46*, 8116-8118; (b) F. H. Stephens, V. Pons, R. T. Baker, *Dalton Trans.*, **2007**, 2613-2626; (c) B. Peng, J. Chen, *Energy Environ. Sci.*, **2008**, *1*, 479-483; (d) A. Staubitz, A. P. M. Robertson, M. E. Sloan, I. Manners, *Chem. Rev.*, **2010**, *110*, 4023-4078; (e) A. Staubitz, A. P. M. Robertson, I. Manners, *Chem. Rev.*, **2010**, *110*, 4079-4124; (f) D. H. A. Boom, A. R. Jupp, J. C. Slootweg, *Chem. Eur. J.*, **2019**, *25*, 9133-9152.

⁵⁹ C. W. Hamilton, R. T. Baker, A. Staubitz, I. Manners, *Chem. Soc. Rev.*, **2009**, *38*, 279-293.

⁶⁰ A. J. M. Miller, J. E. Bercaw, *Chem. Commun.*, **2010**, *46*, 1709-1711.

⁶¹ G. R. Whittell, E. I. Balmond, A. P. M. Robertson, S. K. Patra, M. F. Haddow, I. Manners, *Eur. J. Inorg. Chem.*, **2010**, 3967-3975.

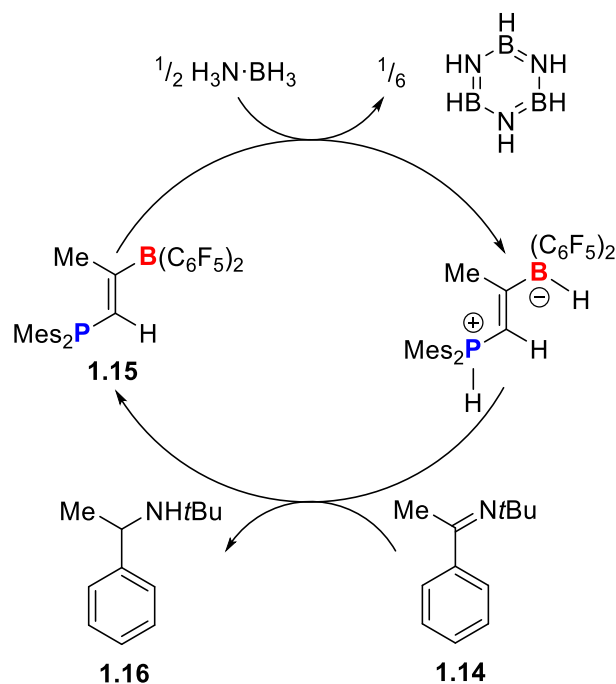
conversion (Scheme 1.7B). Notably, the authors carried out control experiments which confirm that the separate components of the FLP were not able to dehydrogenate the aforementioned aminoboranes. Thus, once again the cooperative action of the acid and the basic functionalities of the FLP system was found to be crucial.



Scheme 1.7. Stoichiometric dehydrogenation of dimethylamine-borane mediated by the FLP: A) $t\text{Bu}_3\text{P}/\text{B}(\text{C}_6\text{F}_5)_3$ and B) TMP/ $n\text{Bu}_3\text{SnOTf}$.

Moreover, the dehydrogenation of aminoboranes mediated by FLPs can be also performed in a catalytic manner. For instance, the Erker group showed that the treatment of imine **1.14** with AB in the presence of catalytic amounts of FLP **1.15** (ca. 10 mol%) leads to the rapid formation of the corresponding amine **1.16** and borazine (Scheme 1.8).^{37a,62}

⁶² (a) S. Schwendemann (2008) Hydrierungsreaktionen mit sterisch gehinderten Phosphan-Boran-Addukten. Diplomarbeit, Münster. See also: (b) D. W. Stephan, G. Erker, *Angew. Chem. Int. Ed.* **2010**, *49*, 46-76.

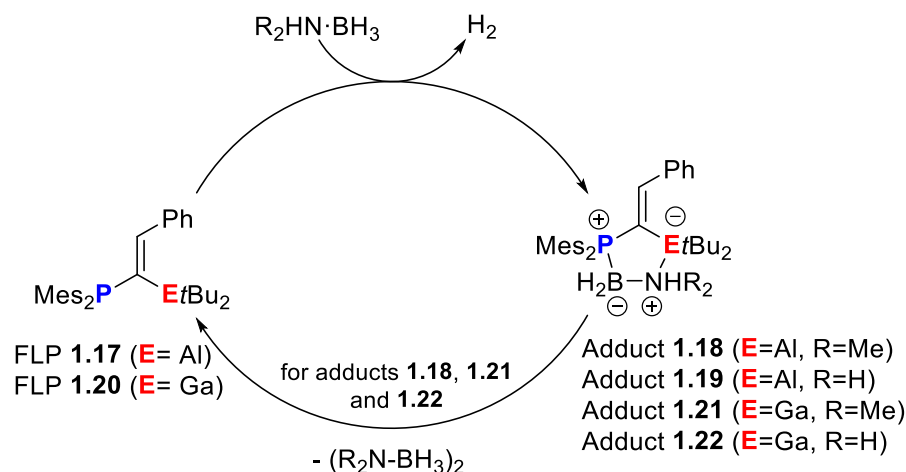


Scheme 1.8. Catalytic reduction of imine **1.14** using ammonia-borane and FLP **1.15**.

Slootweg, Uhl and co-workers also showed that the treatment of FLP **1.17** (9.3 mol%) with DMAB afforded the thermally unstable adduct **1.18** and H_2 . Heating to 90 °C leads to the formation of the dimeric $(\text{Me}_2\text{N}-\text{BH}_2)_2$ and complete regeneration of the FLP **1.17** in 45 min and 71% yield (Scheme 1.9).⁶³ Lower loadings of FLP **1.17** (0.4 mol%) resulted in a similar conversion rate; however, considerably longer reaction times up to 44 hours were required. The reactivity of FLP **1.17** towards the less hindered AB was also investigated but, in this particular case, the adduct **1.19** was remarkably stable and, as a consequence, the starting FLP **1.17** could not be regenerated (Scheme 1.9). In a related study, the reactivity towards aminoboranes of the analogous Ga/P-based FLP was described (Scheme 1.9).⁶⁴ In this case, the same reactivity as the analogous FLP **1.17** towards AB and DMAB was found. However, the corresponding adduct **1.22** was markedly much more unstable than its aluminum counterpart and therefore, regeneration of the FLP **1.20** and formation of oligomeric BN compounds were accomplished. Indeed, small quantities of FLP **1.20** (4 mol%) could be used to catalyze the hydrogen transfer from AB to the imine $\text{PhCH}=\text{N}t\text{Bu}$ affording the corresponding amine.

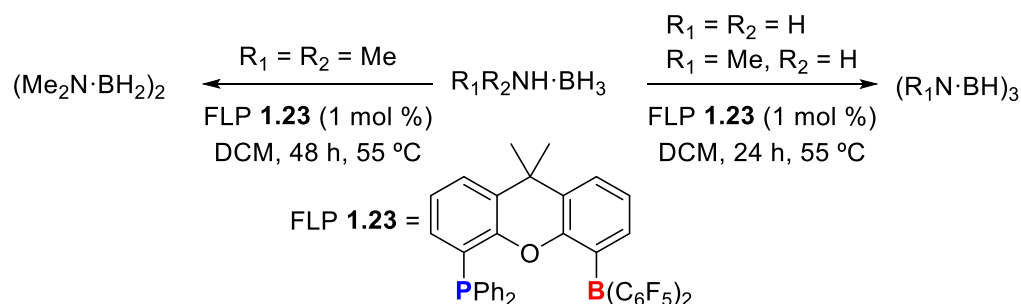
⁶³ C. Appelt, J. C. Slootweg, K. Lammertsma, W. Uhl, *Angew. Chem. Int. Ed.*, **2013**, *52*, 4256-4259.

⁶⁴ J. Possart, W. Uhl, *Organometallics*, **2018**, *37*, 1314-1323.



Scheme 1.9. Catalytic dehydrocoupling of amino-boranes mediated by FLPs **1.17** and **1.20**.

In 2016, Aldridge and co-workers reported the catalytic dehydrogenation of several amine-boranes by a preorganized dimethylxanthene-derived FLP.⁶⁵ Thus, FLP **1.23** was shown to catalyze the dihydrogen release from AB, DMAB, and $\text{MeNH}_2 \cdot \text{BH}_3$ (MAB) at 55 °C employing only 1 mol% catalyst loading (Scheme 1.10).



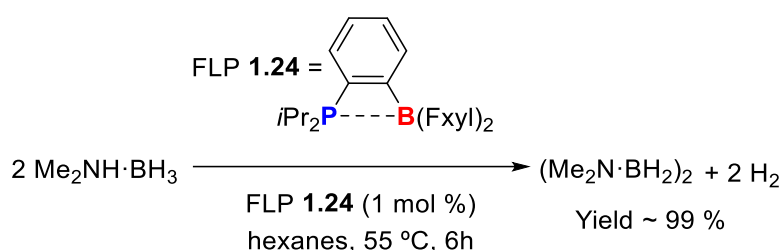
Scheme 1.10. Dehydrogenation of amine-boranes catalyzed by FLP **1.23**.

In a related effort, Bourissou and co-workers employed the *o*-phenylene bridged FLP **1.24** to catalytically dehydrogenate a variety of amine- and diamine-boranes under mild reaction conditions.⁶⁶ By means of different experimental and computational tools, the authors concluded that FLP **1.24** adopts preferably a closed-form where the dative, donor-acceptor bond is formed. However,

⁶⁵ (a) Z. Mo, A. Rit, J. Campos, E. L. Kolychev, S. Aldridge, *J. Am. Chem. Soc.*, **2016**, *138*, 3306-3309; (b) O. Sadek, G. Bouhadir, D. Bourissou, *Chem. Soc. Rev.*, **2021**, *50*, 5777-5805.

⁶⁶ M. Boudjellel, E. D. Sosa Carrizo, S. Mallet-Ladeira, S. Massou, K. Miqueu, G. Bouhadir, D. Bourissou, *ACS Catal.*, **2018**, *8*, 4459-4464.

due to the high ring strain, this bond is labile which makes the open, active geometry accessible. Curiously, although FLP **1.24** did not react with H₂ (2 atm) after days at 50 °C, the catalytic dehydrogenation of DMAB was accomplished employing 1% mol FLP **1.24** loading at 55 °C in 6 hours (Scheme 1.11). This result contrasts with the required 48 h under similar reaction conditions reported by Aldridge and co-workers in the previously commented work (see above). Furthermore, screening of the reaction conditions for this dehydrogenation reaction indicated that the transformation can proceed either by decreasing or increasing the catalytic loading at the expense of time or temperature leading to similar quantitative results.



Scheme 1.11. Catalytic dihydrogen release from dimethylamine-borane mediated by FLP **1.24**.

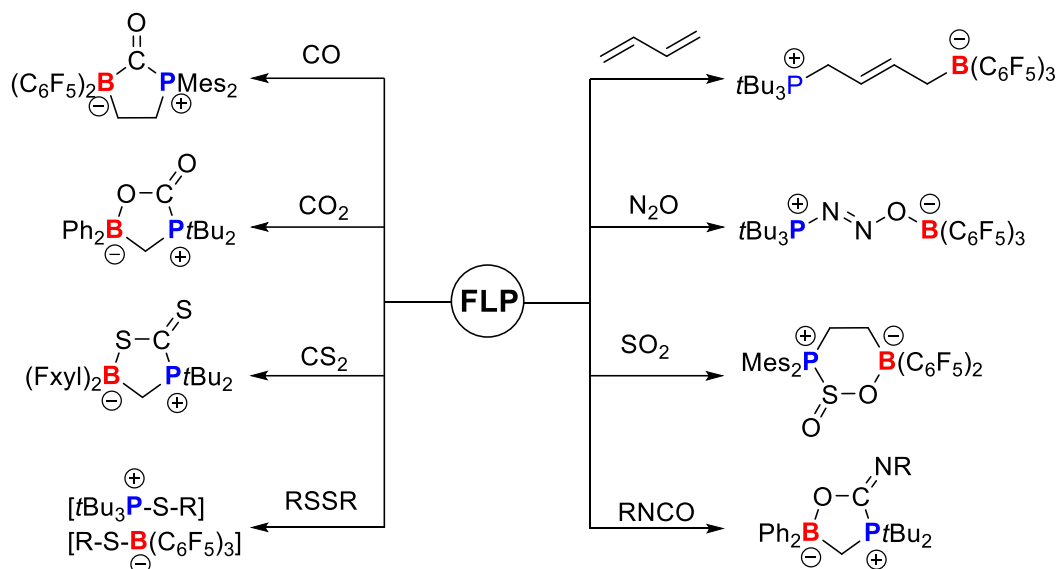
1.2.2. Activation of other small molecules

The cooperative mode of action of the acceptor and donor functionalities of FLPs resembles the way that transition metals act as both acceptors and donors, allowing them to activate a wide range of small molecules. This feature prompted many studies where the use of FLPs has been extended to activate a growing range of small molecules. Indeed, FLPs activate not only dihydrogen but also CO,⁶⁷ CO₂,⁶⁸

⁶⁷ (a) M. Sajid, G. Kehr, C. G. Daniliuc, G. Erker, *Angew. Chem. Int. Ed.*, **2014**, *53*, 1118-1121; (b) M. Sajid, L. M. Elmer, C. Rosorius, C. G. Daniliuc, S. Grimme, G. Kehr, G. Erker, *Angew. Chem. Int. Ed.*, **2013**, *52*, 2243-2246; (c) Q. Sun, C. G. Daniliuc, C. Mück-Lichtenfeld, K. Bergander, G. Kehr, G. Erker, *J. Am. Chem. Soc.*, **2020**, *142*, 17260-17264.

⁶⁸ For a review, see: D. W. Stephan, G. Erker, *Chem. Sci.*, **2014**, *5*, 2625-2641.

CS₂,⁶⁹ SO₂,^{22,70} N₂O,⁷¹ dienes,⁷² ethers,⁷³ isocyanates,⁷⁴ and disulfides,⁷⁵ among others species. Scheme 1.12 shows some selected examples of small molecule activations mediated by FLPs. In this section, we summarize representative examples involving the activation of alkenes/alkynes and CO₂.



Scheme 1.12. Selected examples of small molecule activations promoted by FLPs.

Even though neither tertiary phosphines nor tertiary boranes are known to react with olefins, the combination of both reagents leads to addition reactions to the C=C double bond of different olefins. For instance, Stephan and co-workers reported that the BCF/PtBu₃ FLP reacts with ethylene, propylene, or 1-hexene

⁶⁹ K. Samigullin, I. Georg, M. Bolte, H.-W. Lerner, M. Wagner, *Chem. Eur. J.*, **2016**, *22*, 3478-3484.

⁷⁰ (a) A. Adenot, N. von Wolff, G. Lefèvre, J.-C. Berthet, P. Thuéry, T. Cantat, *Chem. Eur. J.*, **2019**, *25*, 8118-8126; (b) M. Sajid, A. Klose, B. Birkmann, L. Liang, B. Schirmer, T. Wiegand, H. Eckert, A. J. Lough, R. Fröhlich, C. G. Daniliuc, S. Grimme, D. W. Stephan, G. Kehr, G. Erker, *Chem. Sci.*, **2013**, *4*, 213-219; (c) J. Möricke, B. Wibbeling, C. G. Daniliuc, G. Kehr, G. Erker, *Phil. Trans. R. Soc. A*, **2017**, *375*, 20170015; (d) X. Xu, G. Kehr, C. G. Daniliuc, G. Erker, *J. Am. Chem. Soc.*, **2014**, *136*, 12431-12443.

⁷¹ (a) R. C. Neu, E. Otten, A. Lough, D. W. Stephan, *Chem. Sci.*, **2011**, *2*, 170-176; (b) E. Otten, R. C. Neu, D. W. Stephan, *J. Am. Chem. Soc.*, **2009**, *131*, 9918-9919.

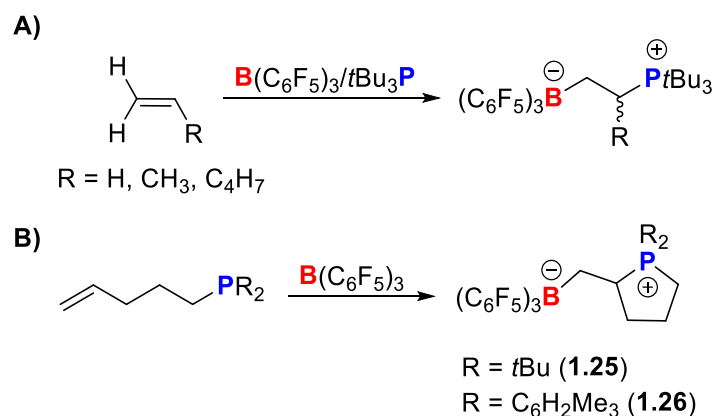
⁷² M. Ullrich, K. S.-H. Seto, A. J. Lough, D. W. Stephan, *Chem. Commun.*, **2009**, 2335-2337.

⁷³ (a) G. C. Welch, L. Cabrera, P. A. Chase, E. Hollink, J. D. Masuda, P. Wei, D. W. Stephan, *Dalton Trans.*, **2007**, 3407-3414; (b) G. C. Welch, J. D. Masuda, D. W. Stephan, *Inorg. Chem.*, **2006**, *45*, 478-480.

⁷⁴ E. Theuergarten, J. Schlösser, D. Schlüns, M. Freytag, C. G. Daniliuc, P. G. Jones, M. Tamm, *Dalton Trans.*, **2012**, *41*, 9101-9110.

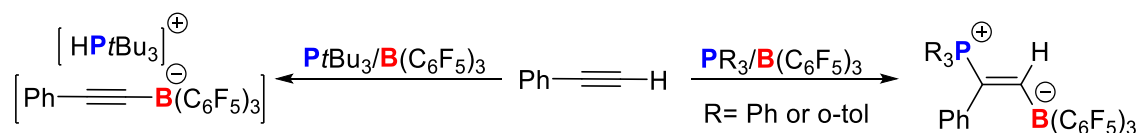
⁷⁵ M. A. Dureen, G. C. Welch, T. M. Gilbert, D. W. Stephan, *Inorg. Chem.*, **2009**, *48*, 9910-9917.

affording the zwitterionic species depicted in Scheme 1.13A.⁷ In the same study, it was confirmed that FLPs can also react with olefins in an intramolecular manner. Thus, the sterically encumbered (pentenyl)PR₂ phosphines (R = *t*Bu, C₆H₂Me₃) react with BCF leading to the cyclic products **1.25** and **1.26** (Scheme 1.13B).



Scheme 1.13. A) Intermolecular and B) intramolecular additions of FLPs to olefins.

Analogous additions of FLPs to alkynes were observed affording the corresponding zwitterionic phosphonium borate products (Scheme 1.14). However, when terminal alkynes are involved, there exists a competition between the activation of the terminal C–H bond and the P/B(Al) addition to the alkyne. Stephan and co-workers demonstrated that the nature of the base is decisive for the outcome of the reaction.⁷⁶ Thus, when phenylacetylene reacts with a combination of the phosphine PPh₃ (or P(*o*-tol)₃) and the LA BCF, the respective zwitterionic products derived from the FLP addition to the alkyne were produced (Scheme 1.14, right). In contrast, when using the bulkier P*t*Bu₃ phosphine as LB, only the C–H activation product of phenylacetylene was observed (Scheme 1.14, left).



Scheme 1.14. Terminal alkyne activation promoted by FLPs.

⁷⁶ M. A. Dureen, D. W. Stephan, *J. Am. Chem. Soc.*, **2009**, *131*, 8396-8397.

Carbon dioxide (CO₂) is one of the main greenhouse gases responsible for global warming. In consequence, strategies to capture, chemically modify or store CO₂ have attracted much interest in the scientific community. The main drawback, which hampers the development of such strategies, is the extraordinarily limited reactivity of CO₂ due to its thermodynamic stability. This issue has been addressed from different approaches such as the use of zeolites,⁷⁷ metal-organic frameworks,⁷⁸ activated carbon,⁷⁹ etc. The ambiphilic nature of FLPs confers them the ability to activate CO₂ by nucleophilic attack to the electrophilic carbon atom and subsequent electrophilic capture of the resulting products.

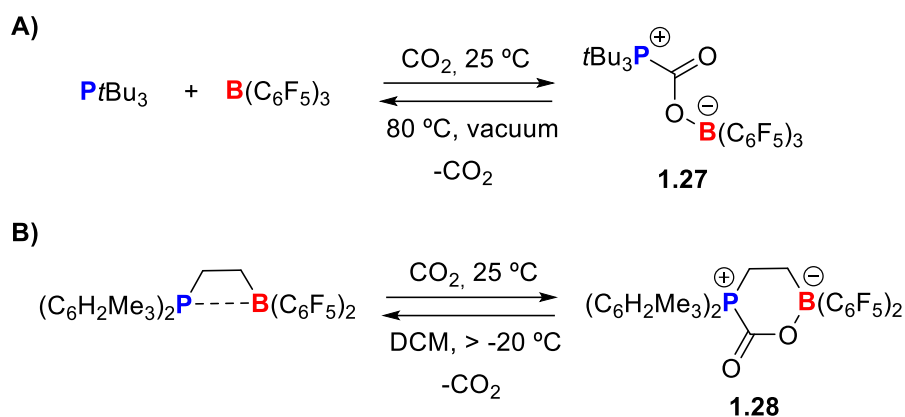
In 2009, Erker and co-workers first described a new approach based on FLPs to reversibly sequester CO₂ under mild reaction conditions.⁸⁰ Thus, a solution of PtBu₃ and BCF in C₆H₅Br under a CO₂ atmosphere at room temperature afforded the CO₂ activation product **1.27** in an excellent 87% yield (Scheme 1.15A). Similarly, CO₂ was captured using the intramolecular FLP (Me₃C₆H₂)₂PCH₂CH₂B(C₆F₅)₂ affording the product **1.28** in 79% yield (Scheme 1.15B). In addition, the thermal stability of the observed CO₂-activation products **1.27** and **1.28** was also analyzed. The authors reported that when a solution of **1.27** in bromobenzene was heated up to 80 °C for 5 hours under vacuum, ca. 50% regeneration of the initial FLP mixture and CO₂ was observed. Strikingly, whereas product **1.28** is relatively stable in the solid-state, dichloromethane or toluene solutions of this species at -20 °C revert to the starting materials.

⁷⁷ For a recent review, see: S. Kumar, R. Srivastava, J. Koh, *J. CO₂ Util.*, **2020**, *41*, 101251, and references therein.

⁷⁸ (a) J. L. C. Rowsell, E. C. Spencer, J. Eckert, J. A. K. Howard, O. M. Yaghi, *Science*, **2005**, *309*, 1350-1354; (b) A. C. Sudik, A. R. Millward, N. W. Ockwig, A. P. Côté, J. Kim, O. M. Yaghi, *J. Am. Chem. Soc.*, **2005**, *127*, 7110-7118; (c) R. Banerjee, A. Phan, B. Wang, C. Knobler, H. Furukawa, M. O'Keeffe, O. M. Yaghi, *Science*, **2008**, *319*, 939-943.

⁷⁹ For a review, see: K. B. Lee, M. G. Beaver, H. S. Caram, S. Sircar, *Ind. Eng. Chem. Res.*, **2008**, *47*, 8048-8062.

⁸⁰ C. M. Mömming, E. Otten, G. Kehr, R. Fröhlich, S. Grimme, D. W. Stephan, G. Erker, *Angew. Chem. Int. Ed.*, **2009**, *48*, 6643-6646.



Scheme 1.15. Reversible CO_2 captures employing A) an intermolecular and B) intramolecular FLP.

After this initial report by Erker and co-workers, several intra- and intermolecular FLPs have been proven to successfully capture CO_2 (Figure 1.5).⁸¹ This transformation can be performed using a wide variety of FLPs having B,⁸² Al,^{13a,13b,83} Si,^{22,84} Ge,²³ Sn,²⁴ as the acceptor partners, and NHCs,⁸⁵ phosphinimines,⁸⁶ or pyrazoles,⁷⁴ as the basic counterpart.

⁸¹ For a review, see: D. W. Stephan, *J. Am. Chem. Soc.*, **2015**, *137*, 10018-10032.

⁸² (a) I. Peuser, R. C. Neu, X. Zhao, M. Ulrich, B. Schirmer, J. A. Tannert, G. Kehr, R. Fröhlich, S. Grimme, G. Erker, D. W. Stephan, *Chem. Eur. J.*, **2011**, *17*, 9640-9650; (b) M. Harhausen, R. Fröhlich, G. Kehr, G. Erker, *Organometallics*, **2012**, *31*, 2801-2809.

⁸³ (a) J. Boudreau, M.-A. Courtemanche, F.-G. Fontaine, *Chem. Commun.*, **2011**, *47*, 11131-11133.

⁸⁴ M. Reissmann, A. Schafer, S. Jung, T. Muller, *Organometallics*, **2013**, *32*, 6736-6744.

⁸⁵ (a) E. L. Kolychev, T. Bannenberg, M. Freytag, C. G. Daniliuc, P. G. Jones, M. Tamm, *Chem. Eur. J.*, **2012**, *18*, 16938-16946; (b) E. Theuergarten, T. Bannenberg, M. D. Walter, D. Holschumacher, M. Freytag, C. G. Daniliuc, P. G. Jones, M. Tamm, *Dalton Trans.*, **2014**, *43*, 1651-1662.

⁸⁶ C. Jiang, D. W. Stephan, *Dalton Trans.*, **2013**, *42*, 630-637.

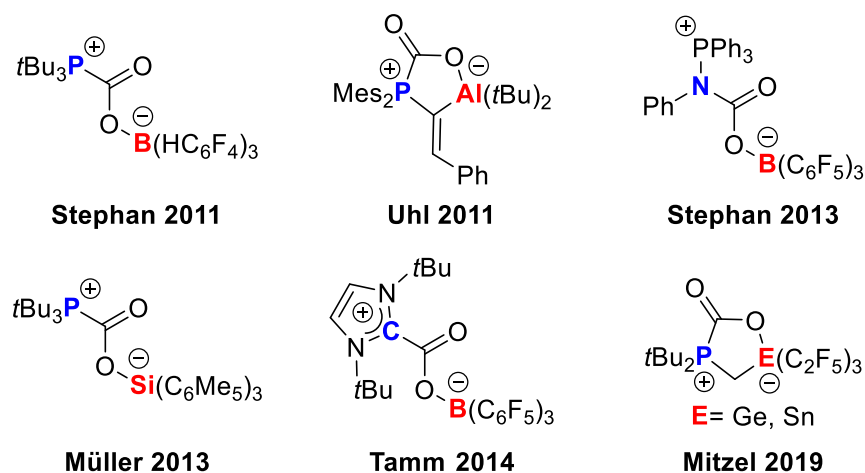


Figure 1.5. Selected examples of CO₂ capture mediated by different FLPs.

Although the sequestration of CO₂ is an attractive alternative in the fight against global warming, it is arguably more interesting not only to capture but also to convert CO₂ into more valuable species. It is well-known that transition metal complexes are able to transform CO₂ into C1-reagents such as formic acid,⁸⁷ formate,⁸⁸ formaldehyde,⁸⁹ methanol,⁹⁰ methane,^{30b, 91} and acetals.⁹² However, metal-free methodologies able to undergo this transformation are still emerging.

⁸⁷ (a) R. Tanaka, M. Yamashita, K. Nozaki, *J. Am. Chem. Soc.*, **2009**, *131*, 14168-14169; (b) C. Federsel, R. Jackstell, M. Beller, *Angew. Chem. Int. Ed.*, **2010**, *49*, 6254-6257; (c) T. Schaub, R. A. Paciello, *Angew. Chem. Int. Ed.*, **2011**, *50*, 7278-7282.

⁸⁸ (a) C. Federsel, A. Boddien, R. Jackstell, R. Jennerjahn, P. J. Dyson, R. Scopelliti, G. Laurenczy, M. Beller, *Angew. Chem. Int. Ed.*, **2010**, *49*, 9777-9780; (b) R. Langer, Y. Diskin-Posner, G. W. Leitner, L. J. Shimon, Y. Ben-David, D. Milstein, *Angew. Chem. Int. Ed.*, **2011**, *50*, 9948-9952; (c) C. A. Huff, M. S. Sanford, *ACS Catal.*, **2013**, *3*, 2412-2416; (d) M. S. Jeletic, M. T. Mock, A. M. Appel, J. C. Linehan, *J. Am. Chem. Soc.*, **2013**, *135*, 11533-11536; (e) L. Zhang, J. Cheng, Z. Hou, *Chem. Commun.*, **2013**, *49*, 4782-4784; (f) R. Shintani, K. Nozaki, K. *Organometallics*, **2013**, *32*, 2459-2462; (g) H.-W. Suh, L. M. Guard, N. Hizari, *Chem. Sci.*, **2014**, *5*, 3859-3872.

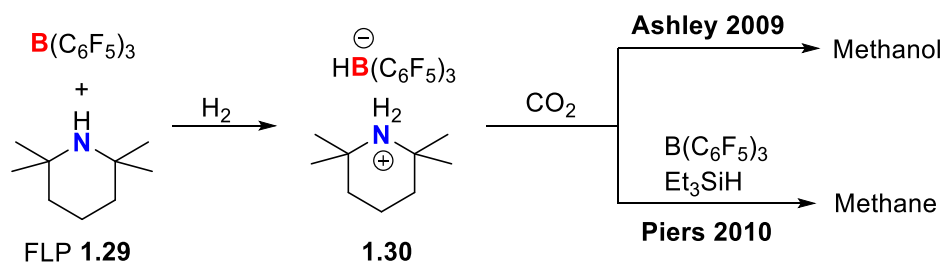
⁸⁹ (a) S. Bontemps, S. Sabo-Etienne, *Angew. Chem. Int. Ed.*, **2013**, *52*, 10253-10255; (b) S. Bontemps, L. Vendier, S. Sabo-Etienne, *J. Am. Chem. Soc.*, **2014**, *136*, 4419-4425.

⁹⁰ (a) S. Chakraborty, J. Zhang, J. A. Krause, H. Guan, *J. Am. Chem. Soc.*, **2010**, *132*, 8872-8873; (b) E. Balaraman, C. Gunanathan, J. Zhang, L. J. W. Shimon, D. Milstein, *Nat. Chem.*, **2011**, *3*, 609-614; (c) C. A. Huff, M. S. Sanford, *J. Am. Chem. Soc.*, **2011**, *133*, 18122-18125; (d) S. Wesselbaum, T. von Stein, J. Klankermayer, W. Leitner, *Angew. Chem. Int. Ed.*, **2012**, *51*, 7499-7502.

⁹¹ (a) T. Matsuo, H. Kawaguchi, *J. Am. Chem. Soc.*, **2006**, *128*, 12362-12363; (b) S. Park, D. Bézier, M. Brookhart, *J. Am. Chem. Soc.*, **2012**, *134*, 11404-11407; (c) S. J. Mitton, L. Turculet, *Chem. Eur. J.*, **2012**, *48*, 15258-15262.

⁹² F. A. LeBlanc, W. E. Piers, M. Parvez, *Angew. Chem. Int. Ed.*, **2014**, *126*, 808-811.

In a seminal report in 2009, Ashley and co-workers described the first conversion of CO₂ into methanol mediated by a FLP.⁹³ Thus, the addition of CO₂ to a solution of the FLP **1.29** (tetramethylpiperidine/BCF) in C₇D₈ under H₂ atmosphere formed CH₃OB(C₆F₅)₂ after 6 days at 160 °C. Subsequent solvent removal allowed the isolation of methanol in 17-25% yield (Scheme 1.16). Despite this modest conversion, this initial report stimulated subsequent studies. For instance, only one year later, Piers and co-workers reported that the treatment of the same FLP **1.29** with H₂ yields the ammonium borate ion-pair **1.30**, which catalytically converts CO₂ into methane employing B(C₆F₅)₃ and triethylsilane as reductant (Scheme 1.16).⁹⁴ Similarly, Stephan and co-workers reported the irreversible capture of CO₂ using a FLP based on AlX₃ (X= Cl or Br) and PMes₃. The corresponding adduct rapidly reacted with an excess of ammonia-borane as the dihydrogen source at room temperature leading to the formation of methanol (37-51% yield).^{13a}



Scheme 1.16. CO₂ conversion into methanol or methane mediated by the ionic pair **1.30**.

In 2013, the Fontaine group also reported a metal-free reduction of CO₂ to methanol using FLPs. In this work, the FLP 1-Bcat-2-PPh₂-C₆H₄ (cat = catechol) efficiently catalyzed the transformation of CO₂ into CH₃OBR₂ or (CH₃OBO)₃ with yields up to 99%.^{95,96} After a final hydrolysis step, both products yield methanol with high turnover numbers (>2950) and turnover frequencies (853 h⁻¹). In 2015, Stephan and Fontaine described the transformation of CO₂/H₂ into formyl, acetal, and methoxy-derivatives mediated by the intramolecular B/N FLP 1-BMes₂-2-NMe₂-C₆H₄.³⁶ More recently, Ozin and co-workers reported an elegant

⁹³ A. E. Ashley, A. L. Thompson, D. O'Hare, *Angew. Chem. Int. Ed.*, **2009**, *48*, 9839-9843.

⁹⁴ A. Berkefeld, W. E. Piers, M. Parvez, *J. Am. Chem. Soc.*, **2010**, *132*, 10660-10661.

⁹⁵ M.-A. Courtemanche, M.-A. Légaré, L. Maron, F.-G. Fontaine, *J. Am. Chem. Soc.*, **2013**, *135*, 9326-9329.

⁹⁶ M.-A. Courtemanche, M.-A. Légaré, L. Maron, F.-G. Fontaine, *J. Am. Chem. Soc.*, **2014**, *136*, 10708-10717.

multidisciplinary work where the replacement of In^{3+} in In_2O_3 by Bi^{3+} generated $\text{Bi}_x\text{In}_{2-x}\text{O}_3$ materials. These materials comprise a surface FLP based on $\text{Bi}^{3+}/\text{O}^{2-}$ which is able to photocatalytically reduce CO_2 to methanol.^{97,98}

1.2.3. Activation of C–F bonds

Organic molecules that contain the electronegative element fluorine are applied in different fields such as medical imaging,⁹⁹ pharmaceutical,¹⁰⁰ materials science¹⁰¹ or agrochemicals.¹⁰² The inclusion of fluorine in organic molecules has a great impact on their physical properties such as significant changes in the polarity,¹⁰³ acidity,¹⁰⁴ biological activity^{100b} and thermal stability.¹⁰⁵ For these reasons, new synthetic strategies towards functionalized organofluorine species are of great interest to the scientific community. However, selective mono C–F activations in $-\text{CHF}_2$ and especially in $-\text{CF}_3$ substrates are particularly challenging due mainly to two reasons. Firstly, the C–F single bonds are renowned for their stability. Indeed, the C–F single bond is the strongest bond (130 kcal/mol)¹⁰⁶ among the single bonds between any element and carbon. In addition, C–F bonds become

⁹⁷ T. Yan, N. Li, L. Wang, W. Ran, P. N. Duchesne, L. Wan, N. T. Nguyen, L. Wang, M. Xia, G. A. Ozin, *Nat. Commun.*, **2020**, *11*, 6095.

⁹⁸ For a recent review, see: J. Wang, G. Zhang, J. Zhu, X. Zhang, F. Ding, A. Zhang, X. Guo, C. Song, *ACS Catal.*, **2021**, *11*, 1406-1423.

⁹⁹ S. M. Ametamey, M. Honer, P. A. Schubiger, *Chem. Rev.*, **2008**, *108*, 1501-1516.

¹⁰⁰ (a) M. Schlosser, *Tetrahedron*, **1978**, *34*, 3-17; (b) J. T. Welch, *Tetrahedron*, **1987**, *43*, 3123-3197; (c) S. Purser, P. R. Moore, S. Swallow, V. Gouverneur, *Chem. Soc. Rev.*, **2008**, *37*, 320-330; (d) V. Gouverneur, *Science*, **2009**, *325*, 1630-1631; (e) T. Taguchi, H. Yanai, Ojima I (ed) *Fluorine in medicinal chemistry and chemical biology*, 2009, Wiley, Chichester, 257-290.

¹⁰¹ (a) M. T. Mocella, *J. Fluorine Chem.*, **2003**, *122*, 87-92; (b) K. K. S. Lau, S. K. Murthy, H. G. Pryce Lewis, J. A. Caulfield, K. K. Gleason, *J. Fluorine Chem.*, **2003**, *122*, 93-96; (c) W. R. Dolbier Jr., W. F. Beach, *J. Fluorine Chem.*, **2003**, *122*, 97-104; (d) S. Ebnesajjad, *Introduction to Fluoropolymers: Materials, Technology and Applications*, 2013, William Andrews: Orlando, Chap. 1, 1.

¹⁰² (a) P. Jeschke, *ChemBioChem*, **2004**, *5*, 570-589; (b) C. Pesenti, F. Viani, *ChemBioChem*, **2004**, *5*, 590-613.

¹⁰³ D. O'Hagan, *Chem. Soc. Rev.*, **2008**, *37*, 308-319.

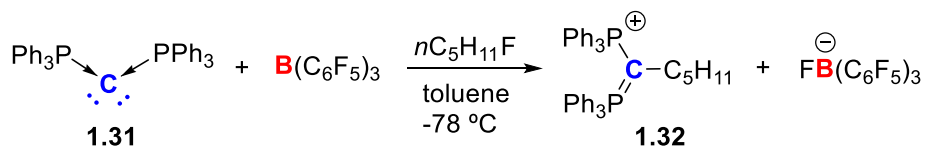
¹⁰⁴ (a) A. Streitwieser Jr., F. Mares, *J. Am. Chem. Soc.*, **1968**, *90*, 2444-2445; (b) F. G. Bordwell, R. J. McCallum, W. N. Olmstead, *J. Org. Chem.*, **1984**, *49*, 1424-1427; (c) F. G. Bordwell, D. Algrim, N. R. Vanier, *J. Org. Chem.*, **1977**, *42*, 1817-1819.

¹⁰⁵ (a) J.-P. Bégué, D. Bonnet-Delpon, *Bioorganic and Medicinal Chemistry of Fluorine*, 2008, John Wiley & Sons: Hoboken, NJ, 72-98; (b) J. Wang, M. Sánchez-Roselló, J. L. Aceña, C. del Pozo, A. E. Sorochinsky, S. Fustero, V. A. Soloshonok, H. Liu, *Chem. Rev.*, **2014**, *114*, 2432-2506.

¹⁰⁶ D. M. Lemal, *J. Org. Chem.*, **2004**, *69*, 1-11.

considerably stronger and shorter as the number of fluorine atoms attached to carbon increases. Thus, the C–F bond dissociation energy typically increases in the order $\text{H}_3\text{C–F}$ (110 kcal/mol) < $\text{H}_2\text{FC–F}$ (120 kcal/mol) < $\text{HF}_2\text{C–F}$ (128 kcal/mol) < $\text{F}_3\text{C–F}$ (130 kcal/mol).¹⁰⁶ Secondly, a common problem in the activation of C–F bonds is the over-reaction derived from the fact that mono- and difluoride substrates are more reactive than trifluoro substrates and, as a result, multiple C–F bonds are usually uncontrollably functionalized.^{3a,107} In other words, it is quite difficult to stop the reaction after the first C–F bond activation in di- and trifluoride substrates. For these reasons, the development of more efficient procedures for the selective C–F bond activation in polyfluorocarbonated species is highly desirable.

In 2010, Alcarazo and co-workers reported the activation of an alkyl monofluoride substrate by a carbon(0)-based FLP.¹⁹ Remarkably, the reaction of one equivalent of 1-fluoropentane to a suspension of carbodiphosphorane **1.31** and BCF, which affords product **1.32**, takes place at $-78\text{ }^\circ\text{C}$ (Scheme 1.17), therefore indicating the high reactivity of this particular FLP.



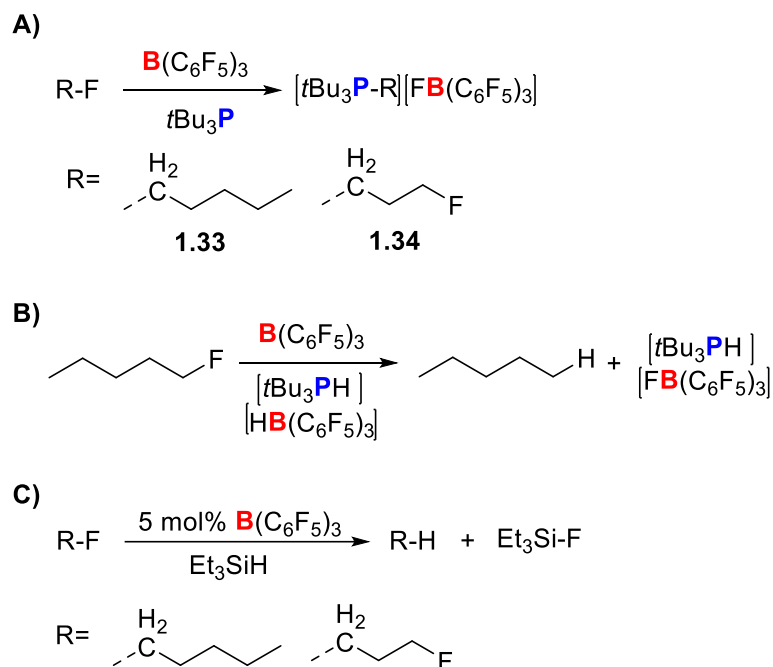
Scheme 1.17. C–F activation reaction mediated by a carbon(0)-based FLP.

In a related effort, Caputo and Stephan described the activation of alkyl C–F bonds employing the LA BCF in combination with sterically demanding phosphines or silanes.¹⁰⁸ Thus, the respective 1:1:1 dichloromethane solutions of BCF, *t*Bu₃P, and substrates **1.33** or **1.34** resulted in the rupture of the C–F bond leading to the formation of the corresponding phosphonium fluoroborate salts (Scheme 1.18A). Transformation of alkyl fluorides into the corresponding alkanes was also achieved through the treatment of BCF/fluoroalkanes with the FLP ionic salt

¹⁰⁷ (a) C. Douvris, O. V. Ozerov, *Science*, **2008**, *321*, 1188-1190; (b) J. Terao, M. Nakamura, N. Kambe, *Chem. Commun.*, **2009**, 6011-6013; (c) M. Janjetovic, A. M. Träff, T. Ankner, J. Wettergren, G. Hilmersson, *Chem. Commun.*, **2013**, *49*, 1826-1828; (d) G. B. Deacon, P. C. Junk, D. Werner, *Eur. J. Inorg. Chem.*, **2015**, 1484-1489; (e) O. Papaianina, K. Y. Amsharov, *Chem. Commun.*, **2016**, *52*, 1505-1508; (f) T. Yamada, K. Saito, T. Akiyama, *Adv. Synth. Catal.*, **2016**, *358*, 62-66.

¹⁰⁸ C. B. Caputo, D. W. Stephan, *Organometallics*, **2012**, *31*, 27-30.

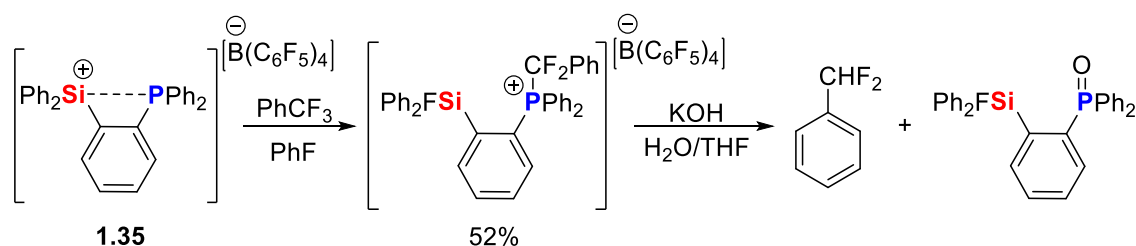
$t\text{Bu}_3\text{PH}/\text{HB}(\text{C}_6\text{F}_5)_3$ (Scheme 1.18B). Strikingly, the well-known fluorophilicity of silanes can be also used to perform C–F bond activations even in a catalytic manner (Scheme 1.18C).¹⁰⁸



Scheme 1.18. Stoichiometric FLP-mediated C–F activations yielding A) phosphonium fluoroborate salts and B) alkanes. C) Catalytic C–F activation affording the corresponding alkanes.

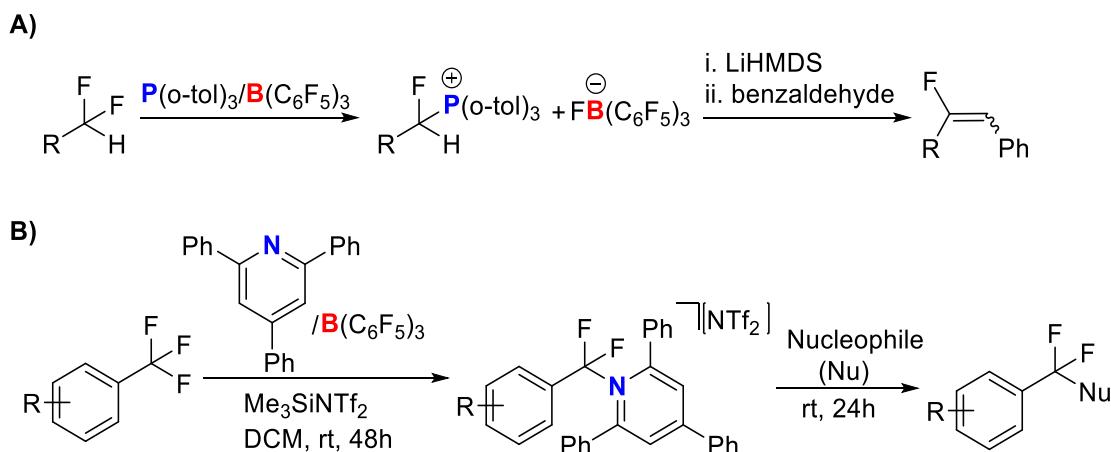
The more challenging selective monodefluorinations of di- and trifluoride substrates are still very scarce and remained elusive to FLPs until Stephan and co-workers reported the first selective mono-hydrodefluorination of aryl polyfluoromethyl functionalities in 2017.¹⁰⁹ Thus, PhCF_3 , PhCF_2H , and Ph_2CF_2 substrates were reacted with the intramolecular FLP **1.35**, containing a phosphorous donor and a silylium cation, to respectively afford PhCF_2H , PhCH_2F , and Ph_2CHF after a Brønsted-base treatment of the corresponding phosphonium salt intermediates (Scheme 1.19). Note that this reaction could be achieved neither with an intermolecular FLP $[\text{Et}_3\text{Si}(\text{tol})]^+/\text{P}(\text{C}_6\text{F}_5)_2\text{Ph}$ nor with electron-rich aromatic solvents due to competitive Friedel-Crafts side-reactions.

¹⁰⁹ I. Mallov, A. J. Ruddy, H. Zhu, S. Grimme, D. W. Stephan, *Chem. Eur. J.*, **2017**, *23*, 17692-17696.



Scheme 1.19. Monoselective C–F bond activation in PhCF₃ mediated by FLP **1.35**.

In 2018, Young and co-workers reported the selective, FLP-mediated, C–F bond activation and subsequent Wittig functionalization of *gem*-difluoromethyl substrates to generate monofluoroalkenes (Scheme 1.20A).¹¹⁰ Two years later, the same group reported an elegant solution to carry out selective monosubstitutions of C–F bonds in the more challenging trifluoride species at remarkably mild reaction conditions using related FLPs (Scheme 1.20B).¹¹¹ This strategy was based on selective monodefluorination and subsequent capture of the fluorocarboanionic intermediates by the LB affording the corresponding cationic phosphonium and pyridinium salts. The positive charge in these intermediates makes them less prone to react with the LAs, therefore overcoming further C–F abstractions and allowing nucleophiles to attack to produce different functionalized fluorine-containing compounds.



Scheme 1.20. FLP strategy to achieve selective monodefluorination over A) difluoro- and B) trifluoro-substrates.

¹¹⁰ D. Mandal, R. Gupta, R. D. Young, *J. Am. Chem. Soc.*, **2018**, *140*, 10682-10686.

¹¹¹ (a) D. Mandal, R. Gupta, A. K. Jaiswal, R. D. Young, *J. Am. Chem. Soc.*, **2020**, *142*, 5, 2572-2578. See also: (b) R. Gupta, A. K. Jaiswal, D. Mandal, R. D. Young, *Synlett*, **2020**, *31*, 933-937.

The same group has recently shown that not only phosphorous and nitrogen bases can be used as FLP partners but also sulfide species successfully enable a similar monoselective C–F activation in difluoro substrates containing geminal and distal C–F sites.¹¹² The substrate scope includes geminal difluoromethyl groups in aromatic, heteroaromatic, oxide, sulfide and alkyl substituents. Importantly, subsequent functionalization through S_N2 substitutions, photo-redox alkylations, and Suzuki couplings allowed the access to a broad range of organofluoride compounds, which illustrates the synthetic usefulness of this FLP-based methodology.

1.2.4. FLPs as ligands in transition metal chemistry

The recent discovery that FLPs are able to act as ambiphilic ligands for transition metals has opened new avenues in organometallic chemistry. According to Bourissou,¹¹³ Fontaine,¹¹⁴ and Owen,¹¹⁵ these types of ligands contain a donor moiety in combination with an acceptor site that directly interacts with the transition metals or with one of their surrounding ligands. Depending on the way the LA moiety interacts with the transition metal fragment, four different modes of coordination have been identified (Figure 1.6):

- i. Mode 1: the donor site interacts with the transition metal, but the acceptor functionality remains pendant.
- ii. Mode 2: both the donor and the acceptor sites interact directly with the transition metal.
- iii. Mode 3: the donor site is directly attached to the transition metal and the acceptor site abstracts a co-ligand from the transition metal.
- iv. Mode 4: the donor site interacts with the transition metal and the acceptor moiety interacts with one of its surrounding ligands that remains coordinated to the metal.

¹¹² R. Gupta, D. Mandal, A. K. Jaiswal, R. D. Young, *Org. Lett.*, **2021**, *23*, 1915-1920.

¹¹³ G. Bouhadir, A. Amgoune, D. Bourissou, *Adv. Organomet. Chem.*, **2010**, *58*, 1-107.

¹¹⁴ F.-G. Fontaine, J. Boudreau, M.-H. Thibault, *Eur. J. Inorg. Chem.*, **2008**, *35*, 5439-5454.

¹¹⁵ G. R. Owen, *Chem. Soc. Rev.*, **2012**, *41*, 3535-3546.

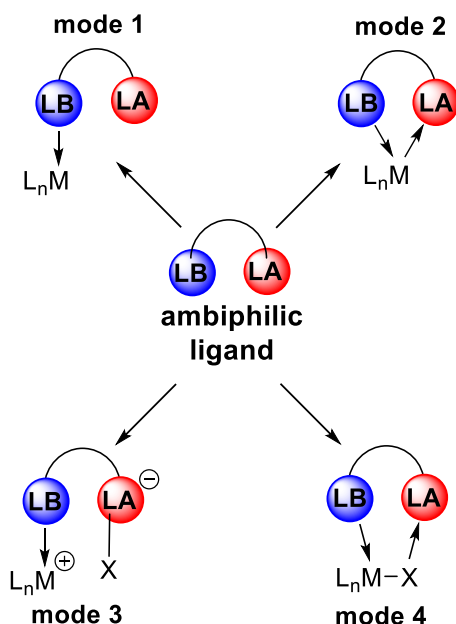
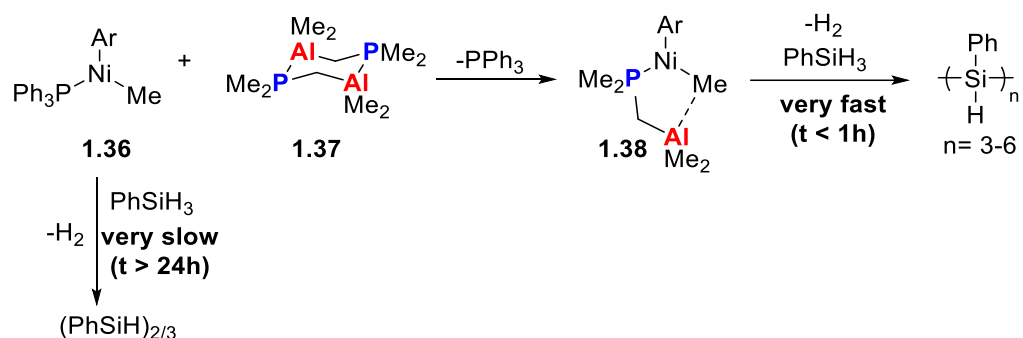


Figure 1.6. Coordination modes of ambiphilic ligands to transition metal complexes.

Several reports have pointed out the strong impact of these ambiphilic ligands on the reactivity of transition metal complexes. In most cases, the interaction of the LA directly with the transition metal is responsible for a unique and enhanced reactivity. For instance, Fontaine and Zargarian reported the first evidence of a positive influence of an ambiphilic ligand on the catalytic activity of transition metal complexes.¹¹⁶ In this study, it is confirmed that intermediate **1.38**, generated by combining the nickel complex **1.36** and the bifunctional reagent **1.37**, is able to convert PhSiH_3 to cyclic oligomers $(\text{PhSiH})_n$ with a turnover frequency 50 times faster than complex **1.36** alone. According to the authors, this remarkably positive effect is due to the coordination of the PMe_2 donor to the Ni center allowing the tethered AlMe_2 acceptor to interact with the Ni–Me moiety. The coordination mode in intermediate **1.38** results in a significant acceleration of both the Si–H bond activation and Si–Si bond-forming reactions (Scheme 1.21).

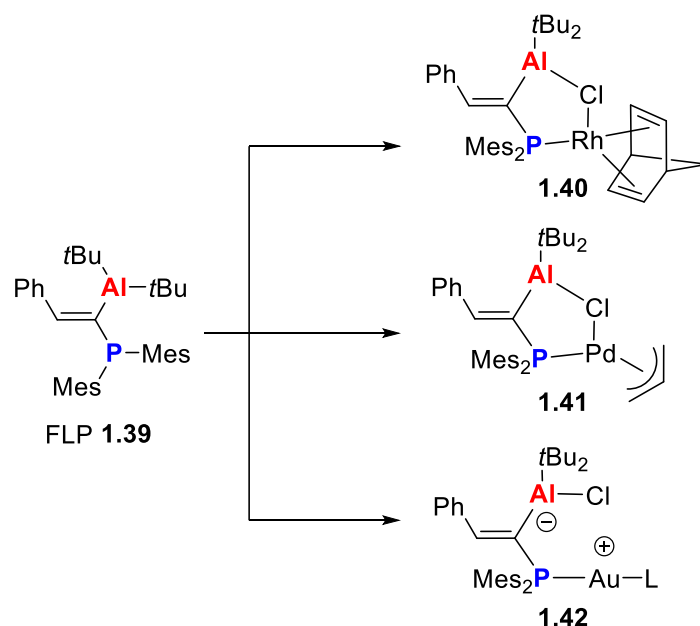
¹¹⁶ F.-G. Fontaine, D. Zargarian, *J. Am. Chem. Soc.*, **2004**, *126*, 8786-8794.



Scheme 1.21. Ambiphilic ligand **1.37** enhances the Ni(II)-catalyzed oligomerization of PhSiH₃.

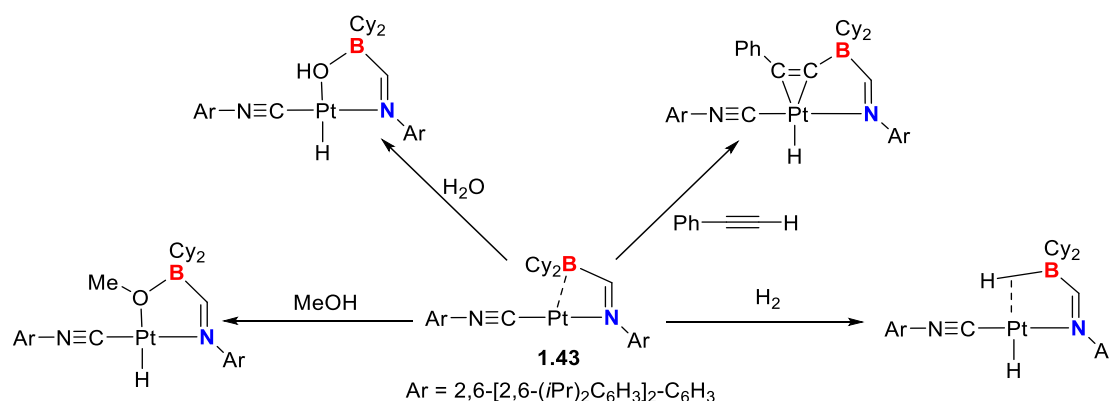
In 2014, Slootweg, Uhl, and Bourissou reported the coordination, as ambiphilic ligand, of the geminal FLP **1.39** to form the transition metal complexes **1.40**, **1.41**, and **1.42**.¹¹⁷ The coordination mode in **1.42** slightly differs from that in complexes **1.40** and **1.41** due to an internal chloride abstraction by the LA from the Au(I)-precursor (Scheme 1.22). Furthermore, the authors suggested that the ambiphilic ligands may offer an alternative to the extended use of silver salts for the activation of Au(I)-Cl precatalysts. For instance, complex **1.42**, bearing FLP **1.39** as ligand, was employed to efficiently catalyze (2 mol%) the cycloisomerization of different propargylamides at room temperature. Note that such transformation is typically mediated by the active catalyst [Ph₃P-Au]⁺ prepared after chloride abstraction from Ph₃P-Au-Cl with the silver salt AgNTf₂.

¹¹⁷ M. Devillard, E. Nicolas, C. Appelt, J. Backs, S. Mallet-Ladeira, G. Bouhadir, J. C. Slootweg, W. Uhl, D. Bourissou, *Chem. Commun.*, **2014**, 50, 14805-14808.



Scheme 1.22. Transition metal complexes bearing an Al/P-based FLP as ambiphilic ligand.

Also in 2014, Figueroa and co-workers reported the platinum complex **1.43**, containing a N/B FLP ligand, which exhibits a significant Pt–B interaction.¹¹⁸ Complex **1.43** is able to exploit this interaction to undergo a rich reactivity towards small molecule activations at room temperature (Scheme 1.23). Interestingly, the free N/B ligand (FNBL) present in complex **41.3** reacts as a FLP activating H₂ or H₂O.¹¹⁸ However, the activation of H₂ by FNBL is conceptually different from that promoted by complex **1.43**. In the former reaction, after an initial H₂ activation step, the reduction of the imine group is then achieved. At variance, a 1,2-addition of H₂ across the Pt–B interaction is observed in the latter case.



Scheme 1.23. Small molecule activation reactions mediated by complex **1.43**.

¹¹⁸ B. R. Barnett, C. E. Moore, A. L. Rheingold, J. S. Figueroa, *J. Am. Chem. Soc.*, **2014**, *136*, 10262-10265.

The rich and synthetically useful chemistry of gold(I)-complexes has also benefited from FLPs as ambiphilic ligands.¹¹⁹ For instance, Bourissou and co-workers described new gold(I)-complexes containing FLPs ligands exhibiting a significant interaction between the transition metal and the LA moiety (Au...B distance of 2.90 Å and 2.66 Å, for **1.44** and **1.45**, respectively) (see, Figure 1.7A).¹²⁰ Similarly, Erker and co-workers reported the Au(I) complexes **1.46**, **1.47**, **1.48** and **1.49**, all of them featuring a P/B-based FLP as ambiphilic ligand and showing a significant Au(I)...B interaction (Figure 1.7B).¹²¹

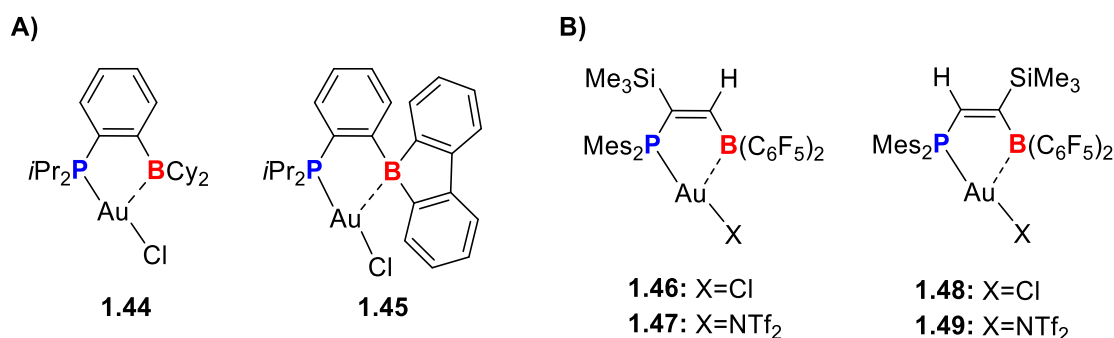


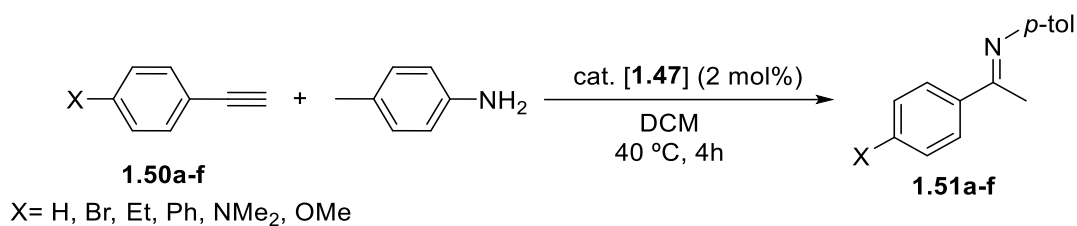
Figure 1.7. Au(I) complexes featuring a FLP as ambiphilic ligands reported by A) Bourissou and co-workers and B) Erker and co-workers.

Such metal-acid interaction has a remarkable influence on the reactivity of these complexes. For instance, complex **1.47** was confirmed to enhance the alkyne hydroamination reactivity as compared to analogous Au(I) complexes lacking the FLP ligand. Thus, catalytic hydroamination of alkynes **1.50a-f** with *p*-toluidine proceeds smoothly at 40 °C affording imines **1.51a-f** in yields around ca. 90% (Scheme 1.24). Although the LA moiety in these complexes is suggested to enhance the electrophilicity of the Au(I)-center,¹²¹ very little is known about the actual role of the ambiphilic FLP ligand in both the electronic properties and reactivity of these complexes.

¹¹⁹ For selected reviews, see: (a) A. Fürstner, P. W. Davies, *Angew. Chem. Int. Ed.*, **2007**, *46*, 3410-3449; (b) A. S. K. Hashmi, *Chem. Rev.*, **2007**, *107*, 3180-3211; (c) A. Arcadi, *Chem. Rev.*, **2008**, *108*, 3266-3325. (d) R. Dorel, A. M. Echavarren, *Chem. Rev.*, **2015**, *115*, 9028-9072.

¹²⁰ S. Bontemps, G. Bouhadir, K. Miqueu, D. Bourissou, *J. Am. Chem. Soc.*, **2006**, *128*, 12056-12057.

¹²¹ A. Ueno, K. Watanabe, C. G. Daniliuc, G. Kehr, G. Erker, *Chem. Commun.*, **2019**, *55*, 4367-4370.



Scheme 1.24. Au(I)-catalyzed hydroamination of terminal alkynes.

1.3. Mechanisms of small molecule activations mediated by FLPs

The rich and genuine reactivity of FLPs has motivated a great number of studies focused on understanding the cooperative mode of action of the FLP antagonists. In this regard, Pápai and co-workers reported the first mechanistic study on the heterolytic splitting of H₂ by FLPs in 2008.¹²² Specifically, the reaction between *t*Bu₃P/BCF and H₂ was explored by means of Density Functional Theory (DFT) and *ab initio* calculations. The formation of a pre-associated LA-LB species, known as “encounter complex”, constitutes the initial step of the process. This intermediate, also called “frustrated complex”, is a weakly bonded species where the LA and LB interact by means of weak non-covalent interactions, mainly C–H···F hydrogen bonds, and dispersion forces. As a consequence, H₂ molecules are able to easily reach the P···B axis and interact with both Lewis functionalities leading to the weakening and successive cleavage of the strong H–H bond. Indeed, a nearly linear transition state (TS) geometry (P···H···H···B) associated with a concerted heterolytic H₂ cleavage was located on the potential energy surface. In such TS, the H–H bond was only slightly elongated suggesting an early TS (Figure 1.8A). According to the computed electron densities and populations, it was found that H₂ becomes polarized in the TS and that a notable amount of electron density is shifted in the *t*Bu₃P → BCF direction (Figure 1.8B). Note that the donor and the acceptor sites of the FLP act synergistically and simultaneously to transfer electron density in a push-pull mode from the phosphine to the antibonding (σ*) molecular orbital of H₂ and to accept electron density in the empty p atomic orbital of the boron from the bonding (σ) molecular orbital of H₂. In this case, such electron

¹²² T. A. Rokob, A. Hamza, A. Stirling, T. Sóos and I. Pápai, *Angew. Chem. Int. Ed.*, **2008**, *47*, 2435-2438.

density transfers can be expressed as $LP(P) \rightarrow \sigma^*(H_2)$ and $\sigma(H_2) \rightarrow p(B)$. The term *electron transfer (ET) model* (schematically shown in Figure 1.9) was coined by the authors to represent this cooperative mode of action between the FLP congeners. This model was also successfully applied to rationalize the reactivity of related FLP systems¹²³ and other activation reactions.¹²⁴

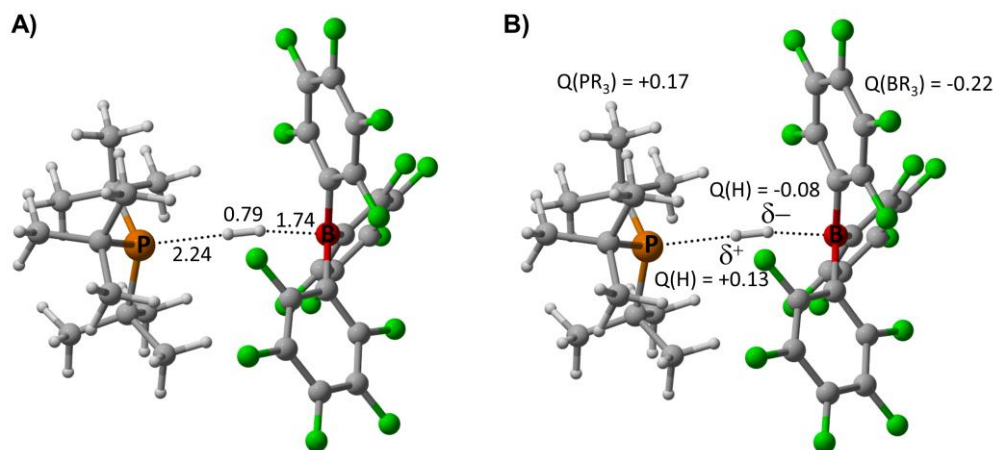


Figure 1.8. A) Optimized geometry (B3LYP/6-31G(d) level) of the transition state associated with the H_2 activation reaction mediated by tBu_3P/BCF reported by Pápai and co-workers (bond distances are given in angstroms). B) Computed charges in the TS where an appreciable polarization of the H_2 molecule is observed.

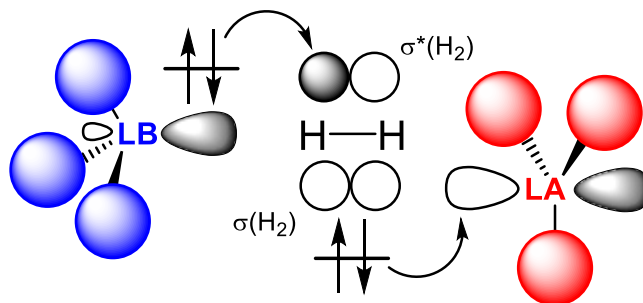


Figure 1.9. Schematic depiction of the ET reactivity model for the H_2 activation reaction mediated by FLPs proposed by Pápai.

One year after, the ET model was reinforced by a new theoretical study on the heterolytic dihydrogen cleavage mediated by the above-commented tBu_3P/BCF FLP.¹²⁵ From the reported results, the authors concluded that the HOMO and the

¹²³ (a) D. Holschumacher, T. Bannenberg, C. G. Hrib, P. G. Jones, M. Tamm, *Angew. Chem. Int. Ed.*, **2008**, *47*, 7428-7432; (b) Y. Guo, S. Li, *Inorg. Chem.*, **2008**, *47*, 6212-6219.

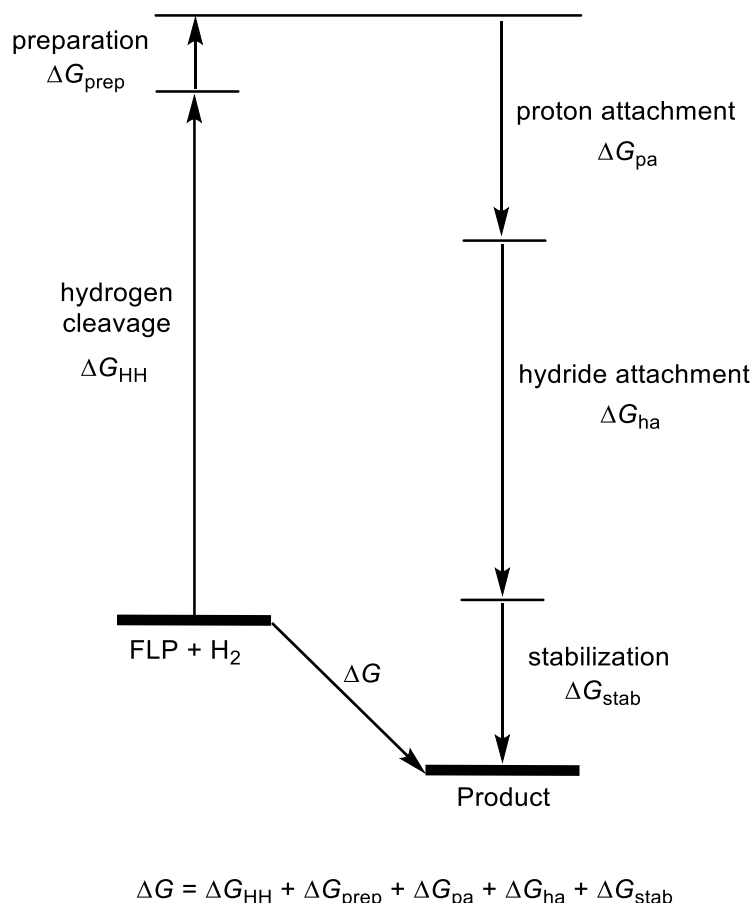
¹²⁴ (a) A. Stirling, A. Hamza, T. A. Rokob, I. Pápai, *Chem. Commun.*, **2008**, 3148-3150; (b) Y. Guo, S. Li, *Eur. J. Inorg. Chem.*, **2008**, 2501-2505; (c) T. A. Rokob, A. Hamza, A. Stirling, I. Pápai, *J. Am. Chem. Soc.*, **2009**, *131*, 2029-2036.

¹²⁵ A. Hamza, A. Stirling, T. A. Rokob and I. Pápai, *Int. J. Quantum Chem.*, **2009**, *109*, 2416-2425.

LUMO of the initial [(*t*Bu)₃P]...[BCF] frustrated complex are located on the sp^3 hybrid lone pair of the phosphorous atom and the empty p boron atomic orbital of the borane, respectively. In addition, these orbitals are practically identical to the respective HOMO/LUMO in the isolated phosphine/borane (the orbital energy changes are -0.009 a.u. and +0.007 a.u., respectively). However, the classical acid-base adduct is not formed due to an inefficient overlap of these orbitals caused by the bulky substituents directly attached to the Lewis centers. According to the authors, the formation of the above-mentioned frustrated complex not only brings the Lewis sites in close proximity but also implies a remarkable preorganization of the HOMO and the LUMO of the Lewis pair to form a “reactive pocket” which is key to the observed reactivity.

Almost simultaneously, the same group reported a different approach to study the H₂ activation mediated by FLPs based on reaction free energy calculations.¹²⁶ In this work, a novel energy partitioning scheme that involves quantitative measures of the acidity and basicity of the reacting Lewis sites was introduced. In this partitioning scheme, the reaction free energy is decomposed into five hypothetical yet chemically meaningful terms (Scheme 1.25). The first term, ΔG_{HH} , is associated with the heterolytic splitting of dihydrogen, which has a free energy of +128.8 kcal/mol in toluene. Note that ΔG_{HH} only depends on the H–H bond strength and therefore is identical for all the FLP systems. The second term, ΔG_{prep} , quantifies the energy required to dissociate the classical acid-base adduct in those cases where the LA–LB dative bond is formed, *i.e.* when there is no frustration. If such dative bond is precluded, this term is zero. The next two terms, ΔG_{pa} and ΔG_{ha} , are the reaction free energies associated with the proton and hydride attachments to the donor and acceptors functionalities of the FLP, respectively. Therefore, these terms are related to the relative Lewis acidity/basicity strengths. The last term, ΔG_{stab} , quantifies the binding free energy of the resulting ion pair once the dihydrogen molecule has been split forming the corresponding zwitterionic species.

¹²⁶ T. A. Rokob, A. Hamza, I. Pápai, *J. Am. Chem. Soc.*, **2009**, *131*, 10701-10710.



Scheme 1.25. Free energy partitioning scheme proposed by the Pápai group.

Within this partitioning scheme, the reactivity of FLPs towards H₂ can be rationalized in terms of thermodynamic energies. To achieve the H₂ splitting, the high energetic cost of the heterolytic H–H bond cleavage should be compensated by the acidity, basicity, and product stabilization. All these factors can be tuned by modifying the electronic properties of the substituents and/or the nature of the acid-basic atoms in the FLP systems. Finally, it was observed that nonlinked (*i.e.* intermolecular) FLPs suffer a more pronounced entropy penalty in comparison with linked (*i.e.* intramolecular) systems, which makes them less prone to activate dihydrogen. Consequently, higher acid/base strength and ion pair stabilization must compensate for this entropy drawback.

In 2010, Grimme, Erker, and co-workers reinvestigated the reactivity of *t*Bu₃P/B(C₆F₅)₃ towards H₂ and proposed a conceptually different mechanism.¹²⁷ This new reactivity model was based on the polarization of H₂ induced by the

¹²⁷ S. Grimme, H. Kruse, L. Goerigk, G. Erker, *Angew. Chem. Int. Ed.*, **2010**, *49*, 1402-1405.

electric field that is generated inside the cavity formed by the FLP (see Figure 1.10). This *electric field (EF) model* is based on the well-known influence of external electric fields on redox processes and other chemical transformations.¹²⁸

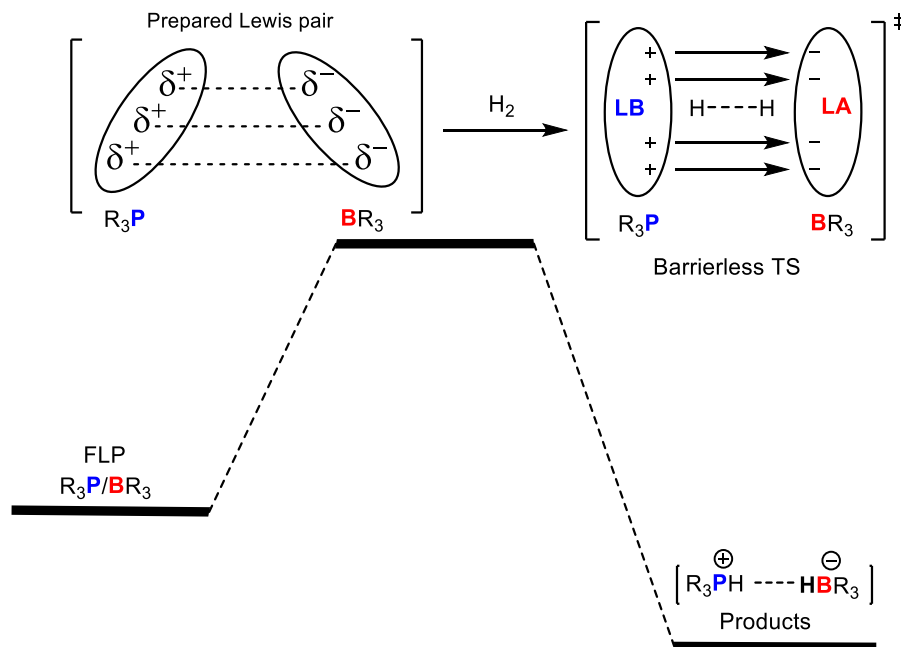


Figure 1.10. Schematic representation of the electric field model proposed by Grimme.

According to this model, it is proposed that once the H₂ molecule has entered in the FLP cavity, the H–H dissociation occurs in an essentially barrierless process. Therefore, the initial entrance of H₂ into the FLP cavity is the key step of the reaction, *i.e.* responsible for the activation barrier. Two important aspects of this model should be highlighted. Firstly, the secondary (non-covalent) interactions between the bulky substituents play a crucial role not only to form the “encounter complex” but also to make the FLP flexible enough to facilitate the entrance of the incoming dihydrogen molecule. The occurrence of such pre-associated complex, also proposed by Pápai (see above), was confirmed experimentally by employing NMR techniques in a milestone study by Rocchigiani and co-workers.¹²⁹ Consequently,

¹²⁸ (a) I. Rozas, I. Alkorta, J. Elguero, *Chem. Phys. Lett.*, **1997**, *275*, 423-428; (b) G. Pacchioni, J. R. Lomas, F. Illas, *J. Mol. Catal. A: Chem.*, **1997**, *119*, 263-273; (c) A. Warshel, *J. Biol. Chem.*, **1998**, *273*, 27035-27038; (d) S. Shaik, S. P. de Visser, D. Kumar, *J. Am. Chem. Soc.*, **2004**, *126*, 11746-11749; (e) R. Meir, H. Chen, W. Lai, S. Shaik, *ChemPhysChem*, **2010**, *11*, 301-310; (f) M. R. Hennefarth, A. N. Alexandrova, *J. Phys. Chem. A*, **2021**, *125*, 1289-1298.

¹²⁹ L. Rocchigiani, G. Ciancaleoni, C. Zuccaccia, A. Macchioni, *J. Am. Chem. Soc.*, **2014**, *136*, 112-115.

computational studies must describe properly the dispersion interactions to correctly characterize the interior of these chemical systems. Secondly, there is no need to involve specific FLP/H₂ orbitals to understand the activation mechanism. Indeed, it is proposed that FLP as molecular systems can be entirely neglected and replaced by a homogenous electric field.

In 2012, Camaioni and co-workers carried out a computational study on the H₂ dissociation promoted by simple Lewis pairs (NH₃ + BX₃, X= H, F, Cl).¹³⁰ Even though the authors pointed out that these systems form classical acid-base adducts, the detailed analysis of the electronic structure and the interaction energies allowed them to explore the potential energy surface from a theoretical point of view. Aiming at assessing the relevance of the ET model reported by Pápai and the EF model proposed by Grimme, the electric field created by the acid/base pairs as well as the relative contributions of electrostatic, dispersion, and charge transfer components to the interaction energy in the respective TS were analyzed. It was concluded that the electric field induced by the Lewis pairs plays a role in polarizing the H₂ molecule, albeit its contribution to the overall interaction energy is small compared to that coming from the orbital overlaps at the TS. Consequently, the electric field by itself seems not sufficient to cleave the strong H–H bond. In addition, it was found that structural reorganization of the precursor complex is key in the activation process and charge-transfer interactions are the dominant stabilizing factor in the TS region.

Even though both the ET and the EF models suggest that the facile heterolytic activation reaction of H₂ takes place via reactive intermediates with preorganized acid/base functionalities, they strongly differ in the mode of action of the active centers. In 2013, several compelling arguments to support the ET model were reported by the Pápai group.¹³¹ Firstly, the ET model strongly resembles the H₂ activation processes mediated by other systems described previously, such as

¹³⁰ D. M. Camaioni, B. Ginovska-Pangovska, G. K. Schenter, S. M. Kathmann, T. Autrey, *J. Phys. Chem. A*, **2012**, *116*, 7228-7237.

¹³¹ T. A. Rokob, I. Bakó, A. Stirling, A. Hamza, I. Pápai, *J. Am. Chem. Soc.*, **2013**, *135*, 4425-4437.

transition metal complexes,¹³² carbenes¹³³ related low-valent species,¹³⁴ and multiply bonded heavier main group species.¹³⁵ Secondly, through a computational analysis of the H₂ activation reaction employing six different FLPs, it was found that although their reactivity was quite similar, they exhibited rather different electric fields.

Similar conclusions have been reported by our research group when exploring the H₂ activation reaction mediated by geminal aminoborane R₂N-CH₂-BR'₂ FLPs.¹³⁶ A detailed analysis of the physical factors controlling these transformations was carried out employing the activation strain model (ASM) of reactivity in combination with the energy decomposition analysis-Natural Orbital for Chemical Valence method (EDA-NOCV). These methods will be described in detail in sections 1.4 and 1.5 of this introduction. The results from this study pointed to a highly orbital-controlled mechanism (see, Figure 1.11) in agreement with the ET model by Pápai. However, the key LP(base) → σ*(H₂) and σ(H₂) → p(B) interactions do not occur simultaneously as proposed by Pápai but at different stages of the reaction coordinate, with the electron density flow σ(H₂) → p(B) being the most emphasized at the beginning of the process and responsible for the early destabilization and polarization of the σ(H₂)-bond (Figure 1.11). In addition, the EDA-NOCV methodology suggested that although the orbital interactions between the reactants become the main factor controlling the reactivity of FLPs, the contribution of the electrostatic attractions in the process is far from being negligible.

¹³² G. J. Kubas, *Chem. Rev.*, **2007**, *107*, 4152-4205.

¹³³ G. D. Frey, V. Lavallo, B. Donnadiou, W. W. Schoeller, G. Bertrand, *Science*, **2007**, *316*, 439-441.

¹³⁴ (a) Y. Peng, B. D. Ellis, X. Wang, P. P. Power, *J. Am. Chem. Soc.*, **2008**, *130*, 12268-12269; (b) Y. Peng, J.-D. Guo, B. D. Ellis, Z. Zhu, J. C. Fettinger, S. Nagase, P. P. Power, *J. Am. Chem. Soc.*, **2009**, *131*, 16272-16282; (c) A. V. Protchenko, K. H. Birjukumar, D. Dange, A. D. Schwarz, D. Vidovic, C. Jones, N. Kaltsoyannis, P. Mountford, S. Aldridge, *J. Am. Chem. Soc.*, **2012**, *134*, 6500-6503.

¹³⁵ (a) G. H. Spikes, J. C. Fettinger, P. P. Power, *J. Am. Chem. Soc.*, **2005**, *127*, 12232-12233; (b) Y. Peng, M. Brynda, B. D. Ellis, J. C. Fettinger, E. Rivard, P. P. Power, *Chem. Commun.*, **2008**, 6042-6044; (c) L. Zhao, F. Huang, G. Lu, Z.-X. Wang, P. v. R. Schleyer, *J. Am. Chem. Soc.*, **2012**, *134*, 8856-8868.

¹³⁶ D. Yepes, P. Jaque, I. Fernández, *Chem. Eur. J.*, **2016**, *22*, 18801-18809.

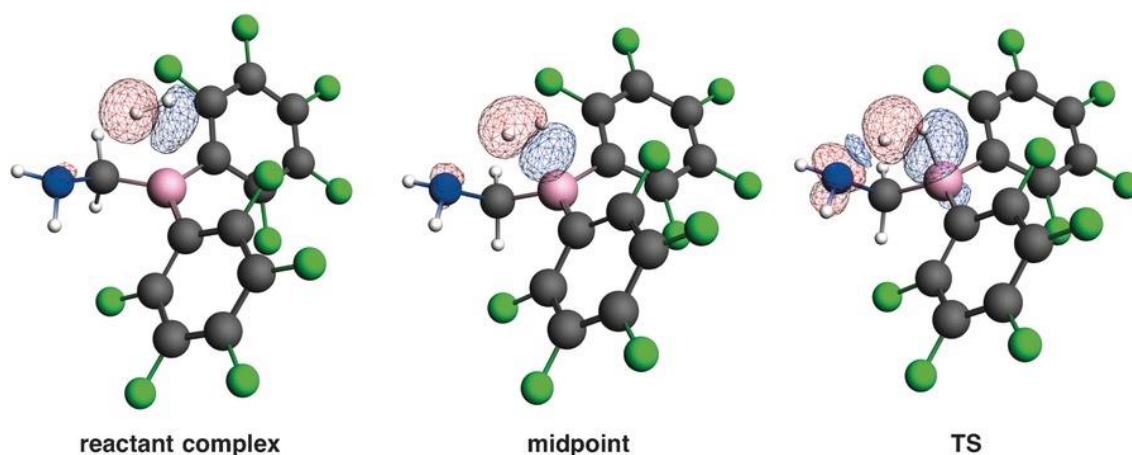


Figure 1.11. Contour plots of NOCV deformation densities for the main orbital interaction between H_2 and geminal aminoborane-based FLPs. Electron density flows from red to blue.

According to these studies, the ET model seems to be more appropriate to rationalize the reactivity of FLPs. However, the EF model suggested by Grimme (or at least, the part related to the electrostatic contribution) cannot be completely neglected. Therefore, as suggested by several authors,^{38r,137} a clear differentiation between pure ET and EF mechanisms for active FLPs is not possible and is more reasonable to consider that both processes occur simultaneously during the H_2 activation reaction.

Both the ET and EF mechanisms involve the occurrence of closed-shell intermediates. However, the involvement of radical species is also possible in the chemistry of FLPs. Piers and co-workers envisioned that the archetypal $t\text{Bu}_3\text{P}/\text{BCF}$ FLP may homolytically cleave dihydrogen after initial oxidation of the phosphine by BCF leading to a Frustrated Radical ion Pair (FRP) (Figure 1.12).¹³⁸ However, such a proposition was initially ruled out due to two reasons: (i) the high ionization energy of the phosphine; indeed, as pointed out by Piers, the disparity in the reduction potential of BCF (1.17 V vs $\text{Cp}_2\text{Fe}^{0/+}$ in THF)¹³⁹ and the oxidation potential of $t\text{Bu}_3\text{P}$ (0.90V vs $\text{Cp}_2\text{Fe}^{0/+}$ in acetonitrile)¹⁴⁰ indicates that any possible formation of the FRP is expected to be limited to sub-nanomolar concentrations;

¹³⁷ (a) G. Kara, F. De Vleeschouwer, P. Geerlings, F. De Proft, B. Pinter, *Sci. Rep.*, **2017**, *7*, 16024-16038.

¹³⁸ W. E. Piers, A. J. V. Marwitz, L. G. Mercier, *Inorg. Chem.*, **2011**, *50*, 12252-12262.

¹³⁹ S. A. Cummings, M. Imura, C. J. Harlan, R. J. Kwaan, I. V. Trieu, J. R. Norton, B. M. Bridgewater, F. Jäkle, A. Sundararaman, M. Tilset, *Organometallics*, **2006**, *25*, 1565-1568.

¹⁴⁰ E. R. M. Habraken, N. P. van Leest, P. Hooijschuur, B. de Bruin, A. W. Ehlers, M. Lutz, J. C. Slootweg, *Angew. Chem. Int. Ed.*, **2018**, *57*, 11929-11933.

(ii) BCF acting as a one-electron oxidant had only been reported in reactions involving transition metal complexes¹⁴¹ but not with metal-free organic molecules.

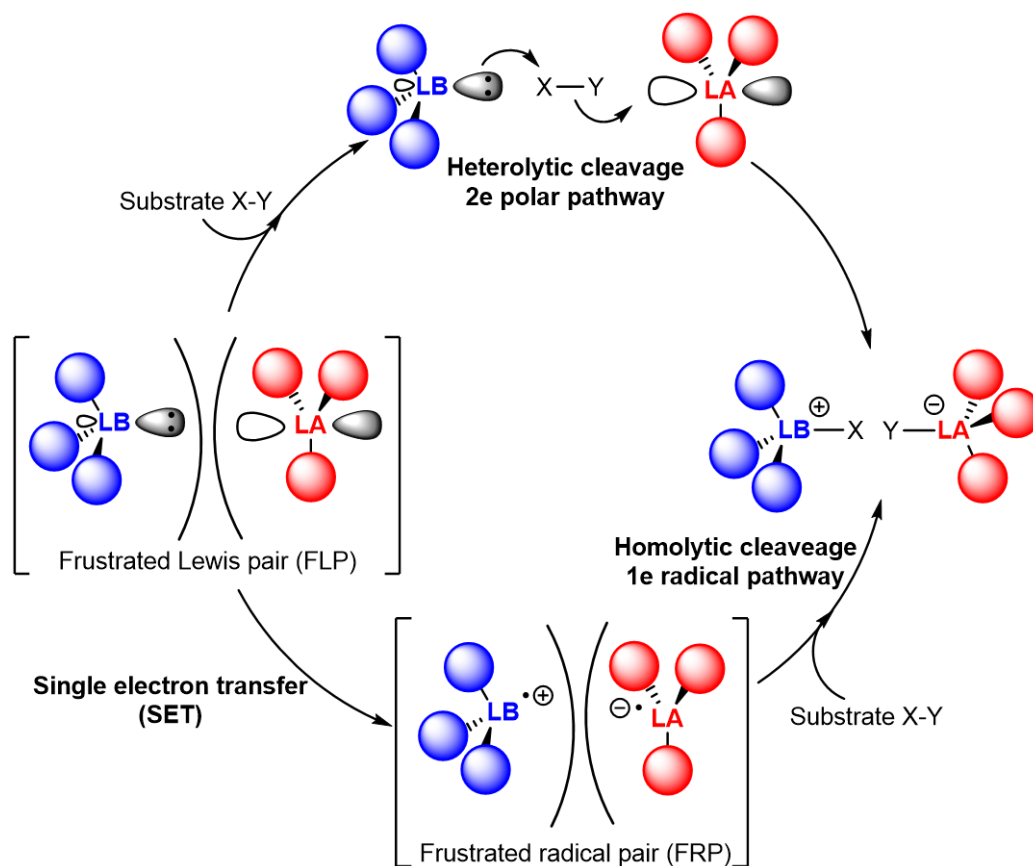


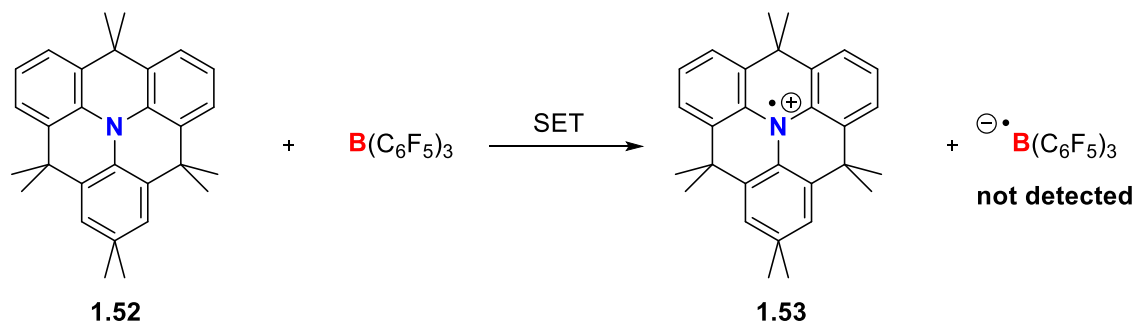
Figure 1.12. Proposed reaction pathways for the small molecule (X–Y) activation mediated by FLPs. Top: representation of the 2e polar pathway leading to the heterolytic cleavage of the substrate. Bottom: depiction of 1e radical pathway featuring a single electron transfer which generates the transient frustrated radical pair and subsequent homolytic splitting of X–Y.

Despite that, in 2013, Wang and co-workers demonstrated the first example of one-electron oxidation of an organic molecule by BCF.¹⁴² In this work, the equimolar combination of the triarylamine **1.52** and BCF led to the planar radical cation **1.53** (Scheme 1.26). A single electron transfer (SET) mechanism was supported by electron paramagnetic resonance (EPR), which confirmed the formation of the radical cation **1.53** but not of the radical anion $[B(C_6F_5)_3]^{•-}$. According to the authors, the absence of an EPR signal corresponding to the latter

¹⁴¹ For selected examples, see: (a) C. J. Harlan, T. Hascall, E. Fujita, J. R. Norton, *J. Am. Chem. Soc.*, **1999**, *121*, 7274-7275; (b) C. J. Beddows, A. D. Burrows, N. Connelly, M. Green, J. M. Lynam, T. J. Paget, *Organometallics*, **2001**, *20*, 231-233.

¹⁴² X. Zheng, X. Wang, Y. Qiu, Y. Li, C. Zhou, Y. Sui, Y. Li, J. Ma, X. Wang, *J. Am. Chem. Soc.*, **2013**, *135*, 14912-14915.

species may be attributed to the known rapid degradation at room temperature of such species.¹⁴³ These data prompted questions about the viability of SET reactions within the FLP field.

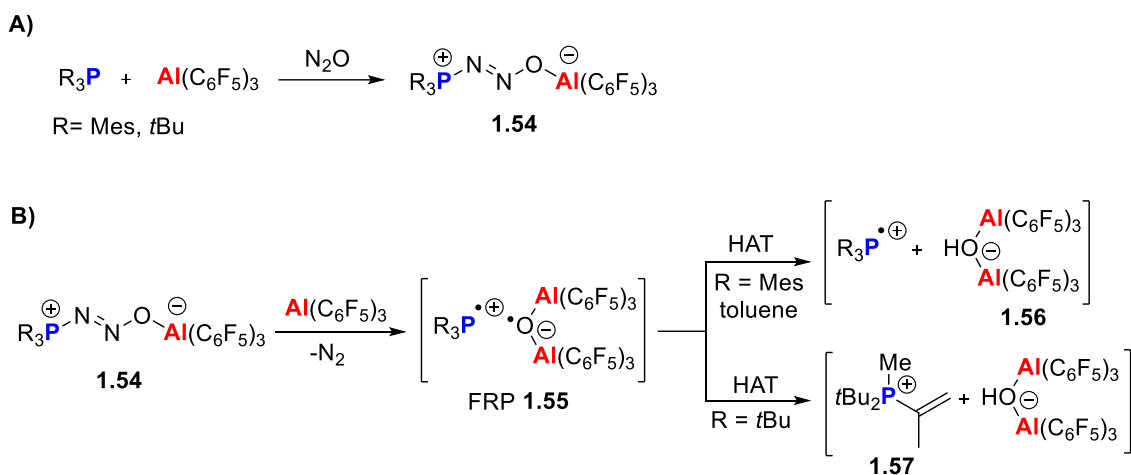


Scheme 1.26. Single electron transfer between the triarylamine **1.52** and BCF.

Indeed, in the same year, Stephan and co-workers reported the reaction between the FLP $\text{R}_3\text{P}/\text{Al}(\text{C}_6\text{F}_5)_3$ ($\text{R} = \text{Mes}$ or $t\text{Bu}$) with nitrous oxide (N_2O).¹⁴⁴ A conventional FLP-type activation was achieved affording the zwitterionic product **1.54** (Scheme 1.27A). Strikingly, this product further reacts with a second equivalent of the alane, releasing N_2 and leading to the formation of the highly reactive FRP **1.55**, which is able to undergo alkyl and aryl C–H bond activations from both the solvent (toluene) or the phosphine (Scheme 1.27B). When Mes_3P was used as a LB, product **1.56** was formed via hydrogen atom abstraction (HAT) from the solvent, and evidence for the formation of the radical cation $[\text{Mes}_3\text{P}]^{\bullet+}$ was provided by EPR, UV-vis spectroscopy and X-ray diffraction. Similarly, species **1.57**, resulting from a HAT from the $t\text{Bu}_3\text{P}$ phosphine to the Al_2 -oxyl radical, could be characterized by X-ray crystallography.

¹⁴³ For studies on the stability of such radical species, see: (a) R. J. Kwaan, C. J. Harlan, J. R. Norton, *Organometallics*, **2001**, *20*, 3818-3820; (b) E. J. Lawrence, V. S. Oganessian, G. G. Wildgoose, A. E. Ashley, *Dalton Trans.*, **2013**, *42*, 782-789; (c) J. Chen, E. Y.-X. Chen, *Dalton Trans.*, **2016**, *45*, 6105-6110.

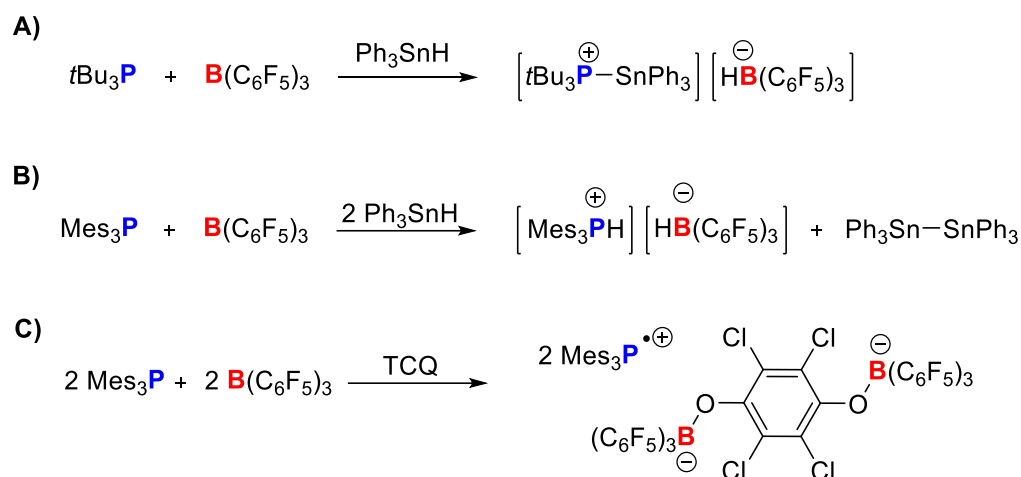
¹⁴⁴ G. Ménard, J. A. Hatnean, H. J. Cowley, A. J. Lough, J. M. Rawson, D. W. Stephan, *J. Am. Chem. Soc.*, **2013**, *135*, 6446-6449.



Scheme 1.27. A) Reactivity of $\text{R}_3\text{P}/\text{Al}$ -based FLP (R = Mes or *t*Bu) with 1 equivalent of N_2O . B) Reaction between product **1.54** with a second equivalent of $\text{Al}(\text{C}_6\text{F}_5)_3$ generating FRP **1.55** via liberation of N_2 and subsequent hydrogen atom transfer (HAT).

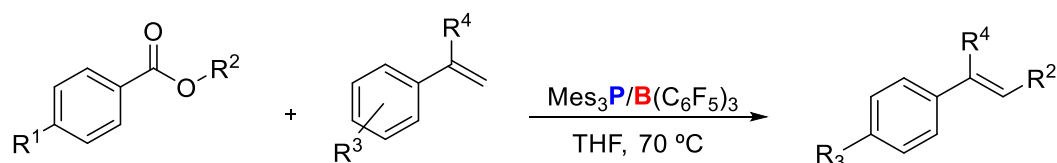
In 2017, the Stephan group also reported the observation of radical intermediates in the archetypal FLPs $\text{Mes}_3\text{P}/\text{E}(\text{C}_6\text{F}_5)_3$ (E = B or Al).¹⁴⁵ Although the $\text{Mes}_3\text{P}/\text{B}(\text{C}_6\text{F}_5)_3$ system displayed a weak EPR signal, the $\text{Mes}_3\text{P}/\text{Al}(\text{C}_6\text{F}_5)_3$ system considerably increased the EPR signal making possible the unambiguous characterization of the phosphine radical cation $[\text{PMes}_3]^{\bullet+}$, thus supporting a SET process. Once again, the corresponding EPR signals for the radical anions $[\text{B}(\text{C}_6\text{F}_5)_3]^{\bullet-}$ or $[\text{Al}(\text{C}_6\text{F}_5)_3]^{\bullet-}$ could not be detected due to the rapid degradation of these species. Moreover, whereas the reaction of $\text{tBu}_3\text{P}/\text{B}(\text{C}_6\text{F}_5)_3$ with Ph_3SnH led to the formation of $[\text{tBu}_3\text{P}-\text{SnPh}_3][\text{HB}(\text{C}_6\text{F}_5)_3]$, which is the expected product for a heterolytic cleavage of the Sn–H bond (Scheme 1.28A), the analogous process involving the $\text{Mes}_3\text{P}/\text{B}(\text{C}_6\text{F}_5)_3$ system resulted in the generation of $[\text{Mes}_3\text{PH}][\text{HB}(\text{C}_6\text{F}_5)_3]$ and $\text{Ph}_3\text{Sn}-\text{SnPh}_3$, which are products consistent with a radical abstraction of H^{\bullet} from the tin reactant (Scheme 1.28B). The observed divergent reactivity between the FLP based on tBu_3P and Mes_3P was proposed to derive from a change in the reaction pathway (heterolytic vs homolytic). Similar results were found in the reaction between the FLPs $\text{R}_3\text{P}/\text{E}(\text{C}_6\text{F}_5)_3$ (R = *t*Bu, Mes; E = B or Al) and tetrachloro-1,4-benzoquinone (TCQ).¹⁴⁵ Thus, as shown in Scheme 1.28C, in the process involving Mes_3P , the radical cationic intermediate $[\text{Mes}_3\text{P}]^{\bullet+}$ was identified, supporting once again that the reaction proceeds via a SET process. In contrast, no traces of radicals were detected when using tBu_3 as the basic partner.

¹⁴⁵ L. Liu, L. L. Cao, Y. Shao, G. Menard, D. W. Stephan, *Chem*, **2017**, *3*, 259-267.



Scheme 1.28. A) Reaction between $t\text{Bu}_3\text{P}/\text{BCF}$ and Ph_3SnH leading to the expected product after a heterolytic cleavage. B) Reaction between $\text{Mes}_3\text{P}/\text{BCF}$ and Ph_3SnH generates different products, which have been proposed to be the result of a homolytic reaction pathway. C) Reactivity of $\text{Mes}_3\text{P}/\text{BCF}$ with TCQ allows the detection of radical species supporting a SET process.

Melen and co-workers recently described the C–C cross-coupling reaction between diaryl esters and styrene mediated by the $\text{Mes}_3\text{P}/\text{B}(\text{C}_6\text{F}_5)_3$ FLP (Scheme 1.29).¹⁴⁶ Similar to the previously commented work from the Stephan group, the cationic radical $[\text{PMes}_3]^{\bullet\oplus}$ was observed by EPR spectroscopy and a mechanism based on a SET pathway was proposed.

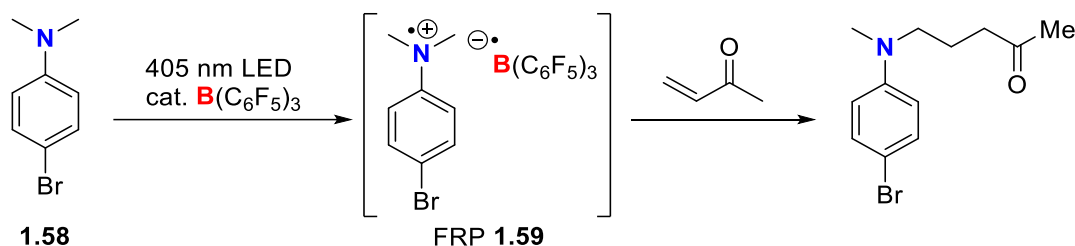


Scheme 1.29. Reaction of the $\text{Mes}_3\text{P}/\text{B}(\text{C}_6\text{F}_5)_3$ FLP with diarylesters leading to the formation of highly functionalized styrenes.

Also, Ooi and co-workers have reported the C–C coupling reaction between methylvinylketone and N,N -dialkylaniline Lewis base **1.58** using catalytic amounts of BCF (scheme 1.30).¹⁴⁷ In this case, the irradiation led to the formation of the transient FRP **1.59** via a photo-induced SET mechanism.

¹⁴⁶ Y. Soltani, A. Dasgupta, T. A. Gazis, D. M. C. Ould, E. Richards, B. Slater, K. Stefkova, V. Y. Vladimirov, L. C. Wilkins, D. Wilcox, R. L. Melen, *Cell Rep. Phys. Chem.*, **2020**, *1*, 10016-10024.

¹⁴⁷ Y. Aramaki, N. Imaizumi, M. Hotta, J. Kumagai, T. Ooi, *Chem. Sci.*, **2020**, *11*, 4305-4311.



Scheme 1.30. C–C coupling between amine **1.58** and methylvinylketone via photo-induced SET to generate FRP **1.59**.

The above-commented reports from Stephan, Melen and Ooi arise several questions that should be addressed in order to rationally design more reactive FRPs from the corresponding LA/LB combinations. For example, why are the reaction pathways of strongly related systems ($t\text{Bu}_3\text{P}/\text{BCF}$ vs $\text{Mes}_3\text{P}/\text{BCF}$) so different? Why are radical anions for BCF and ACF not detected by EPR spectroscopy? Is it due to their short lifetime or because they are not really involved in a SET process? Is light always required to promote SET from a FLP or is it only necessary in specific reactions such as those reported by Ooi and co-workers?

Recent investigations by Slootweg and co-workers shed some light on these questions. In an initial study, they explored the ionization energies and electron affinities of the LB and LA for the $t\text{Bu}_3\text{P}/\text{BCF}$ and $\text{Mes}_3\text{P}/\text{BCF}$ FLPs.¹⁴⁸ It was found that the computed energy gap to generate the respective FRP is too large to be reached in a thermal process. Instead, they proposed a light-induced SET affording the respective FRPs. Indeed, when a frozen toluene solution (at 30 K) of $\text{Mes}_3\text{P}/\text{BCF}$ prepared in the dark was irradiated with visible light (390-500 nm), both radical species $[\text{Mes}_3\text{P}]^{\bullet+}$ and $[\text{B}(\text{C}_6\text{F}_5)_3]^{\bullet-}$ were detected by EPR spectroscopy. Furthermore, by means of transient absorption spectroscopy, a lifetime of 237 ps at room temperature was estimated for the photogenerated FRP. Strikingly, EPR signals for $[t\text{Bu}_3\text{P}]^{\bullet+}$ and $[\text{B}(\text{C}_6\text{F}_5)_3]^{\bullet-}$ were also detected using the same methodology. Despite that, after irradiation, these EPR signals decay much faster than those involved in the $\text{Mes}_3\text{P}/\text{BCF}$ FLP. In addition, a much shorter lifetime of 6 ps was estimated for the corresponding FRP. This fact could be responsible for the lack of radical reactivity reported for this system.

¹⁴⁸ F. Holtrop, A. R. Jupp, N. P. van Leest, M. P. Domínguez, R. M. Williams, A. M. Brouwer, B. de Bruin, A. W. Ehlers, J. C. Slootweg, *Chem. Eur. J.*, **2020**, *26*, 9005-9011.

The finding that FRP formation from these FLPs proceeds via a visible-light-induced SET prompted a subsequent study where the previously reported reactions of FLPs with different substrates were investigated with and without irradiation.¹⁴⁹ For instance, the reaction between the Mes₃P/BCF FLP with H₂ was considered. The authors reasoned that if the FRP formation is a relevant factor in the dihydrogen activation reaction, then a noticeable change in the reaction rate should be observed by performing the reaction in the dark or with visible light. However, nearly identical conversion rates after 2.5 and 4 hours were found. This result allowed the authors to conclude that the FRP concentration is too low and/or its lifetime is too short to significantly affect the reaction rate. Therefore, the dihydrogen activation reaction mediated by Mes₃P/BCF does not seem to proceed via a significant contribution of a radical pathway, and instead, the two-electron (*i.e.* heterolytic splitting) mechanism seems preferred.

The reaction between R₃P/BCF (R = Mes or *t*Bu₃) and Ph₃SnH (see above, Scheme 1.28A and 1.28B) was also explored. It was found that this transformation is again not light-dependent and FRPs are not responsible for the observed reactivity. This is in contrast with the explanation given by Stephan involving a change in the reaction mechanism (from homolytic to heterolytic) to rationalize the formation of the different reaction products ([Mes₃PH][HB(C₆F₅)₃] and Ph₃SnSnPh₃ vs [*t*Bu₃PSnPh₃][HB(C₆F₅)₃], see above). However, Slootweg and co-workers realized that once [*t*Bu₃PSnPh₃][HB(C₆F₅)₃] is formed, the reaction continues to finally afford [*t*Bu₃PH][HB(C₆F₅)₃] and Ph₃SnSnPh₃. Consequently, the authors proposed that for both phosphines (*t*Bu₃P and Mes₃P), a polar, heterolytic cleavage of the Sn–H bond derived from the nucleophilic attack of the phosphine to the tin center is still valid. Consistent with this, Caputo and co-workers have recently demonstrated that the dehydrocoupling of Ph₃SnH to Ph₃SnSnPh₃ mediated by an aminoborane intramolecular FLP proceeds in a heterolytic fashion and that the possible radical pathways were notably higher in energy.¹⁵⁰

Finally, the reaction between the FLP Mes₃P/BCF and tetrachloro-1,4-benzoquinone (TCQ) (see above, Scheme 1.28C) was also investigated. In this case, the reaction in the dark proceeds rapidly and an EPR signal ambiguously assigned

¹⁴⁹ F. Holtrop, A. R. Jupp, B. J. Kooij, N. P. van Leest, B. de Bruin, J. C. Slootweg, *Angew. Chem. Int. Ed.*, **2020**, *59*, 22210-22216.

¹⁵⁰ J. N. Bentley, E. Pradhan, T. Zeng, C. B. Caputo, *Dalton Trans.*, **2020**, *49*, 16054-16058.

to $[\text{Mes}_3\text{P}]^{\bullet+}$ was detected. This finding immediately arises the question of how radicals can be formed in the dark where a photo-induced process is not possible. The authors reasoned that a strong electron acceptor is required to oxidize the Mes_3P , but neither BCF nor TCQ are appropriated for such a task. However, it was found that BCF can coordinate to one of the carbonyl groups of TCQ affording the $\text{TCQ} \cdot \text{BCF}$ Lewis adduct, which has an increased electron affinity and therefore should be capable of oxidizing the phosphine yielding the radical species $[\text{Mes}_3\text{P}]^{\bullet+}$ and $[\text{TCQ} \cdot \text{BCF}]^{\bullet-}$. Indeed, a second molecule of BCF coordinates the other carbonyl group present in TCQ, thus promoting the oxidation of a second equivalent of the phosphine. Note that interactions between Lewis acid and carbonyl groups are known to promote SET processes.¹⁵¹ Furthermore, the authors proposed that in the systems previously reported by Melen and Ooi (see above, Schemes 1.29 and 1.30), which also feature carbonyl groups, the observed SET processes could be facilitated by the same type of carbonyl-BCF interactions.

In summary, recent reports have shown that SET processes generating radical ion pairs could play an important role within the FLP chemistry. Although the $\text{R}_3\text{P}/\text{BCF}$ FLP systems can form high-energy radical ion pairs via photo-induced SET, recent studies have proven that this mechanism is not predominant in the reaction with H_2 or Ph_3SnH . A two-electron, polar, heterolytic mechanism takes place in these reactions instead. Finally, it has been proposed that the reaction of $\text{R}_3\text{P}/\text{BCF}$ systems with substrates bearing carbonyl groups is not the result of a SET from the phosphines to the Lewis acid. Instead, BCF binds the carbonyl oxygen atom of the substrate which results in a significant increase of its electron affinity. It is exciting to think that perhaps in the future radical processes in the FLP chemistry will facilitate the activations of very stable substrates such as N_2 or CH_4 , that remain elusive so far.

¹⁵¹ (a) J. Du, K. L. Skubi, D. M. Schultz, T. P. Yoon, *Science*, **2014**, *344*, 392-396; (b) T. P. Yoon, *Acc. Chem. Res.*, **2016**, *49*, 2307-2315; (c) K. N. Lee, M.-Y. Ngai, *Chem. Commun.*, **2017**, *53*, 13093-13112; (d) E. Speckmeier, P. J. W. Fuchs, K. Zeitler, *Chem. Sci.*, **2018**, *9*, 7096-7103.

1.4. Activation Strain model (ASM) of reactivity

Modern chemistry requires not only new synthetic procedures but also theoretical models which allow us to rationalize the molecular reactivity. Understanding the physical factors which govern the course of chemical reactions is of utmost importance not only to explain the experimental observations but also to predict novel and/or more efficient processes. In this regard, the last century has witnessed a remarkable flowering in the field of theoretical and computational chemistry. For instance, the frontier molecular orbital (FMO) theory,^{152,153} Marcus theory,¹⁵⁴ the curve-crossing model in valence bond (VB) theory^{155,156} and the Woodward-Hoffmann rules^{157, 158} should be especially highlighted. Despite the popularity of these approaches, several deficiencies have been identified and, for this reason, these models have failed to rationalize the experimental findings on different occasions.¹⁵⁹ For instance, in the FMO theory the interactions of the

¹⁵² (a) K. Fukui, T. Yonezawa, H. Shingu, *J. Chem. Phys.*, **1952**, *20*, 722-725; (b) K. Fukui, T. Yonezawa, C. Nagata, H. Shingu, *J. Chem. Phys.*, **1954**, *22*, 1433-1442; (c) I. Fleming, *Frontier Orbitals and Organic Chemical Reactions*, Wiley, New York, 1978; (d) T. A. Albright, J. K. Burdett, M. H. Whangbo, *Orbital Interactions in Chemistry*, 2nd Ed., Wiley, Hoboken, NJ, 2013.

¹⁵³ K. Fukui, *Angew. Chem. Int. Ed. Engl.*, **1982**, *21*, 801-809.

¹⁵⁴ (a) R. A. Marcus, *J. Chem. Phys.*, **1956**, *24*, 966-978; (b) R. A. Marcus, *J. Chem. Phys.*, **1956**, *24*, 979-989.

¹⁵⁵ (a) A. Pross, S. S. Shaik, *Acc. Chem. Res.*, **1983**, *16*, 363-370; (b) A. Sevin, P. C. Hiberty, J.-M. Lefour, *J. Am. Chem. Soc.*, **1987**, *109*, 1845-1852; (c) S. S. Shaik, P. C. Hiberty, *A Chemist's Guide to Valence Bond Theory*, Wiley-Interscience, Hoboken, NJ, 2008.

¹⁵⁶ For some applications, see (a) S. Shaik, A. Shurki, *Angew. Chem. Int. Ed.*, **1999**, *38*, 586-625; (b) W. Lai, C. Li, H. Chen, S. Shaik, *Angew. Chem. Int. Ed.* **2012**, *51*, 5556-5578; (c) B. Braida, C. Walter, B. Engels, P. Hiberty, *J. Am. Chem. Soc.*, **2010**, *132*, 7631-7637; (d) D. Usharani, D. Janardanan, C. Li, S. Shaik, *Acc. Chem. Res.*, **2013**, *46*, 471-482; (e) D. Usharani, D. C. Lacy, A. S. Borovik, S. Shaik, *J. Am. Chem. Soc.*, **2013**, *135*, 17090-17104; (f) J. Li, S. Zhou, J. Zhang, M. Schlangen, T. Weiske, D. Usharani, S. Shaik, H. Schwarz, *J. Am. Chem. Soc.*, **2016**, *138*, 7973-7981; (g) J. Li, S. Zhou, J. Zhang, M. Schlangen, D. Usharani, S. Shaik, H. Schwarz, *J. Am. Chem. Soc.*, **2016**, *138*, 11368-11377.

¹⁵⁷ R. Hoffmann, *Angew. Chem. Int. Ed. Engl.*, **1982**, *21*, 711-724.

¹⁵⁸ (a) R. B. Woodward, R. Hoffmann, *J. Am. Chem. Soc.*, **1965**, *87*, 395-397; (b) R. B. Woodward, R. Hoffmann, *J. Am. Chem. Soc.*, **1965**, *87*, 4388-4389; (c) H. C. Longuet-Higgins, E. W. Abrahamson, *J. Am. Chem. Soc.*, **1965**, *87*, 2045-2046; (d) R. B. Woodward, R. Hoffmann, *Angew. Chem. Int. Ed. Engl.*, **1969**, *8*, 781-853.

¹⁵⁹ (a) S. D. Kahn, C. F. Pau, L. E. Overman, W. J. Hehre, *J. Am. Chem. Soc.*, **1986**, *108*, 7381-7396; (b) C. Spino, H. Rezael, Y. L. Dory, *J. Org. Chem.*, **2004**, *69*, 757-764; (c) B. R. Ussing, C. Hang, D. A. Singleton, *J. Am. Chem. Soc.*, **2006**, *128*, 7594-7607; (d) A. Talbot, D. Devarajan, S. J. Gustafson, I. Fernández, F. M. Bickelhaupt, D. H. Ess, *J. Org. Chem.*, **2015**,

HOMO and LUMO of reactants are emphasized and the strongest interactions are suggested to occur between orbitals that are closest in energy and which have the largest overlap. These FMO interactions, which are computed at the equilibrium geometries of the involved reactants, are suggested to be responsible for the observed reactivity and selectivity (mainly, in pericyclic reactions). This is a rather crude assumption as the interactions occurring in the transition state region, not necessarily identical to those in the initial reactants, are responsible for the activation barriers.

Bickelhaupt and Houk have independently developed a different approach to understand reactivity known as “the activation strain model” of reactivity,¹⁶⁰ also called “the distortion-interaction model”.¹⁶¹ This model has enormously contributed to our current understanding of fundamental transformations in chemistry, such as

80, 548-558; (e) Y. García-Rodeja, M. Solà, F. M. Bickelhaupt, I. Fernández, *Chem. Eur. J.*, **2016**, *22*, 1368-1378.

¹⁶⁰ (a) F. M. Bickelhaupt, *J. Comput. Chem.*, **1999**, *20*, 114-128; (b) I. Fernández, F. M. Bickelhaupt, *Chem. Soc. Rev.*, **2014**, *43*, 4953-4967; (c) L. P. Wolters, F. M. Bickelhaupt, *WIREs Comput. Mol. Sci.*, **2015**, *5*, 324-343; (d) F. M. Bickelhaupt, K. N. Houk, *Angew. Chem. Int. Ed.*, **2017**, *56*, 10070-10086.

¹⁶¹ (a) D. H. Ess, K. N. Houk, *J. Am. Chem. Soc.*, **2007**, *129*, 10646-10647; (b) D. H. Ess, K. N. Houk, *J. Am. Chem. Soc.*, **2008**, *130*, 10187-10198; (c) K. N. Houk, F. Liu, Y.-F. Yang, X. Hong, *Applied Theoretical Organic Chemistry*, Ed. D. Tantillo, World Scientific, 2017, chapter 13; (d) F. Liu, Y. Liang, K. N. Houk, *Acc. Chem. Res.*, **2017**, *50*, 539-543.

cycloadditions,¹⁶² isomerizations,¹⁶³ nucleophilic substitutions,¹⁶⁴ oxidative additions,¹⁶⁵ among other organic or organometallic reactions.¹⁶⁶

The activation strain model (ASM) of reactivity allows us to rationalize the height of reaction barriers in terms of the original reactants. This is achieved by decomposing the activation energy ΔE^\ddagger into two components: the strain energy $\Delta E^\ddagger_{\text{strain}}$ (also called distortion or preparation energy) and the interaction energy $\Delta E^\ddagger_{\text{int}}$ (Eq. 1.1):

¹⁶² For selected examples, see: (a) F. Schoenebeck, D. H. Ess, G. O. Jones, K. N. Houk, *J. Am. Chem. Soc.*, **2009**, *131*, 8121-8133; (b) R. S. Paton, S. Kim, A. G. Ross, S. J. Danishefsky, K. N. Houk, *Angew. Chem. Int. Ed.*, **2011**, *50*, 10366-10368; (c) I. Fernández, F. M. Bickelhaupt, *J. Comput. Chem.*, **2014**, *35*, 371-376; (d) I. Fernández, M. Solà, F. M. Bickelhaupt, *J. Chem. Theory Comput.*, **2014**, *10*, 3863-3870; (e) F. Liu, Y. Liang, K. N. Houk, *J. Am. Chem. Soc.*, **2014**, *136*, 11483-11493; (f) J. J. Cabrera-Trujillo, I. Fernández, *Org. Biomol. Chem.*, **2019**, *17*, 2985-2991; (g) P. Vermeeren, T. A. Hamlin, I. Fernández, F. M. Bickelhaupt, *Angew. Chem. Int. Ed.*, **2020**, *59*, 6201-6206; (h) P. Vermeeren, T. A. Hamlin, I. Fernández, F. M. Bickelhaupt, *Chem. Sci.*, **2020**, *11*, 8105-8112.

¹⁶³ For selected examples, see: (a) I. Fernández, F. M. Bickelhaupt, F. P. Cossío, *Chem. Eur. J.*, **2012**, *18*, 12395-12403; (b) M. El-Hamdi, M. Solà, G. Frenking, J. Poater, *J. Phys. Chem. A*, **2013**, *117*, 8026-8034; (c) M. Contreras, E. Osorio, F. Ferraro, G. Puga, K. J. Donald, J. G. Harrison, G. Merino, W. Tiznado, *Chem. Eur. J.*, **2013**, *19*, 2305-2310; (d) A. C. Castro, E. Osorio, J. L. Cabellos, E. Cerpa, E. Matito, M. Solà, M. Swart, G. Merino, *Chem. Eur. J.*, **2014**, *20*, 4583-4590.

¹⁶⁴ For selected examples, see: (a) M. A. van Bochove, M. Swart, F. M. Bickelhaupt, *J. Am. Chem. Soc.*, **2006**, *128*, 10738-10744; (b) B. Galabov, V. Nikolova, J. J. Wilke, H. F. Schaefer III, W. D. Allen, *J. Am. Chem. Soc.*, **2008**, *130*, 9887-9896; (c) I. Fernández, M. Solà, F. M. Bickelhaupt, *Chem. Eur. J.*, **2013**, *19*, 7416-7422; (d) L. P. Wolters, Y. Ren, F. M. Bickelhaupt, *ChemistryOpen*, **2014**, *3*, 29-36.

¹⁶⁵ For selected examples, see: (a) A. Diefenbach, F. M. Bickelhaupt, *J. Chem. Phys.*, **2001**, *115*, 4030-4040; (b) A. Diefenbach, F. M. Bickelhaupt, *J. Phys. Chem. A*, **2004**, *108*, 8460-8466; (c) J. N. P. van Stralen, F. M. Bickelhaupt, *Organometallics*, **2006**, *25*, 4260-4268; (d) G. T. de Jong, F. M. Bickelhaupt, *J. Chem. Theory Comput.*, **2007**, *3*, 514-529; (e) W.-J. van Zeist, R. Visser, F. M. Bickelhaupt, *Chem. Eur. J.*, **2009**, *15*, 6112-6115; (f) L. P. Wolters, W.-J. van Zeist, F. M. Bickelhaupt, *Chem. Eur. J.*, **2014**, *20*, 11370-11381; (g) Y. Wang, M. S. G. Ahlquist, *Phys. Chem. Chem. Phys.*, **2014**, *16*, 11182-11185; (h) M. Joost, A. Zeineddine, L. Estevez, S. Mallet-Ladeira, K. Miqueu, A. Amgoune, D. Bourissou, *J. Am. Chem. Soc.*, **2014**, *136*, 14654-14657.

¹⁶⁶ For selected examples, see: (a) I. Fernández, F. M. Bickelhaupt, F. P. Cossío, *Chem. Eur. J.*, **2009**, *15*, 13022-13032; (b) S. M. Bronner, J. L. Mackey, K. N. Houk, N. K. Garg, *J. Am. Chem. Soc.*, **2012**, *134*, 13966-13969; (c) J. M. Medina, J. L. Mackey, N. K. Garg, K. N. Houk, *J. Am. Chem. Soc.*, **2014**, *136*, 15798-15805; (d) I. Fernández, F. M. Bickelhaupt, F. P. Cossío, *Chem. Eur. J.*, **2014**, *20*, 10791-10801; (e) M. Joost, L. Estevez, S. Mallet-Ladeira, K. Miqueu, A. Amgoune, D. Bourissou, *J. Am. Chem. Soc.*, **2014**, *136*, 10373-10382.

$$\Delta E^\ddagger = \Delta E_{\text{strain}}^\ddagger + \Delta E_{\text{int}}^\ddagger \quad (\text{Eq. 1.1})$$

The first term, $\Delta E_{\text{strain}}^\ddagger$, is the energy penalty associated with deforming the reagents from a reference state (usually their equilibrium geometries) to the geometries they adopt in the transition states (TS). In general, $\Delta E_{\text{strain}}^\ddagger$ is positive, *i.e.* destabilizing, and thus a factor that gives rise to the activation barrier. The strain energy depends on the rigidity of the reactants, for example, how strong bonds that must break are, how flexible bond angles to be deformed are, as well as, to what extent groups must reorganize during a chemical transformation. On the other hand, the interaction energy, $\Delta E_{\text{int}}^\ddagger$, quantifies the stabilizing interaction between the respective deformed reagents. Consequently, the stabilizing feature of this term is represented with a negative amount of energy and compensates, at least to some extent, the energy penalty associated with the $\Delta E_{\text{strain}}^\ddagger$ term. It is the interplay between these energy terms that determine if, and at which point of the reaction coordinate, a barrier arises, namely, at the point satisfying $d\Delta E_{\text{strain}}(\zeta)/d\zeta = -d\Delta E_{\text{int}}(\zeta)/d\zeta$. A positive aspect of the ASM is the possibility to split the potential energy surface $\Delta E(\zeta)$ not only in the transition state but also along the entire reaction coordinate ζ . Taking this into account, equation 1.1 can be replaced by a more general equation (Eq. 1.2), where all terms can be calculated for any point along the reaction coordinate:

$$\Delta E(\zeta) = \Delta E_{\text{strain}}(\zeta) + \Delta E_{\text{int}}(\zeta) \quad (\text{Eq. 1.2})$$

In addition, the $\Delta E_{\text{strain}}(\zeta)$ can be further decomposed into the individual contributions from different reactants or different fragments (Eq. 1.3). This aspect is very useful because quite often one reactant/fragment requires more energy to be deformed than the other during a chemical transformation. Moreover, the $\Delta E_{\text{int}}(\zeta)$ can also be decomposed into different physical meaningful terms by means of the energy decomposition analysis (EDA) method. This method is described in detail in section 1.5.

$$\Delta E_{\text{strain}}(\zeta) = \Delta E_{\text{strain}}(\zeta)\text{-f1} + \Delta E_{\text{strain}}(\zeta)\text{-f2} \quad (\text{Eq. 1.3})$$

As an illustrative example, Figure 1.13 shows the activation strain diagram (ASD) for the reaction between a P/B-based FLP (**R1**) and dihydrogen (**R2**). Note that the more stable geometry of the FLP **R1** is the closed form, where a strong

interaction between the LA and the LB occurs. Consequently, both functionalities are quenched, and a certain amount of energy must be first employed to make the Lewis sites available to interact with H_2 . Also, the H–H bond in the TS geometry is elongated in comparison with its equilibrium geometry, which is translated into a considerable amount of (strain) energy due to the high H–H bond strength. On the other hand, the interaction energy (ΔE_{int}) becomes increasingly more negative (*i.e.* more stabilizing) as the reaction progresses. This term quantifies the stabilization that occurs when the respective distorted reactants (**R1** and **R2**) approach each other and therefore compensates the destabilizing ΔE_{strain} term.

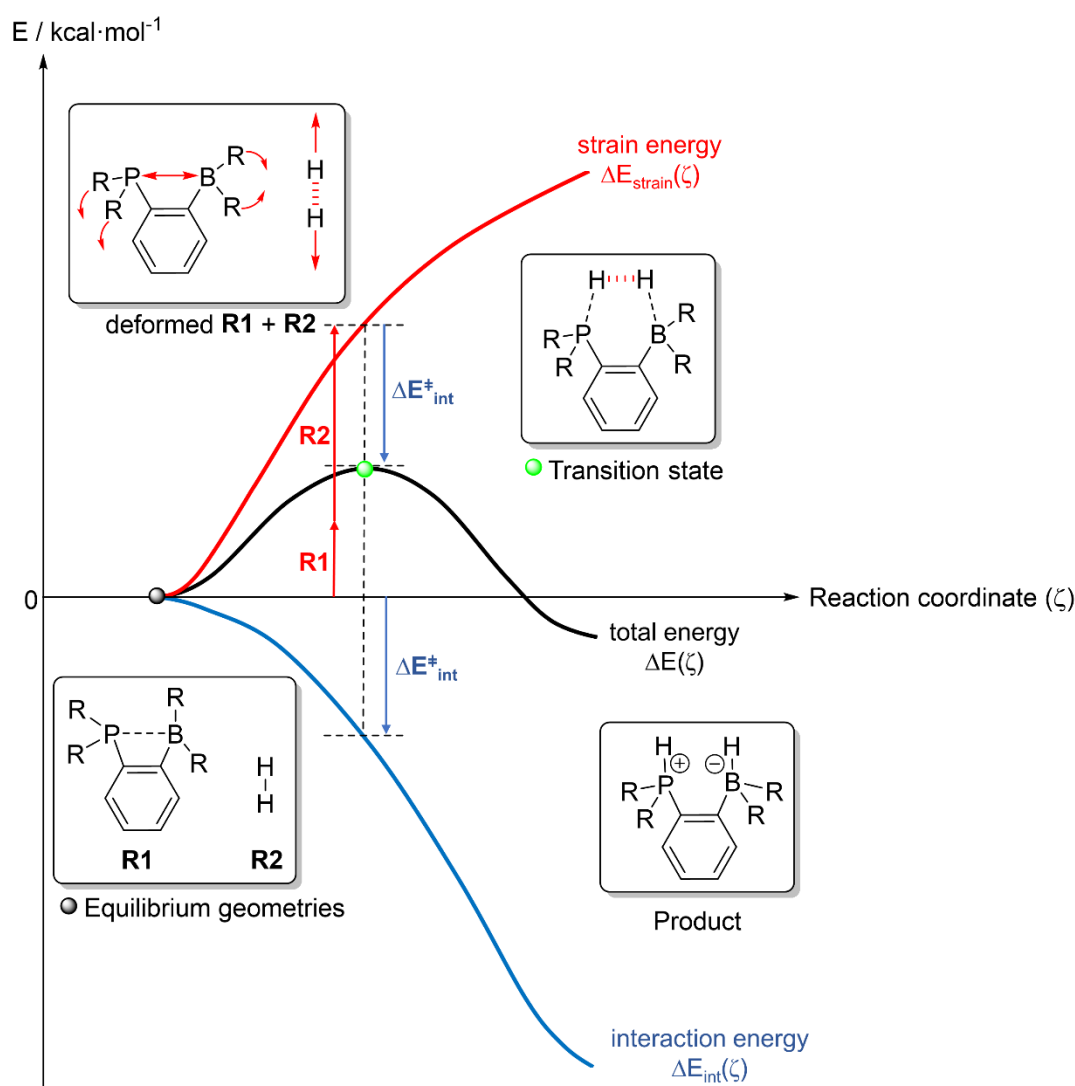


Figure 1.13. Representative activation strain diagram for the H_2 activation reaction mediated by the intramolecular FLP **R1**. Total energy (black line), strain energy (red line), and interaction energy (blue line) are plotted along the entire reaction coordinate (from reactants to the final product). The contribution from the different reactants to the strain energy is shown as red “**R1**” and “**R2**”, respectively.

We want to point out that when comparing two chemical processes using the ASM methodology, the analysis of the strain and interaction energies exclusively in the respective TS geometries may lead to misleading results due to the different position of the TSs on the reaction coordinate. Figure 1.14 graphically illustrates a comparative activation strain diagram (ASD) for two generic reactions “A” and “B” where the respective TSs are represented by a dot. Comparing the strain and interaction energies for both processes at the respective TSs would lead to the erroneous conclusion that the interaction energy is almost identical for both processes and the strain becomes the decisive factor governing the distinct reactivity. However, a simple visual inspection of the evolution of both terms along the reaction coordinates shows that the strain energy is almost identical for both processes and the stronger interaction in reaction B is exclusively the factor responsible for its lower barrier. This example highlights the crucial importance of

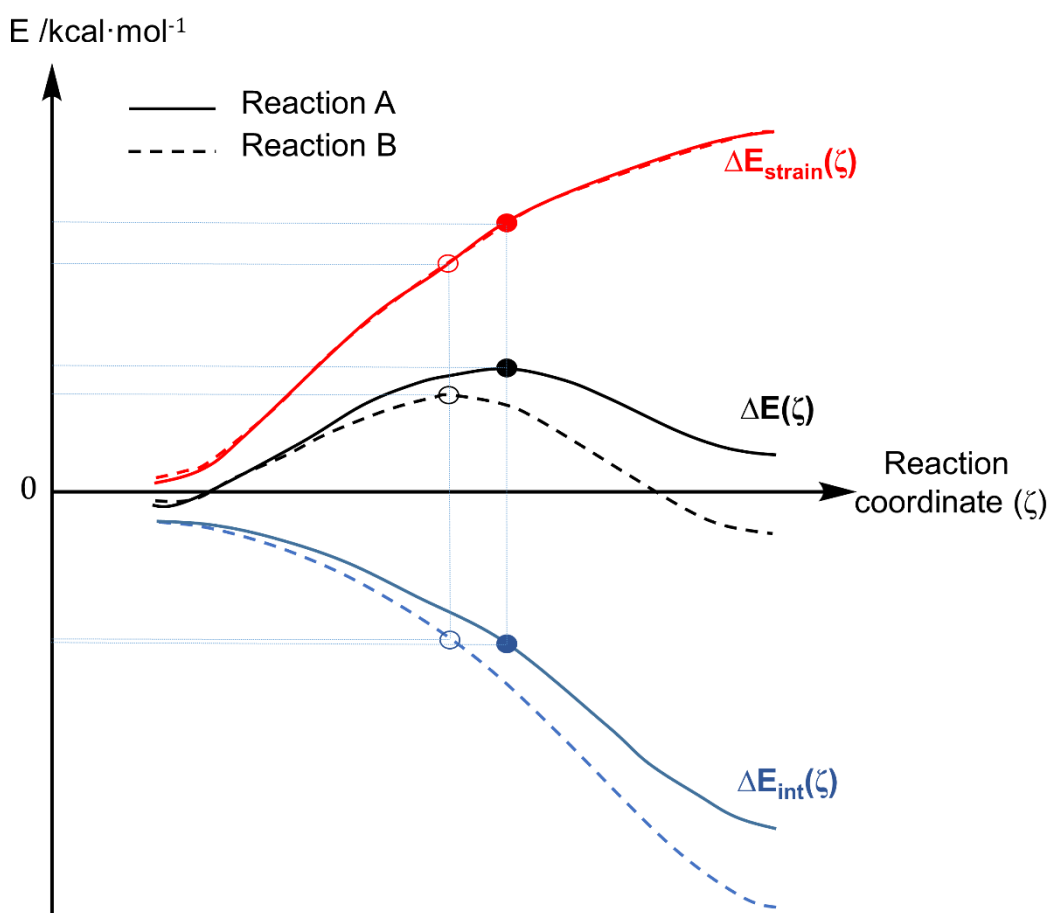


Figure 1.14. Comparison of generic activation strain diagrams having identical strain energy along the entire reaction coordinate. The respective transition states are represented by circles.

considering the evolution of the ASM terms along the entire reaction coordinate and not only at the TS region.

1.5. Energy decomposition analysis (EDA) method

The energy decomposition analysis (EDA), developed by Morokuma¹⁶⁷ and by Ziegler and Rauk,¹⁶⁸ is a powerful method for a quantitative interpretation of the chemical bond. The EDA method decomposes the interaction energy (ΔE_{int}) between two fragments “A” and “B” in a molecule “A-B” into three terms (Eq. 1.4). These terms can be interpreted in a chemically meaningful way, thus providing a bridge between quantum chemical calculations and heuristic bonding models in traditional chemistry.

$$\Delta E_{\text{int}} = \Delta V_{\text{elstat}} + \Delta E_{\text{Pauli}} + \Delta E_{\text{orb}} \quad (\text{Eq. 1.4})$$

The term ΔV_{elstat} corresponds to the quasi-classical electrostatic interaction between the unperturbed charge distributions of the deformed reactants and is usually attractive. The term ΔE_{Pauli} , called “Pauli repulsion”, considers the destabilizing interactions between occupied orbitals. This term considers the repulsive exchange interaction between electrons of both fragments having the same spin and is responsible for any steric interaction. The orbital interaction term, ΔE_{orb} , accounts for the interaction between occupied orbitals on one moiety and unoccupied orbitals on the other (such as HOMO–LUMO interactions), charge-transfer and polarization (empty-occupied orbital mixing on one fragment due to the presence of another fragment).

Dispersion forces, which are crucial in FLP chemistry (see above), arising from the attractive interactions between the induced dipoles of interacting species, have been recently identified as an important factor of chemical bonding.¹⁶⁹ Within the EDA method, there are essentially two ways to consider dispersion forces: (i) using functionals that take into account dispersion forces corrections, as for instance, the

¹⁶⁷ K. Morokuma, *J. Chem. Phys.*, **1971**, *55*, 1236-1244.

¹⁶⁸ T. Ziegler, A. Rauk, *Theor. Chim. Acta*, **1977**, *46*, 1-10.

¹⁶⁹ S. Grimme, *J. Comput. Chem.*, **2004**, *25*, 1463-1473.

Minnesota functionals developed by the Truhlar group,¹⁷⁰ or (ii) considering explicit correction terms for the dispersion interaction such as the Grimme’s dispersion corrections (DFT-D3¹⁷¹ and DFT-D4¹⁷²). In the latter case, a new term (ΔE_{disp}) is summed to equation 1.4 and the total interaction energy is computed as:

$$\Delta E_{\text{int}} = \Delta V_{\text{elstat}} + \Delta E_{\text{Pauli}} + \Delta E_{\text{orb}} + \Delta E_{\text{disp}} \quad (\text{Eq. 1.5})$$

The main orbital contributions to the total ΔE_{orb} term can be visualized and quantified by means of the Natural Orbital for Chemical Valence (NOCV)¹⁷³ extension of the EDA method. Within the EDA-NOCV approach, the orbital interaction (ΔE_{orb}) term is expressed as pairwise contributions of orbitals of the two interacting fragments. The deformation density $\Delta \rho^{\text{orb}}(\mathbf{r})$ represents the density change of the fragment before and after bond formation and can be expressed as a sum of pairs of complementary orbitals ($\Psi_{\mathbf{k}}, \Psi_{-\mathbf{k}}$) corresponding to the eigenvalues ($\mathbf{v}_{\mathbf{k}}, \mathbf{v}_{-\mathbf{k}}$) that are equal in absolute value but opposite in signs (Eq. 1.6).

$$\Delta \rho^{\text{orb}}(\mathbf{r}) = \sum_{\mathbf{k}=1}^{N/2} v_{\mathbf{k}} [-\Psi_{-\mathbf{k}}^2(\mathbf{r}) + \Psi_{\mathbf{k}}^2(\mathbf{r})] = \sum_{\mathbf{k}} \Delta \rho_{\mathbf{k}}(\mathbf{r}) \quad (\text{Eq. 1.6})$$

A particularly helpful feature of the EDA-NOCV method lies in the possibility to graphically depict the total deformation density $\Delta \rho^{\text{orb}}(\mathbf{r})$ in terms of the individual deformation densities $\Delta \rho_{\mathbf{k}}(\mathbf{r})$, which provides a qualitative picture of the different components of the chemical bond (σ , π , δ , etc.). In addition, it is also possible to obtain a quantitative expression for ΔE_{orb} in terms of pairwise orbital interaction energies ($\Delta E_{\text{orb}}^{\mathbf{k}}$) that are associated with the respective $\Delta \rho_{\mathbf{k}}(\mathbf{r})$ (Eq. 1.7),

$$\Delta E_{\text{orb}} = \sum_{\mathbf{k}=1}^{N/2} v_{\mathbf{k}} [-F_{-\mathbf{k},-\mathbf{k}}^{TS} + F_{\mathbf{k},\mathbf{k}}^{TS}] = \sum_{\mathbf{k}} \Delta E_{\text{orb}}^{\mathbf{k}} \quad (\text{Eq. 1.7})$$

¹⁷⁰ For some examples, see: (a) Y. Zhao, D. G. Truhlar, *J. Chem. Phys.*, **2006**, *125*, 194101; (b) Y. Zhao, D. G. Truhlar, *J. Phys. Chem. A* **2006**, *110*, 13126-13130; (c) Y. Zhao, D. G. Truhlar, *Theor. Chem. Acc.*, **2008**, *120*, 215-241; (d) Y. Zhao, D. G. Truhlar, *Acc. Chem. Res.*, **2008**, *41*, 157-167.

¹⁷¹ S. Grimme, J. Antony, S. Ehrlich, H. Krieg, *J. Chem. Phys.*, **2010**, *132*, 154104.

¹⁷² (a) E. Caldeweyher, S. Ehlert, A. Hansen, H. Neugebauer, S. Spicher, C. Bannwarth, S. Grimme, *J. Chem. Phys.*, **2019**, *150*, 154122; (b) E. Caldeweyher, J.-M. Mewes, S. Ehlert, S. Grimme, *Phys. Chem. Chem. Phys.*, **2020**, *22*, 8499-8512.

¹⁷³ M. P. Mitoraj, A. Michalak, T. Ziegler, *J. Chem. Theory Comput.*, **2009**, *5*, 962-975.

where the terms $-F_{-k,-k}^{TS}$ and $F_{k,k}^{TS}$ are the diagonal matrix elements corresponding to NOCVs with eigenvalues $-v_k$ and v_k , respectively.

For further details on the EDA-NOCV method and its application to the analysis of the chemical bond, some recent reviews are recommended.¹⁷⁴

¹⁷⁴ (a) L. Zhao, M. von Hopffgarten, D. M. Andrada, G. Frenking, *WIREs Comput. Mol. Sci.*, **2018**, 8, e1345; (b) G. Frenking, F. M. Bickelhaupt, in *The Chemical Bond. Fundamental Aspects of Chemical Bonding*, G. Frenking and S. Shaik (Eds.), Wiley-VCH, Weinheim, 2014, 121-158; (c) I. Fernández, *Applied Theoretical Organic Chemistry*, D. Tantillo (Ed.), World Scientific, 2017, chapter 7; (d) L. Zhao, M. Hermann, W. H. E. Schwarz, G. Frenking, *Nat. Rev. Chem.*, **2019**, 3, 48-63.

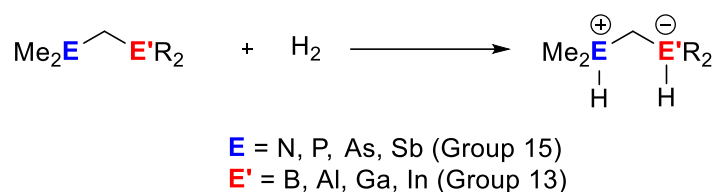
II. OBJECTIVES

*“The scientist is not a person who gives the right answers,
he’s one who asks the right questions.”*

Claude Levi-Strauss

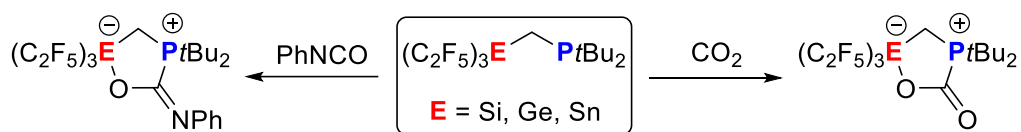
The primary aim of this Ph.D. thesis is to understand the physical factors that govern the reactivity of FLPs by means of state-of-the-art computational methods. To this end, we have used the activation strain model (ASM) of reactivity combined with canonical Energy Decomposition Analysis-Natural Orbital for Chemical Valence (EDA-NOCV) methods to quantitatively unravel those factors responsible for the reactivity of selected FLPs (see below). The results derived from the studies presented herein may contribute not only to rationalize the reactivity of these species but also to the rational design of new and more active FLP systems.

Despite the majority of FLPs are constituted by a combination of Group 13 and Group 15 elements, the influence of the nature of the acid/base pairs on the reactivity of FLPs is essentially unknown. For this reason, in chapter 1 we shall rationalize the reactivity of different LA/LB combinations (LA = B, Al, Ga, In; LB = N, P, As, Sb) in geminal FLPs. To this end, we have selected the archetypal dihydrogen activation reaction (Scheme 2.1). In addition, the influence of the nature of the substituents directly attached to the acid E' atom will be also explored. Besides understanding the factors controlling the dihydrogen activation of these geminal FLPs, the main aim of this chapter is to identify the best combination of the Group 13/Group 15 elements leading to the most active system.



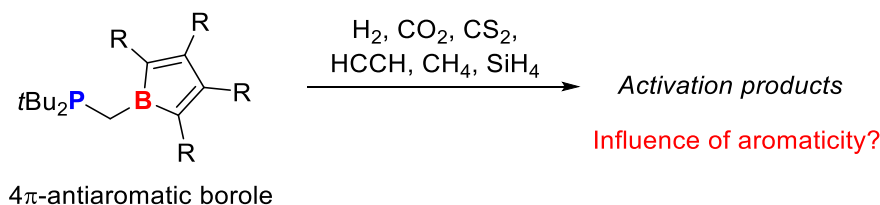
Scheme 2.1. Dihydrogen activation reaction mediated by geminal FLPs considered in chapter 1.

Directly related to the contents of chapter 1, in chapter 2 we will expand the study to geminal FLPs having Group 14 elements as acid functionalities. To this end, we will focus on the experimentally reported $(\text{F}_5\text{C}_2)_3\text{E}-\text{CH}_2-\text{P}(\text{tBu})_2$ (E = Si, Ge, Sn) geminal FLPs. Specifically, the CO_2 and phenylisocyanate activation reactions mediated by these FLPs will be analyzed (Scheme 2.2) and compared to the analogous processes involving the B/P geminal FLP. This will allow us to quantitatively disclose the influence of the nature of the acid functionality on the reactivity of this family of intramolecular FLPs.



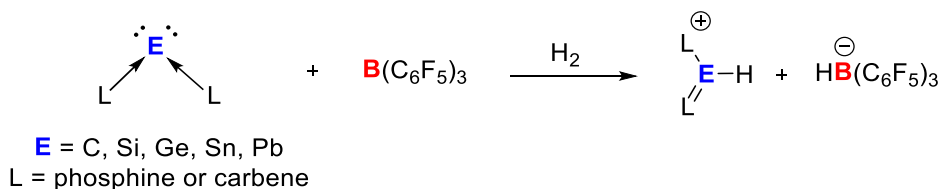
Scheme 2.2. Reactivity of Group 14 element containing geminal FLPs studied in chapter 2.

Aiming at designing highly active FLPs, we will explore the reactivity of geminal FLPs featuring a 4π -antiaromatic borole fragments as the acid sites. To the best of our knowledge, the influence of aromaticity on the reactivity of FLPs was not considered previously. We hypothesize that the loss of antiaromaticity in the borole moiety during the activation of small molecules should result in more favored processes compared to those systems where aromaticity is not involved (Scheme 2.3). Chapter 3 will show the successful application of the aromaticity concept to the reactivity of FLPs.



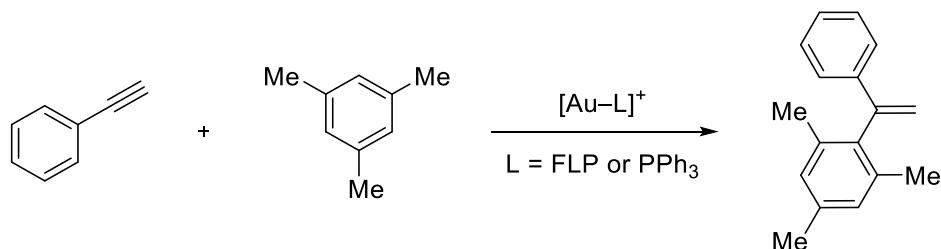
Scheme 2.3. Studied small molecule activation reactions mediated by antiaromatic borole containing FLPs.

Once the reactivity of geminal FLPs is studied, we will next explore intermolecular FLPs featuring ylidenes as the basic functionality. Chapter 4 is therefore inspired by the work by Alcarazo and co-workers who described the reactivity of FLPs composed of BCF and carbenes (unconventional species containing a carbon atom which retain its four valence electrons as two lone pairs). In this chapter, we shall not only focus on carbenes but also on its heavier analogues, known as “ylidenes”. Thus, we will analyze the H_2 activation reactivity of FLPs derived from carbenes or ylidenes with formula EL_2 ($E = C, Si, Ge, Sn, Pb$; $L =$ phosphine or carbene) in combination with $B(C_6F_5)_3$ (Scheme 2.4). Our calculations will allow us to uncover the influence of the nature of both the central atom E and the ligands L on the reactivity of this unconventional family of FLPs.



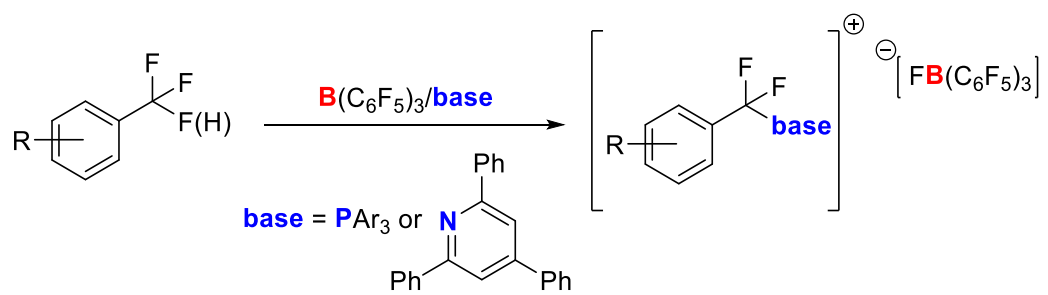
Scheme 2.4. FLP-mediated H_2 activation reactions considered in chapter 4.

In chapter 5, FLPs acting as ambiphilic ligands in Au(I)-complexes will be investigated. Firstly, with the help of the EDA-NOCV method, we will quantitatively analyze the interaction between the LA moiety and the transition metal center. Secondly, we are interested in how such interaction enhances the activity of the corresponding FLP-Au complexes in a representative Au(I)-catalyzed reaction, namely the hydroarylation of phenylacetylene (Scheme 2.5). To this end, we will compare the processes involving these species with that involving the parent $[\text{Au}(\text{PPh}_3)]^+$ catalyst, where no $\text{Au}\cdots\text{LA}$ interaction is present.



Scheme 2.5. Hydroarylation of phenylacetylene catalyzed by Au(I) complexes featuring FLPs as ambiphilic ligands considered in chapter 5.

Finally, we were fascinated by the recent reports by Young and co-workers on the smooth monoselective C–F bond activations in di- and trifluorosubstrates mediated by FLPs (Scheme 2.6). For this reason, in the final chapter 6, we will explore the so far poorly understood role of FLPs in these facile C–F bond activations. Besides exploring the corresponding potential energy surface, the critical influence of non-covalent interactions on the transformation will be also investigated.



Scheme 2.6. Monoselective defluorination reactions in di- and trifluorosubstrates mediated by FLPs studied in chapter 6.

III-VIII. CHAPTERS 1–6

“A thinker sees his own actions as experiments and questions – as attempts to find out something. Success and failure are for him answers above all.”

Friedrich Nietzsche

III. CHAPTER 1

Influence of the Lewis acid/base pairs on the reactivity of geminal E–CH₂–E' frustrated Lewis pairs

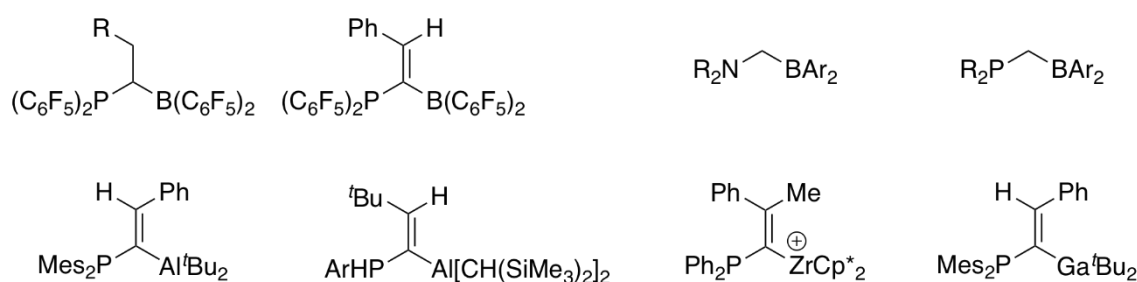
The influence of the nature of the acid/base pairs on the reactivity of geminal frustrated Lewis pairs (FLPs) (Me₂E–CH₂–E'Ph₂) has been computationally explored within the density functional theory framework. To this end, the dihydrogen-activation reaction, one of the most representative processes in the chemistry of FLPs, has been selected. It is found that the activation barrier of this transformation as well as the geometry of the corresponding transition states strongly depend on the nature of the E/E' atoms (E=Group 15 element, E'=Group 13 element) in the sense that lower barriers are associated with earlier transition states. Our calculations identify the geminal N/Al FLP as the most active system for the activation of dihydrogen. Moreover, the barrier height can be further reduced by replacing the phenyl group attached to the acidic atom by C₆F₅ or 3,5-(CF₃)₂C₆H₃ (FxyI) groups. The physical factors controlling the computed reactivity trends are quantitatively described in detail by means of the activation strain model of reactivity combined with the energy decomposition analysis method.

Chem. Eur. J., **2018**, *24*, 17823-17831.

Introduction

The chemistry of frustrated Lewis pairs (FLPs) has arguably experienced a tremendous development since the seminal report by Stephan and co-workers in 2006.¹ These species are characterized by having coordinatively unsaturated Lewis acidic and basic atoms in either single molecules or bimolecular systems where steric hindrance hampers the formation of a classical donor–acceptor dative bond between them. Owing to this peculiar bonding situation, FLPs exhibit a unique reactivity, which allows, among other processes, the activation of different species (*e.g.*, H₂, CO, CO₂, N₂O, etc.) in stoichiometric and catalytic reactions.²

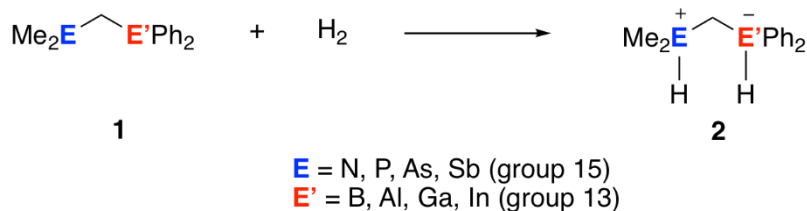
Among the different FLPs described so far, geminal FLPs, that is, systems where the Lewis acidic and basic atoms are separated by a carbon atom, should be especially highlighted (Scheme 3.1). Indeed, geminal P/Al³ and P/B^{4,5} Lewis pairs have attracted considerable interest quite recently due to their remarkable activity in the activation of small molecules. In addition, other geminal FLPs based on N/B,⁶ N/Al,⁷ P/X⁸ (X = Group 14 element), and even P/Ga⁹ have been prepared in order to tune the Lewis acidity/basicity of the FLP antagonists and consequently, to modify the activity of the system. Despite that, the influence of the nature of the Lewis pairs on the reactivity of the FLP is so far not fully understood, which is of crucial importance for further development of FLPs.



Scheme 3.1. Representative examples of geminal FLP systems.

To gain a deeper, quantitative insight into the relationship between the nature of the active sites of geminal FLPs and their reactivity, we explore herein the dihydrogen activation, one of the most important and representative reactions in FLP chemistry,^{2,10} mediated by geminal Me₂E–CH₂–E'Ph₂ (E = Group 15 element, E' = Group 13 element) FLPs (Scheme 3.2). In these systems, which are strongly related to the *t*Bu₂P–CH₂–BPh₂ FLP experimentally described by Lammertsma

and coworkers,^{5a} both the acidic and basic atoms will be modified to identify the E/E' combination leading to the most active geminal FLP (*i.e.*, which exhibits the lowest activation barrier for the considered dihydrogen activation).



Scheme 3.2. FLP-mediated dihydrogen activation reaction considered in this study.

The computed reactivity trends will be analyzed in detail by means of the activation strain model (ASM)¹¹ of reactivity in combination with the energy decomposition analysis (EDA) method.¹² This methodology has been particularly helpful very recently to understand the factors controlling both the H₂ activation and the subsequent dihydrogen release into multiple bonds mediated by geminal B/N FLPs.^{13, 14} Indeed, by means of this state-of-the-art approach we have proposed an orbital-controlled mechanism, complementary to the traditional mechanisms suggested by Pápai et al.¹⁵ and Grimme et al.,¹⁶ where the degree of charge-transfer cooperativity between the key donor–acceptor orbital interactions, that is, LP(N)→σ*(H₂) and σ(H₂)→pπ(B) along the reaction coordinate constitutes a suitable indicator of the reaction barrier.¹³ In addition, a cooperative concerted, yet asynchronous, double hydrogen transfer mechanism was also found for the subsequent hydrogenation of multiple bonds.¹⁴

Theoretical Methods and Computational Details

Geometry optimizations of the molecules were performed without symmetry constraints by using the Gaussian 09 suite of programs¹⁷ employing the meta-hybrid M06-2X exchange-correlation functional¹⁸ combined with the triple-ζ quality def2-TZVPP basis set.¹⁹ Reactants and products were characterized by frequency calculations and have positive definite Hessian matrices. Transition structures (TSs) only show one negative eigenvalue in their diagonalized force constant matrices, and their associated eigenvectors were confirmed to correspond to the motion along the reaction coordinate under consideration by using the intrinsic reaction coordinate (IRC) method.²⁰ In addition, a vibrational calculation provides the thermal Gibbs energy corrections by using the ideal gas/rigid rotor/harmonic

oscillator approximation. Solvent effects were taken into account by means of the polarizable continuum model (PCM)²¹ by using the gas-phase optimized geometries at the same level. This level is denoted PCM(solvent)/M06-2X/def2-TZVPP//M06-2X/def2-TZVPP.

Energy decomposition analyses were carried out by using the ADF.2017 program²² at the same level of theory in conjunction with the triple- ζ quality TZ2P basis set²³ on the geometries optimized at M06-2X/def2-TZVPP. Scalar relativistic effects were accounted for by using the zeroth-order regular approximation (ZORA).²⁴ This level is therefore denoted ZORA-M06-2X/TZ2P//M06-2X/def2-TZVPP.

Activation strain model of reactivity

The ASM of reactivity method¹¹ is a systematic development of the energy decomposition analysis (EDA) method (see below). This method, which is also known as distortion/interaction model,²⁵ is a fragment approach to understanding chemical reactions in which the height of reaction barriers is described and understood in terms of the original reactants. Within this approach, the potential energy surface $\Delta E(\zeta)$ is decomposed along the reaction coordinate ζ into two main contributions, namely the strain $\Delta E_{\text{strain}}(\zeta)$ associated with deforming of the individual reactants plus the actual interaction $\Delta E_{\text{int}}(\zeta)$ between these increasingly deformed reactants [Eq. (3.1)]:

$$\Delta E(\zeta) = \Delta E_{\text{strain}}(\zeta) + \Delta E_{\text{int}}(\zeta) \quad (3.1)$$

Although the strain $\Delta E_{\text{strain}}(\zeta)$ depends on both the rigidity of the reactants and the reaction pathway under consideration, the interaction $\Delta E_{\text{int}}(\zeta)$ between the reactants depends on their electronic structures and on their mutual orientation as they approach each other. The interplay between $\Delta E_{\text{strain}}(\zeta)$ and $\Delta E_{\text{int}}(\zeta)$ determines where the barrier arises, namely, at the point satisfying $d\Delta E_{\text{strain}}(\zeta)/d\zeta = -d\Delta E_{\text{int}}(\zeta)/d\zeta$. This approach has enormously contributed to our current understanding of different fundamental transformations in either organic or organometallic chemistry.²⁶ For further details of the theoretical background and different applications of the ASM method, we refer readers to the review articles that were published recently.¹¹

For consistency reasons, herein the reaction coordinate is defined as the projection of the IRC onto the forming E/E'...H distance. This reaction coordinate ζ undergoes a well-defined change in the course of the reaction from the separate reactants to the equilibrium distance in the corresponding transition states.

Energy decomposition analysis

The interaction $\Delta E_{\text{int}}(\zeta)$ between the strained reactants can be further partitioned into chemically meaningful contributions by means of the EDA method.¹⁴ Thus, $\Delta E_{\text{int}}(\zeta)$ is decomposed into the following terms along the reaction coordinate [Eq. (3.2)]:

$$\Delta E_{\text{int}}(\zeta) = \Delta V_{\text{elstat}}(\zeta) + \Delta E_{\text{Pauli}}(\zeta) + \Delta E_{\text{orb}}(\zeta) + \Delta E_{\text{disp}}(\zeta) \quad (3.2)$$

The term ΔV_{elstat} corresponds to the classical electrostatic interaction between the unperturbed charge distributions of the deformed reactants and is usually attractive. The Pauli repulsion ΔE_{Pauli} comprises the destabilizing interactions between occupied orbitals and is responsible for any steric repulsion. The orbital interaction ΔE_{orb} accounts for charge transfer (interaction between occupied orbitals on one moiety with unoccupied orbitals on the other, including HOMO–LUMO interactions) and polarization (empty–occupied orbital mixing on one fragment due to the presence of another fragment). Finally, the ΔE_{disp} term takes into account the interactions, which are due to dispersion forces. Moreover, the NOCV (natural orbital for chemical valence)²⁷ extension of the EDA method has also been used to further partitioning the ΔE_{orb} term. The EDA-NOCV approach provides pairwise energy contributions for each pair of interacting orbitals to the total bond energy.

Results and Discussion

Similar to the reaction profiles computed previously for the dihydrogen activation mediated by different N/B¹³ or P/B^{5a} geminal FLPs, we found that in all cases the heterolytic H₂ splitting occurs in a concerted manner leading to the corresponding zwitterionic products **2** through the respective five-membered transition states **TS**. These saddle points are therefore associated with the rupture of the H–H bond with the concomitant formation of E–H and E'–H bonds (Figure 3.1). Moreover, the process begins with the formation of an initial van der Waals

reactant complex, which, in all cases, lies approximately 2–3 kcal mol⁻¹ (average value) above the separate reactants (the formation of these species becomes even more endergonic when thermal free-energy corrections at 298.15 K are included, see Table 3.1).

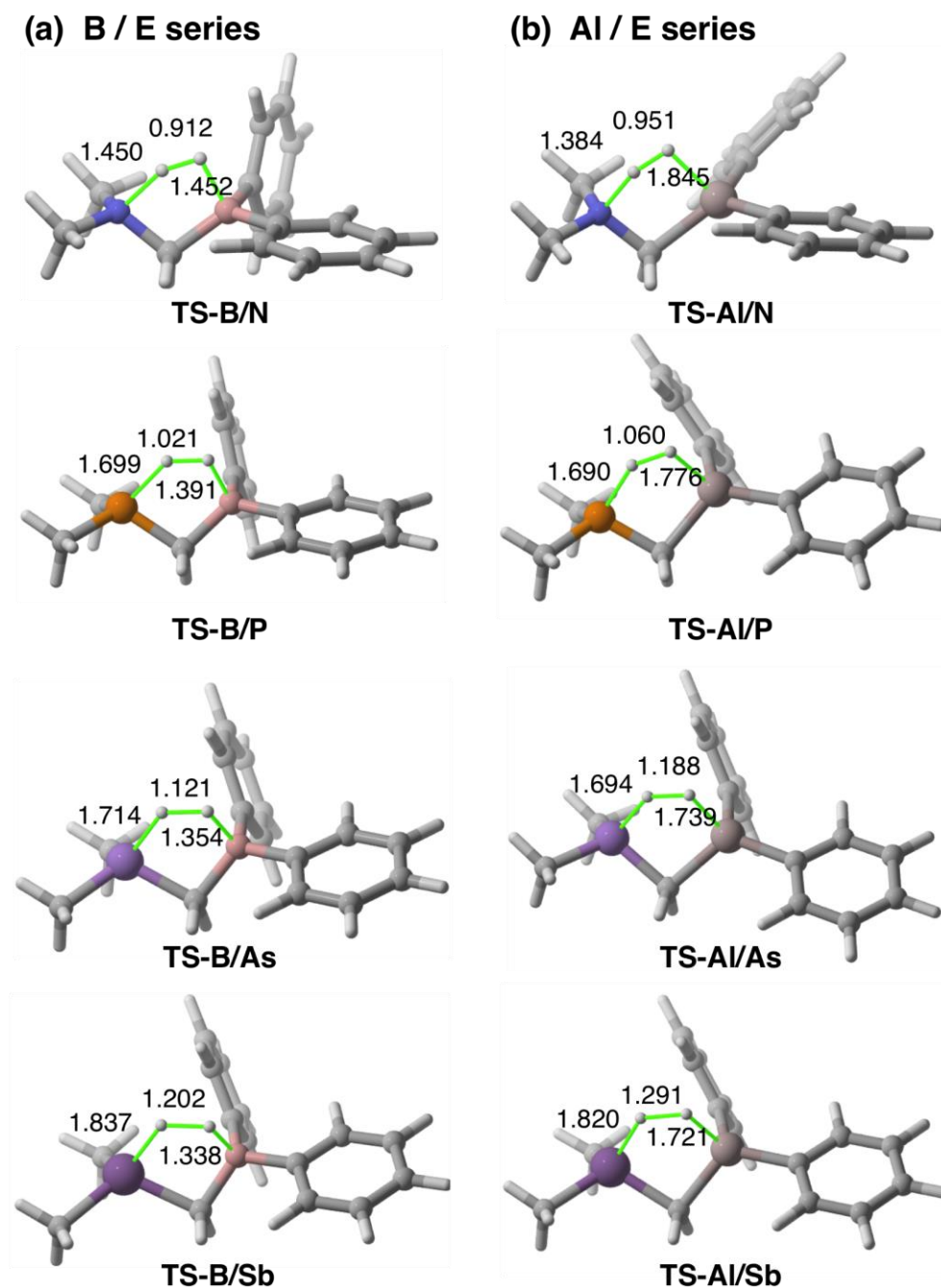


Figure 3.1. Fully optimized geometries (M06-2X/def2-TZVPP level) of the transition states involved in the H₂ activation reactions mediated by FLPs B/E and Al/E (E = Group 15 element). Bond distances are given in Ångstroms.

Closer inspection of the optimized geometries of the transition states (see Figure 3.1 for the representative series involving B/E and Al/E FLPs) clearly indicates that the forming E'...H bond (E'=Group 13 element) becomes shorter and shorter as the basicity of the EMe₂ moiety decreases (E=N>P>As>Sb). At the same time, the H...H bond becomes longer and longer. Therefore, our calculations suggest that the transition state of this FLP-mediated dihydrogen activation is reached later and later as the basicity of the E Lewis base partner becomes lower. Interestingly, for a given E' Lewis acid, the computed activation barrier steadily increases even when the basic E partner goes from nitrogen to antimony (see Table 3.1). For this reason, it is not surprising that very good linear relationships were found when plotting the H...H bond breaking lengths in the transition states versus the corresponding computed activation barriers (correlation coefficients R²>0.99, Figure 3.2). We can then conclude that late transition states in these FLP-mediated reactions are associated with higher activation barriers than earlier transition states, which is fully consistent with the Hammond–Leffer postulate.²⁸ As expected, similar very good linear correlations were also found when plotting the E'...H bond forming length versus the corresponding activation barriers (see Figure 3.S1 in the Supporting Information).

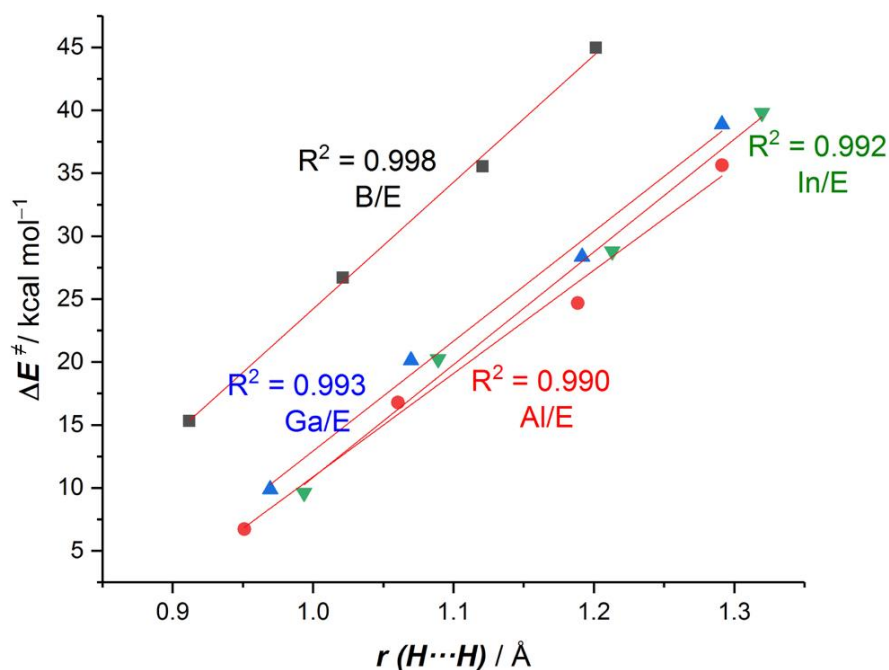


Figure 3.2. Plot of the computed activation barriers (ΔE^\ddagger) vs. the H...H distance in the corresponding transition states. All data were computed at the M06-2X/def2-TZVPP level.

Table 3.1. Computed activation and reaction energies plus ZPVE corrections and corresponding free energies (computed at 298.15 K) for the dihydrogen activation reactions mediated by geminal FLPs **1**. All data (in kcal mol⁻¹), relative to the isolated reactants, were computed at the M06-2X/def2-TZVPP level.

| E'/E | $\Delta E_{\text{RC}}(\text{ZPE})^{[\text{a}]}$ | $\Delta G_{\text{RC}}^{[\text{a}]}$ | $\Delta E^\ddagger(\text{ZPE})^{[\text{b}]}$ | $\Delta G^\ddagger^{[\text{b}]}$ | $\Delta E_{\text{R}}(\text{ZPE})^{[\text{c}]}$ | $\Delta G_{\text{R}}^{[\text{c}]}$ |
|--------------|---|-------------------------------------|--|----------------------------------|--|------------------------------------|
| B/N | 1.7 | 8.3 (5.1) ^[d] | 15.3 | 22.1 (17.6) ^[d] | -1.2 | 6.0 (-6.3) ^[d] |
| B/P | 4.1 | 9.9 (7.7) | 26.7 | 33.5 (30.0) | 3.3 | 10.8 (1.8) |
| B/As | 5.9 | 12.1 (9.1) | 35.5 | 43.2 (38.1) | 18.1 | 26.0 (16.5) |
| B/Sb | 1.3 | 7.6 (5.0) | 45.0 | 52.0 (47.0) | 28.6 | 36.0 (27.1) |
| Al/N | 0.3 | 7.1 (4.0) | 6.7 | 14.0 (10.1) | 1.8 | 8.9 (-2.2) |
| Al/P | 0.1 | 6.0 (3.0) | 16.8 | 23.3 (20.6) | -0.8 | 7.0 (-0.7) |
| Al/As | 0.1 | 7.1 (4.2) | 24.7 | 32.5 (28.9) | 13.3 | 21.8 (13.7) |
| Al/Sb | 2.4 | 8.7 (5.6) | 35.6 | 44.0 (39.7) | 24.4 | 32.8 (24.9) |
| Ga/N | 1.2 | 8.2 (4.7) | 9.9 | 17.6 (13.6) | 5.5 | 12.8 (1.7) |
| Ga/P | 0.1 | 6.4 (3.7) | 20.1 | 26.0 (23.4) | 5.5 | 9.4 (2.0) |
| Ga/As | 0.3 | 7.3 (4.3) | 28.4 | 36.2 (32.5) | 15.9 | 24.5 (16.6) |
| Ga/Sb | 2.4 | 8.4 (5.5) | 38.9 | 47.2 (42.9) | 26.7 | 34.7 (27.2) |
| In/N | 0.8 | 7.8 (4.7) | 9.6 | 17.0 (13.3) | 6.8 | 14.2 (4.5) |
| In/P | 0.4 | 6.8 (3.7) | 20.2 | 27.6 (25.0) | 2.5 | 10.0 (3.9) |
| In/As | -0.2 | 5.7 (4.3) | 28.8 | 35.5 (32.9) | 16.8 | 24.7 (18.3) |
| In/Sb | 2.3 | 6.8 (5.5) | 39.8 | 46.5 (42.5) | 27.8 | 34.4 (27.9) |

[a] $\Delta E_{\text{RC}} = E(\text{RC}) - E(\mathbf{1}) - E(\text{H}_2)$. [b] Activation energy: $\Delta E^\ddagger = E(\text{TS}) - E(\mathbf{1}) - E(\text{H}_2)$. [c] Reaction energy: $\Delta E_{\text{R}} = E(\mathbf{2}) - E(\mathbf{1}) - E(\text{H}_2)$. [d] Values within parentheses indicate the corresponding free energies in toluene solution (computed at the PCM(toluene)-M06-2X/def2-TZVPP//M06-2X-def2-TZVPP level).

Two main reactivity trends can be clearly observed when inspecting the data gathered in Table 3.1. On the one hand and as commented above, the barrier heights for the considered H₂ activation reactions linearly increase upon reducing the basicity strength of the E atom regardless of the nature of the acidic E' atom (ΔE^\ddagger increases in the order N < P < As < Sb). On the other hand, it seems that for a given E atom, the activation barrier decreases when going down in the Group 13 for the acidic E' atom. Strikingly, in all cases, it is found that, regardless of the nature of the basic E atom, the systems having E'=Al as acidic partner systematically exhibit the lowest activation barriers in all of the considered series. Therefore, our calculations identify the geminal Al/N FLP as the most active system for the activation of dihydrogen. Identical reactivity trends are found when considering the effect of the solvent (in this study, toluene was selected because it is the solvent typically used in the experiments). Not surprisingly, the activation

barriers in solution become slightly lower (ca. 5 kcal mol⁻¹) and the reaction energies become systematically less endergonic (ca. 10 kcal mol⁻¹) than those computed in the gas phase. This can be ascribed to the gain of the zwitterionic character of species **2** upon dihydrogen activation.

The activation strain model (ASM) of reactivity was next applied to gain a deeper, quantitative insight into the physical factors controlling the above-commented reactivity trends. Thus, the reduction of the reactivity with decreasing the basicity strength of the E atom was analyzed first. To this end, we focused on the dihydrogen-activation reactions involving the parent geminal Me₂E-CH₂-BPh₂ FLPs (E = N, P, As, Sb). Although all the processes have been studied, Figure 3.3 only shows the corresponding activation strain diagrams (ASDs) from the initial reactant complexes up to the transition states for the reactions involving E = N, P, and Sb for clarity reasons (the remaining ASD for E = As can be found in Figure 3.S2 in the Supporting Information).

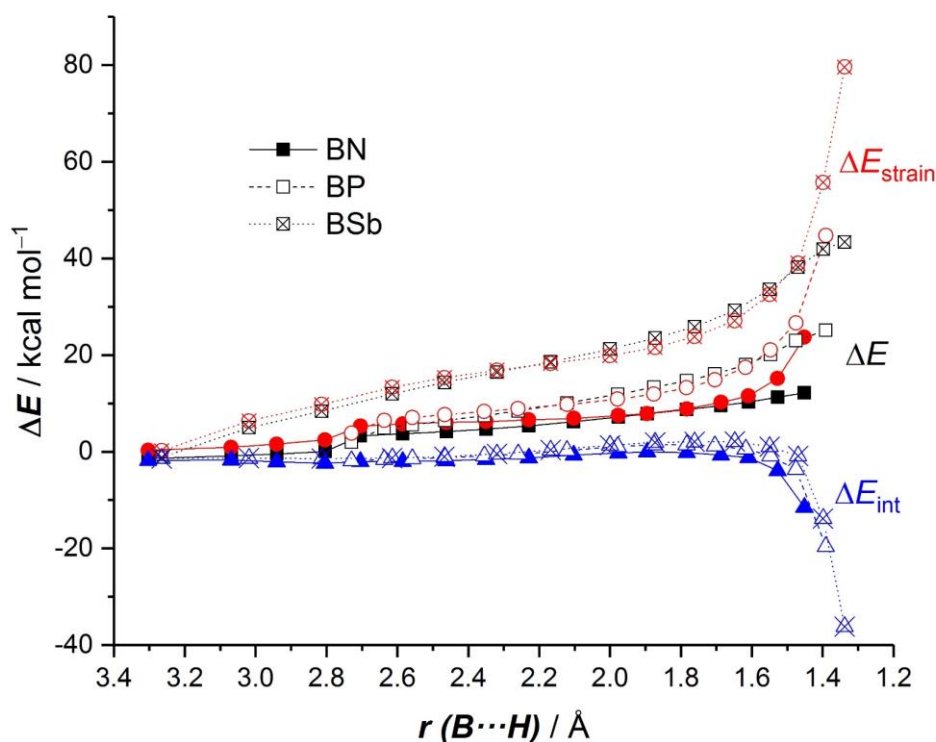


Figure 3.3. Comparative activation strain diagrams of the dihydrogen-activation reactions mediated by geminal B/N (solid lines), B/P (dashed lines) and B/Sb (dotted lines) FLPs along the reaction coordinate projected onto the forming B...H bond length. All data were computed at the M06-2X/def2-TZVPP level and are referenced to the isolated reactants.

All H₂ activation reactions exhibit quite similar ASDs in the sense that the interaction energy between the deformed reactants, measured by the ΔE_{int} term, only becomes clearly stabilizing at the proximity of the transition state region. This behavior has also been observed not only in our previous work focused on the strongly related H₂ activation mediated by geminal B/N FLPs,¹³ but also in completely different processes, such as pericyclic reactions.²⁹ Interestingly, the interaction energy between the deformed reactants (ΔE_{int}), which is rather similar for all systems along the entire reaction coordinate, only becomes significantly different at the corresponding transition states where it increases (*i.e.*, becomes more stabilizing) in the order E = N < P < Sb. This is exactly the opposite trend to the activation barriers, which strongly suggests that the observed reactivity trend is not related to the interaction between the reactants. Instead, the strain energy, that is, the energy required to deform the reactants from their equilibrium geometries, is markedly different for the considered FLP-mediated reactions along the entire transformation and follows the same trend than the activation barriers (ΔE_{strain} increases in the order N < P < Sb). For instance, at the same consistent B...H bond forming length of 1.6 Å, the difference in the computed strain energies ($\Delta\Delta E_{\text{strain}} = 6.4$ and 17.9 kcal mol⁻¹, for B/P and B/Sb with respect to B/N, respectively) roughly matches the difference in the computed total energies ($\Delta\Delta E = 8.1$ and 21.4 kcal mol⁻¹, for B/P and B/Sb, respectively). It can be concluded that the observed trend of the reactivity, which was initially ascribed to the different basicity strength of the EMe₂ moiety, finds its origin mainly in the energy required to deform the reactants to adopt the transition state geometry instead. The ASM method therefore suggests that geminal FLPs having lighter Group 15 elements as basic partner already possess an equilibrium geometry, which better fits into the corresponding transition states, and for this reason, require a much lower deformation energy than their heavier counterparts. This is translated into earlier transition states (see above) and consequently, into lower activation barriers. This conclusion is further confirmed by the partitioning of the total ΔE_{strain} term into contributions coming from both reactants (*i.e.*, H₂ and FLP), which indicates that the strain associated with the deformation of the geminal FLP reactant is mainly responsible for the observed trend in ΔE_{strain} (see Figure 3.S3 in the Supporting Information).

We then analyzed the reactivity trends observed when modifying the acidic E' atom from B to In. As commented above, the activation barriers seem to decrease

systematically when going down in the Group 13 regardless of the nature of the basic E atom with the notable exception of the processes involving $E' = \text{Al}$, which exhibit the lowest computed barrier heights. To understand in detail this peculiar reactivity trend, we again applied the ASM to the H_2 activation reactions involving the geminal $\text{Me}_2\text{N}-\text{CH}_2-\text{E}'\text{Ph}_2$ FLPs ($E' = \text{B}, \text{Al}, \text{In}$). The corresponding ASDs (once again, showing the reaction coordinate from the beginning of the process up to the corresponding transition states) clearly indicate that the processes involving the heavier Group 13 E' atoms ($E = \text{Al}$ or In) benefit from a much lower strain energy along the entire coordinate. Despite that, the lower barrier computed for these systems as compared to $E' = \text{B}$ is not only the result of their less destabilizing deformation energies. As can be clearly seen in Figure 3.4, these systems also benefit from a stronger interaction energy along the entire reaction coordinate and particularly, at the transition state region as compared to the analogous transformation involving the B/N FLP. Therefore, it is the combination of a lower strain energy and a stronger interaction which renders the processes involving the heavier systems kinetically more favorable. Interestingly, the ASDs depicted in Figure 3.4 also explain the anomalous behavior of the system having $E' = \text{Al}$. Indeed, if we compare the processes involving $E' = \text{Al}$ and $E' = \text{In}$, we realize that both systems exhibit a nearly identical strain energy along the entire transformation, which indicates that the ΔE_{strain} term is not at all responsible for this peculiar behavior. At variance, the process involving the $\text{Me}_2\text{N}-\text{CH}_2-\text{AlPh}_2$ FLP clearly benefits from a stronger interaction between the deformed reactants along the entire transformation, which is translated into the lower activation barrier computed for this particular transformation.

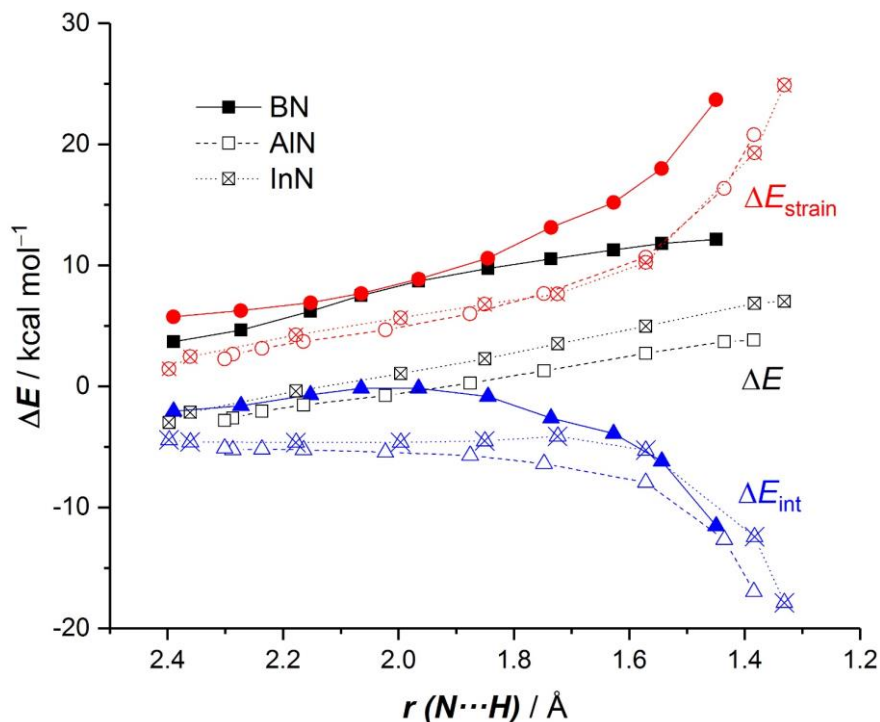


Figure 3.4. Comparative activation strain diagrams of the dihydrogen activation reactions mediated by geminal B/N (solid lines), Al/N (dashed lines), and In/N (dotted lines) FLPs along the reaction coordinate projected onto the forming N \cdots H bond length. All data were computed at the M06-2X/def2-TZVPP level and are referenced to the isolated reactants.

The crucial role of the interaction energy in the processes involving $\text{Me}_2\text{N}-\text{CH}_2-\text{E}'\text{Ph}_2$ ($\text{E}' = \text{B}, \text{Al}, \text{In}$) FLPs deserves further quantitative analysis. To this end, the different contributors to the total interaction energy, ΔE_{int} , are analyzed by applying the energy decomposition analysis (EDA) method.¹² As graphically shown in Figure 3.5, which shows the evolution of the different EDA terms along the reaction coordinate for the H_2 activation involving the $\text{Me}_2\text{N}-\text{CH}_2-\text{E}'\text{Ph}_2$ ($\text{E}' = \text{B}, \text{Al}, \text{In}$) FLPs, it becomes evident that the B/N system presents the strongest orbital interactions between the deformed reactants, particularly at the transition state region. Despite that, the stabilizing ΔE_{orb} term (and ΔV_{elsat} , albeit to a lesser extent) cannot compensate the highly destabilizing effect of the Pauli repulsion term (ΔE_{Pauli}) and for this reason, the total interaction energy for the reaction involving this B/N FLP is comparatively weaker than that computed for the analogous processes involving Al/N or In/N FLPs, which benefit from a much lower destabilizing Pauli repulsion. Interestingly, when comparing these heavier systems, it becomes clear that the differential factor leading to the computed higher interaction energy for the process involving the $\text{E}' = \text{Al}$ system is

the stronger orbital interaction between the reactants for this particular FLP, as the other energy contributors are essentially identical. For instance, at the same N...H bond forming length of 1.5 Å, a value of $\Delta E_{\text{orb}} = -63.6$ kcal mol⁻¹ was computed for the reaction involving the Al/N system whereas a weaker value of $\Delta E_{\text{orb}} = -55.8$ kcal mol⁻¹ ($\Delta V_{\text{elstat}} = -47.3$ kcal mol⁻¹) was found for the process involving the heavier In/N system. This remarkable difference in the orbital interactions is therefore responsible for the lowest barrier height computed for the reaction involving the Al/N FLP.

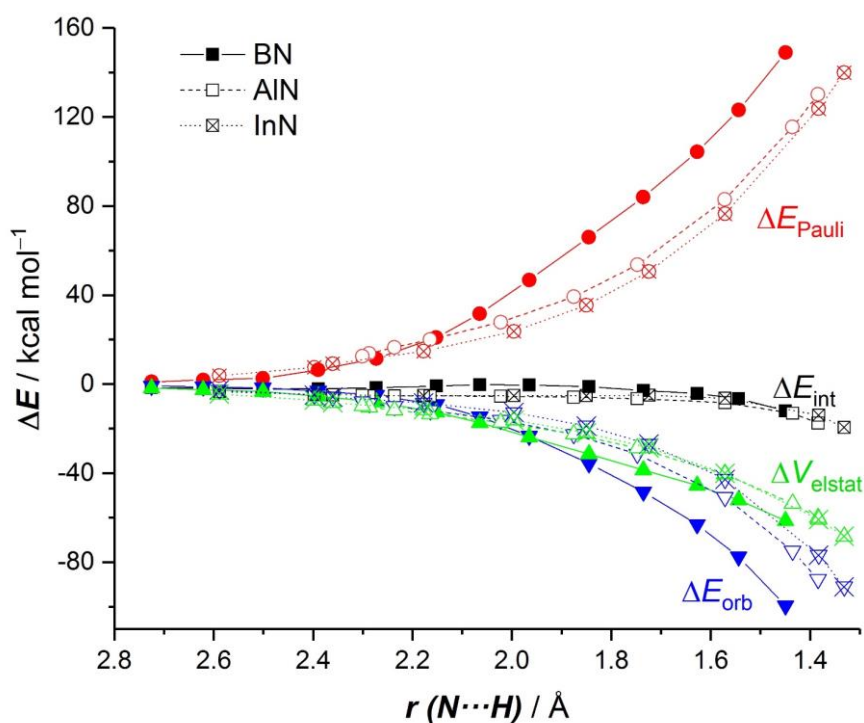


Figure 3.5. Energy decomposition analysis of the dihydrogen activation reactions mediated by geminal B/N (solid lines), Al/N (dashed lines), and In/N (dotted lines) FLPs along the reaction coordinate projected onto the forming N...H bond length. All data were computed at the ZORA-M06-2X/TZ2P//M06-2X/def2-TZVPP level.

By means of the NOCV extension of the EDA,²⁸ the nature of the molecular orbitals involved in the H₂ activation as well as their relative contribution to the total ΔE_{orb} term can be further analyzed. As depicted in Figure 3.6 for the processes mediated by the Al/N and In/N FLPs, the pairwise orbital interaction, which mainly dominates the ΔE_{orb} term (contribution of ca. 90%), involves the cooperative LP(N)→ $\sigma^*(\text{H}_2)$ and $\sigma(\text{H}_2)$ →p $\pi(\text{E}')$ interactions. This orbital interaction is therefore identical to that observed previously by us for the related geminal B/N

FLP-mediated H₂ activations,¹³ which further confirms the generality of the reaction mechanism of this transformation. Despite that, the peculiar behavior of the Al/N system finds its origin in the strength of this particular orbital interaction. Indeed, as shown in Figure 3.6, the associated orbital energy $\Delta E(\rho)$, at the same N...H bond forming length is approximately 8 kcal mol⁻¹ stronger for the process involving Al/N than for the transformation involving its heavier counterpart In/N. This stronger orbital interaction is then responsible for the stronger interaction between the reactants, which, together with the required relatively low strain energy, make the geminal Al/N FLP the most active system of the entire E/E' series for the heterolytic rupture of dihydrogen.

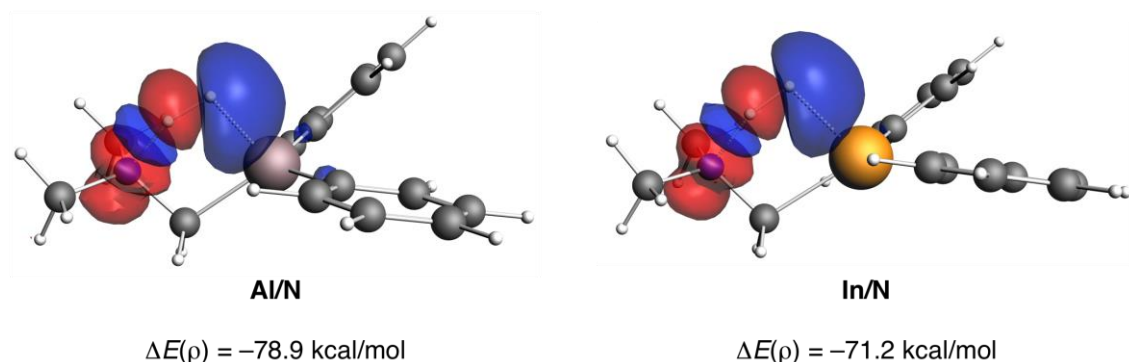


Figure 3.6. Contour plots of NOCV deformation densities $\Delta\rho$ and the associated energies $\Delta E(\rho)$ (in kcal mol⁻¹) for the main orbital interactions between H₂ and geminal FLPs Al/N (left) and In/N (right). The electronic charge flows from red to blue. All data were computed at the ZORA-M06-2X/TZ2P//M06-2X/def2-TZVPP level.

Effect of substituents

In the FLP chemistry, a frequently employed substituent on the acidic atom (usually, boron) is the C₆F₅ group mainly due to its high electron-withdrawing nature, which greatly enhances the acidity of the E' atom. Despite that, in some particular cases (geminal P/B FLPs) the enhanced reactivity of the system leads to a rearrangement side reaction forming a five-membered ring B/P heterocycle, which precludes the preparation of the geminal P/B(C₆F₅)₂ FLP.^{5a} For this reason, different electron-withdrawing substituents, such as the Fxyl group (Fxyl = 3,5-(CF₃)₂C₆H₃) have also been employed quite recently for the preparation of highly active geminal FLPs (*i.e.*, *t*Bu₂P-CH₂-B(Fxyl)₂).^{5c} Taken into account these findings, we finally investigated the effect of these substituents on the reactivity of

the most active geminal FLPs identified above, that is, the B/N and Al/N systems, aiming at further lowering the barrier height of the H₂ activation reaction.

From the data in Table 3.2, which gathers the computed activation and reaction energies of the explored dihydrogen activations, it becomes evident that the C₆F₅ and Fxyl groups significantly favor the transformation, from both thermodynamic and kinetic points of view, as compared to the phenyl group. When comparing both electron-withdrawing groups, it is clear that the C₆F₅ group leads to a more active FLP. Therefore, the geminal FLP Me₂N-CH₂-B(C₆F₅)₂ and particularly, its aluminum counterpart Me₂N-CH₂-Al(C₆F₅)₂, are predicted as the most promising (*i.e.*, active) candidates to perform facile dihydrogen activation reactions (*i.e.*, having relatively low activation barriers).

Table 3.2. Computed activation and reaction energies plus ZPVE corrections and corresponding free energies (computed at 298.15 K) for the dihydrogen activation reactions mediated by B/N and Al/N geminal FLPs. All data (in kcal mol⁻¹), relative to the isolated reactants, were computed at the M06-2X/def2-TZVPP level.

| FLP | $E_{\text{RC}}(\text{ZPE})^{[\text{a}]}$ | $G_{\text{RC}}^{[\text{a}]}$ | $E^\ddagger(\text{ZPE})^{[\text{b}]}$ | $G^\ddagger^{[\text{b}]}$ | $E_{\text{R}}(\text{ZPE})^{[\text{c}]}$ | $G_{\text{R}}^{[\text{c}]}$ |
|--|--|------------------------------|---------------------------------------|---------------------------|---|-----------------------------|
| Me ₂ N-CH ₂ -BPh ₂ | 1.7 | 8.3 | 15.3 | 22.1 | -1.2 | 6.0 |
| | | (5.1) ^[d] | | (17.6) ^[d] | | (-6.3) ^[d] |
| Me ₂ N-CH ₂ -B(C ₆ F ₅) ₂ | 0.5 | 6.3 | 6.6 | 13.7 | -16.2 | -9.3 |
| | | (3.5) | | (9.6) | | (-22.7) |
| Me ₂ N-CH ₂ -B(Fxyl) ₂ | 1.4 | 7.2 | 11.8 | 18.7 | -9.6 | -1.8 |
| | | (4.5) | | (14.6) | | (-14.2) |
| Me ₂ N-CH ₂ -AlPh ₂ | 0.3 | 7.1 | 6.7 | 14.0 | 1.8 | 8.9 |
| | | (4.0) | | (10.1) | | (-2.2) |
| Me ₂ N-CH ₂ -Al(C ₆ F ₅) ₂ | -1.4 | 5.9 | 3.1 ^[e] | 9.2 | -9.9 | -2.5 |
| | | (1.9) | | (5.3) | | (-13.6) |
| Me ₂ N-CH ₂ -Al(Fxyl) ₂ | 0.8 | 8.0 | 3.9 | 11.1 | -4.3 | 3.1 |
| | | (4.0) | | (7.7) | | (-8.3) |

[a] $\Delta E_{\text{RC}} = E(\text{RC}) - E(\mathbf{1}) - E(\text{H}_2)$. [b] Activation energy: $\Delta E^\ddagger = E(\text{TS}) - E(\mathbf{1}) - E(\text{H}_2)$. [c] Reaction energy: $\Delta E_{\text{R}} = E(\mathbf{2}) - E(\mathbf{1}) - E(\text{H}_2)$. [d] Values within parentheses indicate the corresponding free energies in toluene solution (computed at the PCM(toluene)-M06-2X/def2-TZVPP//M06-2X-def2-TZVPP level). [e] Barrier computed with respect to the corresponding reactant complex.

We also applied the ASM to quantitatively understand the reasons behind the remarkably high activity of these geminal FLPs. To this end, we compared the N/B systems having the Ph and C₆F₅ groups together with its N/Al analogue. The corresponding ASDs in Figure 3.7 clearly indicate that the C₆F₅ group enhances the

interaction between the increasingly deformed reactants as compared to the process involving N/BPh₂, which is consistent with the higher electron-withdrawing nature of the C₆F₅ group. In addition, despite its higher steric hindrance, this substituent also induces a significant reduction of the required strain energy. As a consequence of both effects, the barrier computed for the process involving the N/B(C₆F₅)₂ system is significantly lower than that computed for the analogous reaction mediated by the N/BPh₂ FLP. Figure 3.7 also reveals why the barrier of the process involving the N/Al(C₆F₅)₂ system is the lowest of the series. Similar to the trend commented above when comparing the N/E'Ph₂ systems (E' = B, Al, see Figure 3.4), once again, the N/Al FLP induces an additional reduction of the strain energy, which is accompanied by a higher interaction between the deformed reactants along the entire reaction coordinate. Thus, the combination of these favorable effects renders the process mediated by this N/Al(C₆F₅)₂ FLP the kinetically easiest transformation.

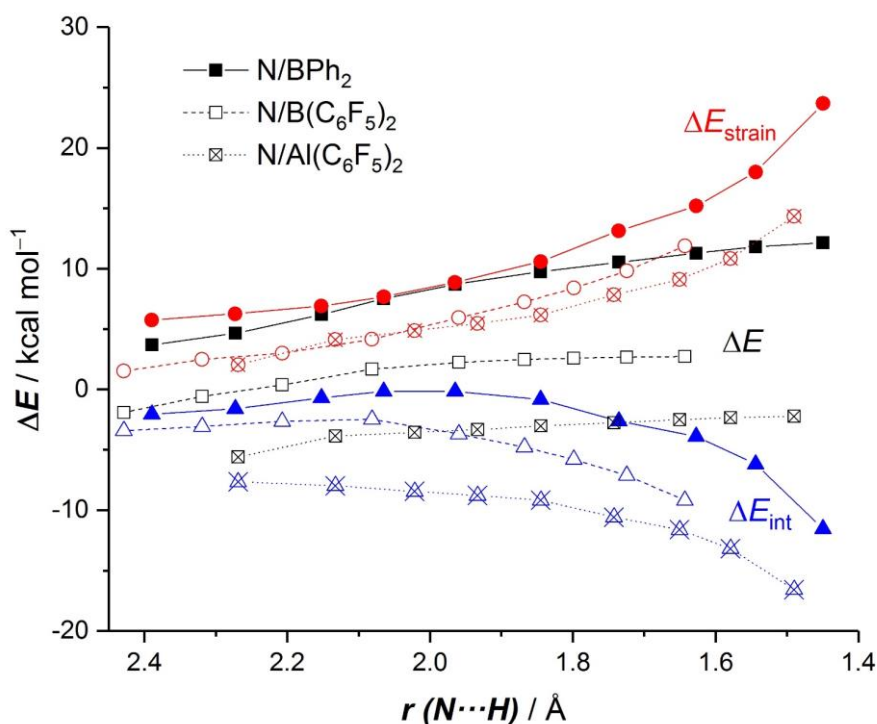


Figure 3.7. Comparative activation strain diagrams of the dihydrogen-activation reactions mediated by geminal N/BPh₂ (solid lines), N/B(C₆F₅)₂ (dashed lines), and N/Al(C₆F₅)₂ (dotted lines) FLPs along the reaction coordinate projected onto the forming N...H bond length. All data were computed at M06-2X/def2-TZVPP level and are referenced to the isolated reactants.

The factors controlling the stronger ΔE_{int} computed for the N/B(C₆F₅)₂ system were also finally analyzed by means of the EDA method. As graphically shown in

Figure 3.8, the beneficial effect of the C_6F_5 group with respect to a phenyl substituent is mainly due to the stronger orbital interactions (mainly the key $\sigma(H_2) \rightarrow p\pi(B)$ interaction) induced by this electron-withdrawing substituent. Once again, the analogous N/Al system, despite inducing weaker orbital and electrostatic interactions between the reactants, benefits from a much less destabilizing Pauli repulsion as compared to its N/B counterpart. As a consequence, the process mediated by the geminal N/Al(C_6F_5)₂ FLP possesses the strongest interaction energy, which is ultimately translated into the lowest activation barrier computed for all the geminal FLPs considered in this study.

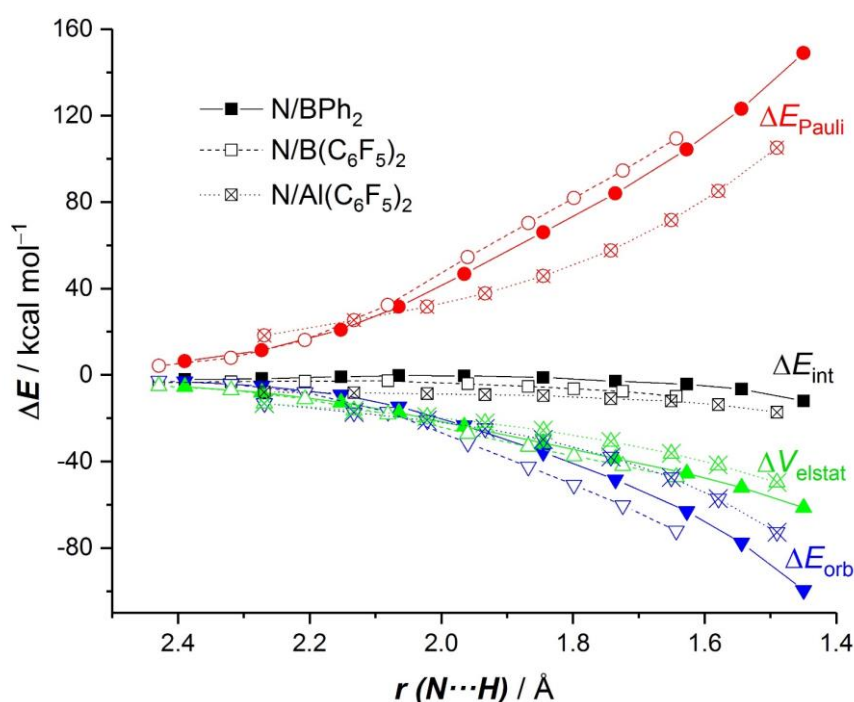


Figure 3.8. Energy decomposition analysis of the dihydrogen-activation reactions mediated by geminal N/BPh₂ (solid lines), N/B(C_6F_5)₂ (dashed lines), and N/Al(C_6F_5)₂ (dotted lines) FLPs along the reaction coordinate projected onto the forming N...H bond length. All data were computed at the ZORA-M06-2X/TZ2P//M06-2X/def2-TZVPP level.

Conclusion

The influence of the nature of the Lewis acid/base antagonists present in geminal FLPs ($Me_2E-CH_2-E'Ph_2$) on their intrinsic reactivity has been computationally explored. By selecting the H_2 activation reaction, it is found that the corresponding barrier height steadily increases when going down in the Group 15 ($N < P < As < Sb$) regardless the nature of the E' (Group 13 element) atom. In

addition, the respective transition states become later and later, which is consistent with the Hammond–Leffer postulate. The influence of the nature of the acidic partner E' (Group 13 element) is opposite (*i.e.*, the barrier decreases from B to In) with the notable exception of systems having E' = Al, which systemically exhibit the lowest activation barriers of each series. Therefore, the geminal N/Al FLP is identified as the most active system for the dihydrogen-activation reaction.

With the help of the ASM method, the reactivity trend computed for the variation of the Lewis base atom is ascribed to the much lower strain energy associated to the FLP having the lighter E atom, and not to its relative basicity strength. The trend computed for the variation of the Lewis acid is not only ascribed to the required deformation energy but also to the stronger interaction between the deformed reactants for processes involving heavier E' atoms. The peculiar behavior of the systems having E' = Al can be mainly ascribed to the combination of the rather low Pauli repulsion computed for these FLPs together with significantly strong $LP(N) \rightarrow \sigma^*(H_2)$ and $\sigma(H_2) \rightarrow p\pi(E')$ orbital interactions.

Finally, the barrier heights can be further reduced by replacing the phenyl groups attached to the E' atom by strong electron-withdrawing groups, such as C_6F_5 or Fxyl. These groups induce a stronger interaction between the reactants along the entire reaction coordinate as compared to phenyl groups. Interestingly, and despite its higher steric volume, the FLPs having these groups require lower deformation energies than their phenyl-substituted counterparts, which is translated into much lower activation barriers computed for the processes involving these systems. Therefore, our calculations predict that geminal N/B(C_6F_5)₂ and especially, N/Al(C_6F_5)₂ FLPs are really promising candidates to achieve facile dihydrogen-activation reactions. In our opinion, the insight gained in this computational study may be important for the rational design of novel FLP hydrogenation catalysts.

References

- ¹ G. C. Welch, R. R. San Juan, J. D. Masuda, D. W. Stephan, *Science* **2006**, *314*, 1124.
- ² For leading reviews, see: a) D. W. Stephan, G. Erker, *Angew. Chem. Int. Ed.* **2010**, *49*, 46; *Angew. Chem.* **2010**, *122*, 50; b) G. Erker, *Pure Appl. Chem.* **2012**, *84*, 2203; c) D. W. Stephan, G. Erker, *Top. Curr. Chem.*, Vol. *332: Frustrated Lewis Pairs I*, Springer, Heidelberg, 2013; d) D. W. Stephan, G. Erker, *Chem. Sci.* **2014**, *5*, 2625; e) D. W. Stephan, *J. Am. Chem. Soc.* **2015**, *137*, 10018; f) D. W. Stephan, G. Erker, *Angew. Chem. Int. Ed.* **2015**, *54*, 6400; *Angew. Chem.* **2015**, *127*, 6498; g) D. W. Stephan, *Acc. Chem. Res.* **2015**, *48*, 306; h) D. W. Stephan, *Science* **2016**, *354*, aaf7229; i) S. Arndt, M. Rudolph, A. S. K. Hashmi, *Gold Bull.* **2017**, *50*, 267.
- ³ Selected examples: a) C. Appelt, H. Westenberg, F. Bertini, A. W. Ehlers, J. C. Sloatweg, K. Lammertsma, W. Uhl, *Angew. Chem. Int. Ed.* **2011**, *50*, 3925; *Angew. Chem.* **2011**, *123*, 4011; b) C. Appelt, J. C. Sloatweg, K. Lammertsma, W. Uhl, *Angew. Chem. Int. Ed.* **2012**, *51*, 5911; *Angew. Chem.* **2012**, *124*, 6013; c) S. Roters, C. Appelt, H. Westenberg, A. Hepp, J. C. Sloatweg, K. Lammertsma, W. Uhl, *Dalton Trans.* **2012**, *41*, 9033; d) C. Appelt, J. C. Sloatweg, K. Lammertsma, W. Uhl, *Angew. Chem. Int. Ed.* **2013**, *52*, 4256; *Angew. Chem.* **2013**, *125*, 4350; e) W. Uhl, E.-U. Würthwein, *Top. Curr. Chem.* **2012**, *334*, 101; f) W. Uhl, C. Appelt, J. Backs, H. Westenberg, A. Wollschläger, J. Tannert, *Organometallics* **2014**, *33*, 1212; g) M. Devillard, R. Declercq, E. Nicolas, A. W. Ehlers, J. Backs, N. Saffon-Merceron, G. Bouhadir, J. C. Sloatweg, W. Uhl, D. Bourissou, *J. Am. Chem. Soc.* **2016**, *138*, 4917; h) L. Keweloh, H. Klöcker, E.-U. Würthwein, W. Uhl, *Angew. Chem. Int. Ed.* **2016**, *55*, 3212; *Angew. Chem.* **2016**, *128*, 3266.
- ⁴ a) A. Stute, G. Kehr, R. Fröhlich, G. Erker, *Chem. Commun.* **2011**, *47*, 4288; b) C. Rosorius, G. Kehr, R. Fröhlich, S. Grimme, G. Erker, *Organometallics* **2011**, *30*, 4211; c) A. Stute, G. Kehr, C. G. Daniliuc, R. Fröhlich, G. Erker, *Dalton Trans.* **2013**, *42*, 4487; d) C. Rosorius, C. G. Daniliuc, R. Fröhlich, G. Kehr, G. Erker, *J. Organomet. Chem.* **2013**, *744*, 149; e) Z. Jian, G. Kehr, C. G. Daniliuc, B. Wibbeling, G. Erker, *Dalton Trans.* **2017**, *46*, 11715.
- ⁵ a) F. Bertini, V. Lyaskoyskyy, B. J. J. Timmer, F. J. J. de Kanter, M. Lutz, A. W. Ehlers, J. C. Sloatweg, K. Lammertsma, *J. Am. Chem. Soc.* **2012**, *134*, 201; b) J. Yu, G. Kehr, C. G. Daniliuc, C. Bannwarth, S. Grimme, G. Erker, *Org. Biomol. Chem.* **2015**, *13*, 5783; c) K. Samigullin, I. Georg, M. Bolte, H.-W. Lerner, M. Wagner, *Chem. Eur. J.* **2016**, *22*, 3478; d) E. R. M. Habraken, L. C. Mens, M. Nieger, M. Lutz, A. W. Ehlers, J. C. Sloatweg, *Dalton Trans.* **2017**, *46*, 12284.
- ⁶ a) E. Theuergarten, J. Schlösser, D. Schlens, M. Freytag, C. G. Daniliuc, P. G. Jones, M. Tamm, *Dalton Trans.* **2012**, *41*, 9101; b) É. Dorkó, E. Varga, T. Gáti, T. Holczbauer, I. Pápai, H. Mehdi, T. Soós, *Synlett* **2014**, *25*, 1525.
- ⁷ W. Zheng, C. Pi, H. Wu, *Organometallics* **2012**, *31*, 4072.
- ⁸ For P/X (X=Ge, Sn, Pb) geminal FLPs, see: a) J. Schneider, K. M. Krebs, S. M. Freitag, K. Eichele, H. Schubert, L. Wesemann, *Chem. Eur. J.* **2016**, *22*, 9812; b) J. Schneider, C. P. Sindlinger, S. M. Freitag, H. Schubert, L. Wesemann, *Angew. Chem. Int. Ed.* **2017**, *56*, 333; *Angew. Chem.* **2017**, *129*, 339.
- ⁹ J. Possart, W. Uhl, *Organometallics* **2018**, *37*, 1314.
- ¹⁰ Selected examples: a) T. Soós, *Pure Appl. Chem.* **2011**, *83*, 667; b) D. W. Stephan, S. Greenberg, T. W. Graham, P. Chase, J. J. Hastie, S. J. Geier, J. M. Farrell, C. C. Brown, Z. M. Heiden, G. C. Welch, M. Ullrich, *Inorg. Chem.* **2011**, *50*, 12338; c) D. W. Stephan, *Org. Biomol. Chem.* **2012**, *10*, 5740; d) J. Paradies, *Synlett* **2013**, *24*, 777; e) J. Paradies, *Angew. Chem. Int. Ed.* **2014**, *53*, 3552; *Angew. Chem.* **2014**, *126*, 3624. For a recent review, see: f) W. Meng, X. Feng, H. Du, *Acc. Chem. Res.* **2018**, *51*, 191.
- ¹¹ For reviews on the ASM method, see: a) W.-J. van Zeist, F. M. Bickelhaupt, *Org. Biomol. Chem.* **2010**, *8*, 3118; b) I. Fernández, F. M. Bickelhaupt, *Chem. Soc. Rev.* **2014**, *43*, 4953; c) L. P. Wolters, F. M. Bickelhaupt, *WIREs Comput. Mol. Sci.* **2015**, *5*, 324; d) F. M. Bickelhaupt, K. N.

Houk, *Angew. Chem. Int. Ed.* **2017**, *56*, 10070; *Angew. Chem.* **2017**, *129*, 10204. See also: e) I. Fernández in *Discovering the Future of Molecular Sciences* (Ed.: B. Pignataro), Wiley-VCH, Weinheim, 2014, pp. 165–187.

¹² For reviews on the EDA method, see: a) F. M. Bickelhaupt, E. J. Baerends in *Reviews in Computational Chemistry, Vol. 15* (Eds.: K. B. Lipkowitz, D. B. Boyd), Wiley-VCH, Weinheim, 2000, pp. 1–86; b) M. von Hopffgarten, G. Frenking, *WIREs Comput. Mol. Sci.* **2012**, *2*, 43; c) L. Zhao, M. von Hopffgarten, D. M. Andrada, G. Frenking, *WIREs Comput. Mol. Sci.* **2018**, *8*, e1345.

¹³ D. Yepes, P. Jaque, I. Fernández, *Chem. Eur. J.* **2016**, *22*, 18801.

¹⁴ D. Yepes, P. Jaque, I. Fernández, *Chem. Eur. J.* **2018**, *24*, 8833.

¹⁵ a) T. A. Rokob, A. Hamza, I. Pápai, *J. Am. Chem. Soc.* **2009**, *131*, 10701; b) T. A. Rokob, I. Bakj, A. Stirling, A. Hamza, I. Pápai, *J. Am. Chem. Soc.* **2013**, *135*, 4425.

¹⁶ a) S. Grimme, H. Kruse, L. Goerigk, G. Erker, *Angew. Chem. Int. Ed.* **2010**, *49*, 1402; *Angew. Chem.* **2010**, *122*, 1444; b) B. Schirmer, S. Grimme, *Chem. Commun.* **2010**, *46*, 7942.

¹⁷ Gaussian 09, Revision D.01, M. J. Frisch, G. W. Trucks, H. B. Schlegel, G. E. Scuseria, M. A. Robb, J. R. Cheeseman, G. Scalmani, V. Barone, B. Mennucci, G. A. Petersson, H. Nakatsuji, M. Caricato, X. Li, H. P. Hratchian, A. F. Izmaylov, J. Bloino, G. Zheng, J. L. Sonnenberg, M. Hada, M. Ehara, K. Toyota, R. Fukuda, J. Hasegawa, M. Ishida, T. Nakajima, Y. Honda, O. Kitao, H. Nakai, T. Vreven, J. A. Montgomery, Jr., J. E. Peralta, F. Ogliaro, M. Bearpark, J. J. Heyd, E. Brothers, K. N. Kudin, V. N. Staroverov, R. Kobayashi, J. Normand, K. Raghavachari, A. Rendell, J. C. Burant, S. S. Iyengar, J. Tomasi, M. Cossi, N. Rega, J. M. Millam, M. Klene, J. E. Knox, J. B. Cross, V. Bakken, C. Adamo, J. Jaramillo, R. Gomperts, R. E. Stratmann, O. Yazyev, A. J. Austin, R. Cammi, C. Pomelli, J. W. Ochterski, R. L. Martin, K. Morokuma, V. G. Zakrzewski, G. A. Voth, P. Salvador, J. J. Dannenberg, S. Dapprich, A. D. Daniels, .: Farkas, J. B. Foresman, J. V. Ortiz, J. Cioslowski, D. J. Fox, Gaussian, Inc., Wallingford CT, 2009.

¹⁸ Y. Zhao, D. G. Truhlar, *Theor. Chem. Acc.* **2008**, *120*, 215.

¹⁹ F. Weigend, R. Ahlrichs, *Phys. Chem. Chem. Phys.* **2005**, *7*, 3297.

²⁰ C. Gonzalez, H. B. Schlegel, *J. Phys. Chem.* **1990**, *94*, 5523.

²¹ a) S. Miertuš, E. Scrocco, J. Tomasi, *Chem. Phys.* **1981**, *55*, 117; b) J. L. Pascual-Ahuir, E. Silla, I. Tuñon, *J. Comput. Chem.* **1994**, *15*, 1127; c) V. Barone, M. Cossi, *J. Phys. Chem. A* **1998**, *102*, 1995.

²² a) C. F. Guerra, J. G. Snijders, G. te Velde, E. J. Baerends, *Theor. Chem. Acc.* **1998**, *99*, 391; b) G. te Velde, F. M. Bickelhaupt, E. J. Baerends, C. F. Guerra, S. J. A. van Gisbergen, J. G. Snijders, T. Ziegler, *J. Comput. Chem.* **2001**, *22*, 931; c) ADF2017, SCM, Theoretical Chemistry, Vrije Universiteit, Amsterdam (The Netherlands), <http://www.scm.com>.

²³ a) E. van Lenthe, E. J. Baerends, *J. Comput. Chem.* **2003**, *24*, 1142; b) M. Franchini, P. H. T. Philipsen, E. van Lenthe, L. Visscher, *J. Chem. Theory Comput.* **2014**, *10*, 1994.

²⁴ a) E. van Lenthe, E. J. Baerends, J. G. Snijders, *J. Chem. Phys.* **1993**, *99*, 4597; b) E. van Lenthe, E. J. Baerends, J. G. Snijders, *J. Chem. Phys.* **1994**, *101*, 9783.

²⁵ a) D. H. Ess, K. N. Houk, *J. Am. Chem. Soc.* **2007**, *129*, 10646; b) D. H. Ess, K. N. Houk, *J. Am. Chem. Soc.* **2008**, *130*, 10187. See reference [11d] for a recent review.

²⁶ Selected representative examples: a) A. P. Bento, F. M. Bickelhaupt, *J. Org. Chem.* **2007**, *72*, 2201; b) I. Fernández, G. Frenking, E. Uggerud, *Chem. Eur. J.* **2009**, *15*, 2166; c) I. Fernández, F. M. Bickelhaupt, F. P. Cossío, *Chem. Eur. J.* **2009**, *15*, 13022; d) W.-J. van Zeist, F. M. Bickelhaupt, *Dalton Trans.* **2011**, *40*, 3028; e) I. Fernández, F. M. Bickelhaupt, F. P. Cossío, *Chem. Eur. J.* **2012**, *18*, 12395; f) L. P. Wolters, F. M. Bickelhaupt, *ChemistryOpen* **2013**, *2*, 106; g) I. Fernández, F. M. Bickelhaupt, F. P. Cossío, *Chem. Eur. J.* **2014**, *20*, 10791; h) E. D. Sosa Carrizo, F. M. Bickelhaupt, I. Fernández, *Chem. Eur. J.* **2015**, *21*, 14362; i) Y. García-Rodeja, M. Solà, F. M. Bickelhaupt, I. Fernández, *Chem. Eur. J.* **2016**, *22*, 1368; j) Y. García-Rodeja, I. Fernández,

Organometallics **2017**, *36*, 460; k) T. A. Hamlin, M. Swart, F. M. Bickelhaupt, *ChemPhysChem* **2018**, *19*, 1315.

²⁷ M. P. Mitoraj, A. Michalak, T. Ziegler, *J. Chem. Theory Comput.* **2009**, *5*, 962.

²⁸ a) J. E. Leffler, *Science* **1953**, *117*, 340; b) G. S. J. Hammond, *J. Am. Chem. Soc.* **1953**, *75*, 334.

²⁹ a) I. Fernández, *Phys. Chem. Chem. Phys.* **2014**, *16*, 7662; b) I. Fernández, F. M. Bickelhaupt, *Chem. Asian J.* **2016**, *11*, 3297; c) I. Fernández, *Eur. J. Org. Chem.* **2018**, 1394, and references therein.

Supporting Information

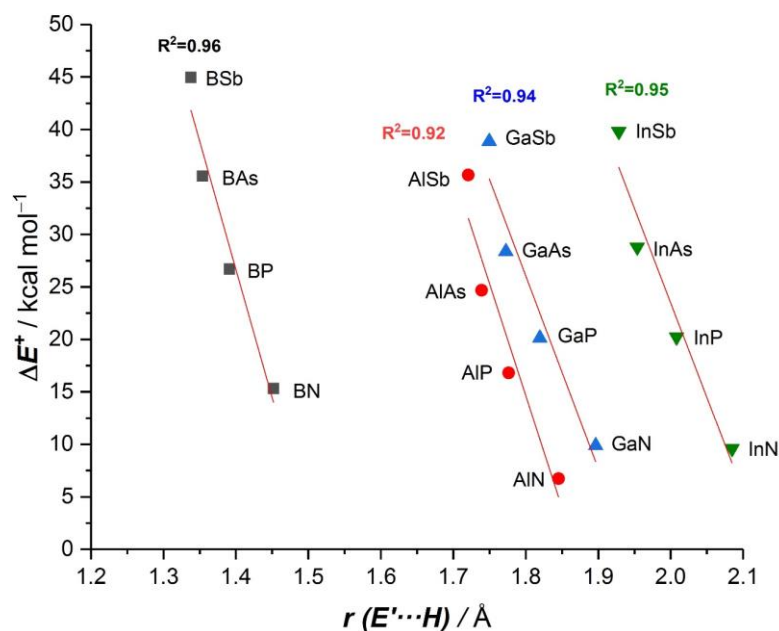


Figure 3.S1. Plot of the computed activation barriers (ΔE^\ddagger) vs the $E'\cdots H$ distance in the corresponding transition states. All data were computed at the M06-2X/def2-TZVPP level.

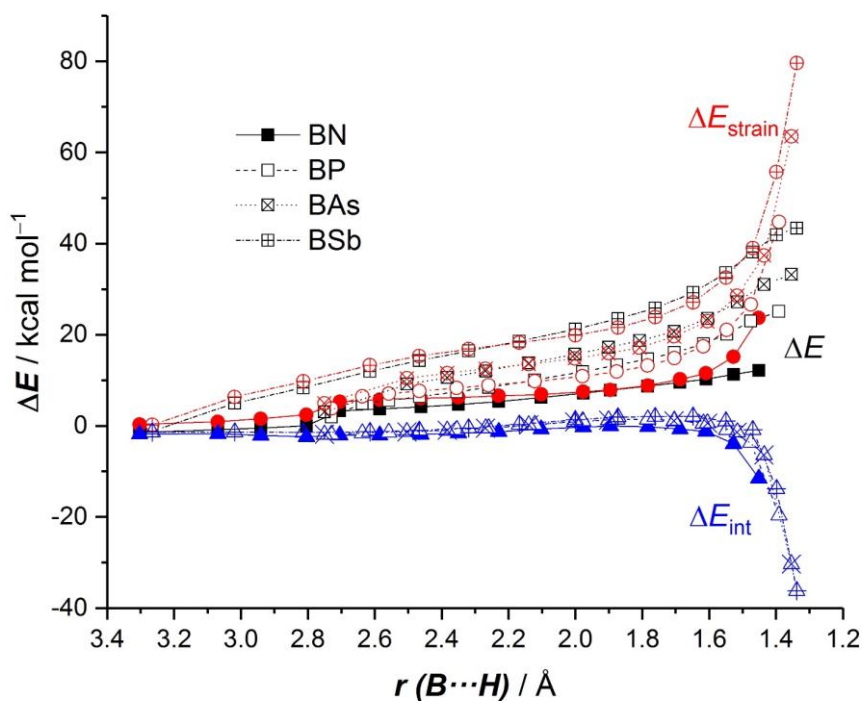


Figure 3.S2. Comparative activation strain diagrams of the dihydrogen activation reactions mediated by geminal B/N (solid lines), B/P (dashed lines), B/As (dotted lines), and B/Sb (dashed dotted lines) FLPs along the reaction coordinate projected onto the forming $B\cdots H$ bond length. All data were computed at the M06-2X/def2-TZVPP level and are referenced to the isolated reactants.

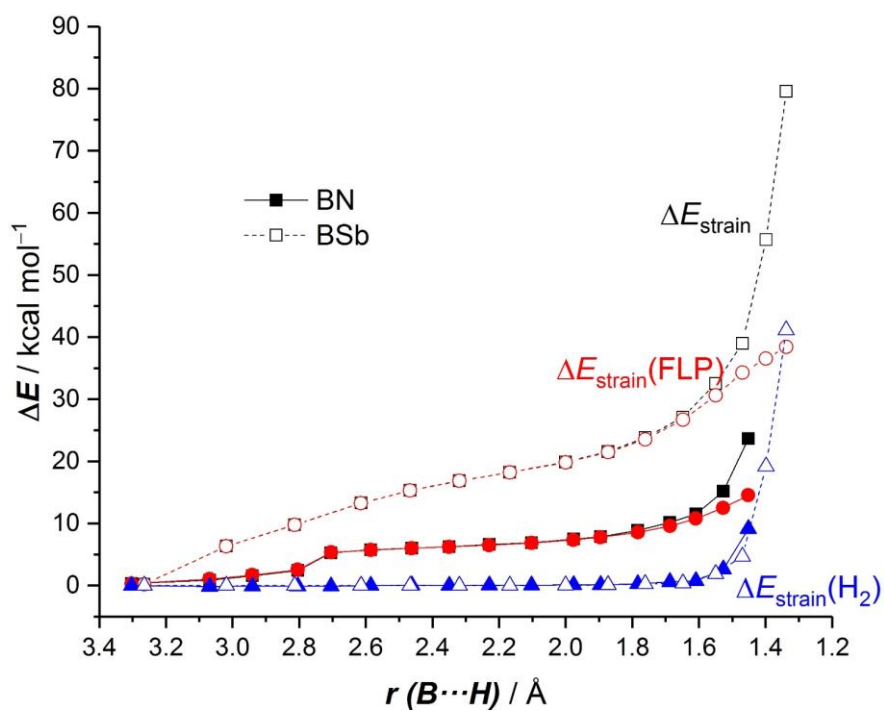


Figure 3.S3. Partitioning of the computed total strain energy ($\Delta E_{\text{strain}}^{\text{total}}$) into its components, $\Delta E_{\text{strain}}^{\text{FLP}}$ (FLP) and $\Delta E_{\text{strain}}^{\text{H}_2}$, for the dihydrogen activation reactions mediated by geminal B/N (solid lines) and B/Sb (dashed lines) FLPs along the reaction coordinate projected onto the forming B \cdots H bond length. All data were computed at the M06-2X/def2-TZVPP level and are referenced to the isolated reactants.

IV. CHAPTER 2

Understanding the reactivity of neutral geminal Group 14 element/phosphorus frustrated Lewis pairs

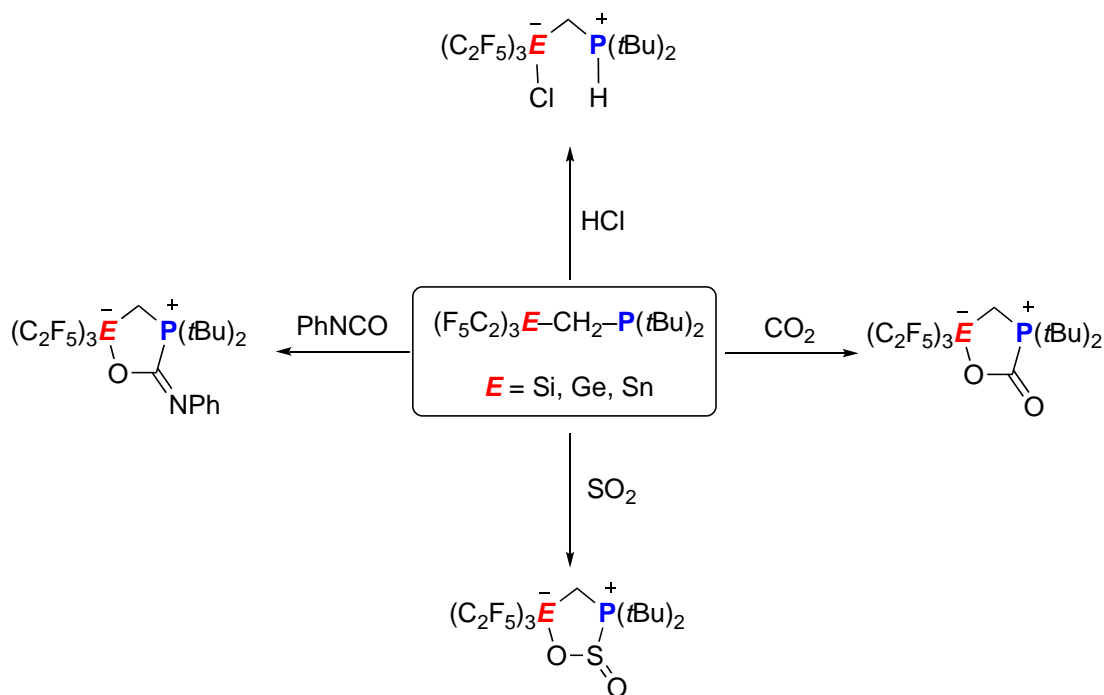
The influence of the nature of the Group 14 elements (E = Si, Ge, Sn) on the reactivity of $(F_5C_2)_3E-CH_2-P(tBu)_2$ geminal frustrated Lewis pairs (FLPs) has been computationally explored by means of density functional theory calculations. To this end, the experimentally described activation reactions of CO_2 and phenyl isocyanate have been investigated and compared to the analogous processes involving the corresponding B/P geminal FLP. It is found that the reactivity of these species is kinetically enhanced when going down the Group 14 (Si < Ge < Sn). This trend of reactivity is quantitatively analyzed in detail by means of the activation strain model of reactivity in combination with the energy decomposition analysis method, which identify the interaction energy between the deformed reactants as the main factor controlling the reactivity of these Group 14 containing geminal FLPs.

J. Phys. Chem. A, **2019**, *123*, 10095-10101.
(Invited for the special issue "Paul Geerlings Festschrift")

Introduction

Since the seminal report by Stephan and co-workers in 2006 of a metal-free molecule that was able to reversibly activate dihydrogen,¹ the chemistry of the so-called frustrated Lewis pairs (FLPs) has experienced an impressive development.²⁻⁷ These species are typically composed of a simple combination of a sterically encumbered Lewis acid and Lewis base, where the severe steric demands hamper the formation of a classical donor–acceptor bond. This particular bonding situation leads to a unique reactivity which allows the relatively facile activation of small molecules (such as H₂, CO, CO₂, N₂O, SO₂,...) or the metal-free hydrogenation of polar multiple bonds, among other processes.²

Aiming at enhancing the activity of these systems, a good number of different FLPs have been prepared. Among them, geminal FLPs, *i.e.*, systems where the donor/acceptor atoms are separated by a carbon atom, should be especially highlighted because their preorganized molecular structure results in a significant enhancement of the reactivity as compared to their corresponding intermolecular FLP counterparts.⁸⁻¹⁴ Although most of these geminal FLPs are typically based on the combination of B/N and B/P pairs, other systems including heavier Group 13 elements^{15,16} or transition metal fragments¹⁷⁻²¹ in their structures have been prepared to tune the Lewis acidity/basicity of the FLP antagonists. In this sense, Mitzel and co-workers have recently prepared a series of Group 14 element containing neutral geminal FLPs, *i.e.*, (F₅C₂)₃E–CH₂–P(*t*Bu)₂, E = Si,²² Ge,²³ Sn,²⁴ which have been proven to readily activate small molecules such as CO₂, SO₂, CS₂, HCl, or phenyl isocyanate (Scheme 4.1), therefore resembling the reactivity of more traditional B/P FLPs.



Scheme 4.1. Reactivity of Group 14 element containing geminal FLPs described by Mitzel and co-workers (see references 22-24).

Despite this evident similarity, very little is known about the actual influence of the nature of the Group 14 element on the reactivity of these novel geminal FLPs. For this reason, herein we decided to computationally explore the reactivity of these species to gain detailed quantitative insight into the impact of the nature of the Group 14 element on the reactivity. To this end, we selected the CO_2 and phenyl isocyanate activation reactions that were experimentally studied by Mitzel and coworkers.²²⁻²⁴ The reactivity trends will be analyzed by means of the combination of the activation strain model (ASM) of reactivity²⁵⁻²⁹ and the energy decomposition analysis (EDA) method.^{30,31} This approach will be used because it has been particularly useful to rationalize the reactivity of both intermolecular and intramolecular (*i.e.*, geminal) FLPs.³²⁻³⁵ Indeed, based on the ASM-EDA method, we proposed an orbital-controlled mechanism, complementary to the widely accepted mechanisms suggested independently by Pápai^{36,37} and Grimme,^{38,39} where the degree of cooperativity between the key donor–acceptor orbital interactions along the reaction coordinate can be used as an indicator of the reaction barrier. Thus, given the good performance of this approach in the chemistry of FLPs, the role of the Group 14 element in the geminal $(\text{F}_5\text{C}_2)_3\text{E}-\text{CH}_2-\text{P}(\text{tBu})_2$ ($\text{E} = \text{Si, Ge, Sn}$) FLPs **1** will be described and compared to their parent B/P

(Ph₂B–CH₂–P(*t*Bu)₂, **2**) counterpart, experimentally described by Slootweg, Lammertsma, and co-workers.¹¹

Theoretical Methods and Computational Details

Geometry optimizations of the molecules were performed without symmetry constraints using the Gaussian09 suite of programs⁴⁰ employing the meta-hybrid M06-2X exchange–correlation functional⁴¹ combined with the double- ζ quality def2-SVP basis set.^{42,43} Reactants and products were characterized by frequency calculations and have positive definite Hessian matrices. Transition structures (TS's) show only one negative eigenvalue in their diagonalized force constant matrices, and their associated eigenvectors were confirmed to correspond to the motion along the reaction coordinate under consideration using the intrinsic reaction coordinate (IRC) method.⁴⁴ In addition, the vibrational calculation provides the thermal Gibbs energy corrections by using the gas ideal-rigid-rotor-harmonic-oscillator approximation. Single-point energy refinements were carried out on the gas-phase optimized M06-2X/def2-SVP geometries at the domain based local pair-natural coupled-cluster, DLPNO-CCSD(T),⁴⁵ as implemented in the program Orca 4.0.1⁴⁶ using the def2-TZVP basis sets^{42,43} and the SMD⁴⁷ solvation model. This level is denoted SMD(toluene)-DLPNO-CCSD-(T)/def2-TZVP//M06-2X/def2-SVP. Quite similar energy values were computed at the PCM(toluene)-M06-2X/def2-TZVPP//M06-2X/def2-SVP level, and for this reason, this level was used for the ASM calculations. In addition, calculations including relativistic effects indicate that the influence of these effects on the activation barriers is negligible (see Table 4.S1 in the Supporting Information).

Activation strain model of reactivity and Energy decomposition analysis

As the ASM method has been the focus of recent reviews,²⁵⁻²⁹ herein we only briefly summarize the basics of this approach. This method is a systematic development of the energy decomposition analysis (EDA) method (see below) used initially to understand the nature of chemical bonding in stable molecules. Within this method, also known as distortion/interaction model,²⁸ the potential energy surface $\Delta E(\zeta)$ is decomposed, along the reaction coordinate ζ , into two main contributions, namely the strain $\Delta E_{\text{strain}}(\zeta)$ associated with the deformation (or

distortion) experienced by the reactants during the transformation plus the interaction $\Delta E_{\text{int}}(\zeta)$ between these increasingly deformed reactants:

$$\Delta E(\zeta) = \Delta E_{\text{strain}}(\zeta) + \Delta E_{\text{int}}(\zeta)$$

Herein the reaction coordinate is defined as the projection of the IRC onto the forming P...C distance. This reaction coordinate ζ undergoes a well-defined change in the course of the reaction from the separate reactants (or the initial reaction complexes) to the equilibrium distance in the corresponding transition states.

The interaction $\Delta E_{\text{int}}(\zeta)$ between the strained reactants can be further partitioned into chemically meaningful contributions by means of the EDA method.^{30,31} Thus, $\Delta E_{\text{int}}(\zeta)$ is decomposed into the following terms along the reaction coordinate:

$$\Delta E_{\text{int}}(\zeta) = \Delta V_{\text{elstat}}(\zeta) + \Delta E_{\text{Pauli}}(\zeta) + \Delta E_{\text{orb}}(\zeta)$$

The term $\Delta V_{\text{elstat}}(\zeta)$ corresponds to the classical electrostatic interaction between the unperturbed charge distributions of the deformed reactants and is usually attractive. The Pauli repulsion $\Delta E_{\text{Pauli}}(\zeta)$ comprises the destabilizing interactions between occupied orbitals and is responsible for any steric repulsion. The orbital interaction $\Delta E_{\text{orb}}(\zeta)$ accounts for charge transfer (interaction between occupied orbitals on one moiety with unoccupied orbitals on the other, including HOMO–LUMO interactions) and polarization (empty-occupied orbital mixing on one fragment due to the presence of another fragment). Moreover, the NOCV (natural orbital for chemical valence)⁴⁸ extension of the EDA method has been also used to further partitioning the ΔE_{orb} term. The EDA-NOCV approach provides pairwise energy contributions for each pair of interacting orbitals to the total bond energy.

Energy decomposition analyses were carried out using the ADF.2017 program^{49,50} at the same DFT level in conjunction with the triple- ζ quality TZ2P basis set⁵¹ on the geometries optimized at the M06-2X/def2-SVP level. This level is therefore denoted M06-2X/TZ2P//M06-2X/def2-SVP.

Results and Discussion

Our calculations suggest that, regardless of the Group 14 element present in the $(\text{F}_5\text{C}_2)_3\text{E}-\text{CH}_2-\text{P}(\text{tBu})_2$ FLP **1**, both the CO_2 and $\text{PhN}=\text{C}=\text{O}$ activation reactions occur in a concerted manner via a five-membered transition state (**TS**) leading to the corresponding zwitterionic adduct **3** (Figure 4.1). In addition, the process begins in most cases with the formation of an initial van der Waals reactant complex (**RC**) which lies ca. 2–3 kcal/mol below the separate reactants (the formation of these species becomes endergonic when thermal free-energy corrections are included). The located saddle points (see also Figure 4.S1 in the Supporting Information) are therefore associated with the simultaneous formation of the P–C and E–O bonds with the concomitant elongation of the reactive C=O double bond of CO_2 or $\text{PhN}=\text{C}=\text{O}$. The computed reaction profiles strongly resemble those reported for dihydrogen activation reactions mediated by related neutral geminal FLPs involving Group 13 and 15 elements as Lewis antagonists,^{11,32,33,52} thus indicating similar reactivity of these systems. Indeed, a similar reaction profile is also computed for the process involving the parent $\text{Ph}_2\text{B}-\text{CH}_2-\text{P}(\text{tBu})_2$ FLP **2** (Figure 4.1), therefore confirming that the replacement of the highly acidic BPh_2 moiety by the $\text{E}(\text{F}_5\text{C}_2)_3$ fragment does not modify the concerted nature of the transformation.

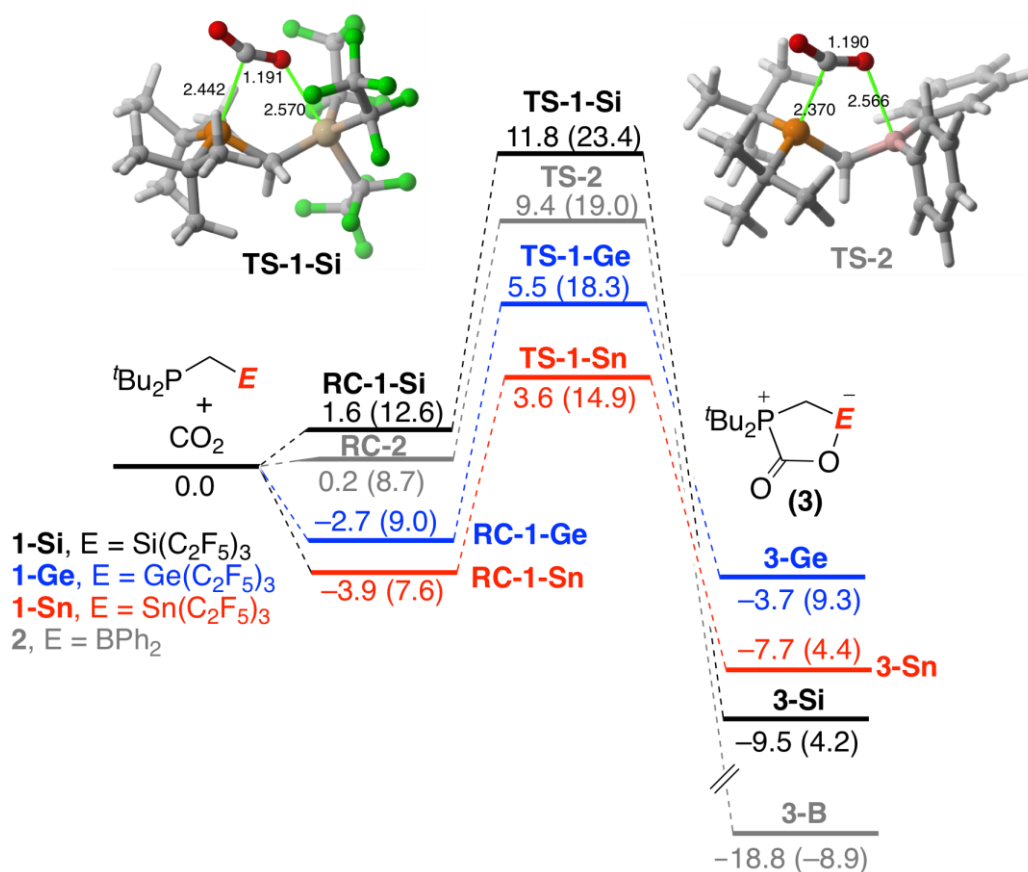


Figure 4.1. Computed reaction profiles for the CO₂ activation reaction mediated by geminal FLPs (1). Relative energies (free energies within parentheses) and bond distances are given in kcal/mol and angstroms, respectively. All data have been computed at the SMD(toluene)-DLPNO-CCSD(T)/def2-TZVP//M06-2X-def2-SVP level.

From the data in Figure 4.1 and Table 4.1, it becomes clear that for both activation reactions the corresponding barrier heights decrease when going down the Group 14 (*i.e.*, ΔE^\ddagger decreases in the order E = Si > Ge > Sn). The computed trend is consistent with the experimental observation that whereas the CO₂ activation involving the silicon FLP **1-Si** occurs at room temperature,²² the analogous process involving its tin counterpart **1-Sn** proceeds at -70 °C.^{24,53} In addition, our calculations are fully consistent with the experimental observation that CO₂ is easily and reversibly bound to FLP **1-Sn** at room temperature, as the barrier for the CO₂ release from **3-Sn** is rather low ($\Delta G^\ddagger = 10.5$ kcal/mol). Closer inspection to the data in Table 4.1 indicates that the **1-Ge** and **1-Sn** geminal FLPs can be even more reactive, from a kinetic point of view, than the parent B/P FLP **2**. This is of course due to the strong electron-withdrawing effect of the three C₂F₅ substituents directly attached to the Group 14 element which greatly enhance the Lewis acidity of the E(C₂F₅)₃ moiety. Indeed, when the fluorine atoms of these

groups were replaced by hydrogen atoms, the CO₂ activation reaction mediated by the corresponding FLP **1-Sn**^{*} ((H₅C₂)₃Sn-CH₂-P(*t*Bu)₂) does not occur. Instead, only the expected nucleophilic addition of the phosphorus lone pair to the electrophilic carbonyl moiety of CO₂ takes place, thus confirming the negligible Lewis acidity of the Sn(C₂H₅)₃ fragment as compared to Sn(C₂F₅)₃.

Table 4.1. Computed activation and reaction energies (in kcal/mol, free energies in parentheses) for geminal FLP-mediated CO₂ and PhNCO activation reactions.

| Reaction | ΔE^\ddagger (ΔG^\ddagger) ^a | ΔE_R (ΔG_R) ^b |
|--|--|--|
| (F ₅ C ₂) ₃ Si-CH ₂ -P(<i>t</i> Bu) ₂ (1-Si) + CO ₂ | 11.8 (23.4) | -9.5 (4.2) |
| (F ₅ C ₂) ₃ Ge-CH ₂ -P(<i>t</i> Bu) ₂ (1-Ge) + CO ₂ | 8.2 (18.3) | -3.7 (9.3) |
| (F ₅ C ₂) ₃ Sn-CH ₂ -P(<i>t</i> Bu) ₂ (1-Sn) + CO ₂ | 7.5 (14.9) | -7.7 (4.4) |
| Ph ₂ B-CH ₂ -P(<i>t</i> Bu) ₂ (2) + CO ₂ | 9.4 (19.0) | -18.8 (-8.9) |
| (F ₅ C ₂) ₃ Si-CH ₂ -P(<i>t</i> Bu) ₂ (1-Si) + PhNCO | 20.0 (28.0) | -21.9 (-5.2) |
| (F ₅ C ₂) ₃ Ge-CH ₂ -P(<i>t</i> Bu) ₂ (1-Ge) + PhNCO | 10.3 (25.0) | -15.8 (1.6) |
| (F ₅ C ₂) ₃ Sn-CH ₂ -P(<i>t</i> Bu) ₂ (1-Sn) + PhNCO | 8.1 (19.8) | -22.0 (-5.8) |
| Ph ₂ B-CH ₂ -P(<i>t</i> Bu) ₂ (2) + PhNCO | 11.6 (20.3) | -33.3 (-19.1) |

^aActivation barriers, ΔE^\ddagger , computed as $\Delta E^\ddagger = E(\mathbf{TS}) - E(\mathbf{RC})$, when $E(\mathbf{RC}) < 0$ kcal/mol, otherwise $\Delta E^\ddagger = E(\mathbf{TS}) - E(\text{FLP}) - E(\text{small molecule})$. Free activation barriers, ΔG^\ddagger , computed as $\Delta G^\ddagger = E(\mathbf{TS}) - E(\text{FLP}) - E(\text{small molecule})$. ^bReaction energies, ΔE_R , computed as $\Delta E_R = E(\text{adduct-3}) - E(\text{FLP}) - E(\text{small molecule})$. All data have been computed at the SMD(toluene)-DLPNO-CCSD(T)/def2-TZVP//M06-2X/def2-SVP level.

The activation strain model (ASM) of reactivity was applied next to gain quantitative insight into the factors controlling the above-commented reactivity trends. To this end, we focused on the activation reaction of phenyl isocyanate mediated by geminal FLPs **1-Si**, **1-Ge** and **1-Sn**. Figure 4.2 shows the corresponding activation strain diagrams (ASDs) from the initial reactant complexes up to the respective transition states along the IRC projected onto the P...C bond forming distance. The considered activation reactions exhibit rather similar ASDs in the sense that the interaction energy between the deformed reactants, measured by the ΔE_{int} term, becomes clearly stabilizing only at the proximity of the transition state region. This behavior resembles that observed by us in the dihydrogen activation reactions mediated by related geminal Group 13/Group 15 FLPs^{32,33} therefore confirming the reactivity likeness of these species. Closer inspection of the different ASDs in Figure 4.2 reveals that the ΔE_{int} term is decisive to govern the different reactivity of FLPs **1**. Thus, the heaviest system

1-Sn benefits from the strongest interaction between the deformed reactants along the entire reaction coordinate. Similarly, the ΔE_{int} term is also slightly more stabilizing for the process involving **1-Ge** than for the process involving the lighter FLP **1-Si**. As a result, the computed trend in reactivity (**1-Si** < **1-Ge** < **1-Sn**) follows the trend in the computed interaction between the deformed reactants. Despite that, the interaction term is not solely responsible for the computed different reactivity. As shown in Figure 4.2, the heavier systems **1-Ge** and **1-Sn** also benefit from a less destabilizing strain energy, albeit to a lesser extent than the ΔE_{int} term. This is mainly due to the fact that the heavier systems already possess an initial equilibrium geometry that better fits into the corresponding transition state structure as compared to its silicon counterpart. Therefore, the stronger interaction between the reactants along the entire process together with a lower energy required to deform them from their equilibrium geometries become the factors which lead to the computed reactivity enhancement of the Group 14/P geminal FLPs when moving down from E = Si to E = Sn.

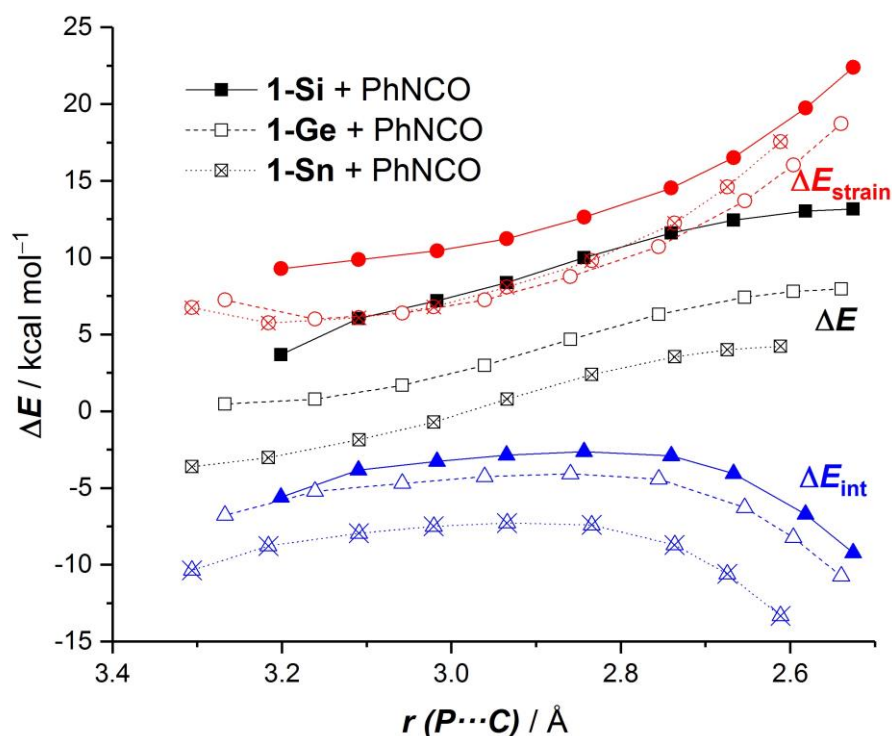


Figure 4.2. Comparative activation-strain diagrams of the phenyl isocyanate activation reactions mediated by geminal FLPs **1-Si** (solid lines), **1-Ge** (dashed lines), and **1-Sn** (dotted lines) along the reaction coordinate projected onto the forming P...C bond distance. All data have been computed at the PCM(toluene)-M06-2X/def2-TZVPP//M06-2X/def2-SVP level.

The crucial role of the interaction between the reactants along the process, which mainly controls the entire transformation, deserves further analysis. To this end, the energy decomposition analysis (EDA) method was next applied to quantitatively assess the different contributors to the total interaction energy. Figure 4.3 graphically shows the evolution of the different EDA terms along the reaction coordinate, once again from the initial reactant complexes up to the respective transition states, for the activation reaction of phenyl isocyanate mediated by geminal FLPs **1-Si**, **1-Ge**, and **1-Sn**. According to the data in Figure 4.3, it becomes evident that the major contributor to the total interaction between the deformed reactants is the electrostatic attractions (ΔV_{elstat}), which is not surprising considering the zwitterionic nature of the reaction product (**3**) in all cases. The orbital interaction, measured by the ΔE_{orb} term, between the reactants, although lower than ΔV_{elstat} , is also remarkable (its contribution amounts ca. 38% to the total interaction in the corresponding transition states).

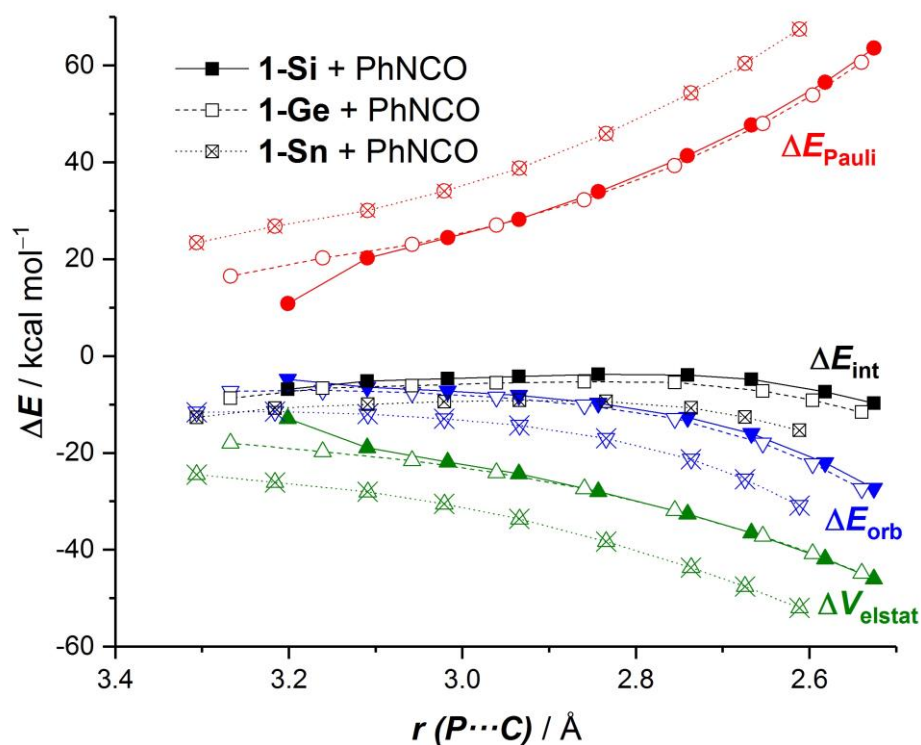


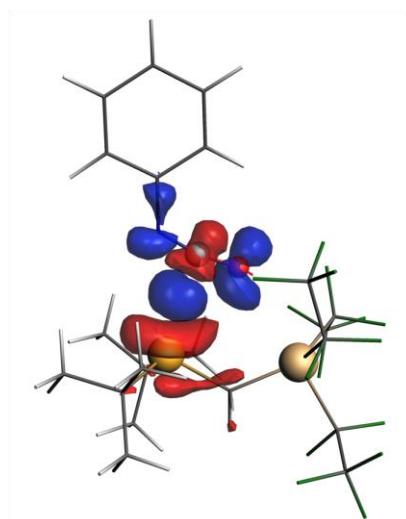
Figure 4.3. Comparative energy decomposition analyses of the phenyl isocyanate activation reactions mediated by geminal FLPs **1-Si** (solid lines), **1-Ge** (dashed lines) and **1-Sn** (dotted lines) along the reaction coordinate projected onto the forming P...C bond distance. All data have been computed at the M06-2X/TZ2P//M06-2X/def2-SVP level.

This finding is compatible with the two widely accepted models for the activation of small molecules by FLPs, namely, Pápai’s electron-transfer model,^{36,37} which is based on cooperative orbital interactions, and Grimme’s electric-field model,^{38,39} where electrostatic interactions are key. Both attractive terms (ΔV_{elstat} and ΔE_{orb}) offset the strong destabilizing effect of the Pauli repulsion term, ΔE_{Pauli} , and as a result, the total interaction energy between the reactants is stabilizing along the entire process, and particularly, at the transition state region.

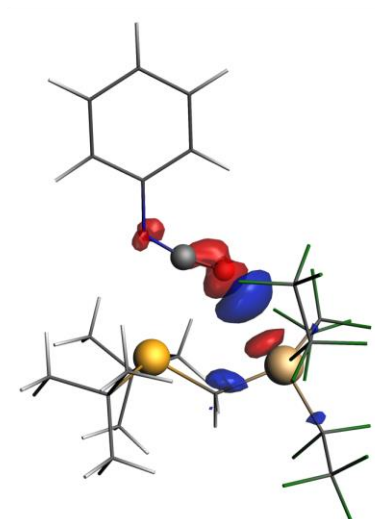
When comparing the different EDA terms for the processes involving **1-Si** and **1-Ge**, one realizes that the origin of the slightly stronger total interaction between the reactants computed for the reaction involving the heavier FLP is mainly due to slightly stronger orbital interactions (and less destabilizing ΔE_{Pauli} , albeit to a lesser extent). The situation for the transformation involving **1-Sn** is much more different. In this particular case, both the electrostatic and orbital interactions are significantly stronger than those for the analogous processes involving **1-Si** or **1-Ge**. For instance, at the same consistent P...C forming bond distance of 2.7 Å, $\Delta V_{\text{elstat}} = -37.4$ kcal/mol, and $\Delta E_{\text{orb}} = -15.7$ kcal/mol for the **1-Si** + PhNCO reaction, whereas much more stabilizing (*i.e.*, more negative) values were computed for the analogous **1-Sn** + PhNCO reaction ($\Delta V_{\text{elstat}} = -45.9$ kcal/mol and $\Delta E_{\text{orb}} = -23.7$ kcal/mol).

The nature of the molecular orbital interactions and their relative contribution to the total orbital interaction term ΔE_{orb} can be further analyzed by means of the NOCV extension of the EDA method. According to the EDA-NOCV data, a main pairwise orbital interaction ($\Delta E(\rho_1)$) dominates the ΔE_{orb} term. This interaction corresponds to the donation of electron density from the lone pair of the phosphorus atom of the FLP (*i.e.*, the HOMO of species **1**) to the LUMO of the phenyl isocyanate, that is, the LP(P)→ $\pi^*(\text{C}=\text{O})$ molecular orbital interaction (see Figure 4.4). According to the evolution of this molecular orbital interaction (see Figure 4.5), the LP(P)→ $\pi^*(\text{C}=\text{O})$ charge transfer continuously reinforces and dominates up to the transition state region, where the reverse donation from the negatively charged oxygen atom of the isocyanate to the E(C₂F₅)₃ moiety ($\Delta E(\rho_2)$, Figure 4.4) starts to take place. Therefore, both key donor–acceptor orbital interactions occur along the reaction path but at different stages of the transformation, which confirms our previously reported cooperative and asynchronous mode of action of FLPs in related dihydrogen activation reactions.^{32,34}

(a) **1-Si + PhNCO**

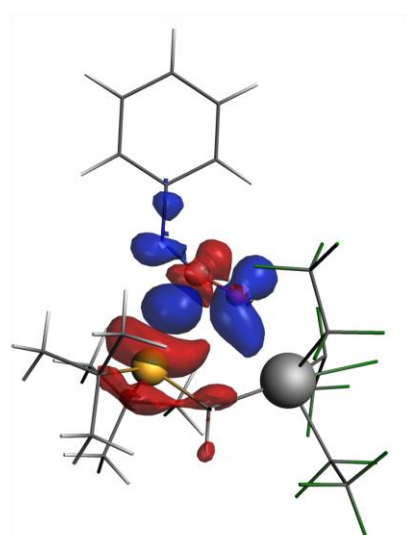


$$\Delta E(\rho_1) = -8.4 \text{ kcal/mol}$$

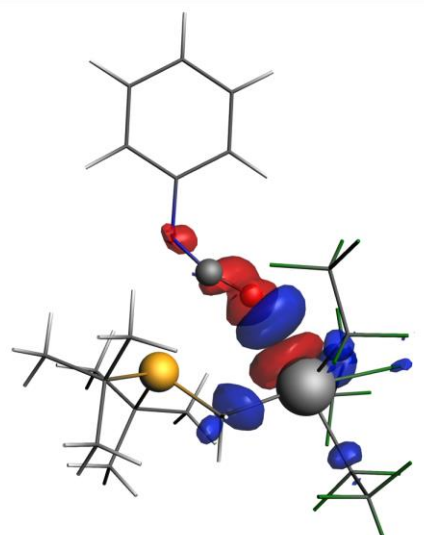


$$\Delta E(\rho_2) = -2.8 \text{ kcal/mol}$$

(b) **1-Sn + PhNCO**



$$\Delta E(\rho_1) = -12.6 \text{ kcal/mol}$$



$$\Delta E(\rho_2) = -5.1 \text{ kcal/mol}$$

Figure 4.4. Contour plots of NOCV deformation densities $\Delta\rho$ and associated energies $\Delta E(\rho)$ (in kcal/mol) for the main orbital interactions between PhNCO and geminal FLPs **1-Si** (a) and **1-Sn** (b) computed at the same consistent P...C forming bond distance of 2.7 Å. Electronic charge flows from red to blue. All data were computed at the M06-2X/TZ2P//M06-2X/def2-TZVPP level.

Interestingly, the data gathered in Figure 4.4 and 4.5 clearly indicate that both orbital interactions are significantly stronger for the process involving the heavier FLP **1-Sn** than for the analogous process involving its silicon counterpart **1-Si**. For instance, at the same consistent P...C forming bond distance of 2.7 Å, $\Delta E(\rho_1) = -12.6$ kcal/mol and $\Delta E(\rho_2) = -5.1$ kcal/mol for the **1-Sn** + PhNCO

reaction, whereas much less stabilizing (*i.e.*, less negative) values were computed for the analogous reaction involving **1-Si** ($\Delta E(\rho_1) = -8.4$ kcal/mol and $\Delta E(\rho_2) = -2.8$ kcal/mol). The higher $\Delta E(\rho_1)$ orbital interaction in the process involving **1-Sn** can be directly ascribed to a more efficient overlap between the involved molecular orbitals ($S = 0.045$ and 0.032 , for the reactions involving **1-Sn** and **1-Si** respectively, at the same consistent $P\cdots C$ forming bond distance of 2.7 Å). Therefore, according to our EDA-NOCV calculations, the origin of the much stronger interaction between the reactants for the process involving the heaviest geminal FLP **1-Sn** as compared to its lighter congeners can be found in the combination of stronger electrostatic and orbital (mainly the $LP(P) \rightarrow \pi^*(C=O)$ interaction) attractions between the reactants along the entire coordinate, and particularly at the transition state region. These factors together with the much lower distortion energy (ΔE_{strain}) computed for this particular system are ultimately responsible for the enhanced reactivity of the geminal FLP **1-Sn** as compared to **1-Si** or **1-Ge**.

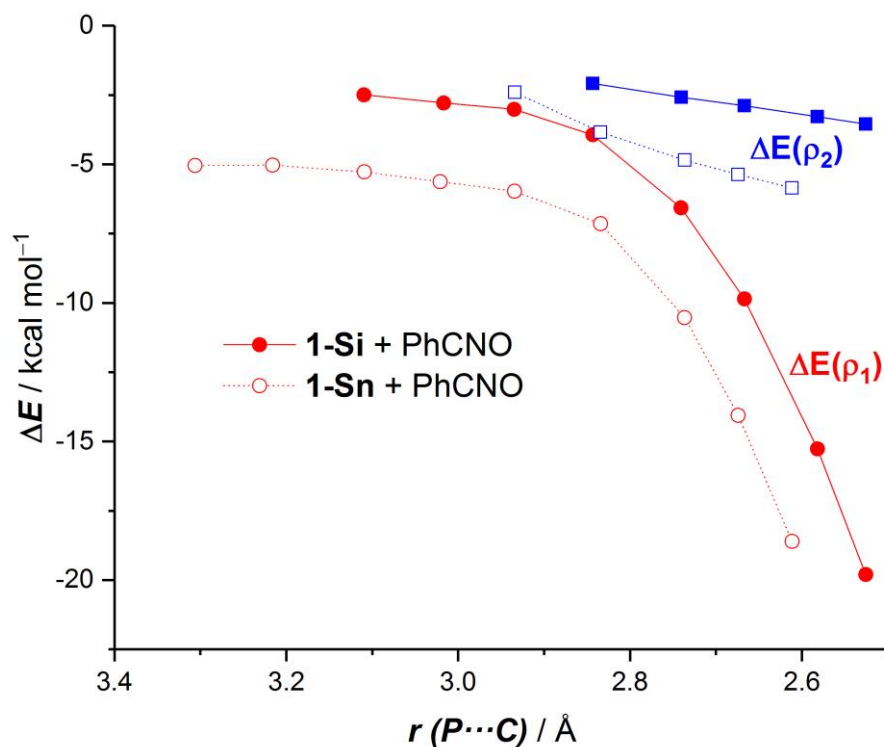


Figure 4.5. Evolution of the NOCV components for the PhNCO activation reactions mediated by FLP **1-Si** (solid lines) and **1-Sn** (dotted lines) along the reaction coordinate projected onto the forming $P\cdots C$ bond distance. All data have been computed at the M06-2X/TZ2P//M06-2X/def2-SVP level.

Conclusion

From the computational study reported herein, the following conclusion can be drawn: (i) Group 14 element containing geminal frustrated Lewis pairs react similarly to more traditional B/P geminal FLPs when the Group 14 element is surrounded by strong electron withdrawing substituents. (ii) In this sense, both the CO₂ and phenyl isocyanate activation reactions proceed in a concerted manner through the corresponding five-membered transition states, which lead to the experimentally observed zwitterionic reaction products. (iii) Despite that, significant reactivity differences are observed when modifying the nature of the Group 14 element. Thus, the process becomes kinetically favored (*i.e.*, it proceeds with a lower activation barrier) when going down in Group 14 (reactivity order: E = Si < Ge < Sn). (iv) According to the ASM approach, this is mainly due to the comparatively much stronger interaction between the deformed reactants along the entire coordinate computed for the reactions involving the heavier systems. In addition, the required strain energy is also less destabilizing for these processes as compared to the analogous activation reaction involving their silicon counterpart. (v) The crucial role of the interaction energy has been also analyzed by means of the EDA-NOCV method. According to this method, the combination of the much stronger electrostatic and orbital (mainly the LP(P)→π*(C=O) interaction) attractions between the reactants along the entire coordinate, and particularly at the transition state region, is responsible for the stronger total interaction computed for the process involving the geminal FLP **1-Sn** as compared to **1-Si**. (vi) Our work has therefore shed more light into the so far poorly understood influence of the nature of the Group 14 element on the reactivity of geminal FLPs, which may be useful for the future rational design of novel systems.

References

- ¹ G. C. Welch, R. R. San Juan, J. D. Masuda, D. W. Stephan, *Science* **2006**, *314*, 1124-1126.
- ² D. W. Stephan, G. Erker, *Angew. Chem., Int. Ed.*, **2010**, *49*, 46-76.
- ³ G. Erker, *Pure Appl. Chem.*, **2012**, *84*, 2203-2217.
- ⁴ D. W. Stephan, G. Erker, *Chem. Sci.*, **2014**, *5*, 2625-2641.
- ⁵ D. W. Stephan, G. Erker, *Angew. Chem., Int. Ed.*, **2015**, *54*, 6400-6441.
- ⁶ D. W. Stephan, *Acc. Chem. Res.*, **2015**, *48*, 306-316.
- ⁷ D. W. Stephan, *Science* **2016**, *354*, aaf7229.
- ⁸ A. Stute, G. Kehr, R. Fröhlich, G. Erker, *Chem. Commun.*, **2011**, *47*, 4288-4290.
- ⁹ C. Rosorius, G. Kehr, R. Fröhlich, S. Grimme, G. Erker, *Organometallics* **2011**, *30*, 4211-4219.
- ¹⁰ A. Stute, G. Kehr, C. G. Daniliuc, R. Fröhlich, G. Erker, *Dalton Trans.* **2013**, *42*, 4487-4499.
- ¹¹ F. Bertini, V. Lyaskovskyy, B. J. J. Timmer, F. J. J. de Kanter, M. Lutz, A. W. Ehlers, J. C. Slootweg, K. Lammertsma, *J. Am. Chem. Soc.*, **2012**, *134*, 201-204.
- ¹² É. Dorkó, E. Varga, T. Gáti, T. Holczbauer, I. Pápai, H. Mehdi, T. Soós, *Synlett* **2014**, *25*, 1525-1528.
- ¹³ K. Samigullin, I. Georg, M. Bolte, H.-W. Lerner, M. Wagner, *Chem. Eur. J.*, **2016**, *22*, 3478-3484.
- ¹⁴ Z. Jian, G. Kehr, C. G. Daniliuc, B. Wibbeling, G. Erker, *Dalton Trans.*, **2017**, *46*, 11715-11721.
- ¹⁵ W. Zheng, C. Pi, H. Wu, *Organometallics* **2012**, *31*, 4072-4075.
- ¹⁶ J. Possart, W. Uhl, *Organometallics* **2018**, *37*, 1314-1323.
- ¹⁷ A. M. Chapman, M. F. Haddow, D. F. Wass, *J. Am. Chem. Soc.*, **2011**, *133*, 18463-18478.
- ¹⁸ D. F. Wass, A. M. Chapman, *Top. Curr. Chem.*, **2013**, *334*, 261-280.
- ¹⁹ A. T. Normand, P. Richard, C. Balan, C. G. Daniliuc, G. Kehr, G. Erker, P. Le Grendre, *Organometallics* **2015**, *34*, 2000-2011.
- ²⁰ X. Xu, G. Kehr, C. G. Daniliuc, G. Erker, *J. Am. Chem. Soc.*, **2015**, *137*, 4550-4557.
- ²¹ J. Campos, *J. Am. Chem. Soc.*, **2017**, *139*, 2944-2947.
- ²² B. Waerder, M. Pieper, L. A. Körte, T. A. Kinder, A. Mix, B. Neumann, H.-G. Stammler, N. W. Mitzel, *Angew. Chem., Int. Ed.*, **2015**, *54*, 13416-13419.
- ²³ T. A. Kinder, R. Pior, S. Blomeyer, B. Neumann, H.-G. Stammler, N. W. Mitzel, *Chem. Eur. J.*, **2019**, *25*, 5899-5903.
- ²⁴ P. Holtkamp, F. Friedrich, E. Stratmann, A. Mix, B. Neumann, H.-G. Stammler, N. W. Mitzel, *Angew. Chem., Int. Ed.*, **2019**, *58*, 5114-5118.
- ²⁵ W.-J. van Zeist, F. M. Bickelhaupt, *Org. Biomol. Chem.*, **2010**, *8*, 3118-3127.
- ²⁶ I. Fernández, F. M. Bickelhaupt, *Chem. Soc. Rev.*, **2014**, *43*, 4953-4967.
- ²⁷ L. P. Wolters, F. M. Bickelhaupt, *WIREs Comput. Mol. Sci.*, **2015**, *5*, 324-343.
- ²⁸ F. M. Bickelhaupt, K. N. Houk, *Angew. Chem., Int. Ed.*, **2017**, *56*, 10070-10086.
- ²⁹ See also: I. Fernández, In *Discovering the future of molecular sciences*, Pignataro, B., Ed.; Wiley-VCH: Weinheim, 2014; pp 165-187.
- ³⁰ M. von Hopffgarten, G. Frenking, *WIREs Comput. Mol. Sci.*, **2012**, *2*, 43-62.
- ³¹ L. Zhao, M. von Hopffgarten, D. M. Andrada, G. Frenking, *WIREs Comput. Mol. Sci.* **2018**, *8*, No. e1345.
- ³² D. Yepes, P. Jaque, I. Fernández, *Chem. Eur. J.*, **2016**, *22*, 18801-18809.
- ³³ D. Yepes, P. Jaque, I. Fernández, *Chem. Eur. J.*, **2018**, *24*, 8833-8840.

- ³⁴ J. J. Cabrera-Trujillo, I. Fernández, *Chem. Eur. J.*, **2018**, *24*, 17823-17831.
- ³⁵ J. J. Cabrera-Trujillo, I. Fernández, *Inorg. Chem.*, **2019**, *58*, 7828-7836.
- ³⁶ T. A. Rokob, A. Hamza, I. Pápai, *J. Am. Chem. Soc.*, **2009**, *131*, 10701-10710.
- ³⁷ T. A. Rokob, I. Bakó, A. Stirling, A. Hamza, I. Pápai, *J. Am. Chem. Soc.*, **2013**, *135*, 4425-4437.
- ³⁸ S. Grimme, H. Kruse, L. Goerigk, G. Erker, *Angew. Chem., Int. Ed.*, **2010**, *49*, 1402-1405.
- ³⁹ B. Schirmer, S. Grimme, *Chem. Commun.*, **2010**, *46*, 7942-7944.
- ⁴⁰ M. J. Frisch, G. W. Trucks, H. B. Schlegel, G. E. Scuseria, M. A. Robb, J. R. Cheeseman, G. Scalmani, V. Barone, B. Mennucci, G. A. Petersson, et al. Gaussian 09, Revision D.01; Gaussian, Inc.: Wallingford, CT, 2009.
- ⁴¹ Y. Zhao, D. G. Truhlar, *Theor. Chem. Acc.*, **2008**, *120*, 215-241.
- ⁴² F. Weigend, R. Ahlrichs, *Phys. Chem. Chem. Phys.*, **2005**, *7*, 3297-3305.
- ⁴³ F. Weigend, *Phys. Chem. Chem. Phys.*, **2006**, *8*, 1057-1065.
- ⁴⁴ C. Gonzalez, H. B. Schlegel, *J. Phys. Chem.*, **1990**, *94*, 5523-5527.
- ⁴⁵ C. Riplinger, B. Sandhoefer, A. Hansen, F. Neese, *J. Chem. Phys.*, **2013**, *139*, 134101-134113.
- ⁴⁶ F. Neese, *WIREs Comput. Mol. Sci.*, **2018**, *8*, No. e1327.
- ⁴⁷ A. V. Marenich, C. J. Cramer, D. G. Truhlar, *J. Phys. Chem. B*, **2009**, *113*, 6378-6396.
- ⁴⁸ M. P. Mitoraj, A. Michalak, T. Ziegler, *J. Chem. Theory Comput.*, **2009**, *5*, 962-975.
- ⁴⁹ G. te Velde, F. M. Bickelhaupt, E. J. Baerends, C. Fonseca Guerra, S. J. A. van Gisbergen, J. G. Snijders, T. Ziegler, *J. Comput. Chem.*, **2001**, *22*, 931-967.
- ⁵⁰ E. J. Baerends, T. Ziegler, A. J. Atkins, J. Autschbach, O. Baseggio, D. Bashford, A. Bérces, F. M. Bickelhaupt, C. Bo, P. M. Boerrigter, et al. ADF2019; SCM, Theoretical Chemistry, Vrije Universiteit: Amsterdam, The Netherlands, <http://www.scm.com>
- ⁵¹ J. G. Snijders, P. Vernooijs, E. J. Baerends, *At. Data Nucl. Data Tables* **1981**, *26*, 483-509.
- ⁵² J. J. Cabrera-Trujillo, I. Fernández, *Chem. Commun.*, **2019**, *55*, 675-678.
- ⁵³ Moreover, the computed reaction rate for the reaction involving **1-Sn** and PhCNO is, according to the Eyring equation, $k^{\text{TST}} = 0.019 \text{ s}^{-1}$, which is translated into $t_{1/2} = 36 \text{ s}$. This indicates that the process should occur almost instantaneously, as experimentally observed (see ref 24). This finding further supports the selected computational methodology for this work.

Supporting Information

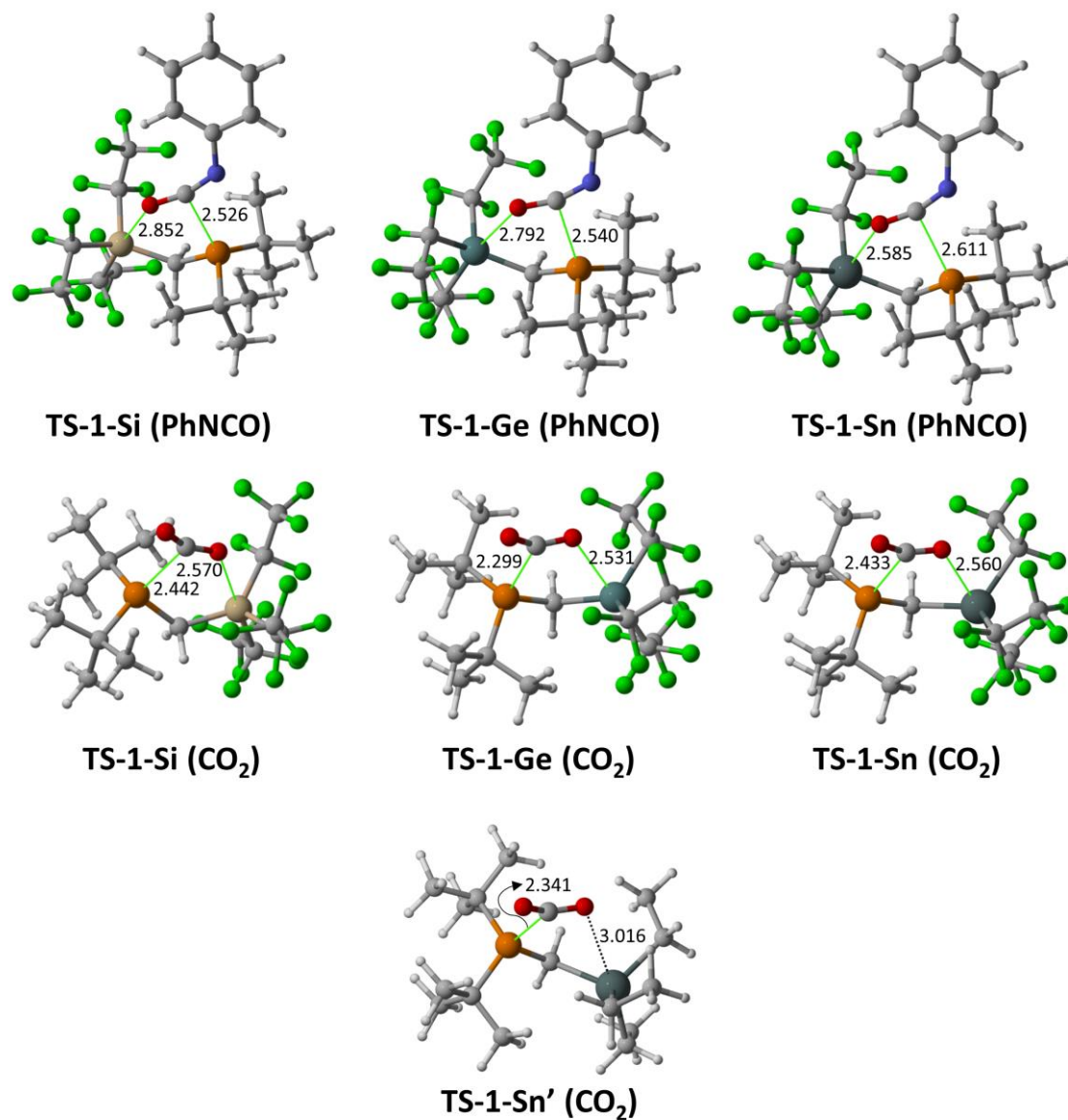


Figure 4.S1. Optimized transition state geometries for the **FLP 1-E** (E=Si, Ge, Sn) and **FLP 1-Sn'** mediated CO₂ and phenyl isocyanate activation reactions. Bond lengths are given in angstroms.

Table 4.S1. Effect of the inclusion of relativistic effects in the calculations on the activation barriers.

| Reaction | ΔE^\ddagger ^[a] | ΔE^\ddagger ^[b] |
|------------------------|------------------------------------|------------------------------------|
| 1-Si + CO ₂ | 10.0 | 10.5 |
| 1-Ge + CO ₂ | 7.6 | 7.8 |
| 1-Sn + CO ₂ | 6.9 | 6.7 |
| 1-Si + PhNCO | 18.5 | 18.3 |
| 1-Ge + PhNCO | 11.3 | 11.3 |
| 1-Sn + PhNCO | 9.8 | 10.2 |

Computed activation barriers, $\Delta E^\ddagger = E(\text{TS}) - E(\text{RC})$. [a] Computed at the PCM(toluene)-M06-2X/def2-TZVPP//M06-2X/def2-SVP level. [b] Computed at the ZORA-COSMO(toluene)-M06-2X/TZ2P//M06-2X/def2-SVP.

V. CHAPTER 3

Aromaticity can enhance the reactivity of P-donor/borole frustrated Lewis pairs

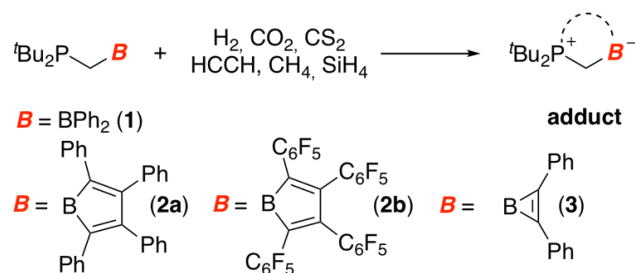
Geminal frustrated Lewis pairs (FLPs) having a borole fragment as the Lewis acid partner constitute really promising candidates to achieve facile small molecule activation reactions. The predicted enhanced reactivity of these species, as compared to more traditional FLPs, finds its origin in the loss of the antiaromatic character of the borole moiety along the reaction coordinate.

Chem. Commun., **2019**, 55, 675-678.

Frustrated Lewis pairs (FLPs) are species typically composed of a pair of a sterically encumbered Lewis acid and Lewis base, which prevents the formation of a classical donor–acceptor bond between both centers.¹ Due to this particular bonding situation, these compounds exhibit a unique reactivity as a result of the cooperative action of the FLP antagonists. Thus, FLPs have emerged as potential metal-free catalysts able to, among other processes, activate small molecules (H₂, CO, CO₂, SO₂, N₂O, etc.).¹ Owing to this rich reactivity, in most cases restricted to transition metals, the chemistry of FLPs has attracted much attention since the seminal report by Stephan and co-workers in 2006.²

Much progress has been made, particularly in recent years, to produce more active systems. Among them, intramolecular FLPs (where the Lewis pairs are part of the same molecule)³ and systems having transition-metal fragments in their structures⁴ should be specially highlighted. Despite that, the vast majority of FLPs are still based on the combination of B/N or B/P pairs, with the boron center typically attached to electron-withdrawing substituents. Aiming at developing more active FLPs, herein we shall introduce a novel concept in FLP chemistry: aromaticity as the key factor enhancing the reactivity of FLPs.

To this end, we focused on a particular FLP, the geminal *t*Bu₂P–CH₂–BPh₂ (**1**) system, synthesized by Slootweg, Lammertsma and co-workers,⁵ whose preorganized structure results in a remarkable reactivity for small molecule activations without the need for strongly electron-withdrawing substituents attached to the boron center. We computationally⁶ replaced the BPh₂ moiety by the sterically hindered tetraphenyl-borole fragment (**2a**, Scheme 5.1), whose antiaromatic nature was confirmed previously by Braunschweig, some of us and co-workers.⁷ Our initial hypothesis follows: the gain of aromaticity in the borole moiety during the activation of a small molecule (H₂, CO₂, CS₂, HC≡CH, SiH₄ and CH₄ in our calculations, Scheme 5.1) should result in a gain of stability in both the corresponding transition state, therefore leading to a lower barrier transformation, and in the final zwitterionic adduct, therefore making the process thermodynamically more favourable.



Scheme 5.1. FLP-mediated small molecule activation reactions considered herein.

In agreement with previous results involving the dihydrogen activation mediated by the parent FLP **1**⁵ and related geminal systems,⁸ our calculations confirm that the heterolytic H₂-splitting occurs in a concerted manner via a five-membered transition state (**TS-1**) and through the formation of an initial van der Waals reactant complex (**RC-1**) which lies ca. 2 kcal mol⁻¹ above the separate reactants (this energy difference becomes higher when including thermal free energy corrections, see Fig. 5.1). Although the computed reaction profile for the process involving the 4π-electrons borole-containing FLP **2a** is rather similar, the dihydrogen activation becomes both kinetically and thermodynamically ($\Delta\Delta E^\ddagger = 5.5$ kcal mol⁻¹ and $\Delta\Delta E_{\text{R}} = 12.5$ kcal mol⁻¹, respect to the separated reactants) more favoured than the analogous process involving FLP **1**.^{9,10} This finding is fully consistent with the Hammond postulate.¹¹ Indeed, closer inspection of the transition states depicted in Fig. 5.1 clearly reveals that **TS-2a** is earlier than its **TS-1** counterpart. Not surprisingly, the replacement of the phenyl groups by the more electron-withdrawing pentafluorophenyl groups in the borole moiety leads to an even more active FLP (compound **2b**) as confirmed by the low barrier and high exothermicity computed for the analogous dihydrogen activation ($\Delta E^\ddagger = 11.7$ kcal mol⁻¹ and $\Delta E_{\text{R}} = -26.4$ kcal mol⁻¹, see Table 5.1). In sharp contrast, the process involving FLP **3**, having a 2π-electrons aromatic borirene fragment in its structure, proceeds with a much higher barrier ($\Delta E^\ddagger = 31.9$ kcal mol⁻¹) in an endothermic reaction ($\Delta E_{\text{R}} = 5.0$ kcal mol⁻¹, see Table 5.1). Therefore, these results point to a clear influence of the aromaticity of the B-heterocycle on the reactivity of these geminal FLPs.

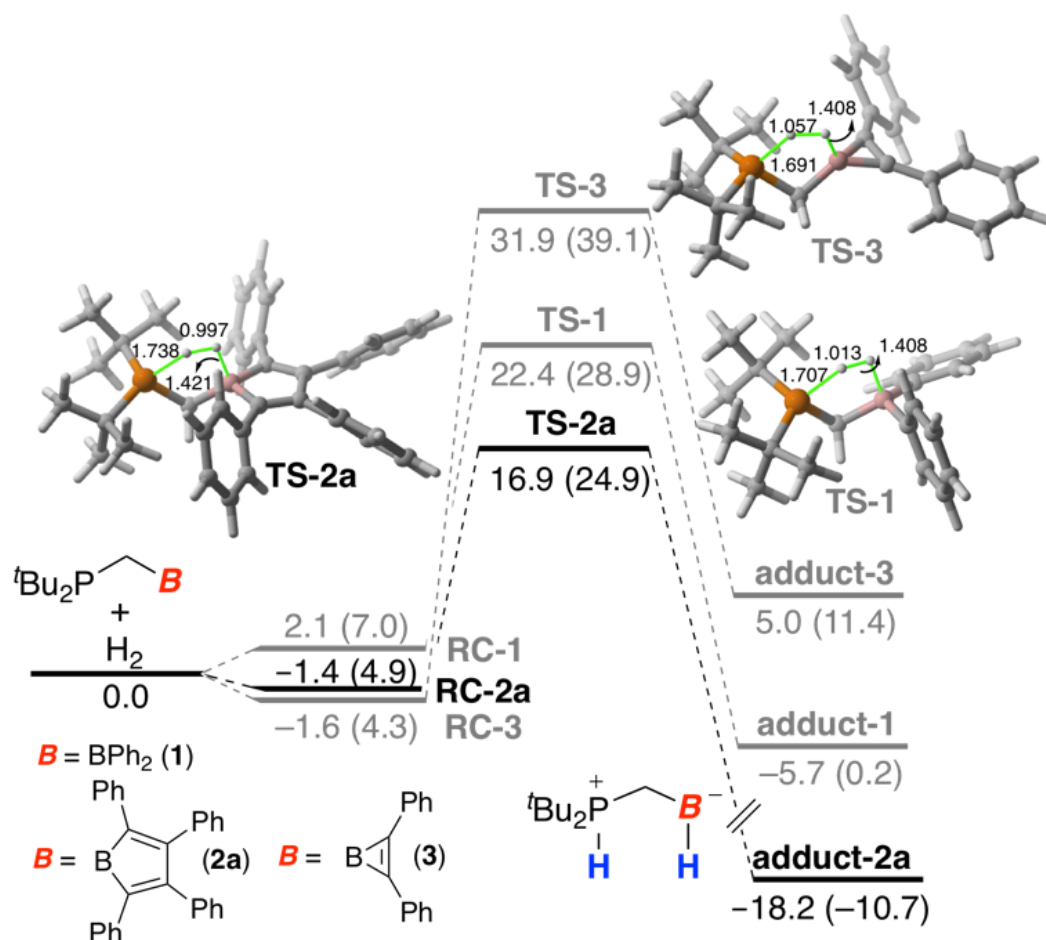


Figure 5.1. Comparative computed reaction profiles for the dihydrogen activation mediated by FLPs **1**, **2a** and **3**. Relative energies (free energies within parentheses) and bond distances are given in kcal mol⁻¹ and angstroms, respectively. All data have been computed at the PCM(toluene)-M06-2X/def2-TZVPP//M06-2X/def2-SVP level.

Similar concerted reaction profiles were also found for the activation of the rest of the small molecules considered in this study (for the corresponding transition state structures involving **2a**, see Fig. 5.S1 in the Supporting Information). Indeed, in all cases, the processes involving the borole-substituted FLPs **2a** and **2b** systematically occur with lower activation barriers and are more exothermic than the analogous processes involving the parent system **1** (Table 5.1). Strikingly, even the C_{sp³}-H activation of methane, a process which has been not achieved in FLP chemistry so far, could be feasible by using the highly active borole-containing FLP **2b** in polar solvents such as dichloromethane ($\Delta E^\ddagger = 32.1$ kcal mol⁻¹ and $\Delta E_R = -16.4$ kcal mol⁻¹, see Table 5.1). Therefore, our calculations predict that the borole containing FLPs (**2a,b**) are really promising candidates to achieve facile small molecule activation reactions. As expected, FLP **3**, which possesses the 2 π -electrons

aromatic borirene, is confirmed to be the least active system in all cases (see Table 5.1).¹²

Table 5.1. Computed activation and reaction energies (in kcal mol⁻¹) for geminal FLP-mediated small molecule activation reactions.

| Reaction | ΔE^\ddagger ^a | ΔG^\ddagger ^a | ΔE_R ^b | ΔG_R ^b |
|--|----------------------------------|----------------------------------|---------------------------|---------------------------|
| 1 + H ₂ | 22.4 (21.1) | 28.9 (27.5) | -5.7 (-6.9) | 0.2 (-1.1) |
| 2a + H ₂ | 16.9 (16.0) | 24.9 (24.0) | -18.2 (-18.8) | -10.7 (-11.3) |
| 2b + H ₂ | 11.7 (11.7) | 19.9 (19.9) | -26.4 (-25.8) | -19.3 (-18.7) |
| 3 + H ₂ | 31.9 (31.3) | 39.1 (38.5) | 5.0 (2.8) | 11.4 (9.2) |
| 1 + CO ₂ | 7.5 (9.6) | 17.0 (19.1) | -18.6 (-18.9) | -8.7 (-9.0) |
| 2a + CO ₂ | 5.8 (7.5) | 17.1 (18.7) | -23.0 (-22.2) | -10.4 (-9.6) |
| 2b + CO ₂ | 5.7 (7.2) | 17.4 (18.9) | -26.6 (-26.3) | -14.8 (-14.5) |
| 3 + CO ₂ | - ^c | | -6.6 (-5.8) | 6.4 (7.2) |
| 1 + CS ₂ | 13.6 (13.7) | 23.8 (23.8) | -22.4 (-25.0) | -10.1 (-12.7) |
| 2a + CS ₂ | 8.3 (6.3) | 20.4 (18.4) | -30.7 (-33.6) | -18.1 (-21.0) |
| 2b + CS ₂ | 7.1 (5.4) | 19.4 (17.7) | -33.9 (-36.9) | -20.8 (-23.8) |
| 3 + CS ₂ | - ^c | | -14.3 (-16.1) | -2.0 (-3.8) |
| 1 + HC≡CH | 23.0 (22.2) | 33.1 (32.3) | -17.3 (-17.6) | -6.9 (-7.3) |
| 2a + HC≡CH | 16.0 (15.2) | 27.3 (26.6) | -25.9 (-26.3) | -14.4 (-14.9) |
| 2b + HC≡CH | 11.0 (11.0) | 21.3 (21.3) | -30.8 (-30.8) | -19.7 (-19.7) |
| 3 + HC≡CH | 29.5 (29.4) | 40.1 (39.9) | -6.7 (-8.1) | 2.7 (1.3) |
| 1 + SiH ₄ | 30.8 (30.4) | 41.3 (41.0) | -3.9 (-4.7) | 6.3 (5.6) |
| 2a + SiH ₄ | 25.3 (25.6) | 36.5 (36.8) | -13.3 (-13.8) | -2.1 (-2.5) |
| 2b + SiH ₄ | 20.1 (21.3) | 30.6 (31.8) | -23.0 (-22.4) | -12.1 (-11.5) |
| 3 + SiH ₄ | 38.1 (38.4) | 49.5 (49.8) | 8.2 (7.1) | 18.7 (17.6) |
| 1 + CH ₄ | 44.5 (44.2) | 54.7 (54.3) | 2.5 (1.5) | 12.4 (11.4) |
| 2a + CH ₄ | 39.2 (38.6) | 49.9 (49.3) | -5.3 (-6.5) | 5.7 (4.5) |
| 2b + CH ₄ | 32.4 (32.8) | 42.1 (42.5) | -14.1 (-13.8) | -4.0 (-3.7) |
| 2b + CH ₄ ^d | 32.1 (32.0) | 41.8 (41.7) | -16.4 (-16.5) | -6.4 (-6.4) |
| 3 + CH ₄ | 55.6 (55.5) | 65.7 (65.6) | 12.1 (10.4) | 22.6 (20.9) |

^a Activation barriers, ΔE^\ddagger , computed as $\Delta E^\ddagger = E(\text{TS}) - E(\text{FLP}) - E(\text{small molecule})$. ^b Reaction energies, ΔE_R , computed as $\Delta E_R = E(\text{adduct}) - E(\text{FLP}) - E(\text{small molecule})$. ^c See reference 12.

^d Data computed using dichloromethane as solvent. Plain values have been computed at the PCM(toluene)-M06-2X/def2-TZVPP//M06-2X/def2-SVP level whereas values within parentheses were computed at the SMD(toluene)-DLPNO-CCSD(T)/def2-TZVP//M06-2X/def2-SVP level.

The influence of the aromaticity of the borole moiety in the reactivity was next analysed in detail. To this end, we first assessed the aromaticity of the key points along the reaction coordinate of borole-FLP mediated dihydrogen activation reaction (*i.e.* initial reactant **2a**, transition state **TS-2a** and corresponding adduct). To this end, we computed the respective isotropic Nuclear Independent Chemical Shift (NICS) values,¹³ NICS(0),¹⁴ as well as its out-of-plane tensor component computed 1 Å above, NICS(1)_{zz}, which typically performs better for planar rings.¹⁵ The data in Table 5.2 and Fig. 5.2 clearly indicate that the highly antiaromatic character of the FLP **2a** (NICS(1)_{zz} = +24.9 ppm) vanishes along the reaction coordinate. This finding becomes evident in the final zwitterionic adduct which can be considered as a non-aromatic species in view of its negligible NICS(1)_{zz} value of

1.3 ppm ($\text{NICS}(0) = 1.4$ ppm). A similar conclusion can be drawn by applying the Anisotropy of the Induced Current Density (ACID) method,¹⁶ which can be used to visualize the nature of the electronic circulation within the ring. As depicted in Fig. 5.2, the strong paratropic (*i.e.* antiaromatic, anticlockwise vectors) ring current in **2a** becomes weaker and weaker as the reaction progresses. Indeed, in the final adduct, the attachment of the hydride to the boron atom provokes a clear interruption of the induced current within the five-membered ring, therefore making this species non-aromatic, which is fully consistent with the computed NICS values.

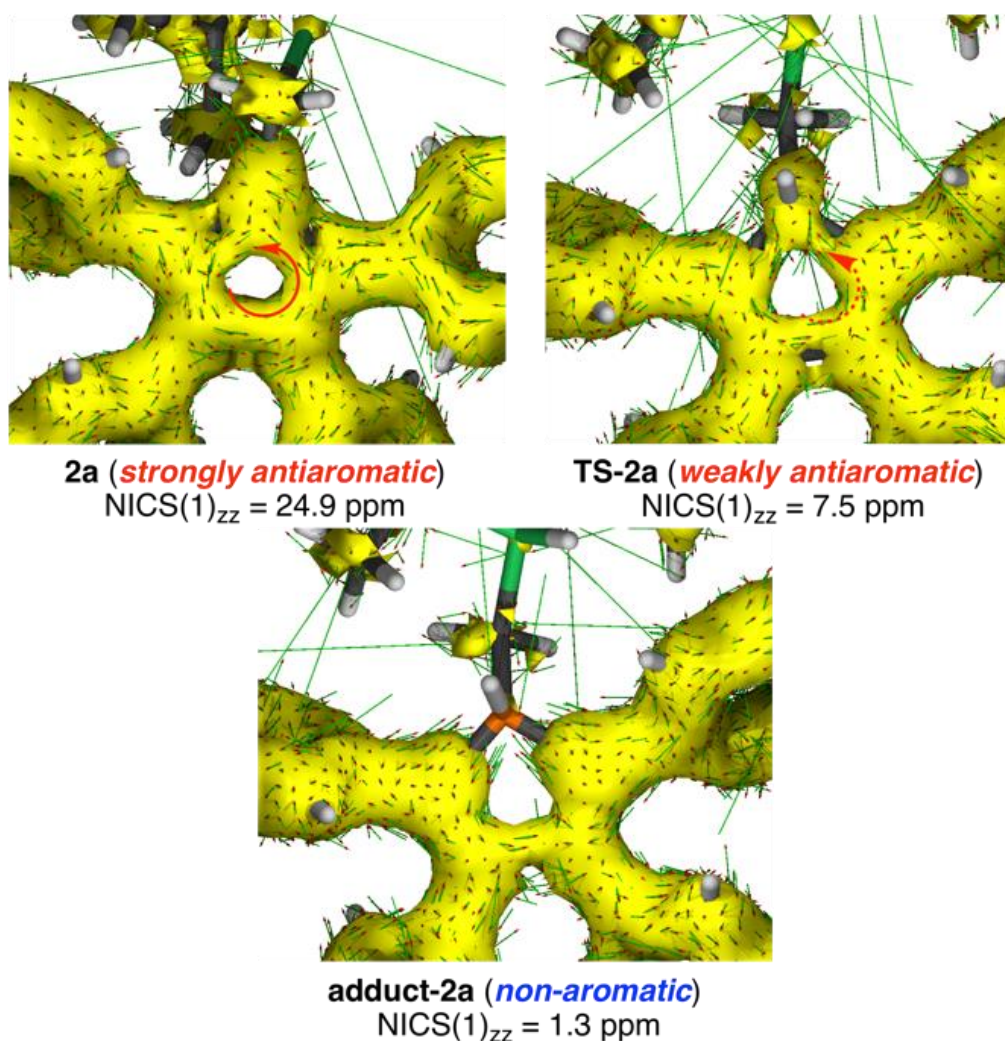


Figure 5.2. Computed ACID plots for the key points of the dihydrogen activation reaction mediated by FLP **2a** (isosurface value of 0.04).

The above results clearly confirm that FLP **2a** becomes more and more aromatic (*i.e.* less and less antiaromatic) as the activation reaction progresses. A similar aromaticity trend is found for the analogous process involving FLP **2b** and for the rest of the small molecule activation reactions considered in this study

(Table 5.2). At variance, the opposite trend is found for the process involving FLP **3**. In this particular case, the initial aromaticity of the 2π -borirene fragment (NICS(1)_{zz} = -15.5 ppm) becomes lower and lower as the reaction progresses. This loss of aromaticity, *i.e.* loss of stability, is reflected into the high barrier and reaction energies computed for the processes involving this FLP, which are even higher than the values computed for the parent FLP system **1** (see Table 5.1). Therefore, it becomes evident that the aromaticity of the B-heterocycle efficiently controls the reactivity of these geminal FLPs.

Table 5.2. Computed isotropic NICS(0) and refined NICS(1)_{zz} (within parentheses), in ppm, of the key points along the reaction coordinate of the considered FLP-mediated small molecule activation reactions.

| Reaction | FLP | TS | Adduct |
|------------------------------|----------------------|----------------------|---------------------|
| 2a + H ₂ | 13.9 (24.9) | 4.2 (7.5) | 1.4 (1.3) |
| 2b + H ₂ | 14.0 (24.4) | 4.4 (7.7) | 1.7 (1.8) |
| 3 + H ₂ | (-15.5) ^a | (-9.4) ^a | (-6.0) ^a |
| 2a + CO ₂ | 13.9 (24.9) | 11.4 (20.7) | 3.8 (7.5) |
| 2b + CO ₂ | 14.0 (24.4) | 7.9 (13.7) | 4.2 (7.5) |
| 3 + CO ₂ | (-15.5) ^a | - ^b | (-8.5) ^a |
| 2a + CS ₂ | 13.9 (24.9) | 7.5 (12.9) | 3.3 (5.6) |
| 2b + CS ₂ | 14.0 (24.4) | 5.7 (9.0) | 3.8 (6.0) |
| 3 + CS ₂ | (-15.5) ^a | - ^b | (-8.5) |
| 2a + HC≡CH | 13.9 (24.9) | 5.2 (7.5) | 1.9 (2.3) |
| 2b + HC≡CH | 14.0 (24.4) | 5.4 (7.4) | 2.1 (2.9) |
| 3 + HC≡CH | (-15.5) ^a | (-9.3) ^a | (-8.7) ^a |
| 2a + SiH ₄ | 13.9 (24.9) | 3.0 (5.6) | 1.6 (1.8) |
| 2b + SiH ₄ | 14.0 (24.4) | 3.6 (5.3) | 2.0 (2.1) |
| 3 + SiH ₄ | (-15.5) ^a | (-11.6) ^a | (-5.9) ^a |
| 2a + CH ₄ | 13.9 (24.9) | 3.3 (5.0) | 1.3 (1.4) |
| 2b + CH ₄ | 14.0 (24.4) | 3.8 (5.2) | 1.5 (1.0) |
| 3 + CH ₄ | (-15.5) ^a | (-9.5) ^a | (-7.7) ^a |

^a Only the NICS(1)_{zz} value is given as the isotropic NICS(0) value is highly contaminated by local shielding effects of the nearby bonds (see ref. 17). ^b See ref. 12. All data (have been computed at the GIAO-B3LYP/def2-SVP//M06-2X/def2-SVP level.

The clear relationship between aromaticity and the computed lower (as compared to the parent system **1**) reaction barriers was finally addressed. Fig. 5.3 shows the evolution of the aromaticity (measured by the NICS values) along the reaction coordinate of the parent dihydrogen activation mediated by **2a** from the initial reactant complex up to the corresponding transition state. As commented above, the NICS values become less and less positive (that is, the system becomes less and less antiaromatic) and reach their minimum value at the transition state, the point where the barrier is defined. Interestingly, both NICS curves are a mirror image of the total energy ΔE , which constitutes a clear indication of a strong correlation between both parameters. Indeed, very good linear correlations were

found when plotting the NICS values versus the ΔE values ($R^2 = 0.992$ and 0.986 , for NICS(0) and NICS(1)_{zz}, respectively, see Fig. 5.4), thus confirming the close relationship between both values. Therefore, it is confirmed that there is a dramatic influence of the aromaticity strength of the 4π -borole moiety on the intrinsic reactivity of the borole-containing FLPs. The gain in aromaticity along the reaction coordinate is translated into a substantial gain in stability which ultimately results in a remarkable enhancement of the reactivity of geminal FLPs having a borole fragment as the Lewis acid partner.

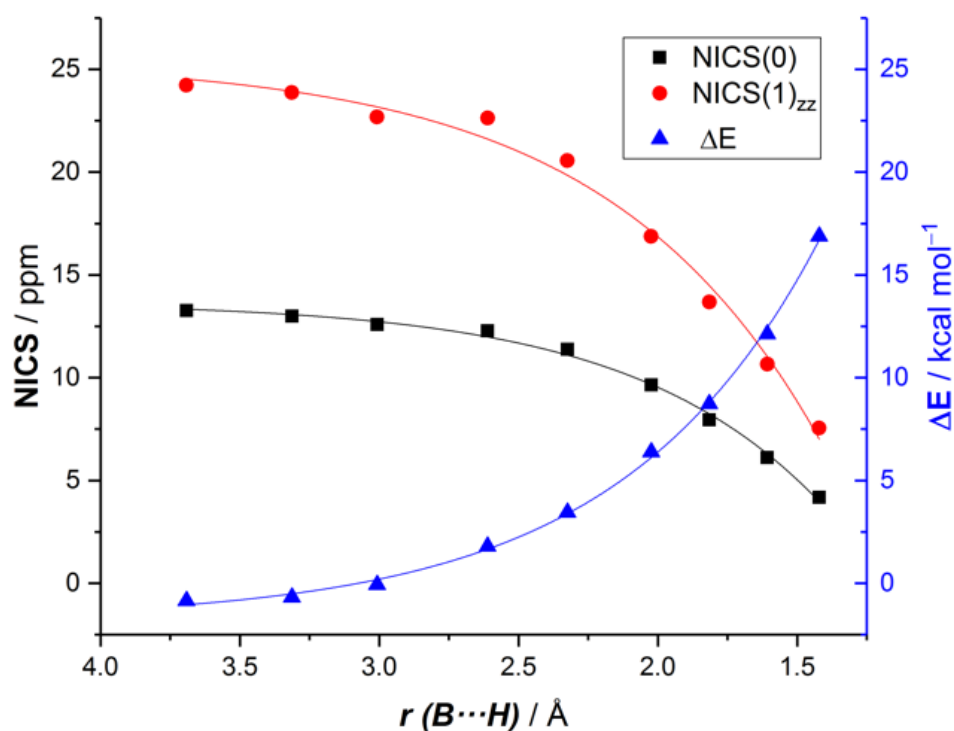


Figure 5.3. Evolution of the aromaticity and energy along the reaction coordinate (from RC to TS) for the dihydrogen activation reaction mediated by FLP **2a**.

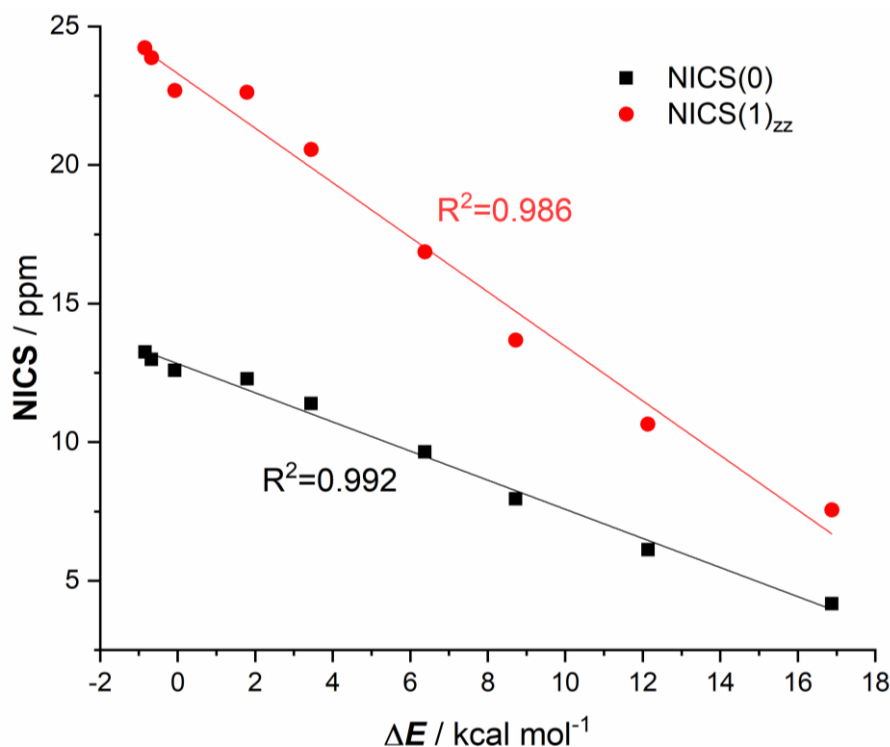


Figure 5.4. Plot of the NICS values vs the energy along the reaction coordinate (from **RC** to **TS**) for the dihydrogen activation reaction mediated by FLP **2a**.

In summary, in this work we have introduced a novel concept in FLP chemistry, *i.e.* aromaticity as a key factor enhancing the reactivity of geminal FLPs. By means of DFT calculations, it is predicted that geminal FLPs having a borole fragment as the Lewis acid partner constitute really promising candidates to achieve facile small molecule activations. This is due to the loss of its antiaromatic character along the reaction coordinate which is translated into much more favourable transformations, as compared to the already active FLP $t\text{Bu}_2\text{P}-\text{CH}_2-\text{BPh}_2$. These predicted highly active borole-FLPs open doors to the otherwise unfeasible activations of inert bonds (such as $\text{C}_{sp^3}-\text{H}$ bonds) mediated by traditional FLPs. In our opinion, the contents of this work will motivate the rational design of novel borole-based FLP species.

References

- ¹ For leading reviews, see: (a) D. W. Stephan and G. Erker, *Angew. Chem., Int. Ed.*, **2010**, *49*, 46; (b) G. Erker, *Pure Appl. Chem.*, **2012**, *84*, 2203; (c) D. W. Stephan and G. Erker, *Frustrated Lewis Pairs I*, Topics in Current Chemistry, 2013, vol. *332*; (d) D. W. Stephan and G. Erker, *Chem. Sci.*, **2014**, *5*, 2625; (e) D. W. Stephan, *J. Am. Chem. Soc.*, **2015**, *137*, 10018; (f) D. W. Stephan and G. Erker, *Angew. Chem., Int. Ed.*, **2015**, *54*, 6400; (g) D. W. Stephan, *Acc. Chem. Res.*, **2015**, *48*, 306; (h) D. W. Stephan, *Science*, **2016**, *354*, aaf7229; (i) W. Meng, X. Feng and H. Du, *Acc. Chem. Res.*, **2018**, *51*, 191; (j) J. Paradies, *Eur. J. Org. Chem.*, **2019**, 283.
- ² G. C. Welch, R. R. San Juan, J. D. Masuda and D. W. Stephan, *Science*, **2006**, *314*, 1124.
- ³ Selected representative examples: (a) C. Appelt, H. Westenberg, F. Bertini, A. W. Ehlers, J. C. Slootweg, K. Lammertsma and W. Uhl, *Angew. Chem., Int. Ed.*, **2011**, *50*, 3925; (b) C. Appelt, J. C. Slootweg, K. Lammertsma and W. Uhl, *Angew. Chem., Int. Ed.*, **2012**, *51*, 5911; (c) S. Roters, C. Appelt, H. Westenberg, A. Hepp, J. C. Slootweg, K. Lammertsma and W. Uhl, *Dalton Trans.*, **2012**, *41*, 9033; (d) C. Appelt, J. C. Slootweg, K. Lammertsma and W. Uhl, *Angew. Chem., Int. Ed.*, **2013**, *52*, 4256; (e) W. Uhl and E.-U. Würthwein, *Top. Curr. Chem.*, **2013**, *334*, 101; (f) W. Uhl, C. Appelt, J. Backs, H. Westenberg, A. Wollschläger and J. Tannert, *Organometallics*, **2014**, *33*, 1212; (g) M. Devillard, R. Declercq, E. Nicolas, A.W. Ehlers, J. Backs, N. Saffon-Merceron, G. Bouhadir, J. C. Slootweg, W. Uhl and D. Bourissou, *J. Am. Chem. Soc.*, **2016**, *138*, 4917; (h) L. Keweloh, H. Klöcker, E.-U. Würthwein and W. Uhl, *Angew. Chem., Int. Ed.*, **2016**, *55*, 3212.
- ⁴ See, for instance: (a) A. M. Chapman, M. F. Haddow and D. F. Wass, *J. Am. Chem. Soc.*, **2011**, *133*, 18463; (b) D. F. Wass and A. M. Chapman, *Top. Curr. Chem.*, **2013**, *334*, 261; (c) A. T. Normand, P. Richard, C. Balan, C. G. Daniliuc, G. Kehr, G. Erker and P. Le Grendre, *Organometallics*, **2015**, *34*, 2000; (d) X. Xu, G. Kehr, C. G. Daniliuc and G. Erker, *J. Am. Chem. Soc.*, **2015**, *137*, 4550; (e) S. Arndt, M. Rudolph and A. S. K. Hashmi, *Gold Bull.*, **2017**, *50*, 267.
- ⁵ (a) F. Bertini, V. Lyaskovskyy, B. J. J. Timmer, F. J. J. de Kanter, M. Lutz, A. W. Ehlers, J. Chris Slootweg and K. Lammertsma, *J. Am. Chem. Soc.*, **2012**, *134*, 201; (b) K. Samigullin, I. Georg, M. Bolte, H.-W. Lerner and M. Wagner, *Chem. Eur. J.*, **2016**, *22*, 3478; (c) E. R. M. Habraken, L. C. Mens, M. Nieger, M. Lutz, A. W. Ehlers and J. C. Slootweg, *Dalton Trans.*, **2017**, *46*, 12284.
- ⁶ All calculations were carried out at the PCM(toluenes)-M06-2X/def2-TZVPP//M06-2X/def2-SVP level. See computational details in the SI.
- ⁷ H. Braunschweig, I. Fernández, G. Frenking and T. Kupfer, *Angew. Chem., Int. Ed.*, **2008**, *47*, 1951.
- ⁸ (a) D. Yepes, P. Jaque and I. Fernández, *Chem. Eur. J.*, **2016**, *22*, 18801; (b) J. J. Cabrera-Trujillo and I. Fernández, *Chem. Eur. J.*, **2018**, *24*, 17823.
- ⁹ Typically, more active FLPs with H₂ also means less effective systems in hydrogenation catalysis. Indeed, despite borole-containing FLP **2a** is more active than **1** for the activation of H₂, our calculations also confirm that the latter species is more efficient for the subsequent hydrogenation of multiple bonds. For instance, the computed free energy barriers for the hydrogenation of formaldehyde mediated by the H₂-adducts derived from **1** and **2a** are 18.8 and 24.0 kcal mol⁻¹, respectively (see Fig. 5.S2 in the SI).
- ¹⁰ Although the use of more acidic B fragment might tolerate a lower basicity donor, our calculations replacing the P*t*Bu₂ fragment by PPh₂ indicate that these related systems are much less active (computed H₂ activation barriers of 27.1 and 22.4 kcal mol⁻¹, for **1-PPh₂** and **2a-PPh₂**, respectively).
- ¹¹ (a) J. E. Leffler, *Science*, **1953**, *117*, 340; (b) G. S. J. Hammond, *J. Am. Chem. Soc.*, **1953**, *75*, 334.

¹² For the processes involving the much less active FLP **3** and CO₂ or CS₂, instead of the expected P/B cooperative activation reaction, only the nucleophilic addition reaction of the phosphine to the electrophilic carbon atom was found.

¹³ Z. Chen, C. S. Wannere, C. Corminboeuf, R. Puchta and P. v. R. Schleyer, *Chem. Rev.*, **2005**, *105*, 3842.

¹⁴ Isotropic NICS(0) values were computed at the [3, +1] ring critical point of the borole moiety. This point was chosen due to its high sensitivity to diamagnetic effects and its unambiguous character.

¹⁵ H. Fallah-Bagher-Shaidaei, C. S. Wannere, C. Corminboeuf, R. Puchta and P. v. R. Schleyer, *Org. Lett.*, **2006**, *8*, 863.

¹⁶ D. Geuenich, K. Hess, F. Köhler and R. Herges, *Chem. Rev.*, **2005**, *105*, 3758.

¹⁷ (a) I. Fernández, M. Duvall, J. I. Wu, P. v. R. Schleyer and G. Frenking, *Chem. Eur. J.*, **2011**, *17*, 2215; (b) I. Fernández, J. I. Wu and P. v. R. Schleyer, *Org. Lett.*, **2013**, *15*, 2990.

Supporting Information

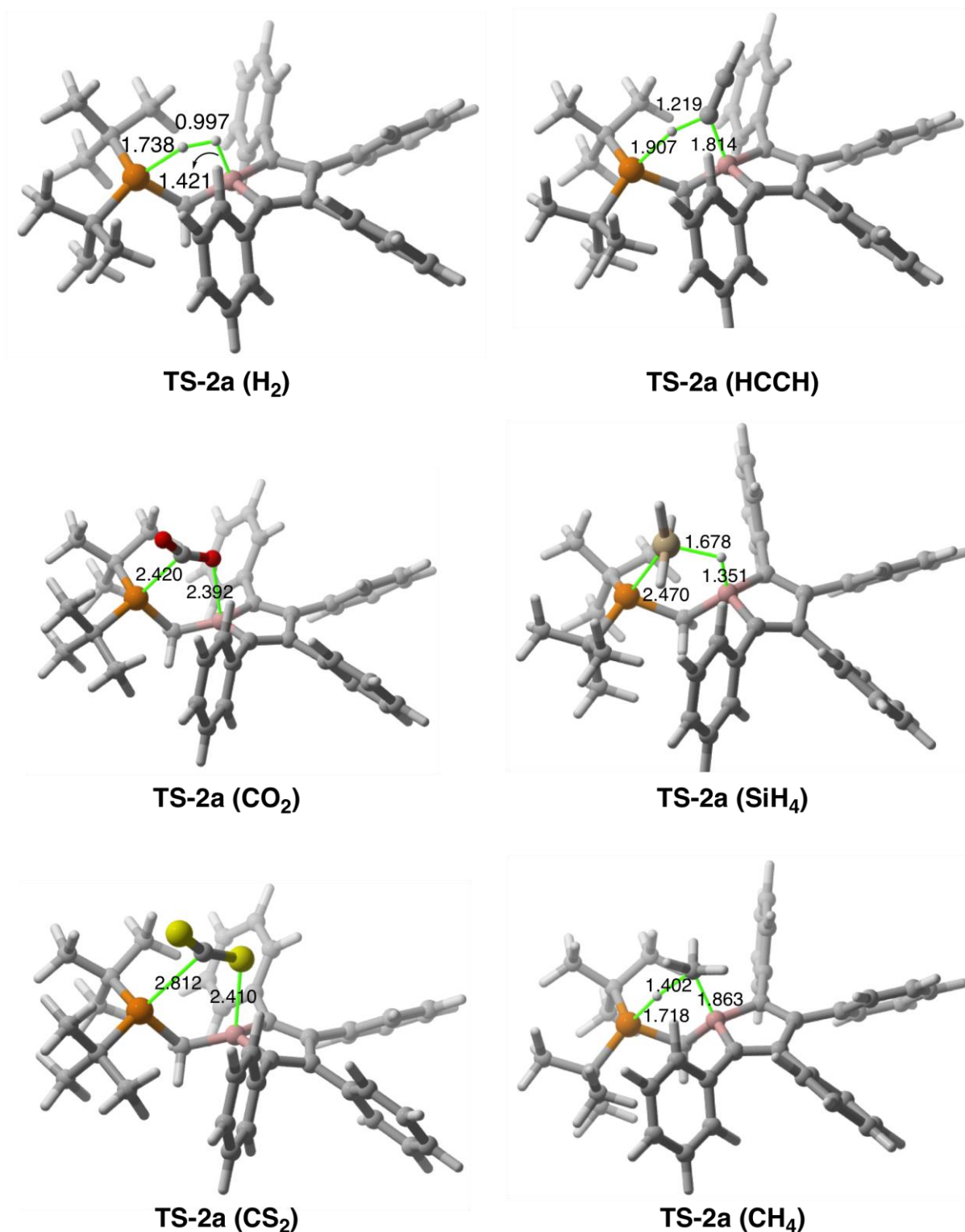


Figure 5.S1. Transition states for the FLP 2a-mediated small molecule activation reactions considered in this study. Bond lengths are given in angstroms. All data have been computed at the M06-2X/def2-SVP level.

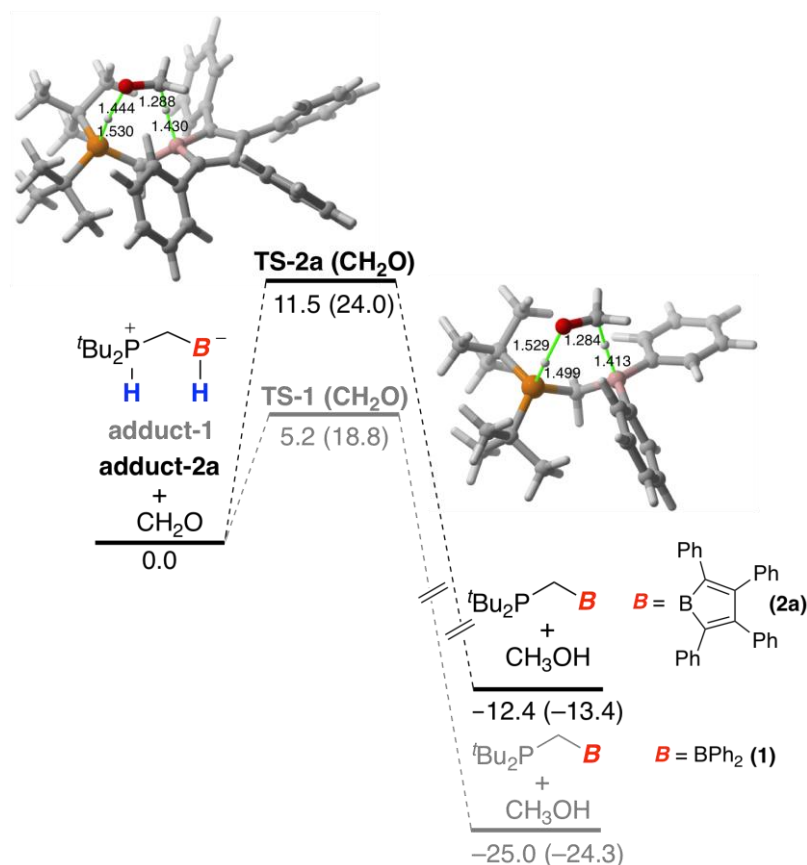


Figure 5.S2. Comparative computed reaction profiles for the hydrogenation reaction of formaldehyde mediated by H₂-adducts derived for FLPs **1** and **2a**. Relative energies (free energies within parentheses) and bond distances are given in kcal/mol and angstroms, respectively. All data have been computed at the PCM(toluene)-M06-2X/def2-TZVPP//M06-2X/def2-SVP level.

Computational details

Geometry optimizations of the molecules were performed without symmetry constraints using the Gaussian09 suite of programs¹ employing the meta-hybrid M06-2X exchange-correlation functional² combined with the double- ζ quality

¹ Gaussian 09, Revision D.01, M. J. Frisch, G. W. Trucks, H. B. Schlegel, G. E. Scuseria, M. A. Robb, J. R. Cheeseman, G. Scalmani, V. Barone, B. Mennucci, G. A. Petersson, H. Nakatsuji, M. Caricato, X. Li, H. P. Hratchian, A. F. Izmaylov, J. Bloino, G. Zheng, J. L. Sonnenberg, M. Hada, M. Ehara, K. Toyota, R. Fukuda, J. Hasegawa, M. Ishida, T. Nakajima, Y. Honda, O. Kitao, H. Nakai, T. Vreven, J. A. Montgomery, Jr., J. E. Peralta, F. Ogliaro, M. Bearpark, J. J. Heyd, E. Brothers, K. N. Kudin, V. N. Staroverov, R. Kobayashi, J. Normand, K. Raghavachari, A. Rendell, J. C. Burant, S. S. Iyengar, J. Tomasi, M. Cossi, N. Rega, J. M. Millam, M. Klene, J. E. Knox, J. B. Cross, V. Bakken, C. Adamo, J. Jaramillo, R. Gomperts, R. E. Stratmann, O. Yazyev, A. J. Austin, R. Cammi, C. Pomelli, J. W. Ochterski, R. L. Martin, K. Morokuma, V. G. Zakrzewski, G. A. Voth, P. Salvador, J. J. Dannenberg, S. Dapprich, A. D. Daniels, Ö. Farkas, J. B. Foresman, J. V. Ortiz, J. Cioslowski, and D. J. Fox, Gaussian, Inc., Wallingford CT, 2009.

² Y. Zhao, D. G. Truhlar, *Theor. Chem. Acc.* **2008**, *120*, 215.

def2-SVP basis set.³ Reactants and products were characterized by frequency calculations, and have positive definite Hessian matrices. Transition structures (TS's) show only one negative eigenvalue in their diagonalized force constant matrices, and their associated eigenvectors were confirmed to correspond to the motion along the reaction coordinate under consideration using the Intrinsic Reaction Coordinate (IRC) method.⁴ In addition, the vibrational calculation provides the thermal Gibbs energy corrections by using the gas ideal-rigid-rotor-harmonic-oscillator approximation. Solvent effects were taken into account by means of the Polarizable Continuum Model (PCM)⁵ using the gas-phase optimized geometries at the same DFT level in conjunction with the triple- ζ quality def2-TZVPP basis set.³ This level is denoted PCM(solvent)/M06-2X/def2-TZVPP//M06-2X/def2-SVP. Moreover, more accurate energies were computed at the Domain Based Local Pair-Natural Coupled-Cluster (DLPNO-CCSD(T))⁶ as implemented in Orca 4.0.1⁷ using the def2-TZVP basis sets³ and the SMD⁸ solvation model on the M06-2X/def2-SVP geometries. This level is denoted SMD(solvent)-DLPNO-CCSD(T)/def2-TZVP//M06-2X-def2-SVP.

The aromaticity of the considered species has been assessed by the computation of the NICS⁹ values computed at the [3,+1] ring critical point of the electron density¹⁰ using the gauge invariant atomic orbital (GIAO) method,¹¹ at the B3LYP¹² level using the def2-SVP basis set, with the optimized M06-2X/def2-SVP geometries. This scheme is denoted as GIAO-B3LYP/def2-SVP//M06-2X/def2-SVP.

³ F. Weigend, R. Ahlrichs, *Phys. Chem. Chem. Phys.* **2005**, *7*, 3297.

⁴ C. Gonzalez, H. B. Schlegel, *J. Phys. Chem.* **1990**, *94*, 5523.

⁵ a) S. Miertuš, E. Scrocco, J. Tomasi, *Chem. Phys.* **1981**, *55*, 117; b) J. L. Pascual-Ahuir, E. Silla, I. Tuñón, *J. Comp. Chem.* **1994**, *15*, 1127; c) Barone, V.; Cossi, M. *J. Phys. Chem. A*, **1998**, *102*, 1995.

⁶ C. Riplinger, B. Sandhoefer, A. Hansen, F. Neese, *J. Chem. Phys.* **2013**, *139*, 134101.

⁷ F. Neese, *WIREs Comput. Mol. Sci.* **2018**, *8*, e1327.

⁸ A. V. Marenich, C. J. Cramer, D. G. Truhlar, *J. Phys. Chem. B* **2009**, *113*, 6378.

⁹ Z. Chen, C. S. Wannere, C. Corminboeuf, R. Puchta, P. v. R. Schleyer, *Chem. Rev.* **2005**, *105*, 3842.

¹⁰ R. F. W. Bader, *Atoms in Molecules - A Quantum Theory*, Clarendon Press: Oxford, 1990.

¹¹ K. Wolinski, J. F. Hilton, P. Pulay, *J. Am. Chem. Soc.* **1990**, *112*, 8251.

¹² a) A. D. Becke, *J. Chem. Phys.* **1993**, *98*, 5648; b) C. Lee, W. Yang, R. G. Parr, *Phys. Rev. B: Condens. Matter Mater. Phys.* **1988**, *37*, 785; c) S. H. Vosko, L. Wilk, M. Nusair, *Can. J. Phys.* **1980**, *58*, 1200.

VI. CHAPTER 4

Carbones and heavier ylidones (EL₂) in frustrated Lewis pair chemistry: Influence of the nature of EL₂ on dihydrogen activation

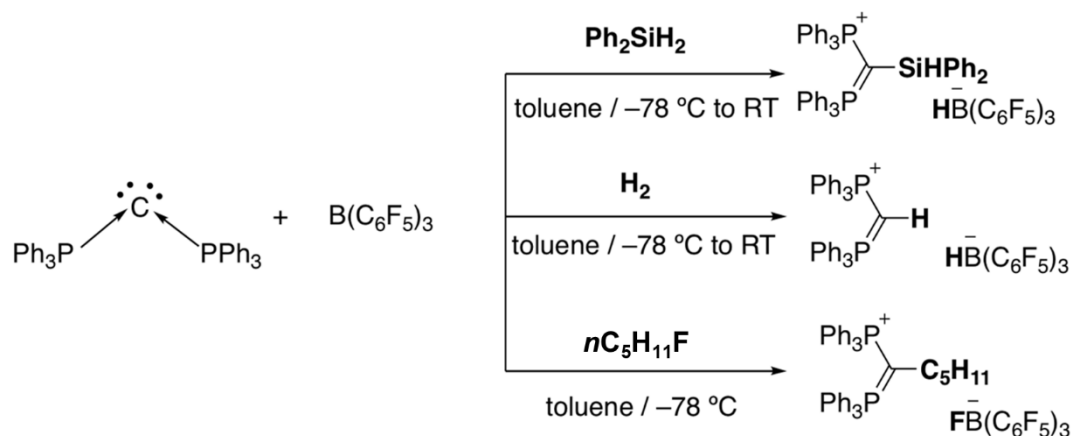
The role of carbones (CL₂; L = phosphines vs carbenes) as Lewis bases in dihydrogen (H₂) activation reactions in the presence of the Lewis acid B(C₆F₅)₃ has been computationally explored by means of density functional theory calculations. To this end, the interaction between H₂ and the [carbone··B(C₆F₅)₃] pair along the reaction coordinate has been quantitatively analyzed in detail and compared to the parent [tBu₃P··B(C₆F₅)₃] frustrated Lewis pair. In addition, the influence on the reactivity of both the nature of the central E atom and the surrounding ligands in ylidones (EL₂) has also been considered. It is found that the activation barrier of the H₂ activation reaction as well as the geometry of the corresponding transition states strongly depends on the nature of both E and L in the sense that lower barriers are systematically associated with earlier transition states. Our calculations identify heavier EL₂ as the most active systems to achieve facile H₂ activation reactions.

Inorg. Chem., **2019**, *58*, 7828-7836.

Introduction

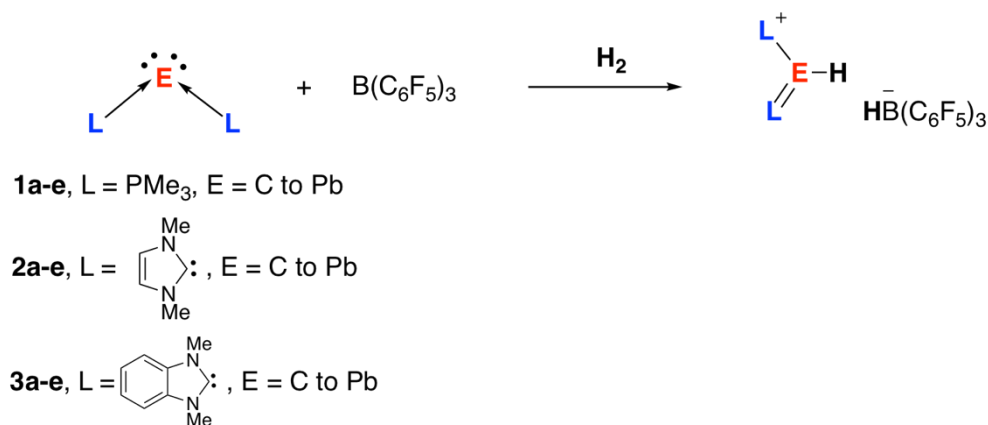
The term “carbone” was coined by Frenking and co-workers to refer to a family of divalent carbon(0) compounds CL_2 whose central carbon atom retains all four valence electrons as two lone pairs and where bonding to the adjacent σ -donor ligands (L) occurs mainly through donor-acceptor interactions (*i.e.*, $L \rightarrow C^0 \leftarrow L$).^{1,2} Since the report by Ramirez and co-workers in 1961 on the first and most representative member of this family of compounds, the parent hexaphenylcarbodiphosphorane $[C(PPh_3)_2]$,³ a good number of carbon(0) species have been prepared and fully characterized.⁴ In addition, this family of compounds has also been expanded to systems having heavier Group 14 elements in their structures [also known as ylidones (EL_2)].^{2a,5} Because of their peculiar bonding situation, these species not only are potential donor ligands in main-group compounds or transition-metal complexes but also exhibit a rich and varied reactivity.^{2,4,6} For instance, carbodicarbenes [carbones where L = carbene or *N*-heterocyclic carbene (NHC)] have attracted considerable attention because of their captodative behavior in catalysis.⁷

In this regard, Alcarazo and co-workers recently found that the parent carbone, $C(PPh_3)_2$, can be used as a carbon-based Lewis base in combination with the Lewis acid $B(C_6F_5)_3$ to form a highly active frustrated Lewis pair (FLP) able to activate not only H–H bonds but also C–O, C–H, Si–H, and C–F bonds (Scheme 6.1).⁸ This behavior therefore strongly resembles that found for typical FLPs based mainly on P-based Lewis bases [for instance, $tBu_3P/B(C_6F_5)_3$ or $Mes_3P/B(C_6F_5)_3$].⁹ Despite this evident similarity, very little is known about the actual role of carbones in the bond activation process compared to analogous transformations involving either intermolecular or intramolecular P/B FLP systems.¹⁰



Scheme 6.1. Activation reactions mediated by hexaphenylcarbodiphosphorane and $\text{B}(\text{C}_6\text{F}_5)_3$ described by Alcarazo and co-workers (see reference 8).

Recently, we combined state-of-the-art computational methods known as the activation strain model (ASM) of reactivity¹¹ and energy decomposition analysis (EDA)¹² to gain more quantitative insight into the factors controlling the dihydrogen (H_2) activation reactions promoted by strongly related intramolecular geminal FLPs.¹³ This approach allowed us to propose an orbital-controlled mechanism, complementary to the widely accepted mechanisms suggested independently by Pápai and co-workers¹⁴ and Grimme and co-workers,¹⁵ where the degree of cooperativity between the key donor-acceptor orbital interactions, *i.e.*, $\text{LP}(\text{Lewis base}) \rightarrow \sigma^*(\text{H}_2)$ and $\sigma(\text{H}_2) \rightarrow \text{p}_z(\text{Lewis acid})$, along the reaction coordinate can be used as an indicator of the reaction barrier. Given the good performance of this approach in the chemistry of FLPs, we decided herein to apply this methodology to explore in detail the role of carbones as Lewis bases in H_2 activation reactions in comparison to the parent process involving the intermolecular $t\text{Bu}_3\text{P}/\text{B}(\text{C}_6\text{F}_5)_3$ FLP. This particular transformation was selected among the other different bond activation reactions described by Alcarazo and co-workers⁸ because it is also one of the most important and representative reactions in FLP chemistry.¹⁰ In addition, the influence of both the nature of the central Group 14 element (E) and the flanking ligands ($\text{L} = \text{phosphine vs carbene}$) on this H_2 activation reaction will also be analyzed (Scheme 6.2) to identify the combination of E and L that leads to the most active ylidone.



Scheme 6.2. FLP-mediated dihydrogen activation reactions considered in this study.

Theoretical Methods and Computational Details

Geometry optimizations of the molecules were performed without symmetry constraints using the Gaussian09 suite of programs,¹⁶ employing the meta-hybrid M06-2X exchange-correlation functional¹⁷ combined with the double- ζ -quality def2-SVP basis set.¹⁸ Reactants and products were characterized by frequency calculations and have positive definite Hessian matrices. Transition states (TSs) show only one negative eigenvalue in their diagonalized force constant matrices, and their associated eigenvectors were confirmed to correspond to the motion along the reaction coordinate under consideration using the intrinsic reaction coordinate (IRC) method.¹⁹ Single-point energy refinements were carried out on the gas-phase optimized geometries using the same functional with the larger triple- ζ -quality plus polarization def2-TZVPP basis set¹⁸ including solvent effects (toluene) by means of the polarizable continuum model (PCM).²⁰ This level is denoted as PCM(toluene)/M06-2X/def2-TZVPP//M06-2X/def2-SVP.

EDAs were carried out using the ADF.2017 program²¹ at the same level of theory in conjunction with the triple- ζ -quality TZ2P basis set²² on the geometries optimized at the M06-2X/def2-SVP level. This level is therefore denoted as M06-2X/TZ2P//M06-2X/def2-SVP.

Activation strain model of reactivity and Energy decomposition analysis

Because the ASM method has been the focus of recent reviews,¹¹ herein we only briefly summarize the basics of this approach. This method is a systematic development of the EDA method (see below) used initially to understand the nature

of chemical bonding in stable molecules. Within this method, also known as the *distortion/interaction* model,²³ the potential energy surface $\Delta E(\zeta)$ is decomposed, along the reaction coordinate ζ , into two main contributions, namely, the strain $\Delta E_{\text{strain}}(\zeta)$ associated with the deformation (or distortion) experienced by the reactants during the transformation plus the interaction $\Delta E_{\text{int}}(\zeta)$ between these increasingly deformed reactants:

$$\Delta E(\zeta) = \Delta E_{\text{strain}}(\zeta) + \Delta E_{\text{int}}(\zeta)$$

Herein the reaction coordinate is defined as the projection of the IRC onto the forming B \cdots H distance. This reaction coordinate ζ undergoes a well-defined change in the course of the reaction from the separate reactants (or the initial reaction complexes) to the equilibrium distance in the corresponding TSs.

The interaction $\Delta E_{\text{int}}(\zeta)$ between the strained reactants can be further partitioned into chemically meaningful contributions by means of the EDA method.¹² Thus, $\Delta E_{\text{int}}(\zeta)$ is decomposed into the following terms along the reaction coordinate:

$$\Delta E_{\text{int}}(\zeta) = \Delta V_{\text{elstat}}(\zeta) + \Delta E_{\text{Pauli}}(\zeta) + \Delta E_{\text{orb}}(\zeta)$$

The term ΔV_{elstat} corresponds to the classical electrostatic interaction between the unperturbed charge distributions of the deformed reactants and is usually attractive. The Pauli repulsion ΔE_{Pauli} comprises the destabilizing interactions between occupied orbitals and is responsible for any steric repulsion. The orbital interaction ΔE_{orb} accounts for charge transfer [interaction between the occupied orbitals on one moiety with the unoccupied orbitals on the other, including highest occupied molecular orbital (HOMO)–lowest unoccupied molecular orbital (LUMO) interactions] and polarization (empty-occupied orbital mixing on one fragment due to the presence of another fragment). Moreover, the natural orbital for chemical valence (NOCV)²⁴ extension of the EDA method has also been used to further partition the ΔE_{orb} term. The EDA-NOCV approach provides pairwise energy contributions for each pair of interacting orbitals to the total bond energy.

Results and Discussion

We first compared the H₂ activation reaction mediated by the intermolecular FLP *t*Bu₃P/B(C₆F₅)₃ and the analogous transformation involving the parent carbene C(PMe₃)₂ (**1a**), a compound experimentally described by Gasser and Schmidbaur in 1975²⁵ that is strongly similar to C(PPh₃)₂ used by Alcarazo and co-workers (see above).⁸ Similar to the reaction profiles computed previously for the H₂ activation mediated by related intra- and intermolecular FLPs,^{13,14,26} we found that, in both cases, heterolytic H₂ splitting occurs in a concerted manner through the formation of an initial reactant complex (**RC**), which evolves into the corresponding reaction product in a strongly exothermic process (Figure 6.1). Therefore, in both cases, the corresponding TSs are associated with the rupture of the H–H bond with the concomitant formation of B–H and P/C–H bonds and lead to an intimate ion pair stabilized by a weak H···H interaction (**PC**, H···H distance of ca. 2 Å), which finally dissociates into the hydride H–B(C₆F₅)₃[−] and the corresponding protonated Lewis base, as experimentally confirmed in the solid state.^{8,9} Despite similar reaction profiles, the process involving the carbene **1a** is clearly favored over the process involving *t*Bu₃P along the entire reaction coordinate and, particularly, at the reaction product region (*i.e.*, $\Delta\Delta E_{\text{R}} = 33.2$ kcal/mol). In addition, the computed low barrier and strong exothermicity computed for the **1a**/B(C₆F₅)₃ + H₂ reaction are fully consistent with the reaction conditions used experimentally (−78 °C to room temperature),⁸ which nicely confirms the high activity of the carbene/B(C₆F₅)₃ system.

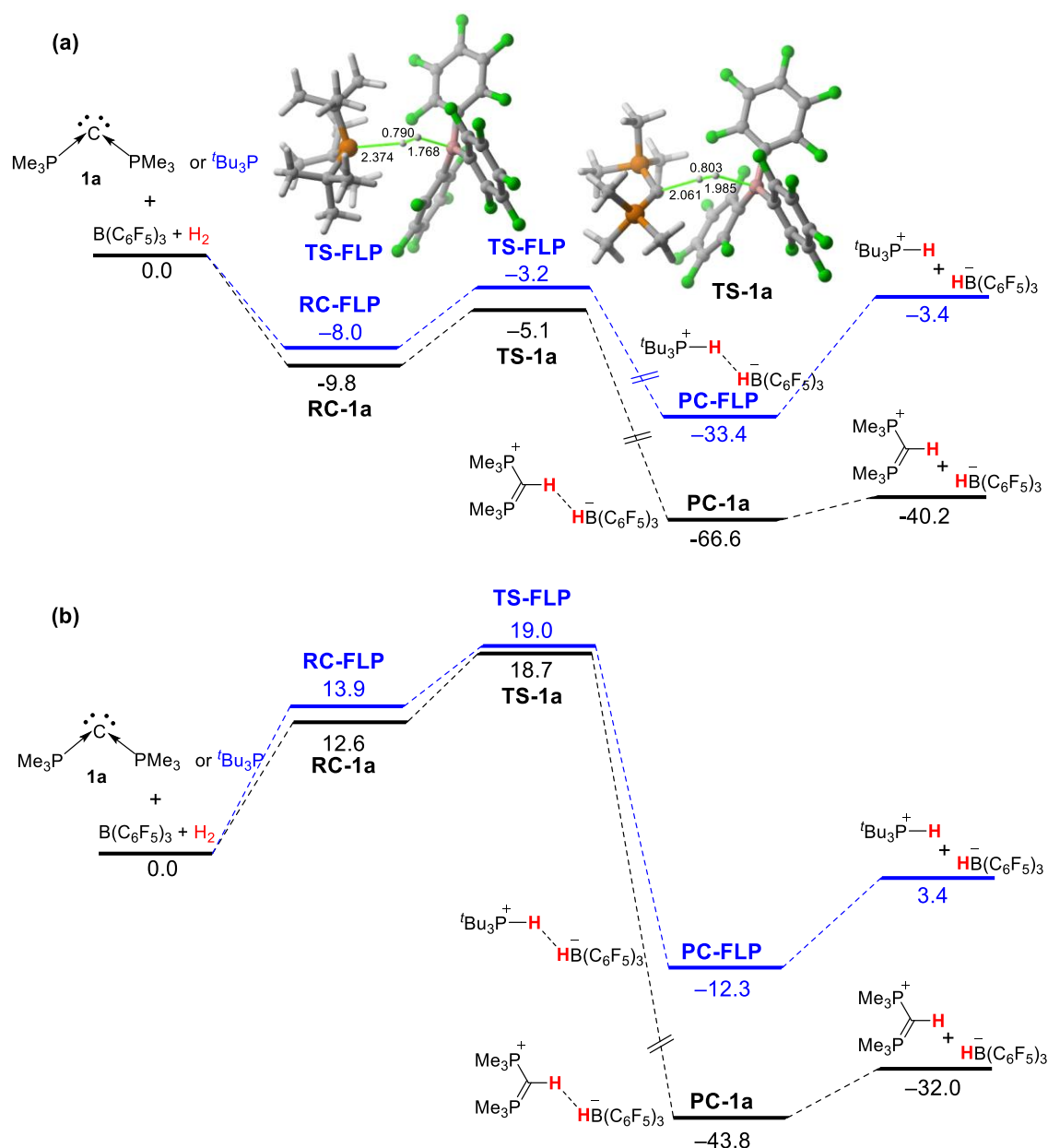


Figure 6.1. Computed reaction profiles for the H₂ activation reactions mediated by carbene **1a** (black lines) and *t*Bu₃P (blue lines) in the presence of B(C₆F₅)₃: relative energies (a); free energies at 298 K (b), given in kcal/mol. The bond lengths are given angstrom. All data were computed at the PCM(toluenes)-M06-2X/def2-TZVPP//M06-2X/def2-SVP level.

According to the ASM of reactivity, the process involving **1a** benefits from a much stronger interaction between the deformed H₂ and [1a⋯B(C₆F₅)₃] reactants, particularly at the TS region, compared to the process involving *t*Bu₃P (the corresponding activation strain diagrams are given in Figure 6.S1). Despite that, this latter reaction benefits from less deformation energy, which offsets the computed weaker interaction for this system. As a result, both processes present rather similar activation barriers (see above).

The reasons behind the computed different interaction energies between H₂ and the *t*Bu₃P/B(C₆F₅)₃ and **1a**/B(C₆F₅)₃ pairs can be quantitatively analyzed by means of the EDA method. This approach has greatly contributed to our current understanding of the H₂ activation reaction mediated by either intramolecular¹³ or similar intermolecular FLPs.²⁷ Figure 6.2 graphically shows the evolution of the different EDA terms along the reaction coordinate from the initial reactant complexes up to the corresponding TSs for both transformations. Although the interaction between H₂ and the [*t*Bu₃P⋯B(C₆F₅)₃] or [(Me₃P)₂C⋯B(C₆F₅)₃] pairs is rather similar (slightly stronger for the process involving **1a**), the attractive interactions (ΔV_{elstat} and ΔE_{orb}) are clearly more stabilizing for the H₂ activation mediated by the **1a**/B(C₆F₅)₃ system along the entire reaction coordinate. Nevertheless, these stronger stabilizing interactions are nearly offset by the Pauli repulsion term, which is clearly much more destabilizing for the process involving **1a** from the very beginning of the transformation. Therefore, although the attractive interactions between H₂ and the [*t*Bu₃P⋯B(C₆F₅)₃] pair are comparatively less stabilizing, this system benefits from a less destabilizing Pauli repulsion, which is translated into the computed nearly identical total interaction (ΔE_{int}) between the reactants. Therefore, our EDA study clearly shows that there exist significant differences in the mode of action of phosphines and carbones as Lewis bases for the activation of H₂. In addition, our EDA calculations suggest that the electrostatic and orbital interactions contribute to a nearly similar extent to the total attractions in both systems, which is compatible with the two widely accepted models for H₂ activation by FLPs, namely, Pápai's electron-transfer model,¹⁴ which is based on cooperative orbital interactions involving the LP(base)→ σ^* (H₂) and σ (H₂)→p π (acid) interactions, and Grimme's electric-field model,¹⁵ where electrostatic interactions are key.

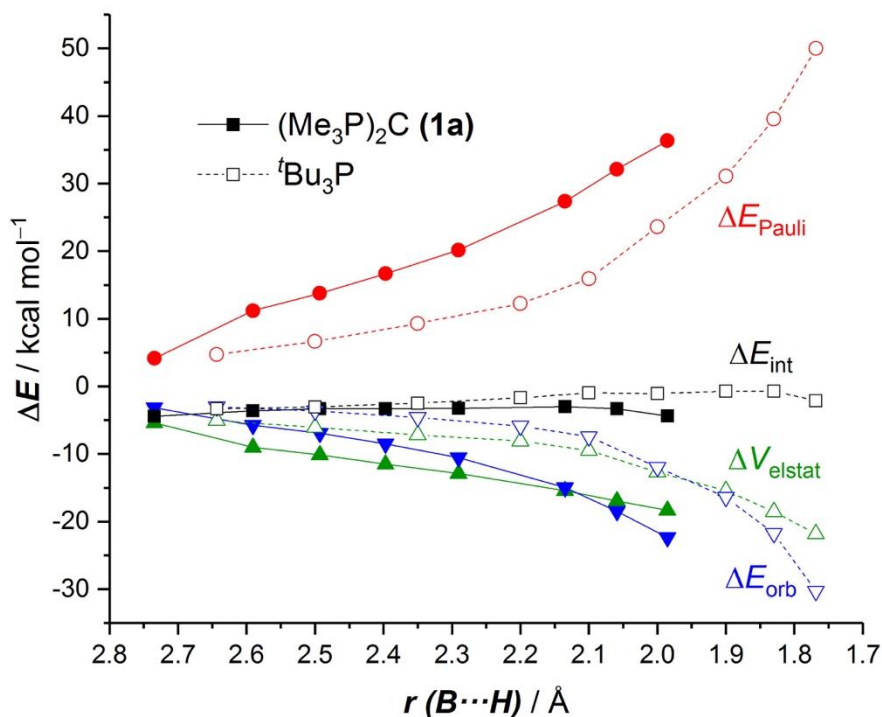


Figure 6.2. EDA of the H_2 activation reactions mediated by **1a** (solid lines) and $t\text{Bu}_3\text{P}$ (dashed lines) in the presence of $\text{B}(\text{C}_6\text{F}_5)_3$ along the reaction coordinate projected onto the forming $\text{B}\cdots\text{H}$ bond length. All data were computed at the M06-2X/TZ2P//M06-2X/def2-SVP level.

The NOCV extension of the EDA method was applied next to understand the nature of the orbital interactions as well as their relative contribution to the total ΔE_{orb} term involved in the H_2 splitting promoted by $t\text{Bu}_3\text{P}/\text{B}(\text{C}_6\text{F}_5)_3$ and **1a**/ $\text{B}(\text{C}_6\text{F}_5)_3$. To this end, we selected three key points along the reaction coordinate, namely, the initial reactant complex, the TS, and a midpoint between them. Figure 6.3 shows snapshots of the corresponding NOCV deformation densities ($\Delta\rho$) together with their associated stabilization energies [$\Delta E(\rho)$]. As can be seen for the process involving the FLP $t\text{Bu}_3\text{P}/\text{B}(\text{C}_6\text{F}_5)_3$ (Figure 6.3a), at a very early stage of the reaction, the principal charge depletion region (in red) belongs to the $\text{H}-\text{H}$ σ orbital, while the charge accumulation (in blue) corresponds to the empty p_π atomic orbital at the boron center. As the H_2 activation reaction progresses, this charge-transfer process continuously reinforces and dominates up to the TS region, where $\text{LP}(\text{P})\rightarrow\sigma^*(\text{H}-\text{H})$ starts to take place. Therefore, although the activation reaction is concerted, it does not occur in a synchronous manner; *i.e.*, the $\sigma(\text{H}_2)\rightarrow p_z(\text{B})$ orbital interaction takes place first and is responsible for the polarization of the $\text{H}-\text{H}$ σ bond, which allows subsequent interaction with the phosphorus lone pair. A similar orbital scenario was found by us in the analogous process involving intramolecular geminal N/B or P/B FLPs.^{13a,c} According to the data in Figure 6.3, the charge flow computed for the analogous process involving

1a along the reaction coordinate is rather similar. However, the associated orbital energies are comparatively higher along the entire process.²⁸ This is mainly due to involvement of the $\text{LP}(\text{C}) \rightarrow \sigma^*(\text{H}-\text{H})$ orbital interaction from the beginning of the process (see Figure 6.3b) as a consequence of the higher σ -donor ability of **1a** compared to $t\text{Bu}_3\text{P}$, which is then translated into the stronger orbital interactions computed for the **1a**/ $\text{B}(\text{C}_6\text{F}_5)_3 + \text{H}_2$ reaction along the entire reaction coordinate (see above).

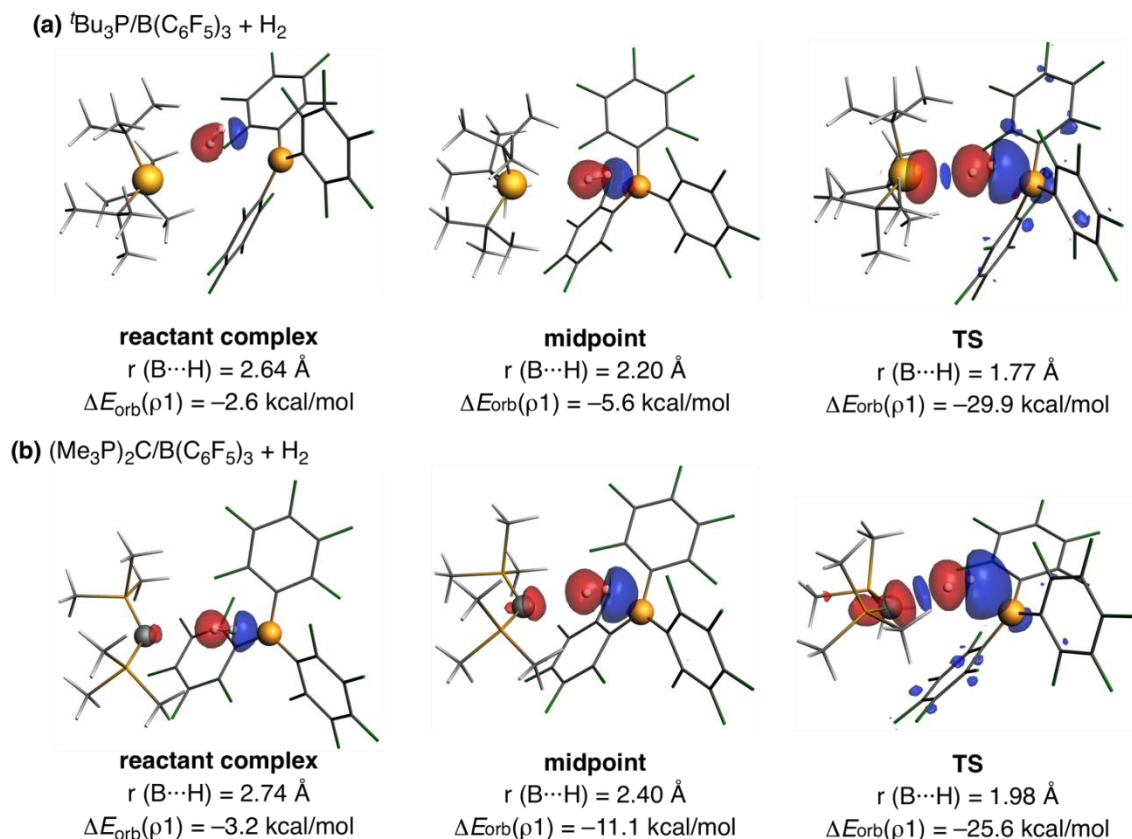


Figure 6.3. Contour plots of NOCV deformation densities $\Delta\rho$ and associated energies $\Delta E(\rho)$ (in kcal/mol) for the main orbital interactions between H_2 and $[t\text{Bu}_3\text{P}\cdots\text{B}(\text{C}_6\text{F}_5)_3]$ (a) and $[\mathbf{1a}\cdots\text{B}(\text{C}_6\text{F}_5)_3]$ (b). Electronic charge flows from red to blue. All data were computed at the M06-2X/TZ2P//M06-2X/def2-SVP level.

Another remarkable difference between the considered FLP and carbene-mediated H_2 activations is found in the nature of the corresponding reaction products. The presence of the two carbon lone pairs in the initial **1a** necessarily involves that the reaction product formed upon H_2 activation; *i.e.*, $[(\text{Me}_3\text{P})_2\text{CH}]^+$ should possess a free lone pair available for a new activation process. Indeed, Alcarazo and co-workers already confirmed this point by reacting the analogous cation $[(\text{Me}_3\text{P})_2\text{CMe}]^+$ with H_2 or methanol in the presence of $\text{B}(\text{C}_6\text{F}_5)_3$.⁸

Although the H₂ activation could not be experimentally achieved, the system successfully cleaved the O–H bond of methanol. This finding prompted us to computationally explore this second activation reaction, which, of course, is unfeasible for the process involving *t*Bu₃P because no lone pairs are available in the corresponding reaction product ([*t*Bu₃PH]⁺).

From the computed reaction profiles depicted in Figure 6.4, which clearly shows the occurrence of the lone pair at the carbon atom in [(Me₃P)₂CH]⁺ (see the inset in Figure 6.4), it becomes evident that the second H₂ activation reaction is much more difficult than the first H₂ activation mediated by **1a**, from both kinetic ($\Delta\Delta G^\ddagger = 7.9$ kcal/mol) and, particularly, thermodynamic ($\Delta\Delta G_R = 48.5$ kcal/mol) points of view, which is consistent with the experimental findings by Alcarazo's group. This markedly reduced reactivity of [**1a-H**]⁺ also agrees with the much lower second proton affinities (PAs) computed for carbones compared to their first PAs,^{2a} and further confirms the lower Lewis base ability of the remaining lone pair in protonated carbones. Not surprisingly, activation of the O–H bond of methanol is computed to be much more favorable than the H₂ activation, which is also in agreement with the experimental results. This can be, of course, ascribed to polarization of the O–H bond, which allows a more facile heterolytic splitting than that involving the H–H bond. A similar result was found by us in the activation of X–H σ bonds mediated by slightly related Group 13 carbenoids.²⁹ The same reactivity trend is found when using a more polar solvent (*o*-dichlorobenzene or nitrobenzene; see Figure 6.4). As expected, the final dicationic reaction products (**PC1a-H**) and also the corresponding TSs (albeit to a lesser extent) become more and more stabilized with increasing polarity of the solvent.

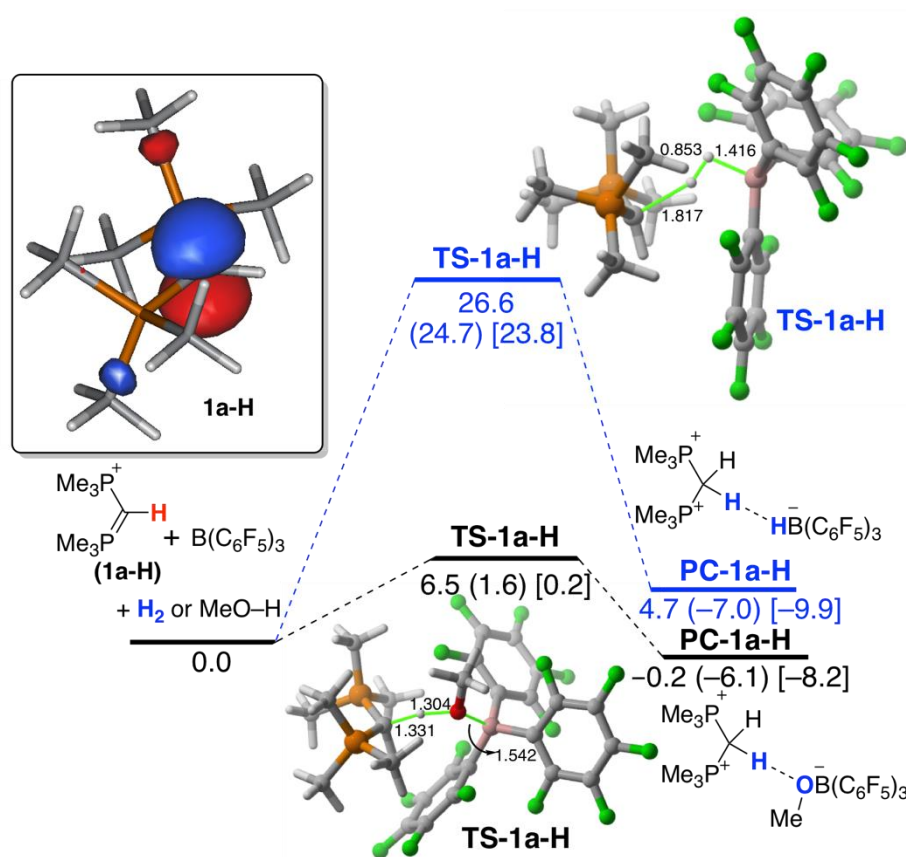


Figure 6.4. Computed reaction profiles for the H–H (blue lines) and CH₃O–H (black lines) bond activation reactions mediated by cationic **1a–H** in the presence of B(C₆F₅)₃. Relative free energies (at 298 K) and bond lengths are given in kcal/mol and Ångstrom, respectively. Plain values were computed in toluene, whereas values within parentheses and brackets were computed in *o*-dichlorobenzene and nitrobenzene, respectively. Inset: computed HOMO of **1a–H** (isosurface value of 0.045 au). All data were computed at the PCM(solvent)-M06-2X/def2-TZVPP//M06-2X/def2-SVP level.

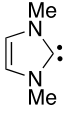
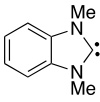
Influence of the Nature of E and L

Once the process involving the parent carbene **1a** had been studied, we then explored the influence of both the nature of the central Group 14 element and the ligand L on the selected H₂ activation reaction in the presence of B(C₆F₅)₃. Table 6.1 gathers the computed free barrier and reaction energies for the processes involving ylidenes **1a–1e**, **2a–2e**, and **3a–3e**.³⁰

Two main reactivity trends can be clearly observed upon inspection of the data gathered in Table 6.1.³¹ On the one hand, the activation barrier systematically decreases upon moving down Group 14 (E = C > Si > Ge > Sn > Pb) regardless of the ligand L present in the ylide. In addition, the corresponding reaction energies become less and less exergonic, which can be ascribed to the different bond

strengths of the newly formed E–H bonds in the process (*i.e.*, the E–H bond dissociation energies decrease from E = C to E = Pb: 337, 321, and 176 kJ/mol for C–H, Ge–H, and Pb–H, respectively).³²

Table 6.1. Computed HOMO energies (in eV) and free activation and reaction energies (computed at 298.15 K) for the H₂ activation reactions mediated by **1-3** in the presence of B(C₆F₅)₃.^a

| EL ₂ | E | L | E _{HOMO} / eV | ΔG _{RC} ^a | ΔG ^{#b} | ΔG _R ^c |
|-----------------|----|---|------------------------|-------------------------------|------------------|------------------------------|
| 1a | C | | -5.58 | 12.6 | 18.7 | -43.8 |
| 1b | Si | | -4.23 | 9.6 | 14.4 | -33.8 |
| 1c | Ge | PMe ₃ | -4.15 | 9.6 | 13.5 | -30.4 |
| 1d | Sn | | -3.88 | 10.8 | 13.1 | -27.8 |
| 1e | Pb | | -3.70 | 10.5 | 11.3 | -18.5 |
| 2a | C | | -4.68 | 10.8 | 15.5 | -58.0 |
| 2b | Si |  | -3.72 | 11.5 | 14.8 | -44.3 |
| 2c | Ge | | -3.66 | 11.1 | 13.8 | -43.2 |
| 2d | Sn | | -3.35 | 9.7 | 13.6 | -43.8 |
| 2e | Pb | | -3.04 | 9.1 | 10.6 | -42.7 |
| 3a | C | | -5.47 | 12.6 | 16.6 | -46.0 |
| 3b | Si |  | -4.35 | 15.5 | 17.9 | -38.2 |
| 3c | Ge | | -4.25 | 14.2 | 16.7 | -32.1 |
| 3d | Sn | | -3.86 | 9.9 | 14.9 | -39.7 |
| 3e | Pb | | -3.52 | 7.7 | 12.4 | -39.4 |

^a All data (in kcal/mol), relative to the isolated reactants, were computed at the PCM(toluene)-M06-2X/def2-TZVPP//M06-2X-def2-SVP level. ^b ΔG_{RC} = G(**RC**) - G(**1-3**) - G[B(C₆F₅)₃] - G(H₂). ^c Activation energy: ΔG[#] = G(**TS**) - G(**1-3**) - G(B(C₆F₅)₃) - G(H₂). ^d Reaction energy: ΔG_R = G(**adduct**) - G(**1-3**) - G(B(C₆F₅)₃) - G(H₂).

On the other hand, it seems that, when E = C, the activation barrier decreases upon replacement of the phosphine ligands (compound **1a**) by NHCs (compounds **2a** and **3a**). This enhanced reactivity computed for carbones having carbenes in their structures (ΔG[#] increases in the order **2a** < **3a** < **1a**) is fully consistent with the reported computed first PAs (294.3 > 284.7 > 278.4 kcal/mol for **2a**, **3a**, and **1a**, respectively),^{2a} which suggests that the PA values can be, at least qualitatively, used for predicting the relative reactivity of carbones. From the data in Table 6.1, it can then be concluded that ylidones are clearly more reactive than *t*Bu₃P (ΔG[#] = 19.0 kcal/mol) to promote H₂ activation reactions in the presence of the highly acidic B(C₆F₅)₃ Lewis acid. Our calculations predict that the activation barrier of

the process can even be reduced up to ca. 11–13 kcal/mol when heavier ylidenes (E = Sn, Pb) are used.

Closer inspection of the optimized geometries of the corresponding TSs (see Figure 6.5 for the representative series involving ylidenes **1a–1e** and **2a–2e**) clearly indicates that the breaking H···H bond becomes shorter and shorter upon moving down Group 14, therefore indicating that the corresponding TSs are reached earlier and earlier from E = C to E = Pb. According to the computed activation barriers, which become lower and lower also upon moving down Group 14 (see Table 6.1), it seems that the Hammond–Leffer postulate³³ is fully satisfied in these transformations. Indeed, a very good linear relationship was found upon plotting these parameters (correlation coefficient $R^2 = 0.96$; see Figure 6.6 for the processes involving **1a–1e**). According to this postulate, one should expect that those processes having lower barriers (*i.e.*, possessing earlier TSs) should also be more exergonic. However, the opposite is found (see Table 6.1), which further confirms the strong influence of the strength of the newly formed E–H bonds on the computed reaction energies. For this reason, although a nearly perfect linear relationship was found upon plotting the breaking H···H distances versus the computed reaction energies (correlation coefficient $R^2 = 0.99$; see Figure 6.6), the straight line possesses a negative slope. Similar very good linear correlations were also found for the processes involving ylidenes **2** or **3** (see, for instance, Figure 6.S2 for the H₂ activations mediated by **2a–2e**).

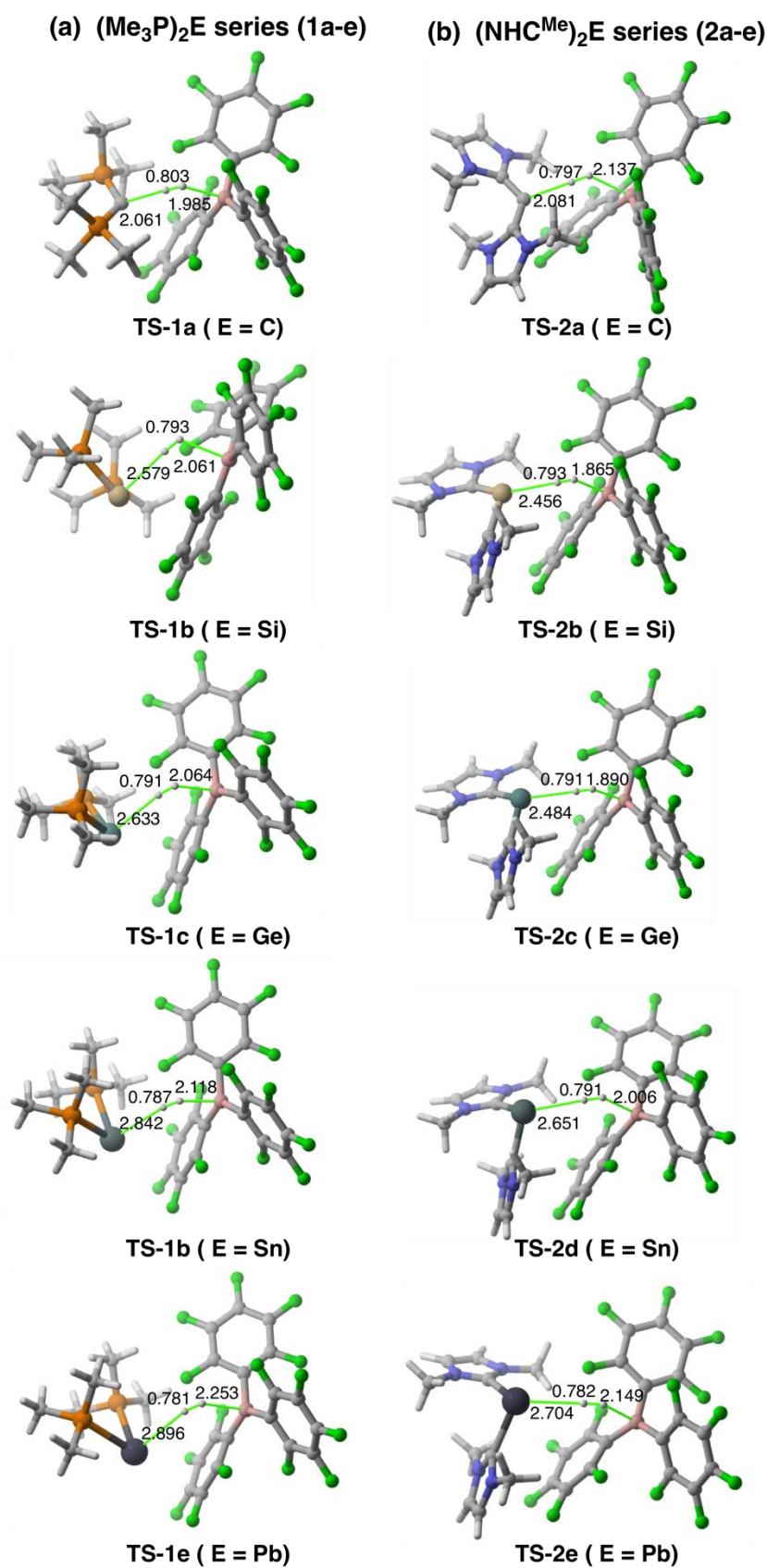


Figure 6.5. Fully optimized geometries (M06-2X/def2-SVP level) of the TSs involved in the H_2 activation reactions mediated by ylidenes **1a-e** and **2a-e** in the presence of $\text{B}(\text{C}_6\text{F}_5)_3$. Bond lengths are given in Ångstroms.

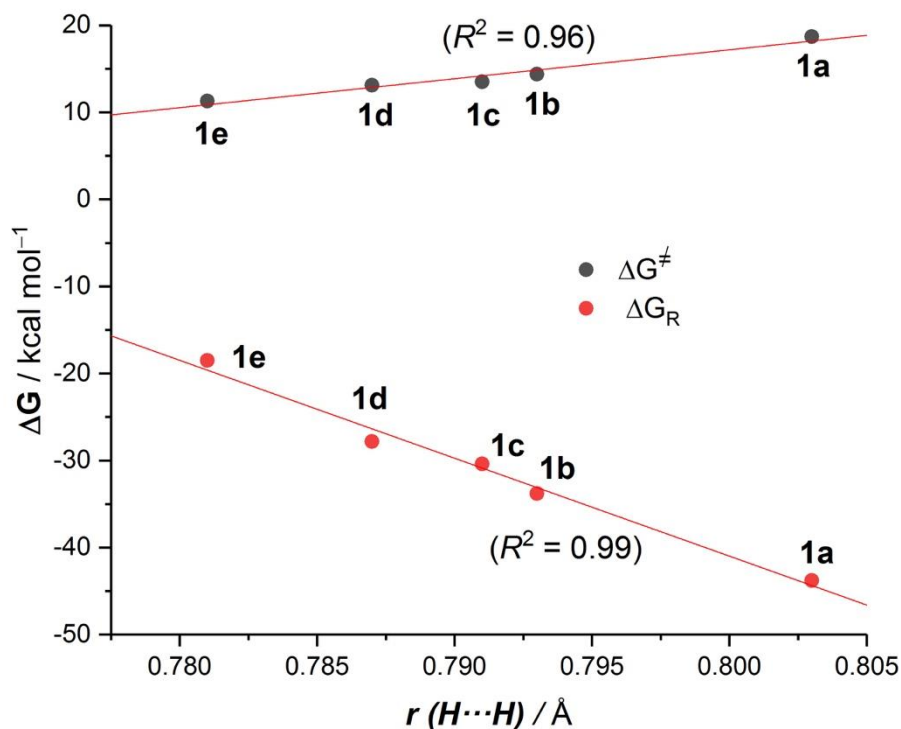


Figure 6.6. Plot of the computed activation barriers (ΔG^\ddagger ; black circles) and reaction energies (ΔG_R ; red circles) vs the breaking H \cdots H distance in the corresponding TSs involved in the **1a-e** + B(C₆F₅)₃ + H₂ reaction. All data were computed at the PCM(toluene)-M06-2X/def2-TZVPP//M06-2X/def2-SVP level.

We then applied a combination of the ASM of reactivity and EDA methods to understand the enhanced reactivity (in terms of the computed activation barriers) of ylidenes when the central E atom changes from E = C to E = Pb. To this end, we focused on the H₂ activation reactions mediated by carbene **1a** (E = C) and germylene **1c** (E = Ge) in the presence of B(C₆F₅)₃ as representative transformations (Figure 6.7). The ASM clearly ascribed the lower activation barrier computed for the process involving **1c** mainly to the much stronger interaction between the deformed H₂ and [**1c**···B(C₆F₅)₃] reactants along the entire reaction coordinate compared to the analogous reaction involving **1a** (the corresponding activation strain diagrams are given in Figure 6.S3). In addition, the former system also benefits from a less destabilizing deformation energy (ΔE_{strain}).

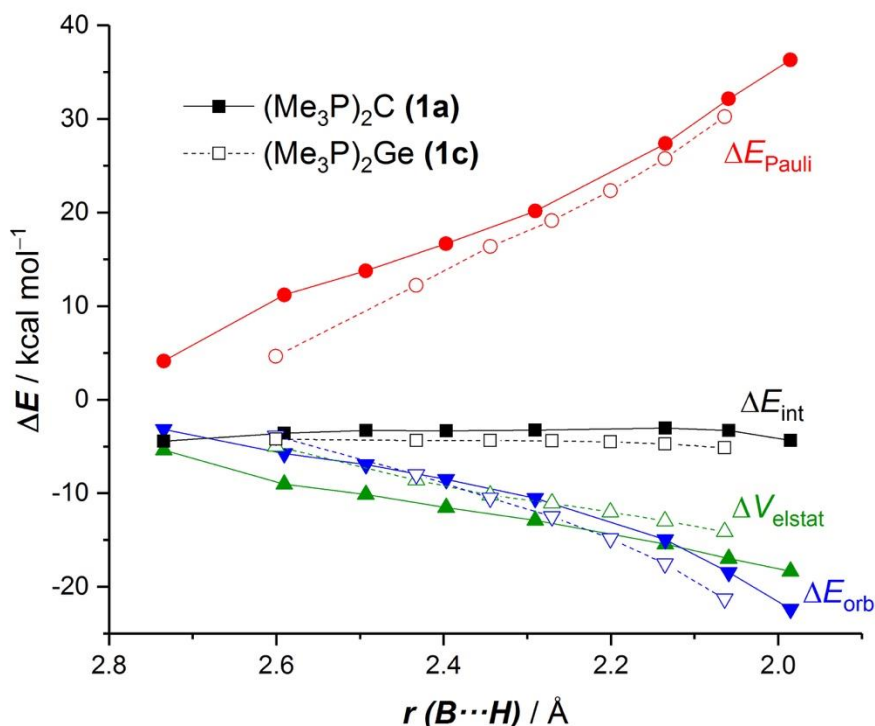


Figure 6.7. EDA of the H_2 activation reactions mediated by carbene **1a** (solid lines) and germylone **1c** (dashed lines) in the presence of $\text{B}(\text{C}_6\text{F}_5)_3$ along the reaction coordinate projected onto the forming $\text{B}\cdots\text{H}$ bond length. All data were computed at the M06-2X/TZ2P//M06-2X/def2-SVP level.

The crucial role of the interaction energy in these H_2 activation reactions can be quantitatively analyzed by means of the EDA method. As graphically shown in Figure 6.7, the electrostatic interactions (ΔV_{elstat}) between $[\mathbf{1a}\cdots\text{B}(\text{C}_6\text{F}_5)_3]$ and H_2 are clearly more stabilizing than those computed for the process involving its germylone counterpart. Despite that, the latter process benefits from both a less destabilizing Pauli repulsion and stronger orbital attractions along the entire reaction coordinate which are therefore responsible for the stronger interaction computed for the reaction involving **1c** ($\text{E} = \text{Ge}$). Although the energies of the HOMO of the initial ylidone qualitatively agree with the higher orbital interactions computed for the process involving **1c** (see Table 6.1), we applied the EDA–NOCV to quantitatively decompose the ΔE_{orb} term. Once again, the NOCV method identifies the $\sigma(\text{H}_2) \rightarrow \text{p}_z(\text{B})$ and $\text{LP}(\text{E}) \rightarrow \sigma^*(\text{H}-\text{H})$ interactions as the main orbital interactions taking place in these H_2 activation reactions (Figure 6.8). Interestingly, the associated stabilizing energy $[\Delta E(\rho)]$ is comparatively stronger for the process involving the heavier ylidone **1c**. For instance, at the same consistent forming $\text{B}\cdots\text{H}$ bond distance of 2.15 Å, $\Delta E(\rho)$ amounts to -16.6 kcal/mol for the H_2 activation mediated by carbene **1a**, whereas a higher value of -22.1 kcal/mol was computed

for the analogous process involving germylone **1c**. As a result of this higher orbital interaction, a much stronger total orbital interaction (ΔE_{orb}) was computed for the latter transformation.

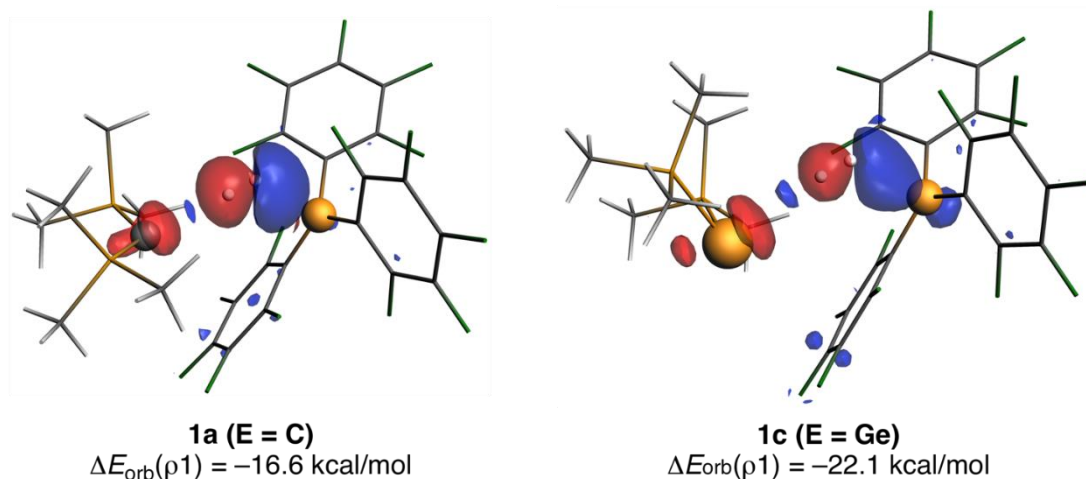


Figure 6.8. Contour plots of NOCV deformation densities $\Delta\rho$ and associated energies $\Delta E(\rho)$ (in kcal/mol) for the main orbital interactions between H_2 and $[\mathbf{1a}\cdots\text{B}(\text{C}_6\text{F}_5)_3]$ (left) and $[\mathbf{1c}\cdots\text{B}(\text{C}_6\text{F}_5)_3]$ (right) at the same consistent forming B \cdots H distance of 2.15 Å. Electronic charge flows from red to blue. All data were computed at the M06-2X/TZ2P//M06-2X/def2-SVP level.

Conclusions

By means of state-of-the-art computational tools, we found that carbones present significant differences with respect to phosphines when used as Lewis bases in H_2 activation reactions in the presence of $\text{B}(\text{C}_6\text{F}_5)_3$. Although the interaction between H_2 and the $[\text{tBu}_3\text{P}\cdots\text{B}(\text{C}_6\text{F}_5)_3]$ or $[(\text{Me}_3\text{P})_2\text{C}\cdots\text{B}(\text{C}_6\text{F}_5)_3]$ pairs is similar, the latter system benefits from stronger electrostatic and orbital attractions along the entire reaction coordinate. Indeed, the key $\text{LP}(\text{C})\rightarrow\sigma^*(\text{H}-\text{H})$ orbital interaction, which takes place from the beginning of the transformation, induces a stronger interaction as a consequence of the higher σ -donor ability of carbone compared to tBu_3P . Moreover, the corresponding reaction product, $[(\text{Me}_3\text{P})_2\text{CH}]^+$, is able to undergo a second activation reaction because of the presence of an available lone pair on the carbon atom. However, this second H_2 activation is considerably less favored than the first one due to the less Lewis base ability of this remaining lone pair.

We also explored the influence on the reactivity of the nature of both the central E atom (E = C–Pb) and the surrounding ligands L (L = phosphine vs

carbene) in EL_2 compounds. It was found that the barrier height of the H_2 activation reaction steadily decreases upon moving down Group 14 regardless of the attached ligand. This enhanced reactivity of the heavier ylides finds its origin mainly in the computed stronger interaction between the deformed reactants along the reaction coordinate as a consequence of a less destabilizing Pauli repulsion and more stabilizing orbital interactions. In addition, carbenes having NHCs in their structures are more reactive than those having phosphines as σ -donor ligands. Our calculations predict that heavier ylides are really promising candidates to achieve facile H_2 activation reactions. In our opinion, the insight gained in this computational study is important not only for our understanding of the actual role of ylides as Lewis bases but also for the rational design of novel FLP-type systems.

References

- ¹ (a) R. Tonner, F. Öxler, B. Neumüller, W. Petz, G. Frenking, *Angew. Chem., Int. Ed.*, **2006**, *45*, 8038-8042; (b) R. Tonner, G. Frenking, *Angew. Chem., Int. Ed.*, **2007**, *46*, 8695-8698; (c) R. Tonner, G. Frenking, *Chem. Eur. J.*, **2008**, *14*, 3260-3272; (d) R. Tonner, G. Frenking, *Chem. Eur. J.*, **2008**, *14*, 3273-3289.
- ² For recent reviews, see: (a) G. Frenking, R. Tonner, S. Klein, N. Takagi, T. Shimizu, A. Krapp, K. K. Pandey, P. Parameswaran, *Chem. Soc. Rev.*, **2014**, *43*, 5106-5139; (b) G. Frenking, M. Hermann, D. M. Andrada, N. Holzmann, *Chem. Soc. Rev.*, **2016**, *45*, 1129-1144; (c) L. Zhao, M. Hermann, N. Holzmann, G. Frenking, *Coord. Chem. Rev.*, **2017**, *344*, 163-204.
- ³ F. Ramirez, N. B. Desai, B. Hansen, N. McKelvie, *J. Am. Chem. Soc.*, **1961**, *83*, 3539-3540.
- ⁴ For representative examples, see: (a) C. A. Dyker, V. Lavallo, B. Donnadiu, G. Bertrand, *Angew. Chem., Int. Ed.*, **2008**, *47*, 3206-3209; (b) C. A. Dyker, G. Bertrand, *Nat. Chem.*, **2009**, *1*, 265-266; (c) M. Alcarazo, C. W. Lehmann, A. Anoop, W. Thiel, A. Fürstner, *Nat. Chem.*, **2009**, *1*, 295-301; (d) A. Fürstner, M. Alcarazo, R. Goddard, C. W. Lehmann, *Angew. Chem., Int. Ed.*, **2008**, *47*, 3210-3214; (e) M. Melaimi, P. Parameswaran, B. Donnadiu, G. Frenking, G. Bertrand, *Angew. Chem., Int. Ed.*, **2009**, *48*, 4792-4795; (f) I. Fernández, C. A. Dyker, A. DeHope, B. Donnadiu, G. Frenking, G. Bertrand, *J. Am. Chem. Soc.*, **2009**, *131*, 11875-11881.
- ⁵ For representative examples for EL₂ compounds (E = Si, Ge; L = σ donors), see: (a) K. C. Mondal, H. W. Roesky, M. C. Schwarzer, G. Frenking, B. Niepötter, H. Wolf, R. Herbst-Irmer, D. Stalke, *Angew. Chem., Int. Ed.*, **2013**, *52*, 2963-2967; (b) Y. Li, K. C. Mondal, H. W. Roesky, H. Zhu, P. Stollberg, R. Herbst-Irmer, D. Stalke, D. M. Andrada, *J. Am. Chem. Soc.*, **2013**, *135*, 12422-12428; (c) Y. Xiong, S. Yao, G. Tan, S. Inoue, M. Driess, *J. Am. Chem. Soc.*, **2013**, *135*, 5004-5007; (d) Y. Xiong, S. Yao, S. Inoue, J. D. Epping, M. Driess, *Angew. Chem., Int. Ed.*, **2013**, *52*, 7147-7150; (e) T. Chu, L. Belding, A. van der Est, T. Dudding, I. Korobkov, G. I. Nikonov, *Angew. Chem., Int. Ed.*, **2014**, *53*, 2711-2715; (f) B. Su, R. Ganguly, Y. Li, R. Kinjo, *Angew. Chem., Int. Ed.*, **2014**, *53*, 13106-13109; (g) T. Sugahara, T. Sasamori, N. Tokitoh, *Angew. Chem., Int. Ed.*, **2017**, *56*, 9920-9923; (h) Y. Wang, M. Karni, S. Yao, Y. Apeloig, M. Driess, *J. Am. Chem. Soc.*, **2019**, *141*, 1655-1664.
- ⁶ For a recent review, see: M. Alcarazo, *Struct. Bonding (Berlin, Ger.)* **2017**, *177*, 25-51.
- ⁷ For a recent review, see: S.-k. Liu, W.-C. Shih, W.-C. Chen, T.-G. Ong, *ChemCatChem* **2018**, *10*, 1483-1498.
- ⁸ M. Alcarazo, C. Gomez, S. Holle, R. Goddard, *Angew. Chem., Int. Ed.*, **2010**, *49*, 5788-5791.
- ⁹ G. C. Welch, D. W. Stephan, *J. Am. Chem. Soc.*, **2007**, *129*, 1880-1881.
- ¹⁰ For leading reviews on FLP chemistry, see: (a) D. W. Stephan, G. Erker, *Angew. Chem., Int. Ed.*, **2010**, *49*, 46-76; (b) G. Erker, *Pure Appl. Chem.*, **2012**, *84*, 2203-2217; (c) D. W. Stephan, G. Erker, Topics in Current Chemistry. *Frustrated Lewis Pairs I*; Springer Press, 2013; Vol. 332; (d) D. W. Stephan, G. Erker, *Chem. Sci.*, **2014**, *5*, 2625-2641; (e) D. W. Stephan, *J. Am. Chem. Soc.*, **2015**, *137*, 10018-10032; (f) D. W. Stephan, G. Erker, *Angew. Chem., Int. Ed.*, **2015**, *54*, 6400-6441; (g) D. W. Stephan, *Acc. Chem. Res.*, **2015**, *48*, 306-316; (h) D. W. Stephan, *Science* **2016**, *354*, aaf7229.
- ¹¹ For reviews on the ASM, see: (a) W.-J. van Zeist, F. M. Bickelhaupt, *Org. Biomol. Chem.*, **2010**, *8*, 3118-3127; (b) I. Fernández, F. M. Bickelhaupt, *Chem. Soc. Rev.*, **2014**, *43*, 4953-4967; (c) L. P. Wolters, F. M. Bickelhaupt, *WIREs Comput. Mol. Sci.*, **2015**, *5*, 324-343; (d) F. M. Bickelhaupt, K. N. Houk, *Angew. Chem., Int. Ed.*, **2017**, *56*, 10070-10086; See also: (e) I. Fernández, In *Discovering the Future of Molecular Sciences*; Pignataro, B., Ed.; Wiley-VCH: Weinheim, Germany, 2014; pp 165-187.

- ¹² For reviews on the EDA method, see: (a) M. von Hopffgarten, G. Frenking, *WIREs Comput. Mol. Sci.*, **2012**, *2*, 43-62; (b) L. Zhao, M. von Hopffgarten, D. M. Andrada, G. Frenking, *WIREs Comput. Mol. Sci.*, **2018**, *8*, No. e1345.
- ¹³ (a) D. Yepes, P. Jaque, I. Fernández, *Chem. Eur. J.*, **2016**, *22*, 18801-18809; (b) D. Yepes, P. Jaque, I. Fernández, *Chem. Eur. J.*, **2018**, *24*, 8833-8840; (c) J. J. Cabrera-Trujillo, I. Fernández, *Chem. Eur. J.*, **2018**, *24*, 17823-17831.
- ¹⁴ (a) T. A. Rokob, A. Hamza, I. Pápai, *J. Am. Chem. Soc.*, **2009**, *131*, 10701-10710; (b) T. A. Rokob, I. Bakó, A. Stirling, A. Hamza, I. Pápai, *J. Am. Chem. Soc.*, **2013**, *135*, 4425-4437.
- ¹⁵ (a) S. Grimme, H. Kruse, L. Goerigk, G. Erker, *Angew. Chem., Int. Ed.*, **2010**, *49*, 1402-1405. (b) B. Schirmer, S. Grimme, *Chem. Commun.*, **2010**, *46*, 7942-7944.
- ¹⁶ M. J. Frisch, G. W. Trucks, H. B. Schlegel, G. E. Scuseria, M. A. Robb, J. R. Cheeseman, G. Scalmani, V. Barone, B. Mennucci, G. A. Petersson, H. Nakatsuji, M. Caricato, X. Li, H. P. Hratchian, A. F. Izmaylov, J. Bloino, G. Zheng, J. L. Sonnenberg, M. Hada, M. Ehara, K. Toyota, R. Fukuda, J. Hasegawa, M. Ishida, T. Nakajima, Y. Honda, O. Kitao, H. Nakai, T. Vreven, J. A. Montgomery, Jr., J. E. Peralta, F. Ogliaro, M. Bearpark, J. J. Heyd, E. Brothers, K. N. Kudin, V. N. Staroverov, R. Kobayashi, J. Normand, K. Raghavachari, A. Rendell, J. C. Burant, S. S. Iyengar, J. Tomasi, M. Cossi, N. Rega, J. M. Millam, M. Klene, J. E. Knox, J. B. Cross, V. Bakken, C. Adamo, J. Jaramillo, R. Gomperts, R. E. Stratmann, O. Yazyev, A. J. Austin, R. Cammi, C. Pomelli, J. W. Ochterski, R. L. Martin, K. Morokuma, V. G. Zakrzewski, G. A. Voth, P. Salvador, J. J. Dannenberg, S. Dapprich, A. D. Daniels, Ö. Farkas, J. B. Foresman, J. V. Ortiz, J. Cioslowski, and D. J. Fox, Gaussian 09, Revision D.01, Gaussian, Inc., Wallingford CT, 2009.
- ¹⁷ Y. Zhao, D. G. Truhlar, *Theor. Chem. Acc.*, **2008**, *120*, 215-241.
- ¹⁸ (a) F. Weigend, R. Ahlrichs, *Phys. Chem. Chem. Phys.*, **2005**, *7*, 3297-3305; (b) F. Weigend, *Phys. Chem. Chem. Phys.*, **2006**, *8*, 1057-1065.
- ¹⁹ C. Gonzalez, H. B. Schlegel, *J. Phys. Chem.*, **1990**, *94*, 5523-5527.
- ²⁰ (a) S. Miertuš, E. Scrocco, J. Tomasi, *Chem. Phys.*, **1981**, *55*, 117-129; (b) J. L. Pascual-Ahuir, E. Silla, I. Tuñón, *J. Comput. Chem.*, **1994**, *15*, 1127-1138; (c) V. Barone, M. Cossi, *J. Phys. Chem. A*, **1998**, *102*, 1995-2001.
- ²¹ (a) G. te Velde, F. M. Bickelhaupt, E. J. Baerends, C. Fonseca Guerra, S. J. A. van Gisbergen, J. G. Snijders, T. Ziegler, *Comput. Chem.*, **2001**, *22*, 931-967; (b) *ADF2017, SCM*; Theoretical Chemistry, Vrije Universiteit: Amsterdam, The Netherlands, <http://www.scm.com>.
- ²² J. G. Snijders, P. Vernooijs, E. J. Baerends, *At. Data Nucl. Data Tables*, **1981**, *26*, 483-509.
- ²³ (a) D. H. Ess, K. N. Houk, *J. Am. Chem. Soc.*, **2007**, *129*, 10646-10647; (b) D. H. Ess, K. N. Houk, *J. Am. Chem. Soc.*, **2008**, *130*, 10187-10198. See also ref 11d for a recent review.
- ²⁴ M. P. Mitoraj, A. Michalak, T. Ziegler, *J. Chem. Theory Comput.*, **2009**, *5*, 962-975.
- ²⁵ O. Gasser, H. Schmidbaur, *J. Am. Chem. Soc.*, **1975**, *97*, 6281-6282.
- ²⁶ (a) F. Bertini, V. Lyaskovskyy, B. J. J. Timmer, F. J. J. de Kanter, M. Lutz, A. W. Ehlers, J. C. Slootweg, K. Lammertsma, *J. Am. Chem. Soc.*, **2012**, *134*, 201-204; (b) J. J. Cabrera-Trujillo, I. Fernández, *Chem. Commun.*, **2019**, *55*, 675-678.
- ²⁷ M. Heshmat, T. Privalov, *J. Phys. Chem. A*, **2018**, *122*, 7202-7211.
- ²⁸ At the same consistent forming B··H distance of 2.0 Å, $\Delta E(\rho) = -12.3$ kcal/mol for the process involving *t*Bu₃P, whereas a higher value of $\Delta E(\rho) = -25.6$ kcal/mol was computed for the process involving **1a**.
- ²⁹ Y. García-Rodeja, F. M. Bickelhaupt, I. Fernández, *Chem. Eur. J.*, **2016**, *22*, 13669-13676.
- ³⁰ Calculations including relativistic effects indicate that the influence of these effects on the activation barriers is negligible. See Table 6.S1.
- ³¹ The decomposition of the free activation barriers indicates that all processes present rather similar activation entropies ranging from -74 (**3d**) to -87 (**1a**) cal/(mol K). These negative values are fully compatible with the concerted nature of the TSs located on the potential energy surface.

³² Values taken from the *National Standard Reference Data Series 31*; National Bureau of Standards: Washington, DC, 1970.

³³ (a) J. E. Leffler, *Science* **1953**, *117*, 340-341; (b) G. S. Hammond, *J. Am. Chem. Soc.*, **1955**, *77*, 334-338.

Supporting Information

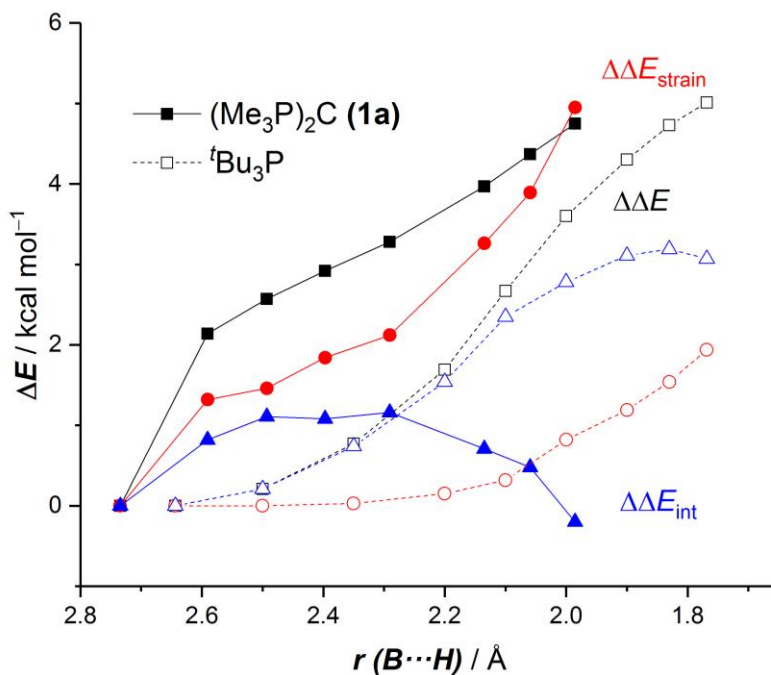


Figure 6.S1. Comparative activation-strain diagrams of the dihydrogen activation reactions mediated by carbene **1a** (solid lines) and $t\text{Bu}_3\text{P}$ (dashed lines) in the presence of $\text{B}(\text{C}_6\text{F}_5)_3$ along the reaction coordinate projected onto the forming $\text{B}\cdots\text{H}$ bond length. All data were computed at the M06-2X/TZ2P//M06-2X/def2-SVP level and are referenced to the corresponding reactant complexes.

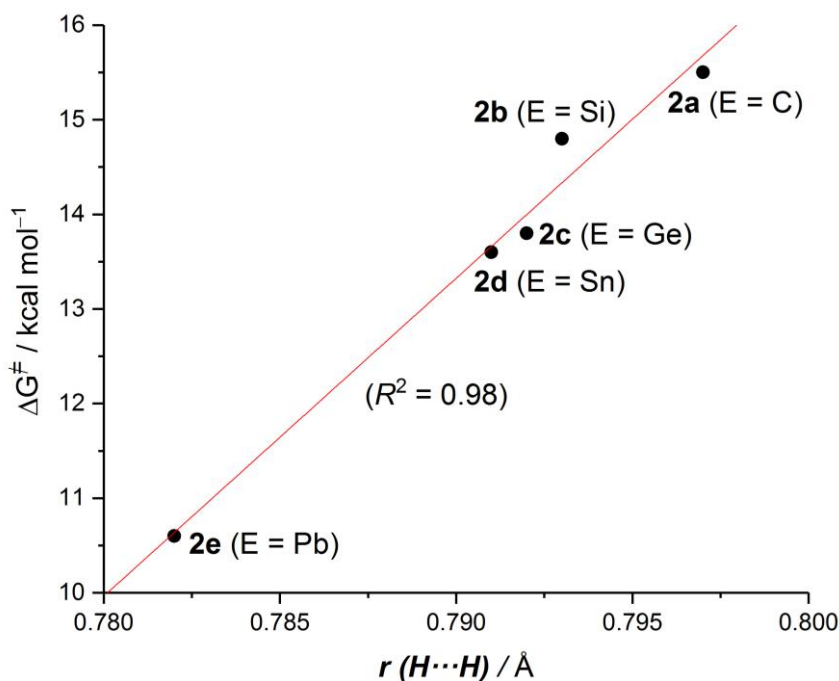


Figure 6.S2. Plot of the computed activation barriers (ΔG^\ddagger) vs the breaking $\text{H}\cdots\text{H}$ distance in the corresponding transition states involved in the **2a-e** + $\text{B}(\text{C}_6\text{F}_5)_3$ + H_2 reaction. All data were computed at the PCM(toluene)-M06-2X/def2-TZVPP//M06-2X-def2-SVP level.

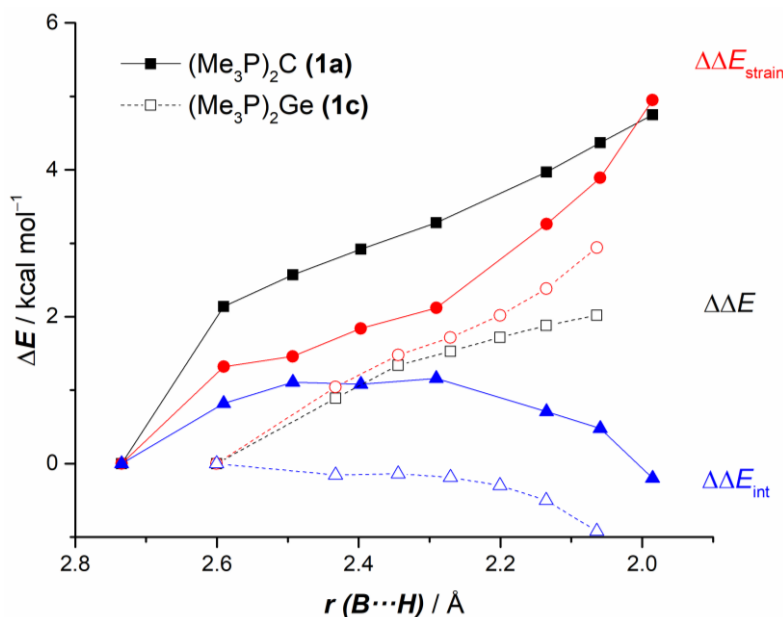


Figure 6.S3. Comparative activation-strain diagrams of the dihydrogen activation reactions mediated by carbene **1a** (solid lines) and germylene **1c** (dashed lines) in the presence of $B(C_6F_5)_3$ along the reaction coordinate projected onto the forming $B\cdots H$ bond length. All data were computed at the M06-2X/TZ2P//M06-2X/def2-SVP level and are referenced to the corresponding reactant complexes.

Table 6.S1. Comparison of the computed activation barriers including relativistic effects.

| <i>ylidone</i> | $\Delta E^\ddagger^{[a]}$ | $\Delta E^\ddagger^{[b]}$ |
|----------------|---------------------------|---------------------------|
| 1a | 4.7 | 4.7 |
| 1b | 1.9 | 2.3 |
| 1c | 1.5 | 1.7 |
| 1d | 1.0 | 1.3 |
| 1e | 0.3 | 0.1 |
| 2a | 2.0 | 1.7 |
| 2b | 3.1 | 3.1 |
| 2c | 2.7 | 3.0 |
| 2d | 3.0 | 2.8 |
| 2e | 0.6 | 0.5 |
| 3a | 4.5 | 4.1 |
| 3b | 2.3 | 1.9 |
| 3c | 4.0 | 3.7 |
| 3d | 4.2 | 4.4 |
| 3e | 3.0 | 3.0 |

Computed activation barriers, $\Delta E^\ddagger = E(\text{TS}) - E(\text{RC})$. [a] Computed at the PCM(toluene)-M06-2X/def2-TZVPP//M06-2X/def2-SVP level. [b] Computed at the ZORA-COSMO(toluene)-M06-2X/TZ2P//M06-2X/def2-SVP.

VII. CHAPTER 5

Understanding the role of frustrated Lewis pairs as ligands in transition metal-catalyzed reactions

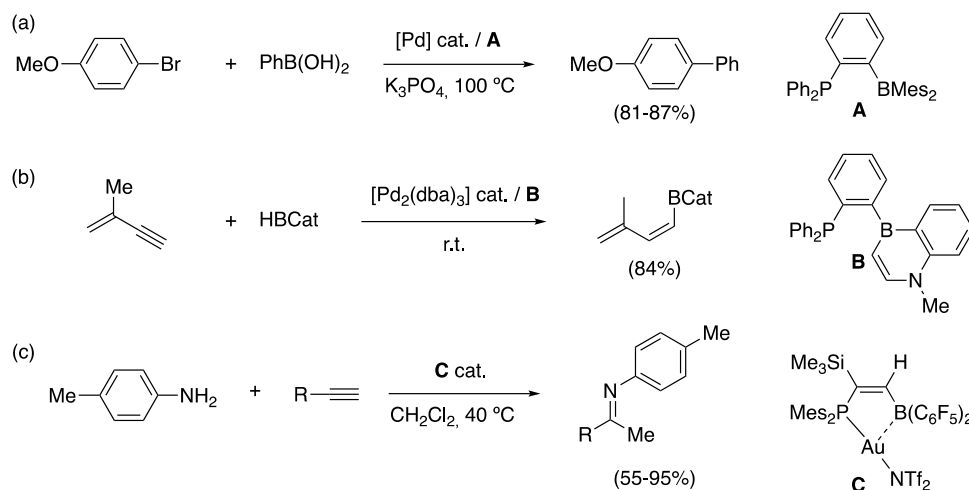
The role of frustrated Lewis pairs (FLPs) as ligands in gold(I) catalyzed-reactions has been computationally investigated by using state-of-the-art density functional theory calculations. To this end, the nature of (P,B)-FLP-transition metal interactions in different gold(I)-complexes has been first explored in detail with the help of the energy decomposition analysis method, which allowed us to accurately quantify the so far poorly understood Au \cdots B interactions present in these species. The impact of such interactions on the catalytic activity of gold(I)-complexes has been then evaluated by performing the Au(I)-catalyzed hydroarylation reaction of phenylacetylene with mesitylene. With the help of the activation strain model of reactivity, the factors governing the higher activity of Au(I)-complexes having a FLP as a ligand as compared to that of the parent PPh₃ system have also been quantitatively identified.

Dalton Trans., **2020**, *49*, 3129-3137.

Introduction

Since the seminal work by Stephan and co-workers in 2006 on reversible dihydrogen activation mediated by a system having a Lewis acid and a Lewis base in its structure,¹ the so-called frustrated Lewis pairs (FLPs) have emerged as powerful species to activate small molecules under metal-free conditions in both stoichiometric and catalytic reactions.² These species are typically composed of a pair of sterically encumbered Lewis acidic and Lewis basic centers, in either single molecules or bimolecular systems, which severely hampers the formation of a classical donor–acceptor bond between them. This peculiar bonding situation is responsible for the unique and rich reactivity of these compounds, which in many instances was traditionally restricted to transition metals.²

FLPs have also been used as ambiphilic ligands in transition metal chemistry.^{3,4} Interestingly, the presence of a Lewis acid moiety nearby transition metals can significantly influence their reactivity. For instance, Bourissou and co-workers reported that, in comparison with PPh₃ as a ligand, FLP **A** improved the efficiency of the Pd-catalyzed Suzuki–Miyaura coupling of *p*-bromoanisole with PhB(OH)₂ (Scheme 7.1a).⁵ Similarly, Liu and co-workers used related FLP **B** in the Pd-catalyzed hydroboration of enynes (Scheme 7.1b).⁶ As compared to the analogous process involving *o*-naphthalenyl phosphine, FLP **B** not only improves the activity of the catalyst but also provides a markedly different selectivity as a *trans*-hydroboration product is almost exclusively formed. In contrast, a 1,4-hydroboration reaction product is formed in the analogous reaction involving a phosphine lacking the Lewis acidic fragment.

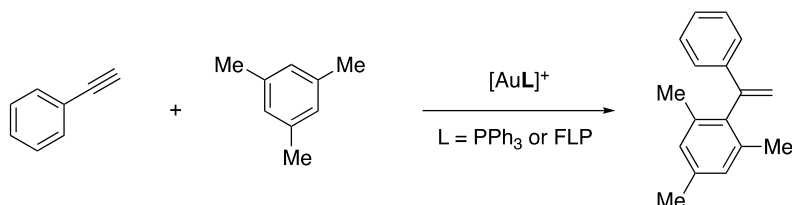


Scheme 7.1. Representative examples of transition metal-catalyzed reactions using FLPs as ligands.

Related intramolecular FLPs have also been used as ligands in gold(I)-catalyzed transformations such as, among others, the intramolecular cyclization reactions of propargylamides⁷ or, quite recently, the intra- and intermolecular hydroamination reactions of alkynes (Scheme 7.1c).⁸ Based on X-ray diffraction studies, it is assumed that the interaction between the strong Lewis acid moiety and the transition metal in either the FLP_{Au}X (X = Cl, NTf) complex or the active catalytic species FLP(Au)⁺ significantly enhances the electrophilic properties of the catalyst, which ultimately results in an enhancement of its catalytic activity. Despite that, very little is known about the actual nature of such transition metal–Lewis acid interaction and its direct consequences on the catalysis, which hampers the further development of novel FLP ligands which are able to increase the activity of transition metal catalysts. For these reasons, we decided to carry out a detailed computational study focused on both unabated issues, namely (i) the nature of the transition metal–Lewis acid interaction in FLP–metal complexes and (ii) its impact on their catalytic activity. Once both aspects are fully and quantitatively understood, the insight gained in this study will be used to conveniently modify the FLP ligand towards the rational design of highly active catalysts.

To this end, we selected a prototypical reaction in transition metal π -catalysis, namely the gold(I)-catalyzed hydroarylation reaction of phenylacetylene with mesitylene,⁹ and compared the reactivities of the processes mediated by typical phosphines (such as PPh₃) with the analogous transformations involving P/B FLPs as ligands (Scheme 7.2). The bonding situation in these complexes and the

computed reactivity trends will be quantitatively analyzed by means of the energy decomposition analysis (EDA)¹⁰ method and the so-called activation strain model (ASM) of reactivity.¹¹ These state-of-the-art computational tools were selected because they were particularly helpful for our current understanding of the chemistry of FLPs¹² and related gold(I)-catalyzed reactions.¹³



Scheme 7.2. Hydroarylation reaction considered in this study.

Theoretical Methods and Computational Details

Geometry optimizations of the molecules were performed without symmetry constraints using the Gaussian16¹⁴ suite of programs with the BP86¹⁵ functional in conjunction with the D3 dispersion correction suggested by Grimme and coworkers.¹⁶ Gold atoms were described using the scalar-relativistic Stuttgart-Dresden SDD effective core potentials and their associated double- ζ basis sets,¹⁷ complemented with a set of polarization functions.¹⁸ The 6-31G(d) basis set was used for the rest of the atoms. Solvent effects (solvent = dichloromethane, DCM) have been taken into account using the Polarizable Continuum Model (PCM)¹⁹ of solvation during the geometry optimizations. This level is denoted as PCM(DCM)-BP86-D3/6-31G(d)&SDD(f) and was chosen because it has been used for related gold complexes.²⁰ Reactants and adducts were characterized by frequency calculations, and have positive definite Hessian matrices. Transition states (TSs) show only one negative eigenvalue in their diagonalized force constant matrices, and their associated eigenvectors were confirmed to correspond to the motion along the reaction coordinate under consideration using the Intrinsic Reaction Coordinate (IRC) method.²¹ Single-point energy refinements in solution were carried out using the M06L²² functional in conjunction with the D3 correction and the triple- ζ -quality plus polarization basis set def2-TZVPP for all atoms.²³ This level is therefore denoted as PCM(DCM)-M06L-D3/def2-TZVPP//PCM(DCM)-BP86-D3/6-31G(d)&SDD(f).

The bonding situation of the species considered in this study was quantitatively analyzed with the help of the energy decomposition analysis (EDA) method.¹⁰ Within this method, the interaction energy between the selected fragments can be decomposed into the following chemically meaningful terms: $\Delta E_{\text{int}}(\zeta) = \Delta E_{\text{elstat}}(\zeta) + \Delta E_{\text{Pauli}}(\zeta) + \Delta E_{\text{orb}}(\zeta) + \Delta E_{\text{disp}}(\zeta)$. The term ΔE_{elstat} corresponds to the quasi-classical electrostatic interaction between the unperturbed charge distributions of the deformed reactants and is usually attractive. The Pauli repulsion, ΔE_{Pauli} , corresponds to the destabilizing interactions between the occupied orbitals and is responsible for any steric repulsion. The orbital interaction term, ΔE_{orb} , accounts for bond pair formation, charge transfer (interaction between occupied orbitals on one moiety and unoccupied orbitals on the other, including HOMO–LUMO interactions), and polarization (empty-occupied orbital mixing on one fragment due to the presence of another fragment). Finally, the ΔE_{disp} term takes into account those interactions derived from dispersion forces. Moreover, the NOCV (natural orbital for chemical valence)²⁴ extension of the EDA method has also been used to further partition the ΔE_{orb} term. The EDA–NOCV approach provides pairwise energy contributions for each pair of interacting orbitals to the total bond energy.

The EDA calculations were carried out with the ADF2019 program package²⁵ using the PCM(DCM)-BP86-D3/6-31G(d)&SDD(f) optimized geometries at the same DFT level in conjunction with a triple- ζ -quality basis set using uncontracted Slater-type orbitals (STOs) augmented by two sets of polarization functions with a frozen-core approximation for the core electrons.²⁶ Auxiliary sets of s, p, d, f, and g STOs were used to fit the molecular densities and to represent the Coulomb and exchange potentials accurately in each SCF cycle.²⁷ Scalar relativistic effects were incorporated by applying the zeroth-order regular approximation (ZORA).²⁸ This level of theory is denoted as ZORA-BP86-D3/TZ2P//PCM(DCM)-BP86-D3/6-31G(d)&SDD(f) and has been selected because of its good performance in the analysis of the bonding situation of a wide variety of transition metal complexes including Au(I) species.^{20,29}

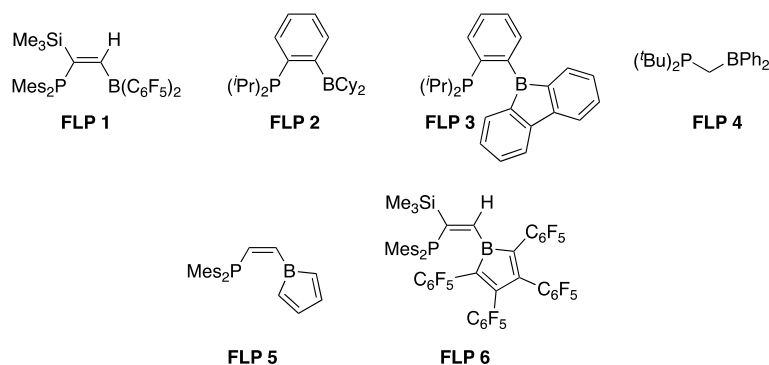
Results and Discussion

(a) Nature of the [Au–FLP] bond

We first quantitatively analyzed the nature of the Au–FLP bond with the help of the Energy decomposition analysis – natural orbital for chemical valence (EDA–NOCV) method. To this end, we investigated the interaction between the FLPs **1–6** (see Table 7.1) and the Au(I) fragment in FLP–AuX complexes (X = NTf₂, Cl). FLPs **1–3** were selected because they have been experimentally used as ligands in transition metal chemistry by Erker and co-workers (FLP **1**)⁸ and Borissou and co-workers (FLPs **2** and **3**).³⁰ Geminal P/B FLP **4** was also included in our study because this particular system shows a remarkable reactivity towards the activation of small molecules.³¹ Similarly, FLPs **5** and **6** were included as the 4π-antiaromatic borole fragment has proved to greatly enhance the Lewis acidity of the boron moiety and, as a consequence, the activity of borole containing FLPs.³²

Table 7.1 shows the relativistic and dispersion corrected (ZORA-BP86-D3/TZ2P//PCM-BP86-D3/6-31G(d)&SDD(f) level) EDA–NOCV calculations for the considered FLP–AuNTf₂ complexes and the parent Ph₃P–AuNTf₂ system. From the data in Table 7.1, it becomes evident that the interaction between the FLP and AuNTf₂ fragments is clearly much stronger than that in the parent Ph₃P–AuNTf₂ ($\Delta E_{\text{int}} = -86.7 \text{ kcal mol}^{-1}$ vs. -103.0 to $-108.7 \text{ kcal mol}^{-1}$). In all cases, this is due to the enhancement of all the attractive interactions, namely electrostatic, orbital and also dispersion interactions (measured by the ΔE_{elstat} , ΔE_{orb} and ΔE_{disp} terms, respectively), which are significantly stronger in the FLP–AuNTf₂ complexes than in Ph₃P–AuNTf₂. Further inspection of the EDA values reveals that the major contribution to the total interaction in all L–AuNTf₂ complexes comes from the electrostatic term ΔE_{elstat} (~ 58 – 65% to ΔE_{int}), which indicates that the Au–L bond is highly polarized. Despite this, the orbital interactions (measured by the ΔE_{orb} term) are also quite significant ($\sim 30\%$ to ΔE_{int}) and remarkably higher in the complexes having the FLPs as ligands, which suggests an important contribution of the Au⋯B orbital interaction to the bonding situation (see below).

Table 7.1. EDA-NOCV analyses of the bonding situation of L–AuNTf₂ complexes. Energy values (in kcal mol⁻¹) were computed at the ZORA-BP86-D3/TZ2P//PCM(DCM)-BP86-D3/6-31G(d)&SDD(f) level.



| L–AuNTf ₂ | L = PPh ₃ | L = FLP 1 | L = FLP 2 | L = FLP 3 | L = FLP 4 | L = FLP 5 | L = FLP 6 |
|--|-------------------------|----------------------|--------------|--------------|--------------|--------------|--------------|
| ΔE_{int} | -86.7 | -103.0 | -105.6 | -105.1 | -106.8 | -103.3 | -108.7 |
| ΔE_{Pauli} | 169.1 | 212.6 | 210.5 | 224.6 | 199.2 | 231.2 | 254.8 |
| $\Delta E_{\text{elstat}}^{\text{[a]}}$ | -167.6 | -182.8 | -199.5 | -207.0 | -195.6 | -201.9 | -209.8 |
| | (65.5%) | (57.9%) | (63.1%) | (62.8%) | (63.9%) | (60.4%) | (57.7%) |
| $\Delta E_{\text{orb}}^{\text{[a]}}$ | -77.8 | -98.9 | -87.4 | -96.1 | -85.2 | -107.7 | -117.6 |
| | (30.4%) | (31.3%) | (27.7%) | (29.2%) | (27.8%) | (32.2%) | (32.4%) |
| $\Delta E_{\text{disp}}^{\text{[a]}}$ | -10.4 | -33.9 | -29.1 | -26.6 | -25.3 | -24.9 | -36.0 |
| | (4.1%) | (10.7%) | (9.2%) | (8.1%) | (8.3%) | (7.4%) | (9.9%) |
| $\Delta E_{\text{orb1}}^{\text{[b]}}$ | -48.7 | -50.6 | -48.3 | -47.4 | -49.5 | -48.0 | -52.3 |
| | (62.6%) | (51.2%) | (55.3%) | (49.3%) | (58.1%) | (44.6%) | (44.5%) |
| $\Delta E_{\text{orb2}}^{\text{[b]}}$ | – | -15.9 | -10.4 | -17.4 | -8.3 | -25.4 | -30.8 |
| | | (16.2%) | (11.9%) | (18.1%) | (9.7%) | (23.6%) | (26.2%) |
| $\Delta E_{\text{orb3}}^{\text{[b]}}$ | -8.3 | -6.8 | -7.7 | -7.9 | -7.8 | -8.3 | -7.2 |
| | (10.6%) | (6.8%) | (8.8%) | (8.2%) | (9.2%) | (7.7%) | (6.1%) |
| $\Delta E_{\text{orb4}}^{\text{[b]}}$ | -7.8 | -6.4 | -7.1 | -7.6 | -6.8 | -7.2 | -6.1 |
| | (10.0%) | (6.4%) | (8.2%) | (7.9%) | (8.0%) | (6.7%) | (5.2%) |
| $\Delta E_{\text{orb(rest)}}^{\text{[b]}}$ | -13.0 | -19.2 | -13.9 | -15.9 | -12.8 | -18.7 | -21.3 |
| | (16.7%) | (19.5%) | (15.9%) | (16.5%) | (15.0%) | (17.4%) | (18.1%) |
| $q(\text{Au})^{\text{c}}$ | 0.354 | 0.478 | 0.413 | 0.498 | 0.370 | 0.580 | 0.596 |
| $r(\text{Au}\cdots\text{B})/\text{\AA}$ | – | 2.720 | 2.953 | 2.619 | 3.167 | 2.407 | 2.345 |
| | | (2.712) ^d | | | | | |

^aThe values in parentheses give the percentage contribution to the total attractive interactions $\Delta E_{\text{elstat}} + \Delta E_{\text{orb}} + \Delta E_{\text{disp}}$. ^bThe values in parentheses give the percentage contribution to the total orbital interactions ΔE_{orb} . ^cNatural charges computed at the PCM(DCM)-BP86-D3/6-31G(d)&SDD(f) level. ^dExperimental value taken from ref. 8.

According to the NOCV method, the orbital term in the parent $\text{Ph}_3\text{P-AuNTf}_2$ system is dominated by three orbital interactions, namely the donation from the P-lone pair to the AuNTf_2 fragment (*i.e.* σ -type $\text{P} \rightarrow \text{Au}$ dative bond, denoted as ΔE_{orb1}) together with two weak π -backdonations from the transition metal fragment to the PPh_3 ligand (denoted as ΔE_{orb3} and ΔE_{orb4} , respectively, see Table 7.1 and Fig. 7.1). Strikingly, in the FLP-AuNTf_2 systems, there exists an additional orbital interaction (denoted as ΔE_{orb2}) which involves the donation of electron density from the transition metal atom to the vacant p_z atomic orbital of the boron atom. This additional orbital interaction, which is much stronger than the corresponding π -backdonations, significantly reduces the electron density at the transition metal fragment, therefore enhancing its electrophilicity as compared to the parent $\text{Ph}_3\text{P-AuNTf}_2$ system. This can be confirmed by the computed NBO(Au) charges, which are clearly more positive than those in the parent Au(I)-PPh_3 complex. Not surprisingly, the systems having **FLP2** and **FLP4** show a comparatively weaker $\text{Au}\cdots\text{B}$ interaction, which is reflected in the computed longer $\text{Au}\cdots\text{B}$ distances. This is due, in the case of the **FLP2** complex, to the donor nature of the cyclohexyl groups attached to the boron atom, which reduces its ability to accept electron density from the transition metal. In the case of the **FLP4** system, the shorter tether connecting the P and B fragments hampers the $\text{Au}\cdots\text{B}$ interaction, which indicates that the nature of this tether is crucial to achieving a significant Au-B interaction. In sharp contrast, **FLP5**, which contains a borole in its structure, exhibits a much stronger ΔE_{orb2} interaction as a consequence of the high acidity of this fragment. This is well reflected not only in the highly positive charge at the transition metal ($+0.580e$) but also in the computed markedly short $\text{Au}\cdots\text{B}$ bond distance of 2.470 Å. The effect of the borole fragment becomes even more evident in the **FLP6** system which possesses highly electron-withdrawing C_6F_5 groups attached to the borole fragment, as can be viewed from the computed strongest ΔE_{orb2} interaction ($-30.8 \text{ kcal mol}^{-1}$, which is half as strong as the dominant $\text{P} \rightarrow \text{Au}$ dative bond) and a rather short $\text{Au}\cdots\text{B}$ bond distance of 2.345 Å.

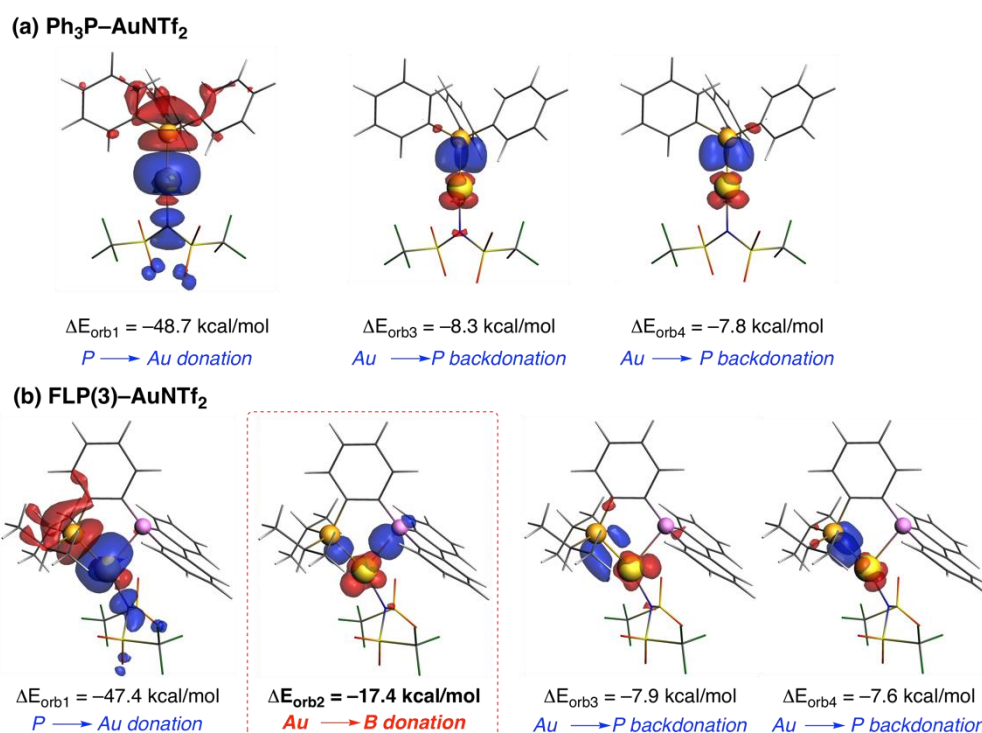


Figure 7.1. Plot of the deformation densities $\Delta\rho$ of the pairwise orbital interactions between AuNTf₂ and PPh₃ (a) or **FLP3** (b) ligands and associated stabilization energies $\Delta E(\rho)$. The code of the charge flow is red→blue.

Similar results were found in the analogous FLP–AuCl complexes. From the data in Table 7.2, which shows the most representative EDA–NOCV values (for the complete set of values, see Table 7.S1 in the Supporting Information), it is confirmed that the total interaction between the FLP and AuCl fragments is stronger than that in the parent Ph₃P–AuCl system. Interestingly, although the trends are essentially identical, the interaction in the chloride complexes is weaker than that in their bistriflimide counterparts, as a result of the lower acceptor nature of the AuCl fragment as compared to that of AuNTf₂. For this reason, the main orbital interaction involving the P → Au dative bond (measured by ΔE_{orb1}) is weaker in all the considered chloride derivatives. As a consequence of the higher electron density at the transition metal, the Au⋯B orbital interaction (measured by ΔE_{orb2}) is slightly stronger in the chloride complexes, which is then translated into slightly shorter Au⋯B distances. Despite this, based on these EDA–NOCV calculations, it can then be concluded that, regardless of the nature of the X counteranion, the FLP ligand induces a significant enhancement of the electrophilicity of the AuX moiety. This effect can be mainly ascribed to the occurrence of a significant Au(d) → B(p_z) molecular orbital interaction, not present

in the parent $\text{Ph}_3\text{P-AuX}$ system, which in addition is manifested in a marked increase in the positive charge at the transition metal.

Table 7.2. EDA-NOCV analyses of the bonding situation of L-AuCl complexes. Energy values (in kcal mol^{-1}) were computed at the ZORA-BP86-D3/TZ2P//PCM(DCM)-BP86-D3/6-31G(d)&SDD(f) level.

| L-AuCl | $\text{L} =$ PPh_3 | $\text{L} =$ FLP 1 | $\text{L} =$ FLP 2 | $\text{L} =$ FLP 3 | $\text{L} =$ FLP 4 | $\text{L} =$ FLP 5 | $\text{L} =$ FLP 6 |
|--|--------------------------------|------------------------------|------------------------------|------------------------------|------------------------------|------------------------------|------------------------------|
| ΔE_{int} | -74.2 | -87.6 | -89.4 | -89.3 | -88.8 | -87.7 | -92.8 |
| $\Delta E_{\text{orb}}^{\text{a}}$ | -72.0 (29.5%) | -94.8 (31.2%) | -80.1 (27.6%) | -89.7 (29.3%) | -76.9 (27.3%) | -100.4 (32.4%) | -111.1 (32.7%) |
| $\Delta E_{\text{orb1}}^{\text{b}}$ | -43.1 (59.8%) | -44.6 (47.1%) | -43.3 (54.1%) | -42.5 (47.4%) | -44.0 (57.2%) | -42.6 (42.5%) | -44.6 (40.2%) |
| $\Delta E_{\text{orb2}}^{\text{b}}$ | — | -20.8 (21.9%) | -10.4 (13.0%) | -17.8 (19.8%) | -8.0 (10.4%) | -27.3 (27.2%) | -34.5 (31.0%) |
| $q(\text{Au})^{\text{c}}$ | 0.280 | 0.453 | 0.343 | 0.432 | 0.305 | 0.514 | 0.548 |
| $r(\text{Au}\cdots\text{B})/\text{\AA}^{\text{d}}$ | — | 2.592 (2.347) | 2.963 (2.903) | 2.610 (2.663) | 3.126 | 2.416 | 2.322 |

^a The values in parentheses give the percentage contribution to the total attractive interactions $\Delta E_{\text{elstat}} + \Delta E_{\text{orb}} + \Delta E_{\text{disp}}$. ^b The values in parentheses give the percentage contribution to the total orbital interactions ΔE_{orb} . ^c Natural charges computed at the PCM(DCM)-BP86-D3/6-31G(d)&SDD(f) level. ^d Experimental values are given within parentheses.

(b) Impact of the $\text{Au}\cdots\text{B}$ interaction on the reactivity

From the results described above, it can be anticipated that the activity of gold(I) catalysts having a FLP ligand leading to a significant $\text{Au}\cdots\text{B}$ interaction will be higher than that of their PPh_3 counterpart and those systems exhibiting a weaker $\text{Au}\cdots\text{B}$ interaction (*i.e.* XAu-FLP4). To confirm this hypothesis, we explored the hydroarylation reaction of phenylacetylene with mesitylene mediated by gold(I)-catalysts (see Scheme 7.2), a process experimentally studied by Alcarazo and co-workers using cationic phosphines as ligands.³³ This transformation begins from an initial π -complex, formed upon coordination of the triple bond of phenylacetylene to the active gold(I) catalyst (*i.e.* AuL^+), which then suffers a nucleophilic attack from the mesitylene to produce a new C–C bond. Then, the Au–C protonolysis reaction produces the observed final alkene with the concomitant regeneration of the active catalyst. As previously reported for strongly

related processes,^{13,34} the initial nucleophilic addition reaction constitutes the rate-limiting step of the entire transformation and for this reason, herein we exclusively focused on the C–C bond forming reaction. Besides considering the processes involving the complexes having **FLP4**, **FLP5** and **FLP6** as ligands, we also considered the analogous reactions involving the slightly modified **FLP1'** and **FLP3'**, where the mesityl and isopropyl groups in **FLP1** and **FLP3**, respectively, were replaced with phenyl groups to enable a direct comparison with the analogous process involving PPh₃ as the ligand.

Figure 7.2 shows the computed reaction profile for the transformations involving the parent PPh₃ ligand and **FLP3'** as a representative ligand for the FLP containing Au(I)-complexes. As readily seen in Fig. 7.2, the process begins with the formation of a weakly bonded van der Waals complex (**RC–L**), which lies 5–10 kcal mol⁻¹ below the separate reactants (the formation of these species becomes endergonic when thermal free-energy corrections are included, see also Table 7.3). From this species, the nucleophilic addition takes place via **TS–L**, a saddle point associated with the formation of the new C–C bond. Despite rather similar reaction profiles, the transformation involving **FLP3'** as the ligand is clearly favored over the analogous process involving PPh₃ along the entire reaction coordinate, and particularly, in the transition state region ($\Delta\Delta E^\ddagger = 3.7$ kcal mol⁻¹; $\Delta\Delta G^\ddagger = 1.5$ kcal mol⁻¹). Therefore, our calculations clearly confirm the anticipated (and experimentally observed) higher activity of the FLP containing gold(I)-catalysts as compared to their parent PPh₃ counterpart.

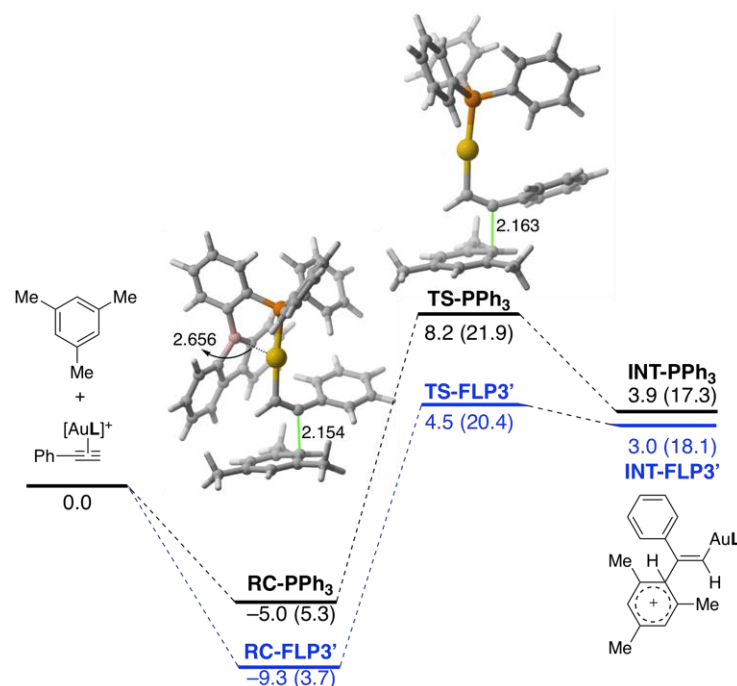


Figure 7.2. Computed reaction profiles for the hydroarylation reaction of phenylacetylene and mesitylene mediated by $[\text{Au}-\text{PPh}_3]^+$ (black lines) and $[\text{Au}-\text{FLP3}']^+$ (blue lines). Relative total energies (free energies, at 298.15 K, are given within parentheses) and bond lengths are given in kcal/mol^{-1} and angstroms, respectively. All data have been computed at the PCM(DCM)-M06L-D3/def2-TZVPP//PCM(DCM)-BP86-D3/6-31G(d)SDD(f) level.

Table 7.3. Computed energies (in kcal mol^{-1}) and free energies (within parentheses) for the L–Au(I)-catalyzed hydroarylation reactions involving phenylacetylene and mesitylene. All data have been computed at the PCM(DCM)-M06L-D3/def2-TZVPP//PCM(DCM)-BP86-D3/6-31G(d)&SDD(f) level.

| L | $\Delta E(\text{RC-L})^a$ | $\Delta E(\text{TS-L})^b$ | ΔE_R^c | BVD ^d |
|------------------------|---------------------------|---------------------------|----------------|------------------|
| PPh₃ | -5.0 (5.3) | 8.2 (21.9) | 3.9 (17.3) | – |
| FLP1' | -7.2 (5.9) | 6.5 (21.0) | 1.4 (17.6) | 0.55 |
| FLP3' | -9.3 (3.7) | 4.5 (20.4) | 3.0 (18.1) | 0.57 |
| FLP4 | -8.6 (2.3) | 8.7 (21.4) | 5.2 (20.1) | 0.56 |
| FLP5 | -7.7 (5.2) | 4.1 (19.5) | -1.6 (13.4) | 0.59 |
| FLP6 | -11.4 (2.5) | -0.9 (13.6) | -7.3 (9.5) | 0.65 |

^a Reactant complex (RC) energy: $\Delta E(\text{RC-L}) = E(\text{RC-L}) - E(\text{mesitylene}) - E(\pi\text{-complex})$.

^b Transition state (TS) energy: $\Delta E(\text{TS-L}) = E(\text{TS-L}) - E(\text{mesitylene}) - E(\pi\text{-complex})$. ^c

Reaction energies: $\Delta E_R = E(\text{INT-L}) - E(\text{mesitylene}) - E(\pi\text{-complex})$. ^d Boron valence deficiency (BVD) computed for the corresponding H-BR₂ systems.

Similar reaction profiles were found for the rest of the considered hydroarylation reactions. From the data in Table 7.3, it is confirmed that the corresponding reactions involving the FLPs are favored along the entire reaction

coordinate and proceed faster than the analogous reaction involving the PPh₃ ligand, with the exception of the process involving **FLP4** as the ligand. In particular, the processes involving **FLP5** and especially **FLP6**, having a borole fragment as a Lewis acid, are predicted to proceed with the lowest activation barriers in all the considered hydroarylation reactions ($\Delta G^\ddagger = 19.5$ kcal mol⁻¹ and $\Delta G^\ddagger = 13.6$ kcal mol⁻¹ for **FLP5** and **FLP6**, respectively). This can mainly be attributed to the high acidity of the borole moiety, which significantly enhances the Au···B interaction as compared to the rest of the FLPs herein considered (see above). The computed high boron valence deficiency (BVD) values, which are suggested as a direct measure of boron Lewis acidity,³⁵ confirm the high acidity of the borole fragment in **FLP5** and, particularly, in **FLP6** (see Table 7.3). For the same reason, it is not surprising that the process involving **FLP4**, which exhibits the weakest Au···B interaction (and the lowest BVD of 0.56), proceeds with a rather similar barrier to that of the parent hydroarylation reaction involving PPh₃ ($\Delta E^\ddagger = 8.7$ kcal mol⁻¹; $\Delta G^\ddagger = 21.4$ kcal mol⁻¹). Therefore, these findings strongly suggest that there exists a direct causal correlation between the strength of the Au···B interaction and the activity of the gold(I)-catalysts.

To gain further quantitative insight into the impact of the Au···B interaction on the reactivity, we next applied the activation strain model (ASM) of reactivity. This approach, which has been really helpful for our current understanding of a number of fundamental reactions including transition metal-catalyzed processes,¹¹ decomposes the total energy into two contributions, namely the strain energy (ΔE_{strain}) that results from the distortion experienced by the individual reactants during the transformation and the interaction energy (ΔE_{int}) between these distorted reactants along the reaction coordinate. Figure 7.3 shows the activation strain diagrams (ASDs) for the hydroarylation reactions involving mesitylene and the initially formed π -complexes [Ph₃P–Au–phenylacetylene]⁺ or [**FLP3'**–Au–phenylacetylene]⁺ from the corresponding reactant complexes (**RC-L**) up to the respective transition states (**TS-L**) projected onto the forming C···C bond distance. As readily seen in Fig. 7.3, the energy required to deform the reactants from their equilibrium geometries to the geometry that they adopt at the transition state (measured by the ΔE_{strain} term) is nearly identical for both processes, which indicates that the required distortion is not all decisive for the observed difference of reactivity. At variance, the interaction energy between the deformed reactants (ΔE_{int}) is clearly much stronger for the process involving **FLP3'** as the ligand from

the very beginning of the process up the transition state region. This stronger interaction, as compared to the parent process involving the PPh_3 ligand, is then solely responsible for the lower barrier computed for the process involving the **FLP3'** ligand. Therefore, it can be concluded that the FLP ligand, when able to establish a significant $\text{Au}\cdots\text{B}$ interaction, makes the corresponding π -complex more prone to undergo the nucleophilic addition reaction, which is ultimately translated into a lower activation barrier.

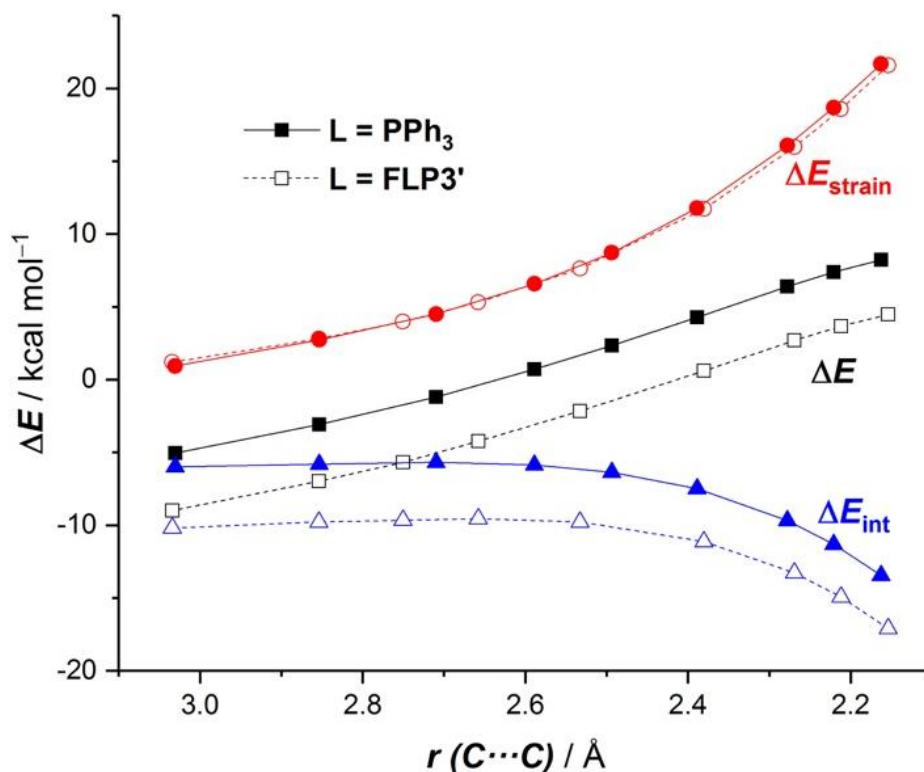


Figure 7.3. Comparative activation strain diagrams for the hydroarylation reactions involving mesitylene and the π -complexes $[\text{Ph}_3\text{P-Au-phenylacetylene}]^+$ (solid lines) or $[\text{FLP3}'\text{-Au-phenylacetylene}]^+$ (dashed lines) along the reaction coordinate projected onto the forming $\text{C}\cdots\text{C}$ bond. All data have been computed at the PCM(DCM)-M06L-D3/def2-TZVPP//PCM(DCM)-BP86-D3/6-31G(d)&SDD(f) level.

The origins of the above-mentioned enhanced interaction between the reactants along the reaction coordinate for the processes involving FLPs as ligands can be found by analyzing the main features of the initial π -complexes formed upon the coordination of phenylacetylene to the active $[\text{Au-L}]^+$ catalysts. As can be seen in Table 7.4, the Au-C bond length, involving the reactive C2 carbon atom of phenylacetylene, becomes systematically longer in all the complexes having the FLP ligand as compared to the analogous π -complex involving the parent PPh_3 ligand.

This is particularly evident in those species having the highly acidic borole moiety in their structures (**FLP5** and **FLP6**), which show the longest Au–C(2) bonds. As a result of this $\eta^2 \rightarrow \eta^1$ slippage (as compared to the PPh₃ system, where the extent of asymmetry of both Au–C bonds is much lower), the electrophilicity of the reactive carbon atom of the coordinated phenylacetylene (*i.e.* C2) is significantly enhanced. This can be confirmed by the increase in the positive charge at this carbon atom and by the stabilization of the corresponding LUMO (*i.e.* the orbital accepting the electron density coming from the nucleophile). Indeed, a good linear correlation was found when plotting these LUMO energies versus the computed activation barriers (correlation coefficient of 0.91, see Fig. 7.S1 in the Supporting Information). These findings are in line with the earlier seminal work by Eisenstein and Hoffmann about the impact of the $\eta^2 \rightarrow \eta^1$ slippage on the shape and energy of the LUMO of related transition metal activated olefins.³⁶ More recently, this idea has also been successfully applied to nucleophilic additions to Pt(II),³⁷ Rh(I)³⁸ or Au(I)-coordinated alkenes.^{12a}

Table 7.4. Main features (Au–C2 distance, natural charge at C2 and LUMO energy) of the initial π -complexes [L–Au–phenylacetylene]⁺ in kcal mol⁻¹. All data have been computed at the PCM(DCM)-BP86-D3/6-31G(d)&SDD(f) level.

| L | $r(\text{Au}-\text{C}2)/\text{\AA}$ | $q(\text{C}2)$ | $E_{\text{LUMO}}/\text{eV}$ | $r(\text{Au}\cdots\text{B})/\text{\AA}$ |
|------------------|-------------------------------------|----------------|-----------------------------|---|
| PPh ₃ | 2.348 | 0.050 | -3.66 | – |
| FLP1' | 2.440 | 0.062 | -3.80 | 3.079 |
| FLP3' | 2.397 | 0.052 | -3.73 | 2.818 |
| FLP4 | 2.425 | 0.058 | -3.51 | 3.457 |
| FLP5 | 2.467 | 0.071 | -4.07 | 2.430 |
| FLP6 | 2.544 | 0.093 | -4.59 | 2.371 |

Not surprisingly, the systems having the borole fragment, which exhibit the strongest Au \cdots B interaction as viewed from the computed shortest Au \cdots B distances (see Table 7.4), present the most stabilized LUMOs and the highest value of the positive charge at C2. Consequently, we predict that these particular complexes having a borole as a Lewis acid partner constitute promising candidates to achieve facile nucleophilic additions. Therefore, it can be concluded that the Au \cdots B

interaction in these species induces a remarkable enhancement of the electrophilicity of the corresponding reactive π -complexes (E_{LUMO} ranging from -3.73 eV to -4.59 eV) as compared to those species lacking this interaction (*i.e.* PPh₃ ligand, $E_{\text{LUMO}} = -3.66$ eV) or where the Au \cdots B interaction is almost negligible (*i.e.* FLP4 ligand, $E_{\text{LUMO}} = -3.51$ eV, and $r(\text{Au}\cdots\text{B}) = 3.457$ Å).

Conclusion

From the results of the computational study reported herein, it can be concluded that P/B FLPs are able to establish relatively strong Au \cdots B interactions, whose strength is directly related to the acidity of the boron moiety. This interaction involves the donation of electron density from the transition metal atom to the vacant p_z atomic orbital of the boron atom and significantly reduces the electron density at the transition metal fragment, therefore enhancing its electrophilicity as compared to the parent Ph₃P–AuX system. In the particular gold(I)-catalyzed hydroarylation reaction considered in this study, which can be used as a model for a transformation involving π -catalysis, the Au \cdots B interaction makes the corresponding π -complex, initially formed upon coordination of the triple bond of phenylacetylene to the active [Au–FLP]⁺ catalyst, much more prone to undergo a nucleophilic addition reaction. This is confirmed by the higher positive charge at the reactive C2 carbon atom and the stabilization of the LUMO of these π -complexes as compared to their PPh₃ π -complex counterpart. As a consequence, the interaction energy between the reactants, from the very beginning of the transformation up to the corresponding transition states associated with the C–C bond formation, is stronger than that of the analogous process involving the parent PPh₃ as the ligand. This stronger interaction is ultimately translated into the lower activation barriers computed for the processes involving FLPs as ligands and is therefore the main factor behind the observed higher activity of these species. Finally, our calculations suggest that FLPs having a borole fragment as an acidic partner lead to markedly strong Au \cdots B interactions, which indicates that the corresponding catalysts constitute really promising candidates to achieve facile nucleophilic addition. In our opinion, the present study not only rationalizes, in a quantitative manner, the nature of the so far poorly understood interaction between FLPs and transition metals but also provides novel insights that can be further applied to modify FLP ligands towards the rational design of highly active catalysts.

References

- ¹ G. C. Welch, R. R. San Juan, J. D. Masuda, D. W. Stephan, *Science* **2006**, *314*, 1124-1126.
- ² For recent reviews, see: (a) D. W. Stephan, G. Erker, *Angew. Chem. Int. Ed.*, **2010**, *49*, 46-76; (b) G. Erker, *Pure Appl. Chem.*, **2012**, *84*, 2203-2217; (c) D. W. Stephan, G. Erker, *Chem. Sci.*, **2014**, *5*, 2625-2641; (d) D. W. Stephan, G. Erker, *Angew. Chem. Int. Ed.*, **2015**, *54*, 6400-6441; (e) D. W. Stephan, *Acc. Chem. Res.*, **2015**, *48*, 306-316; (f) D. W. Stephan, *Science*, **2016**, *354*, aaf7229.
- ³ Selected examples: (a) F. Fontaine, J. Boudreau, M.-H. Thibault, *Eur. J. Inorg. Chem.*, **2008**, 5439-5454; (b) M. Sircoglou, M. Mercy, N. Saffon, Y. Coppel, G. Bouhadir, L. Maron, D. Bourissou, *Angew. Chem. Int. Ed.*, **2009**, *48*, 3454-3457; (c) A. J. M. Miller, J. A. Labinger, J. E. Bercaw, *J. Am. Chem. Soc.*, **2010**, *132*, 3301-3303; (d) A. Amgoune, S. Ladeira, K. Miqueu, D. Bourissou, *J. Am. Chem. Soc.*, **2012**, *134*, 6560-6563.
- ⁴ For a recent review, see: G. Bouhadir, D. Bourissou, *Chem. Soc. Rev.* **2016**, *45*, 1065-1079.
- ⁵ (a) R. Malacea, N. Saffon, M. Gómez, D. Bourissou, *Chem. Commun.*, **2011**, *47*, 8163-8165. See also, (b) R. Malacea, F. Chahdoura, M. Devillard, N. Saffon, M. Gómez, D. Bourissou, *Adv. Synth. Catal.*, **2013**, *355*, 2274-2284.
- ⁶ S. Xu, F. Haeffner, B. Li, L. N. Zakharov, S. Y. Liu, *Angew. Chem. Int. Ed.*, **2014**, *53*, 6795-6799.
- ⁷ M. Devillard, E. Nicolas, C. Appelt, J. Backs, S. Mallet-Ladeira, G. Bouhadir, J. C. Slootweg, W. Uhl, D. Bourissou, *Chem. Commun.*, **2014**, *50*, 14805-14808.
- ⁸ A. Ueno, K. Watanabe, C. G. Daniliuc, G. Kehr, G. Erker, *Chem. Commun.*, **2019**, *55*, 4367-4370.
- ⁹ Selected reviews on transition metal catalyzed hydroarylation reactions: (a) X. Zeng, *Chem. Rev.*, **2013**, *113*, 6864-6900; (b) M. E. Muratore, A. M. Echavarren, Gold-catalyzed hydroarylation of alkynes, *PATAI's Chemistry of Functional Groups* (Ed. Z. Rappoport), Wiley, Hoboken, 2015; (c) L. Yang, H. Huang, *Chem. Rev.*, **2015**, *115*, 3468-3571; (d) Z. Dong, Z. Ren, S. J. Thompson, Y. Xu, G. Dong, *Chem. Rev.*, **2017**, *117*, 9333-9403; (e) *Catalytic hydroarylation of carbon-carbon multiple bonds* (eds.: L. Ackerman, T. B. Gunnoe, L. G. Habgood), Wiley, Hoboken, 2018.
- ¹⁰ For reviews on the EDA method, see: (a) F. M. Bickelhaupt, E. J. Baerends, in *Reviews in Computational Chemistry*, (Eds. K. B. Lipkowitz, D. B. Boyd), Wiley-VCH: New York, 2000, Vol. 15, pp. 1-86; (b) M. von Hopffgarten, G. Frenking, *WIREs Comput. Mol. Sci.*, **2012**, *2*, 43; (c) L. Zhao, M. von Hopffgarten, D. M. Andrada, G. Frenking, *WIREs Comput. Mol. Sci.*, **2018**, *8*, e1345.
- ¹¹ (a) I. Fernández, F. M. Bickelhaupt, *Chem. Soc. Rev.*, **2014**, *43*, 4953; (b) L. P. Wolters, F. M. Bickelhaupt, *WIREs Comput. Mol. Sci.*, **2015**, *5*, 324; (c) F. M. Bickelhaupt, K. N. Houk, *Angew. Chem. Int. Ed.*, **2017**, *56*, 10070. See also, (d) I. Fernández, in *Discovering the Future of Molecular Sciences* (Ed.: B. Pignataro), Wiley-VCH, Weinheim, 2014, pp. 165-187.
- ¹² (a) D. Yepes, P. Jaque, I. Fernández, *Chem. Eur. J.*, **2016**, *22*, 18801-18809; (b) D. Yepes, P. Jaque, I. Fernández, *Chem. Eur. J.*, **2018**, *24*, 8833-8840; (c) J. J. Cabrera-Trujillo, I. Fernández, *Chem. Eur. J.*, **2018**, *24*, 17823-17831; (d) J. J. Cabrera-Trujillo, I. Fernández, *Inorg. Chem.*, **2019**, *58*, 7828-7836; (e) J. J. Cabrera-Trujillo, I. Fernández, *J. Phys. Chem. A*, **2019**, *123*, 10095-10101.
- ¹³ (a) A. Couce-Rios, A. Lledós, I. Fernández, G. Ujaque, *ACS Catal.*, **2019**, *9*, 848-858; (b) Y. García-Rodeja, I. Fernández, *Organometallics*, **2017**, *36*, 460-466.
- ¹⁴ Gaussian 16, Revision B.01, M. J. Frisch, G. W. Trucks, H. B. Schlegel, G. E. Scuseria, M. A. Robb, J. R. Cheeseman, G. Scalmani, V. Barone, G. A. Petersson, H. Nakatsuji, X. Li, M. Caricato, A. Marenich, J. Bloino, B. G. Janesko, R. Gomperts, B. Mennucci, H. P. Hratchian,

J. V. Ortiz, A. F. Izmaylov, J. L. Sonnenberg, D. Williams-Young, F. Ding, F. Lipparini, F. Egidi, J. Goings, B. Peng, A. Petrone, T. Henderson, D. Ranasinghe, V. G. Zakrzewski, J. Gao, N. Rega, G. Zheng, W. Liang, M. Hada, M. Ehara, K. Toyota, R. Fukuda, J. Hasegawa, M. Ishida, T. Nakajima, Y. Honda, O. Kitao, H. Nakai, T. Vreven, K. Throssell, J. A. Montgomery, Jr., J. E. Peralta, F. Ogliaro, M. Bearpark, J. J. Heyd, E. Brothers, K. N. Kudin, V. N. Staroverov, T. Keith, R. Kobayashi, J. Normand, K. Raghavachari, A. Rendell, J. C. Burant, S. S. Iyengar, J. Tomasi, M. Cossi, J. M. Millam, M. Klene, C. Adamo, R. Cammi, J. W. Ochterski, R. L. Martin, K. Morokuma, O. Farkas, J. B. Foresman, D. J. Fox, Gaussian, Inc., Wallingford CT, 2016.

¹⁵ (a) A. D. Becke, *Phys. Rev. A*, **1988**, 38, 3098-3100; (b) J. P. Perdew, *Phys. Rev. B*, **1986**, 33, 8822-8824.

¹⁶ S. Grimme, J. Antony, S. Ehrlich, H. Krieg, *J. Chem. Phys.*, **2010**, 132, 154104-154119.

¹⁷ D. Andrae, U. Häussermann, M. Dolg, H. Stoll, H. Preuss, *Theor. Chim. Acta*, **1990**, 77, 123-141.

¹⁸ A. W. Ehlers, M. Böhme, S. Dapprich, A. Gobbi, A. Hollwarth, V. Jonas, K. G. Köhler, R. Stegmann, A. Veldkamp, G. Frenking, *Chem. Phys. Lett.*, **1993**, 208, 111-114.

¹⁹ (a) S. Miertuš, E. Scrocco, J. Tomasi, *Chem. Phys.* **1981**, 55, 117-129; (b) J. L. Pascual-Ahuir, E. Silla, I. Tuñón, *J. Comput. Chem.* **1994**, 15, 1127-1138; (c) V. Barone, M. Cossi, *J. Phys. Chem. A* **1998**, 102, 1995-2001.

²⁰ (a) M. Baya, U. Belío, I. Fernández, S. Fuertes, A. Martín, *Angew. Chem. Int. Ed.*, **2016**, 55, 6978-6982; (b) M. Baya, U. Belío, D. Campillo, I. Fernández, S. Fuertes, A. Martín, *Chem. Eur. J.*, **2018**, 24, 13879-13889.

²¹ C. González, H. B. Schlegel, *J. Phys. Chem.*, **1990**, 94, 5523-5527.

²² Y. Zhao, D. G. Truhlar, *Theor. Chem. Acc.*, **2008**, 120, 215-241.

²³ F. Weigend, R. Ahlrichs, *Phys. Chem. Chem. Phys.*, **2005**, 7, 3297-3305.

²⁴ M. P. Mitoraj, A. Michalak, T. A. Ziegler, *J. Chem. Theory Comput.*, **2009**, 5, 962-975.

²⁵ (a) G. te Velde, F. M. Bickelhaupt, E. J. Baerends, C. Fonseca Guerra, S. J. A. van Gisbergen, J. G. Snijders, T. Ziegler, *J. Comput. Chem.*, **2001**, 22, 931-967; (b) *ADF2019*, SCM, Theoretical Chemistry, Vrije Universiteit, Amsterdam, The Netherlands, <http://www.scm.com>.

²⁶ J. G. Snijders, P. Vernooijs, E. J. Baerends, *At. Data Nucl. Data Tables*, **1981**, 26, 483-509.

²⁷ J. Krijn, E. J. Baerends, *Fit Functions in the HFS-Method*, Internal Report (in Dutch), Vrije Universiteit Amsterdam, The Netherlands, 1984.

²⁸ (a) E. van Lenthe, E. J. Baerends, J. G. Snijders, *J. Chem. Phys.*, **1993**, 99, 4597-4610; (b) E. van Lenthe, E. J. Baerends, J. G. Snijders, *J. Chem. Phys.*, **1994**, 101, 9783-9792; (c) E. van Lenthe, A. Ehlers, E. J. Baerends, *J. Chem. Phys.*, **1999**, 110, 8943-8953.

²⁹ Selected recent examples: (a) K. Freitag, M. Molon, P. Jerabek, K. Dilchert, C. Rösler, R. W. Seidel, C. Gemel, G. Frenking, R. A. Fischer, *Chem. Sci.*, **2016**, 7, 6413-6421; (b) C. Poggel, G. Frenking, *Chem. Eur. J.*, **2018**, 24, 11675-11682; (c) C. Chi, S. Pan, L. Meng, M. Luo, L. Zhao, M. Zhou, G. Frenking, *Angew. Chem. Int. Ed.*, **2019**, 58, 1732-1738.

³⁰ S. Bontemps, G. Bouhadir, K. Miqueu, D. Bourissou, *J. Am. Chem. Soc.*, **2006**, 128, 12056-12057.

³¹ F. Bertini, V. Lyaskovskyy, B. J. J. Timmer, F. J. J. de Kanter, M. Lutz, A. W. Ehlers, J. C. Slootweg, K. Lammertsma, *J. Am. Chem. Soc.*, **2012**, 134, 201-204.

³² (a) J. J. Cabrera-Trujillo, I. Fernández *Chem. Commun.*, **2019**, 55, 675-678. See also, (b) A. Y. Houghton, J. Hurmalainen, A. Mansikkamäli, W. E. Piers, H. M. Tuononem, *Nat. Chem.*, **2014**, 6, 983-988.

³³ H. Tinnermann, C. Wille, M. Alcarazo, *Angew. Chem. Int. Ed.*, **2014**, 53, 8732-8736.

³⁴ (a) A. S. K. Hashmi, *Acc. Chem. Res.*, **2014**, *47*, 864-876; (b) E. Soriano, I. Fernández, *Chem. Soc. Rev.*, **2014**, *43*, 3041-3105; (c) A. M. Asiri, A. S. K. Hashmi, *Chem. Soc. Rev.*, **2016**, *45*, 4471-4503.

³⁵ J. A. Plumley, J. D. Evanseck, *J. Phys. Chem. A* **2009**, *113*, 5985-5992.

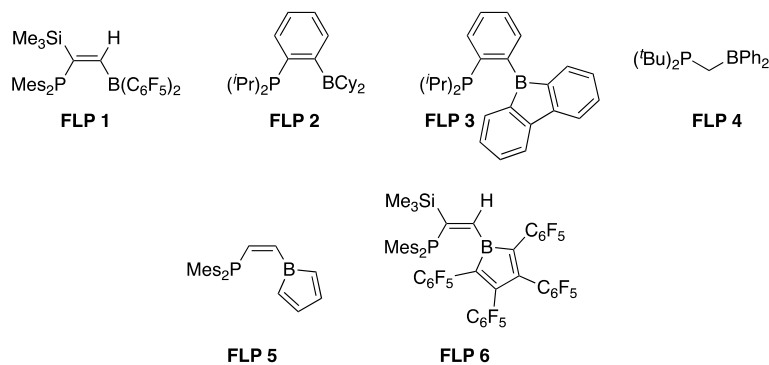
³⁶ (a) O. Eisenstein, R. Hoffmann, *J. Am. Chem. Soc.*, **1980**, *102*, 6148-6149; (b) O. Eisenstein, R. Hoffmann, *J. Am. Chem. Soc.*, **1981**, *103*, 4308-4320.

³⁷ C. R. Barone, R. Cini, E. Clot, O. Eisenstein, L. Maresca, G. Natile, G. Tamasi, G. J. *Organomet. Chem.*, **2008**, *693*, 2819-2827.

³⁸ A. Couce-Rios, A. Lledós, G. Ujaque, *Chem. Eur. J.*, **2016**, *22*, 9311-9320.

Supporting Information

Table 7.S1. EDA-NOCV analyses of the bonding situation of L–AuCl complexes. Energy values (in kcal mol⁻¹) were computed at the ZORA-BP86-D3/TZ2P//PCM(DCM)-BP86-D3/6-31G(d)&SDD(f) level.



| L–AuNTf ₂ | L = PPh ₃ | L = FLP 1 | L = FLP 2 | L = FLP 3 | L = FLP 4 | L = FLP 5 | L = FLP 6 |
|--|-------------------------|------------------|------------------|------------------|--------------|--------------|--------------|
| ΔE_{int} | -74.2 | -87.6 | -89.4 | -89.3 | -88.8 | -87.7 | -92.8 |
| ΔE_{Pauli} | 169.6 | 215.8 | 200.7 | 217.3 | 192.6 | 221.9 | 246.4 |
| $\Delta E_{\text{elstat}}^{\text{[a]}}$ | -163.5 | -188.3 | -192.1 | -199.9 | -188.2 | -194.4 | -205.7 |
| | (61.1%) | (62.1%) | (66.2%) | (65.2%) | (66.9%) | (62.8%) | (60.7%) |
| $\Delta E_{\text{orb}}^{\text{[a]}}$ | -72.0 | -94.8 | -80.1 | -89.7 | -76.9 | -100.4 | -111.1 |
| | (29.5%) | (31.2%) | (27.6%) | (29.3%) | (27.3%) | (32.4%) | (32.7%) |
| $\Delta E_{\text{disp}}^{\text{[a]}}$ | -8.3 | -20.3 | -17.9 | -17.0 | -16.4 | -14.9 | -22.4 |
| | (3.4%) | (6.7%) | (6.2%) | (5.6%) | (5.8%) | (4.8%) | (6.6%) |
| $\Delta E_{\text{orb1}}^{\text{[b]}}$ | -43.1 | -44.6 | -43.3 | -42.5 | -44.0 | -42.6 | -44.6 |
| | (59.8%) | (47.1%) | (54.1%) | (47.4%) | (57.2%) | (42.5%) | (40.2%) |
| $\Delta E_{\text{orb2}}^{\text{[b]}}$ | – | -20.8 | -10.4 | -17.8 | -8.0 | -27.3 | -34.5 |
| | | (21.9%) | (13.0%) | (19.8%) | (10.4%) | (27.2%) | (31.0%) |
| $\Delta E_{\text{orb3}}^{\text{[b]}}$ | -8.7 | -7.0 | -8.1 | -8.0 | -8.0 | -8.5 | -7.7 |
| | (12.1%) | (7.4%) | (10.1%) | (9.0%) | (10.4%) | (8.4%) | (6.9%) |
| $\Delta E_{\text{orb4}}^{\text{[b]}}$ | -8.7 | -6.9 | -7.3 | -8.3 | -7.3 | -7.5 | -6.8 |
| | (12.1%) | (7.3%) | (9.1%) | (9.2%) | (9.4%) | (7.4%) | (6.2%) |
| $\Delta E_{\text{orb(rest)}}^{\text{[b]}}$ | -11.5 | -15.5 | -11.0 | -13.0 | -9.5 | -14.5 | -17.4 |
| | (16.0%) | (16.4%) | (13.7%) | (14.5%) | (12.4%) | (14.5%) | (15.7%) |
| $q(\text{Au})^{\text{c}}$ | 0.280 | 0.453 | 0.343 | 0.432 | 0.305 | 0.514 | 0.548 |
| $r(\text{Au}\cdots\text{B})/\text{\AA}^{\text{[d]}}$ | – | 2.592 (2.347) | 2.963 (2.903) | 2.610 (2.663) | 3.126 | 2.416 | 2.322 |

^a The values in parentheses give the percentage contribution to the total attractive interactions $\Delta E_{\text{elstat}} + \Delta E_{\text{orb}} + \Delta E_{\text{disp}}$. ^b The values in parentheses give the percentage contribution to the total orbital interactions ΔE_{orb} . ^c Natural charges computed at the PCM(DCM)-BP86-D3/6-31G(d)&SDD(f) level. ^d Experimental values are given within parentheses (see ref. 8).

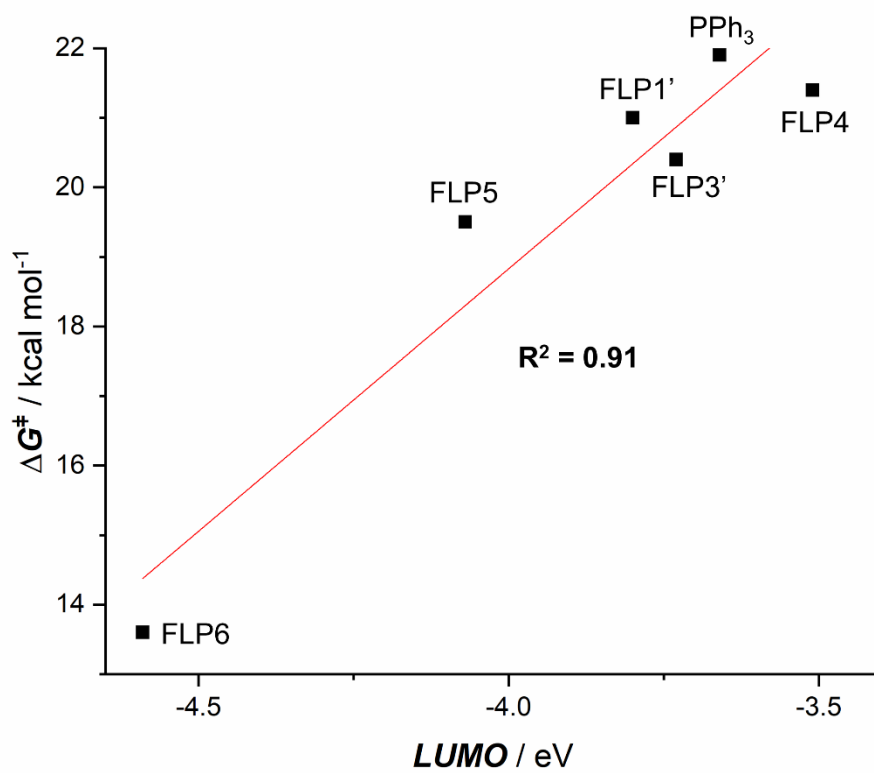


Figure 7.S1. Plot of the free energy barriers of the hydroarylation *vs.* LUMO values.

VIII. CHAPTER 6

Understanding the C–F bond activation mediated by frustrated Lewis pairs: Crucial role of non-covalent interactions

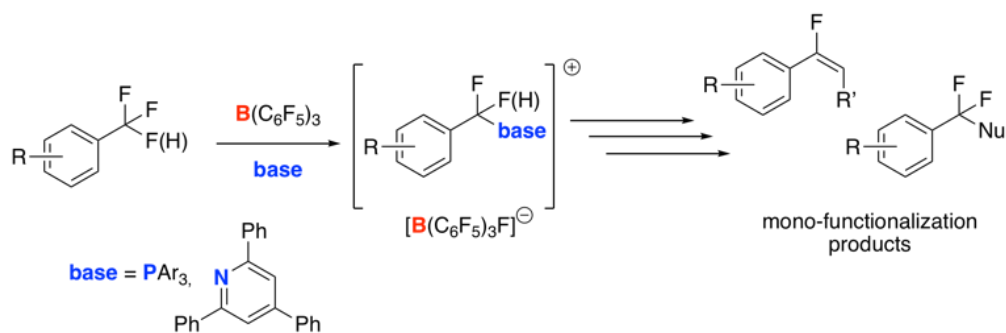
The activation of a single C–F bond in di- and trifluoromethyl groups by frustrated Lewis pairs (FLPs) has been computationally explored by means of Density Functional Theory calculations. It is found that in this activation reaction the FLP partners exhibit a peculiar cooperative action, which is markedly different from related FLP-mediated processes, and where non-covalent interactions established between the Lewis base and the substrate play a decisive role. In addition, the process proceeds through the intermediacy of a hypervalent species featuring a pentacoordinate carbon atom, which is rare in the chemistry of FLPs. The physical factors controlling this process as well as the bonding situation of these hypervalent intermediates have been quantitatively analyzed in detail by using state-of-the-art computational methods to not only rationalize the mechanism of the transformation but also to guide experimentalists towards the realization of these so far elusive hypervalent systems.

Chem. Eur. J., **2021**, *27*, 3823-3831.

Introduction

The discovery in 2006 by Stephan and co-workers that combinations of sterically encumbered Lewis acids and bases can activate dihydrogen¹ constituted the starting point of the so-called Frustrated Lewis Pairs (FLPs) chemistry. Owing to the cooperative action of the FLP antagonists, where the formation of a donor–acceptor bond between them is precluded, these species exhibit a unique and rich reactivity, which in most cases is restricted to transition-metal complexes.^{2,3} Since the seminal work by Stephan, impressive progress in this field has been made. As a result, a good number of highly active FLPs have been developed including, among others, intramolecular species⁴ or systems having transition-metal fragments in their structures.⁵ In addition, the number of applications of FLPs has broadened significantly, particularly in recent years. Indeed, FLPs have been not only successfully applied to activate different small molecules (H₂, CO, CO₂, N₂O, SO₂, etc.) but also have been used in asymmetric syntheses⁶ and polymerization reactions.⁷ More recently, the concept of FLPs has been even applied towards the development of heterogeneous catalysts and new materials,⁸ which clearly illustrates the current growing interest in this area of main group chemistry.

In this regard, FLPs were recently applied by Young and co-workers to activate a single C–F bond in di- and trifluoromethyl groups (Scheme 8.1).^{9–11,12} The use of FLPs in this reaction constitutes an elegant solution to the longstanding problem of multiple C–F functionalizations typically observed in Lewis acid-catalyzed reactions, which derives from the lower reactivity of the polyfluoride starting materials with respect to their substituted products.¹³ In contrast, the resulting phosphonium or pyridinium salts formed in this novel FLP-mediated process are “deactivated” intermediates that can be further functionalized by nucleophilic substitutions or electrophilic transfer reactions, therefore leading to a wide variety of products with potential applications in medicinal chemistry or materials science.^{9–11}



Scheme 8.1. Mono-selective functionalization of C-F bonds in di- and trifluoromethyl groups described by Young and co-workers (see refs. [9]-[11]).

Despite the evident synthetic potential of this transformation, which can be even performed catalytically in the Lewis acid by the addition of TMSNTf₂ as a fluoride sequestering agent,^{10,14} very little is known about the actual role of the FLP in the process. For this reason, we decided to gain a detailed understanding of the unknown cooperative action of the FLP partners in the transformation. The physical factors controlling this novel and synthetically useful FLP-mediated C–F activation reaction will be quantitatively analyzed by the combination of the Activation Strain Model (ASM)¹⁵ of reactivity and the Energy Decomposition Analysis (EDA)¹⁶ methods. This approach has been chosen because it has not only contributed to our current understanding of fundamental reactions in organic, organometallic, and also main group chemistry,^{15–17} but also because it has been particularly helpful to rationalize small molecule activation reactions mediated by related FLPs.¹⁸ As it will be described herein, our state-of-the-art quantum chemical calculations suggest that this reaction proceeds via the intermediacy of hypervalent species featuring a pentacoordinate carbon atom, which is rare in the chemistry of FLPs. The bonding situation in these intermediates will be also investigated in detail to stimulate experimentalists towards the experimental realization of these elusive species.

Computational Details

Geometry optimizations of the molecules were performed without symmetry constraints by using the Gaussian 09 (Rev D.01)¹⁹ suite of programs at the dispersion corrected B3LYP²⁰-D3²¹/def2-SVP²² level including solvent effects (solvent = dichloromethane) with the Polarization Continuum Model (PCM) method.²³ Reactants and adducts were characterized by frequency calculations, and have positive definite Hessian matrices. Transition states show only one negative

eigenvalue in their diagonalized force constant matrices, and their associated eigenvectors were confirmed to correspond to the motion along the reaction coordinate under consideration by using the Intrinsic Reaction Coordinate (IRC) method.²⁴ Energy refinements were carried out by means of single-point calculations at the same DFT level using the much larger triple-z basis set def2-TZVPP.²² This level is denoted PCM(DCM)-B3LYP-D3/def2-TZVPP//PCM(DCM)-B3LYP-D3/def2-SVP. Additional single-point refinements were carried out at the same DFT level using the much larger def2-QZVPP basis set for the process depicted in Figure 8.1 to check the reliability of the selected computational level. It was found (see Figure 8.S1 in the Supporting Information) that the relative energy differences are almost negligible, which indicates that the selected level is sufficient for the purpose of the present study.

Charges and donor-acceptor interactions were computed at the same DFT level with the NBO6.0 method.²⁵ The QTAIM results described in this work were also computed at the same computational level. The topology of the electron density was conducted by using the AIMAll program package.²⁶

Activation strain model of reactivity and energy decomposition analysis

Within the ASM method,¹⁵ also known as distortion/interaction model,^{15c} the potential energy surface $\Delta E(\zeta)$ is decomposed along the reaction coordinate, ζ , into two contributions, namely the strain $\Delta E_{\text{strain}}(\zeta)$ associated with the deformation (or distortion) required by the individual reactants during the process and the interaction $\Delta E_{\text{int}}(\zeta)$ between these increasingly deformed reactants [Eq. (8.1)]:

$$\Delta E(\zeta) = \Delta E_{\text{strain}}(\zeta) + \Delta E_{\text{int}}(\zeta) \quad (8.1)$$

Within the EDA method,¹⁶ the interaction energy can be further decomposed into the following chemically meaningful terms [Eq. (8.2)]:

$$\Delta E_{\text{int}}(\zeta) = \Delta V_{\text{elstat}}(\zeta) + \Delta E_{\text{Pauli}}(\zeta) + \Delta E_{\text{orb}}(\zeta) + \Delta E_{\text{disp}}(\zeta) \quad (8.2)$$

The term ΔV_{elstat} corresponds to the classical electrostatic interaction between the unperturbed charge distributions of the deformed reactants and is usually attractive. The Pauli repulsion ΔE_{Pauli} comprises the destabilizing interactions

between occupied orbitals and is responsible for any steric repulsion. The orbital interaction ΔE_{orb} accounts for bond pair formation, charge transfer (interaction between occupied orbitals on one moiety with unoccupied orbitals on the other, including HOMO–LUMO interactions), and polarization (empty–occupied orbital mixing on one fragment owing to the presence of another fragment). Finally, the ΔE_{disp} term accounts for the interactions coming from dispersion forces. Moreover, the NOCV (Natural Orbital for Chemical Valence)²⁷ extension of the EDA method has been also used to further partitioning the ΔE_{orb} term. The EDA-NOCV approach provides pairwise energy contributions for each pair of interacting orbitals to the total bond energy.

The program package ADF²⁸ was used for EDA calculations using the optimized PCM-B3LYP-D3/def2-SVP geometries at the same B3LYP-D3 level in conjunction with a triple- ζ -quality basis set using uncontracted Slater-type orbitals (STOs) augmented by two sets of polarization functions with a frozen-core approximation for the core electrons.²⁹ Auxiliary sets of s, p, d, f, and g STOs were used to fit the molecular densities and to represent the Coulomb and exchange potentials accurately in each SCF cycle.³⁰ Scalar relativistic effects were incorporated by applying the zeroth-order regular approximation (ZORA).³¹ This level of theory is denoted ZORA-B3LYP-D3/TZ2P//PCM(DCM)-B3LYP-D3/def2-SVP.

Results and Discussion

We first explored the experimentally studied C–F activation reaction in *p*-Me-trifluoromethylbenzene (**1a**) mediated by the BCF/TPPY pair (BCF=B(C₆F₅)₃, TPPY=triphenylpyridine) leading to the experimentally observed¹⁰ pyridinium salt **2a** (Figure 8.1). Two possible reaction pathways can be envisaged, namely (i) the non-cooperative pathway, where the Lewis acid solely activates the C–F bond and then the resulting cationic intermediate reacts with the Lewis base (*i.e.*, S_N1-type mechanism) or (ii) the cooperative path, where the C–F activation by the Lewis acid is also mediated by the base (*i.e.*, FLP mechanism). For the non-cooperative mechanism, the process begins with the exothermic formation of an initial reactant complex (**RC-1a'**) where the boron atom of the Lewis acid weakly interacts with the reactive fluorine atom of **1a**. Not surprisingly, the formation of this species becomes only slightly exergonic ($\Delta G=$

$-0.6 \text{ kcal mol}^{-1}$) when thermal free energy corrections at 298.15 K are considered, mainly as a result of entropic effects. From this intermediate, the activation reaction occurs via the transition state **TS1-1a'**, a saddle point associated with the simultaneous rupture of the C–F bond and formation of the new B–F bond. A rather similar reaction profile was computed for the cooperative pathway (Figure 8.1, blue pathway).³² Despite that, the presence of the TPPY Lewis base clearly favors this FLP pathway over the non-cooperative reaction along the entire reaction coordinate. Strikingly, whereas the non-FLP pathway leads to the formation of the $[p\text{-tolyl-CF}_2]^+$ cation, the process via **TS1-1a** affords the neutral intermediate **INT-1a**, a species where the reactive carbon atom is simultaneously bonded to the released fluoride (C⋯F bond length of 2.425 Å) and the nitrogen atom of the Lewis base (C⋯N bond length of 2.613 Å). Therefore, this intermediate can be viewed as a hypervalent system featuring a pentacoordinate carbon atom. We will describe the bonding situation of this unusual intermediate in detail later on.

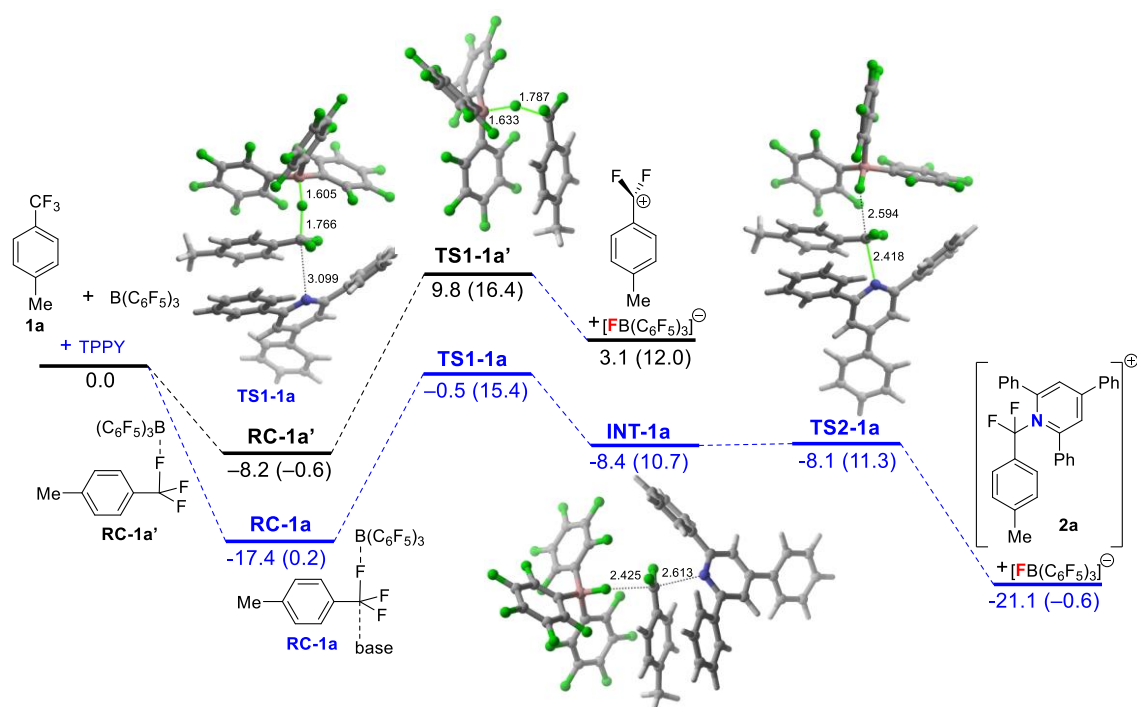


Figure 8.1. Computed reaction profile for the BCF-mediated (black lines) and BCF/TPPY-mediated (blue lines) C–F activation reaction involving the trifluoromethyl system **1a**. Relative energies (computed at the PCM(DCM)-B3LYP-D3/def2-TZVPP//PCM(DCM)-B3LYP-D3/def2-SVP level) and bond lengths are given in kcal mol⁻¹ and Å, respectively. Relative free energies (ΔG , 298 K) are given within parentheses and were computed at the PCM(DCM)-B3LYP-D3/def2-SVP level.

Once the C–F activation has occurred, an intramolecular S_N2-type reaction takes place via **TS2-1a** affording the experimentally isolated pyridinium cation **2a** and [(C₆F₅)₃B-F]⁻. The easiness of this S_N2 reaction ($\Delta E^\ddagger = 0.3$ kcal mol⁻¹, $\Delta G^\ddagger = 0.6$ kcal mol⁻¹) sharply contrasts to the analogous process (**1a**+TPPY) occurring in the absence of the Lewis acid ($\Delta E^\ddagger = 56.3$ kcal mol⁻¹, $\Delta G^\ddagger = 81.6$ kcal mol⁻¹), which is mainly due to the weaker C–F bond owing to Lewis acid coordination and a build-up of positive charge on the reactive carbon atom. Therefore, our calculations indicate that the cooperative action of the FLP antagonists not only makes the process more favorable but also leads to a hypervalent intermediate, which undergoes an extraordinarily easy intramolecular S_N2 reaction leading to the experimentally observed pyridinium salt **2a**.

The Activation Strain Model (ASM) of reactivity was applied next to understand why the key C–F activation reaction is energetically favored in the presence of the Lewis base (FLP cooperative mechanism) over the analogous non-cooperative pathway. Figure 8.2 shows the corresponding Activation Strain Diagrams (ASDs) for both processes from the respective initial reactant complexes up to the corresponding transition states projected onto the forming B··F bond length. Similar to related intermolecular FLP-mediated activation reactions,^{18e} we used **1a** and [BCF··TPPY] as fragments for the analysis of the cooperative mechanism. According to the data in Figure 8.2, the FLP pathway benefits from a less destabilizing strain energy along the entire reaction coordinate and, particularly, at the transition state region. This can be mainly ascribed to the less deformation energy required by the substrate **1a** to adopt the geometry of the corresponding transition state. Indeed, **TS1-1a** is reached earlier (C··F breaking distance of 1.766 Å) than **TS1-1a'** (C··F breaking distance of 1.787 Å), which results in the lower ΔE_{strain} computed for the FLP pathway. In addition, the interaction energy between the deformed reactants is clearly stronger for the FLP pathway also along the entire C–F activation reaction. Therefore, the combined effects of a less destabilizing strain and a stronger (*i.e.*, more stabilizing) interaction along the entire transformation make the cooperative C–F activation more favorable than the analogous reaction occurring in the absence of the Lewis base.

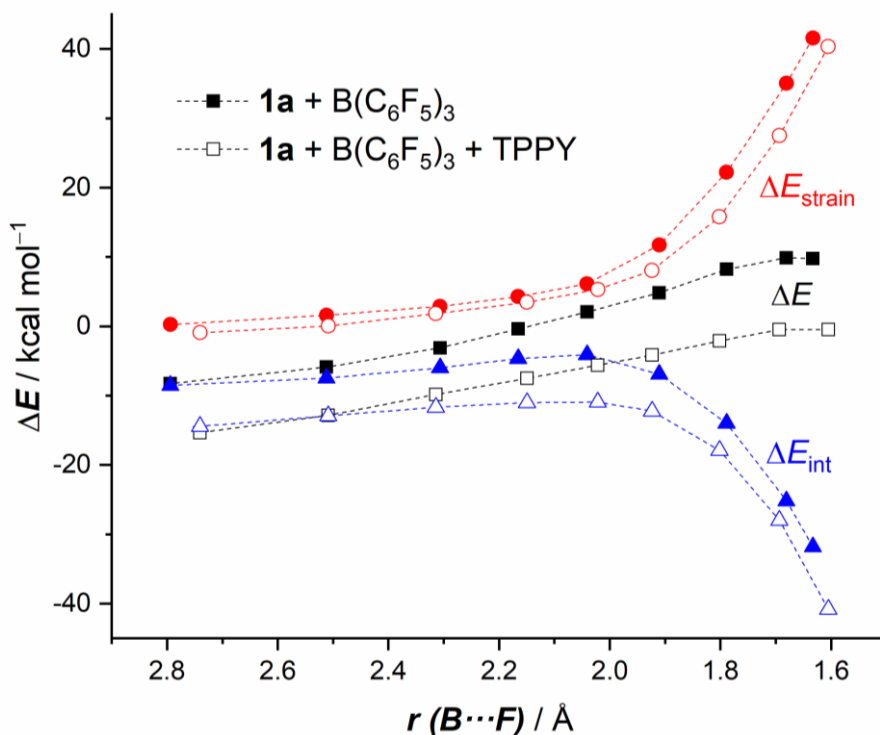


Figure 8.2. Comparative activation strain diagrams for the non-cooperative (solid lines) and cooperative (dashed lines) C–F activation reaction in **1a** along the reaction coordinate projected onto the forming B···F bond length. All data were computed at the PCM(DCM)-B3LYP-D3/def2-TZVPP//PCM(DCM)-B3LYP-D3/def2-SVP level.

The stronger interaction between the deformed reactants computed for the FLP pathway deserves further analysis. With the help of the EDA method, the different contributors to the total interaction energy can be quantified. On the basis of the behavior of other Lewis bases in related FLP-mediated activation reactions,^{18,33} one might initially think that the stronger interaction computed for the FLP pathway directly derives from stronger orbital interactions as a consequence of the polarization of the reactive C–F bond induced by the Lewis base. However, as readily seen in Figure 8.3, which graphically shows the evolution of the EDA terms along the reaction coordinate once again from the respective initial reactant complexes up to the corresponding transition states, the computed orbital term (ΔE_{orb}) is only slightly more stabilizing for the cooperative pathway. According to the NOCV extension of the EDA method, the main orbital interaction in the FLP mechanism is exclusively dominated by the $\sigma(\text{C-F}) \rightarrow \text{B}(p_z)$ interaction with no measurable contribution of the Lewis base (Figure 8.4), which is consistent with the rather long C···N distance of 3.099 Å in **TS1-1a**. This is exactly the same orbital interaction occurring in the absence of the Lewis base, and therefore it is not surprising that both processes exhibit nearly identical orbital interactions. At

variance, the FLP-mediated C–F activation benefits from stronger electrostatic interactions and, to a higher extent, from much more stabilizing dispersion interactions (measured by the ΔE_{elstat} and ΔE_{disp} terms, respectively). Both contributions offset the less destabilizing Pauli repulsion (ΔE_{Pauli}) computed for the non-cooperative pathway and are therefore responsible for the stronger interaction computed for the favored FLP mechanism.

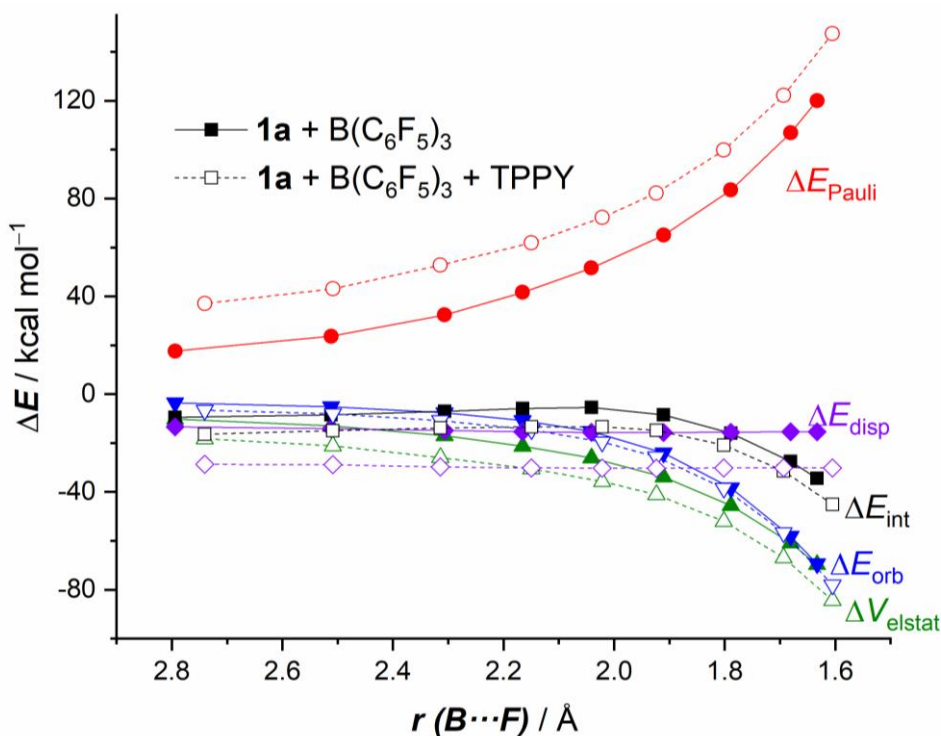


Figure 8.3. Comparative energy decomposition analyses for the non-cooperative (solid lines) and cooperative (dashed lines) C–F activation reactions involving **1a** along the reaction coordinate projected onto the forming B···F bond length. All data were computed at the ZORA-B3LYP-D3/TZ2P//PCM(DCM)-B3LYP-D3/def2-SVP level.

The significant role of dispersion interactions in the C–F activation reaction occurring in the presence of the Lewis base can be readily understood with the help of the non-covalent interaction (NCI) method.³⁴ This method has been particularly useful to understand the influence of dispersion on the stabilization of intermediates and transition states and its impact on reactivity.³⁵ As illustrated in Figure 8.4 for the transition state **TS1-1a**, there exist two stabilizing non-covalent interactions (green surfaces) established between TPPY and the substrate, namely a $\pi\cdots\pi$ stacking between the aryl fragment of **1a** and a phenyl group of TPPY ($\text{Ar}_{\text{centroid}}\cdots\text{Ph}_{\text{centroid}}$ distance of 3.62 Å) and two additional C–F··· π interactions

involving the non-reactive fluorine atoms of **1a** and a different phenyl group of the base (shortest F \cdots Ph_{centroid} distance of 3.08 Å). Both non-covalent interactions are present along the entire activation reaction and up to the formation of the intermediate **INT-1a** ($\Delta E_{\text{disp}} = -27.8$ kcal mol⁻¹, see Figure 8.S2 in the Supporting Information) and are mainly responsible for the stronger dispersion interactions computed for the FLP pathway. The occurrence of such stabilizing non-covalent interactions also explains (at least, in part) why the analogous reactions involving lutidine or pyridine instead of TPPY as the base partner, where these dispersion interactions are absent, experimentally gave poor conversion or failed to react with **1a**.¹⁰ Indeed, our calculations confirm that the process involving lutidine is both kinetically and thermodynamically less favored than the process involving TPPY (see Figure 8.S3 in the Supporting Information). A similar result was found when using NTf₂⁻ as a base (see Figure 8.S4 in the Supporting Information), which further supports the crucial role of these non-covalent interactions in the transformation.

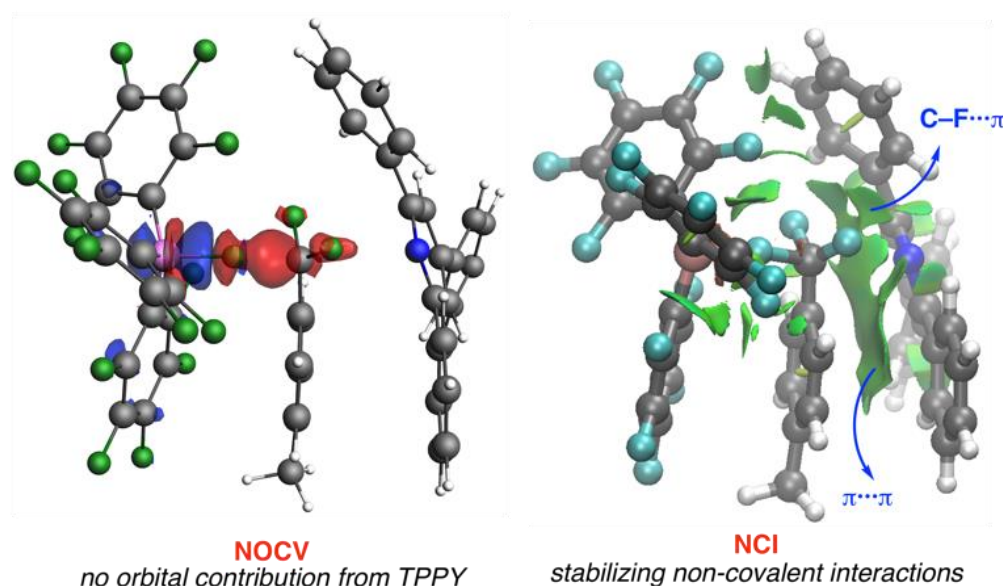


Figure 8.4. (Left) Plot of the deformation densities $\Delta\rho$ of the pairwise orbital interactions occurring in **TS1-1a** (isovalue of 0.0015 a.u.). The color code of the charge flow is red→blue. (Right) Contour plots of the reduced density gradient isosurfaces (density cutoff of 0.03 a.u.) for **TS1-1a**. The green surfaces indicate attractive non-covalent interactions.

In addition, we also explored the analogous C–F activation reaction involving a substrate with an aliphatic (instead of aromatic) substituent, which experimentally is seen to be much more challenging¹⁰ and where the crucial $\pi\cdots\pi$ non-covalent interaction is not possible. Our calculations, involving either H₃C–CF₃ or H₃C–CHF₂, indicate that the corresponding hypervalent intermediate is not a

stable intermediate on the potential energy surface but a transition state associated with the displacement of the BCF-activated fluorine atom by the base. Therefore, the lack of this critical stabilizing non-covalent interaction turns the C–F activation mechanism into a standard S_N2 reaction (see Figure 8.S5 in the Supporting Information), which highlights the influence of the non-covalent interactions on the mechanism of the transformation.

Once the transition state **TS1-1a** is reached (*i.e.*, the C–F is broken), the Lewis base further approaches the electron-deficient ($q = +1.16$) carbon atom of the substrate. As a consequence, TPPY not only interacts via the above commented non-covalent interactions but also through a potent LP(N)→C(p_z) two-electron donation. Indeed, snapshots of the NOCV deformation densities at the final intermediate **INT-1a** and a midpoint after **TS1-1a** (Figure 8.5) clearly confirm that whereas this orbital interaction is negligible in the transition state (see above), it becomes increasingly more significant when approaching the intermediate. As a result, the main orbital interaction in the transition state ($\Delta E(\rho) = -51.4$ kcal mol⁻¹, Figure 8.4) is continuously reinforced by the LP(N)→p_z(C) interaction ($\Delta E(\rho) = -94.2$ kcal mol⁻¹ at the midpoint), reaching its maximum at the final intermediate ($\Delta E(\rho) = -107.1$ kcal mol⁻¹, Figure 8.5). Therefore, our calculations indicate that similar to dihydrogen activations mediated by either inter- or intramolecular FLPs,^{18, 33} the key $\sigma(\text{substrate}) \rightarrow p_z(\text{B})$ and LP(N)→ $\sigma^*/p_z(\text{vacant orbital of the substrate})$ molecular orbital interactions take place cooperatively along the reaction coordinate. However, and at variance with typical FLP-mediated processes, in the considered C–F bond activation these interactions do not occur in a concerted manner but at rather different stages of the transformation, which ultimately leads to the formation of a hypervalent intermediate. Despite that, the Lewis base is not a mere spectator at the beginning of the process (where the interaction of the substrate with the Lewis acid dominates) but significantly contributes to the stabilization of the entire reaction coordinate through non-covalent interactions. These findings, namely (i) non-concerted cooperation between the FLP partners, (ii) the intermediacy of a hypervalent intermediate with a pentacoordinate carbon atom, and (iii) the critical role of non-covalent interactions, are genuine features of the activation of C–F bonds promoted by FLPs.

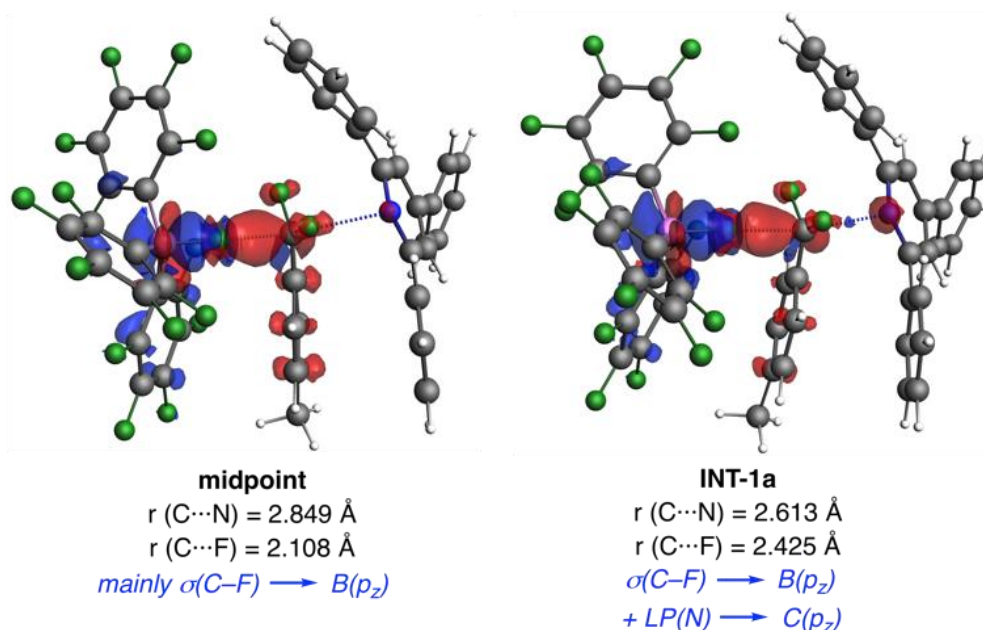


Figure 8.5. Plot of the deformation densities $\Delta\rho$ of the pairwise orbital interactions occurring in **INT-1a** (right) and at a midpoint between **TS1-1a** and this intermediate (left). The color code of the charge flow is red→blue (isovalue of 0.0015 au).

The bonding situation of the intermediate **INT-1a** deserves further analysis. As depicted in Figure 8.1, this species presents a slightly distorted trigonal bipyramidal (TBP) pentacoordinate structure (av. F–C–C_{Ar} angle of 122.6°) with relatively long apical distances (C⋯F=2.425 Å and C⋯N=2.613 Å, F⋯C⋯N angle of 167.1°). The geometry of this intermediate strongly resembles those of the hypervalent pentacoordinate carbon compounds bearing an oxygen-donating anthracene skeleton experimentally characterized by Yamamoto, Akiba, and co-workers.³⁶ Note, however, that in **INT-1a** the apical substituents are not geometrically confined by a molecular scaffold.³⁷ Such unconstrained species with a TBP structure are extraordinarily rare and, to the best of our knowledge, only a few systems including the cationic [Me₃Si–CH₃–SiMe₃]⁺ have been experimentally detected.^{38,39} Related cationic and also anionic hypervalent species have been also proposed computationally⁴⁰ together with the experimentally well-known [R₃Al–CH₃–AlR₃][–] anions.⁴¹

The nature of the C–F(BCF) and C–N(TPPY) interactions was also investigated with the QTAIM and NBO methods. Figure 8.6(top), which shows the Laplacian distribution in the F⋯C⋯N plane, clearly confirms the occurrence of C–F and C–N bond critical points together with the corresponding bond paths running

between the involved atoms. Not surprisingly, the C–F and C–N bonds are weak and partly ionic as confirmed by the small values of the electron density [$\rho(\mathbf{r})$: 0.021 and 0.022 eÅ⁻³, respectively] and the small positive Laplacian values [$\nabla^2\rho(\mathbf{r})$: 0.087 and 0.065 eÅ⁻⁵] computed at the bond critical points. Rather similar values were reported for the C–O bonds of the hypervalent species described by Yamamoto and co-workers.³⁶ In addition, the respective delocalization indices, which have been suggested as a measure of the bond strength,⁴² are relatively low but not negligible: $\delta(\text{C}\cdots\text{F})=0.05$ and $\delta(\text{C}\cdots\text{N})=0.09$. The computed δ values also suggest that the C–N interaction is almost twice as strong as the C–F interaction. The second-order perturbation theory (SOPT) of the NBO method nicely agrees with that. Indeed, this method locates two donor–acceptor interactions involving the two-electron donations from the LP(F) and LP(N) orbitals to the vacant p_z atomic orbital of the trigonal carbon atom (Figure 8.6, bottom). The associated SOPT energies are –17.5 and –28.7 kcal mol⁻¹ for the LP(F)→p_z(C) and LP(N)→p_z(C) interactions, respectively, thus confirming the much higher strength of the latter interaction as a consequence of the higher donor ability of the nitrogen atom compared with fluorine. Moreover, and as commented above, **INT-1a** is further stabilized by $\pi\cdots\pi$ (Ar_{centroid}⋯Ph_{centroid} distance of 3.62 Å) and C–F⋯ π (shortest F⋯Ph_{centroid} distance of 3.07 Å) stabilizing non-covalent interactions, similar to those occurring in **TS-1a** (see corresponding NCI plot in Figure 8.S2 in the Supporting Information). These findings firmly indicate that intermediate **INT-1a** can be considered as a three-center, four-electron (3c–4e) hypervalent system featuring a pentacoordinate carbon atom.

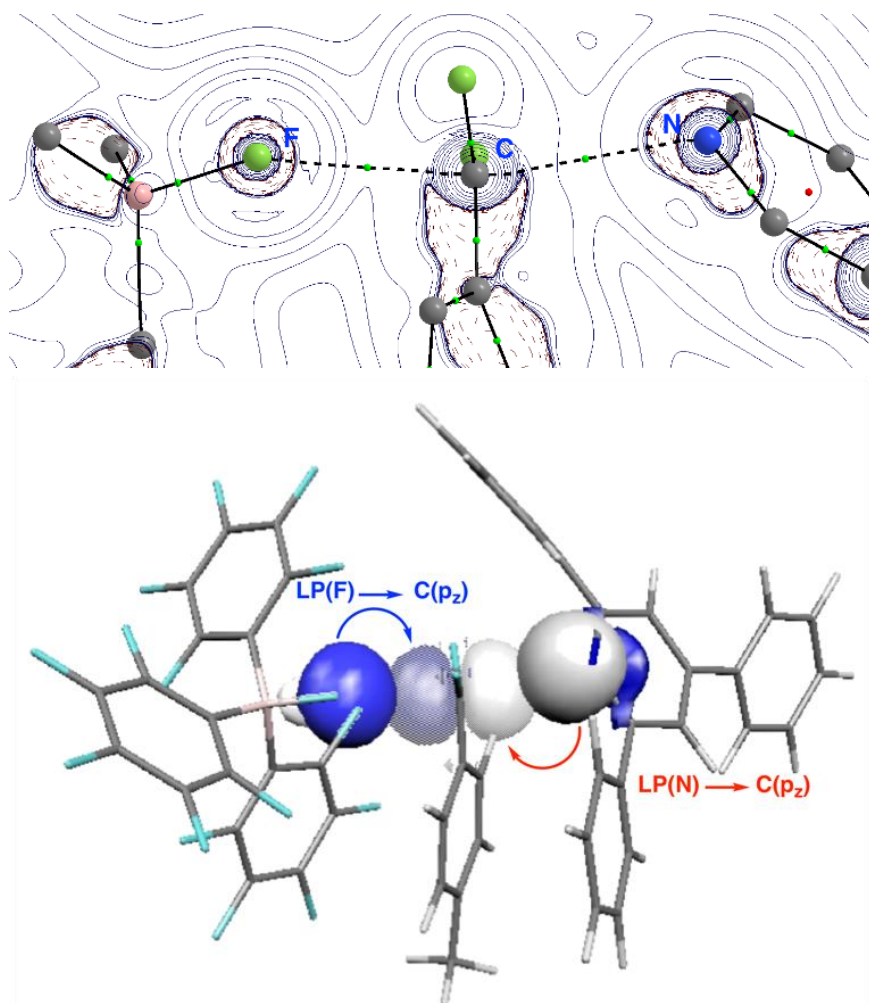


Figure 8.6. Laplacian distribution of **INT-1a** in the F–C–N plane. Bond critical points are represented as small green spheres (top). Donor-acceptor interactions located by the SOPT of the NBO method (bottom).

As described above, the hypervalent intermediate **INT-1a** readily undergoes a fast S_N2-type intramolecular reaction ($\Delta E^\ddagger = 0.3 \text{ kcal mol}^{-1}$) leading to the experimentally isolated pyridinium cation **2a** in a strongly exothermic process. For this reason, no traces of this intermediate were detected in the experiments.¹⁰ Despite that, we hypothesized that a further stabilization of the incipient positive charge of the trigonal, pentacoordinate carbon atom ($q = +1.11$ in **INT-1a**) would increase the chances of isolating/detecting such species. To this end, we simply placed π electron-donor substituents (NMe₂ and OMe) at the *para* position of the phenyl group of **1a**. From the data in Figure 8.7, which shows the corresponding computed reaction profiles, it becomes evident that both substituents stabilize the initial transition state as well as the hypervalent intermediate compared with the lower electron-donating methyl group (**1a**). In addition, the subsequent

intramolecular S_N2 reaction also proceeds slower than the analogous process involving **1a**. As expected, the influence of the NMe_2 group on the process is much greater than that of the methoxy substituent as a consequence of the higher π -donor ability of the NMe_2 group (corresponding Hammett σ_p^+ constants of -1.70 and -0.78 , respectively),⁴³ which results in a significant increase of the barrier of the S_N2 reaction ($\Delta E^\ddagger = 8.2 \text{ kcal mol}^{-1}$, $\Delta G^\ddagger = 7.4 \text{ kcal mol}^{-1}$). Strikingly, the intermediate derived from the **1a-NMe}_2** is even slightly more stable than the final $[\mathbf{2a-NMe}_2]^+[\text{BCF-F}]^-$ product. This result is also markedly different from the processes involving **1a** or **1a-OMe**.

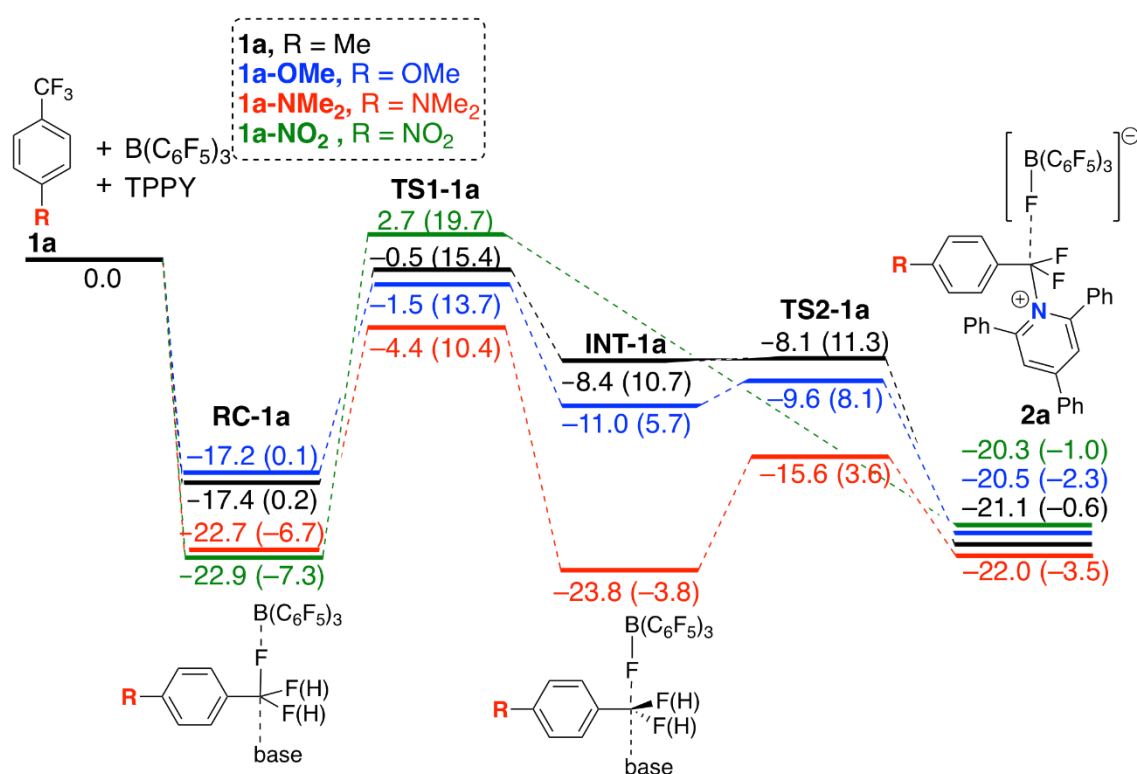


Figure 8.7. Comparative reaction profiles for the C–F activation reactions involving *p*-substituted CF_3 -benzenes **1a**. Relative energies were computed at the PCM(DCM)-B3LYP-D3/def2-TZVPP//PCM(DCM)-B3LYP-D3/def2-SVP level. Relative free energies (ΔG , 298 K) are given within parentheses and were computed at the PCM(DCM)-B3LYP-D3/def2-SVP level.

Not surprisingly, the replacement of the methyl group in **1a** by an electron-withdrawing group such as NO_2 ($\sigma_p^+ = 0.72$) provokes the opposite effect. Indeed, the corresponding hypervalent intermediate could not be located on the potential energy surface and the respective transition state **TS1-1a-NO}_2** directly converges into the final reaction products (see the corresponding IRC plot in Figure 8.S6 of the Supporting Information). This result is consistent with the reactivity profile reported experimentally by Young and co-workers (*i.e.*, electron-withdrawing

groups at the *para* position slowed the rate of the C–F activation).¹⁰ Therefore, we predict that substrate **1a-NMe₂** and related systems with strong π -donor substituents in their structures constitute really promising candidates to, at least, detect under controlled experimental conditions these rare (and still elusive) hypervalent systems featuring a pentacoordinate carbon atom.

We finally compared the rate-limiting C–F bond activation step involving the trifluoromethyl reactant **1a** with the analogous process involving **1b**, which bears a difluoromethyl group. For completeness, we also considered the substrate **1c** with a CH₂F group. As shown in Figure 8.8, it is confirmed that the FLP cooperative mechanism is favored regardless of the number of fluorine atoms in the initial reactant. Interestingly, the replacement of fluorine by hydrogen atoms steadily favors the entire transformation from the initially formed reactant complex up to the corresponding hypervalent intermediates. Thus, the transformation becomes kinetically easier (*i.e.*, proceeds with a lower barrier) and even exergonic when going from **1a** to **1b** or **1c**. The computed reactivity trend is consistent with the reported C–F bond dissociation energies, which decreases with the number of hydrogen atoms (131, 128, 120, and 110 kcal mol⁻¹ for CF₄, CHF₃, CH₂F₂, and CH₃F, respectively)^{10,44} and, interestingly, nicely follows the Hammond–Leffer postulate.⁴⁵ Indeed, the corresponding transition states are reached earlier and earlier (C··F=1.766 Å, 1.760 Å, and 1.751 Å, for **TS1-1a**, **TS1-1b**, and **TS1-1c**, respectively) with the reduction of the number of fluorine atoms attached to the reactive carbon atom.

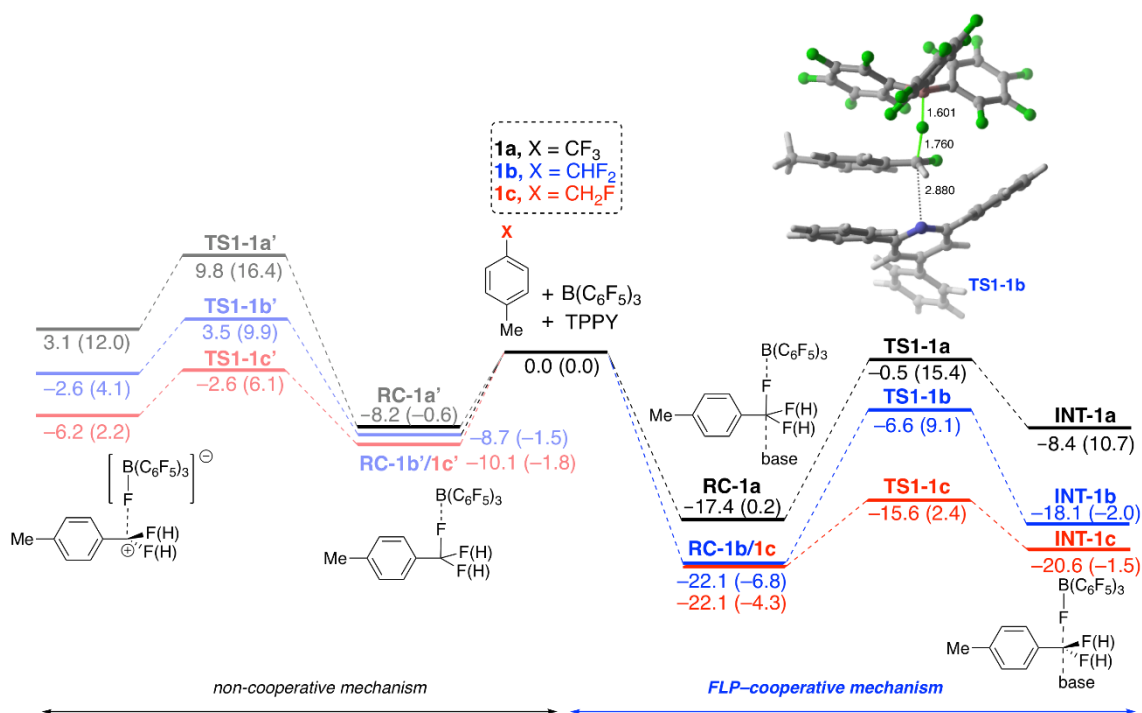


Figure 8.8. Computed reaction profiles for the C–F activation of **1a**, **1b**, and **1c** mediated by the BCF/TPPY FLP. Relative energies (computed at the PCM(DCM)-B3LYP-D3/def2-TZVPP//PCM(DCM)-B3LYP-D3/def2-SVP level) and bond lengths are given in kcal mol⁻¹ and Å, respectively. Relative free energies (ΔG , 298 K) are given within parentheses and were computed at the PCM(DCM)-B3LYP-D3/def2-SVP level.

The stabilization of the hypervalent intermediate upon the replacement of fluorine by hydrogen atoms can be easily understood in terms of the lower stabilization of the positive charge of the trigonal carbon atom induced by the fluorine atoms compared with hydrogen atoms. This is confirmed by the computed charges at such carbon atom (+1.11, +0.81, and +0.46, summed with hydrogen atoms, for **1a**, **1b**, and **1c**, respectively), which follows the same trend as the relative stability of the intermediate. Therefore, it is confirmed that the stabilization of the incipient positive charge of the sp²-carbon atom either by the substituents directly attached to it or by remote substituents in the adjacent aryl ring constitutes a promising approach towards the realization of these new hypervalent species.

On the other hand, the reduction of the activation barrier should mainly derive, according to the above-mentioned earlier nature of **TS1-1b** and **TS1-1c** with respect to **TS1-1a**, from a lower, less destabilizing strain energy. To check this, we applied once again the ASM to compare the processes involving **1a** and **1b**. As graphically shown in Figure 8.9, the interaction energy for the process

involving **1b** is only more stabilizing at the beginning of the transformation and is therefore responsible for the higher stability (with respect to the separate reactants) of the reactant complex **RC-1b** (or **RC-1c**) compared with **RC-1a**. At variance, at the proximities of the transition state region (where the barrier arises), the ΔE_{int} term computed for both processes is nearly identical and therefore is not at all responsible for the reduction of the barrier upon F/H replacement. Instead, the reaction involving **1b** benefits from a less destabilizing strain energy, which is translated into the computed lower barrier. As commented above, this lower strain exclusively originates from the less distortion energy required by the substrate **1b** compared with **1a** ($\Delta\Delta E_{\text{strain}}^{\ddagger} = 5.0 \text{ kcal mol}^{-1}$), which roughly matches the computed transition state energy difference ($\Delta\Delta E^{\ddagger} = 6.1 \text{ kcal mol}^{-1}$).

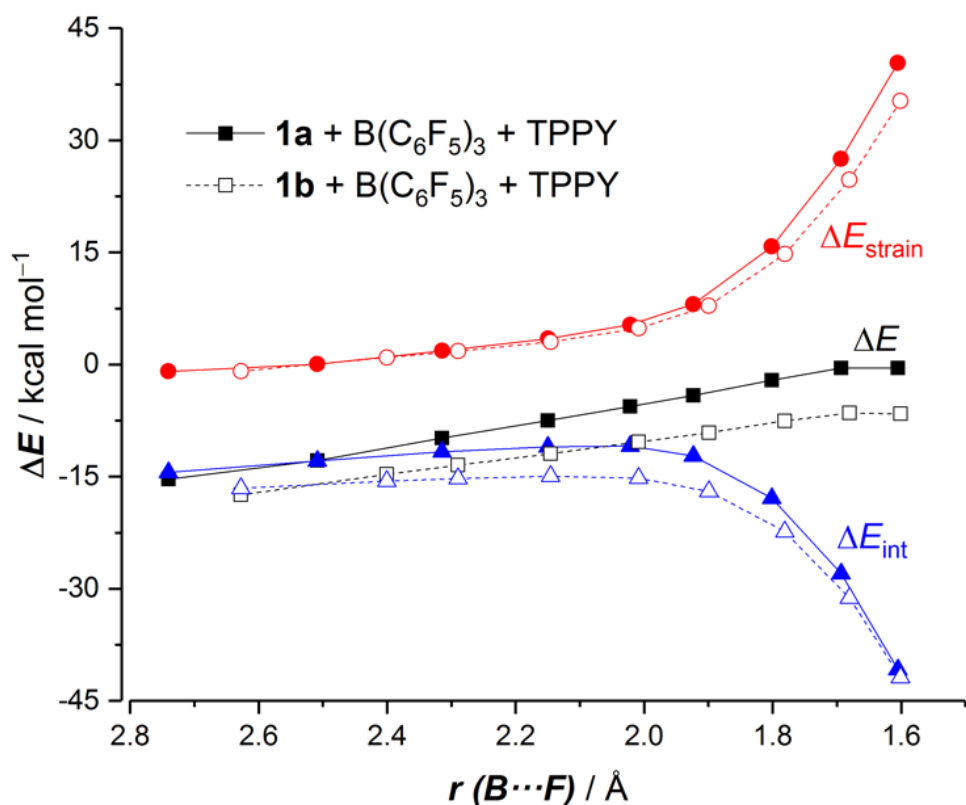


Figure 8.9. Comparative activation strain diagrams for the BCF/TPPY-mediated C–F activation reactions involving **1a** (solid lines) and **1b** (dashed lines) along the reaction coordinate projected onto the forming B...F bond length. All data were computed at the PCM(DCM)-B3LYP-D3/def2-TZVPP//PCM(DCM)-B3LYP-D3/def2-SVP level.

Conclusion

Our computational study reveals that the activation of a single C–F bond in di- and trifluoromethyl groups by FLPs exhibit a peculiar cooperative action

between the FLP partners, which is markedly different from related FLP-mediated activation reactions. In this particular transformation, the cooperation does not take place in a concerted manner but at different stages of the transformation, that is, the $\text{LP}(\text{N}) \rightarrow \text{p}_z(\text{C})$ interaction only occurs once the C–F bond is significantly activated by the Lewis acid. Despite that, the Lewis base is not a mere spectator at the beginning of the process (where the interaction of the substrate with the Lewis acid dominates) but significantly contributes to the stabilization of the entire reaction coordinate through stabilizing non-covalent interactions ($\pi \cdots \pi$ and $\text{C}–\text{F} \cdots \pi$ interactions). As a result, this C–F bond activation proceeds through the intermediacy of a three-center, four-electron (3c–4e) hypervalent species featuring a pentacoordinate carbon atom. Our calculations predict that the stabilization of the incipient positive charge of the trigonal carbon atom in these hypervalent intermediates might be used towards the isolation/detection of these elusive species. These findings, namely (i) non-concerted cooperation between the FLP partners, (ii) the intermediacy of a hypervalent intermediate with a pentacoordinate carbon atom, and (iii) the critical role of non-covalent interactions, are genuine features of the studied C–F bond activation reactions and may stimulate future experimental work toward the design of novel bond activation reactions mediated by FLPs.

References

- ¹ G. C. Welch, R. R. San Juan, J. D. Masuda, D. W. Stephan, *Science* **2006**, *314*, 1124.
- ² For leading reviews, see: a) D. W. Stephan, G. Erker, *Angew. Chem. Int. Ed.* **2010**, *49*, 46; *Angew. Chem.* **2010**, *122*, 50; b) G. Erker, *Pure Appl. Chem.* **2012**, *84*, 2203; c) D. W. Stephan, G. Erker, *Top. Curr. Chem.* **2013**, *332*, 85, in *Frustrated Lewis Pairs I*; d) D. W. Stephan, G. Erker, *Chem. Sci.* **2014**, *5*, 2625; e) D. W. Stephan, *J. Am. Chem. Soc.* **2015**, *137*, 10018; f) D. W. Stephan, G. Erker, *Angew. Chem. Int. Ed.* **2015**, *54*, 6400; *Angew. Chem.* **2015**, *127*, 6498; g) D. W. Stephan, *Acc. Chem. Res.* **2015**, *48*, 306; h) D. W. Stephan, *Science* **2016**, *354*, aaf7229.
- ³ See also: a) A. R. Jupp, D. W. Stephan, *Trends Chem.* **2019**, *1*, 35; b) D. W. Stephan, *Chem.* **2020**, *6*, 1520.
- ⁴ Selected representative examples: a) C. Appelt, H. Westenberg, F. Bertini, A. W. Ehlers, J. C. Slootweg, K. Lammertsma, W. Uhl, *Angew. Chem. Int. Ed.* **2011**, *50*, 3925; *Angew. Chem.* **2011**, *123*, 4011; b) C. Appelt, J. C. Slootweg, K. Lammertsma, W. Uhl, *Angew. Chem. Int. Ed.* **2012**, *51*, 5911; *Angew. Chem.* **2012**, *124*, 6013; c) S. Roters, C. Appelt, H. Westenberg, A. Hepp, J. C. Slootweg, K. Lammertsma, W. Uhl, *Dalton Trans.* **2012**, *41*, 9033; d) C. Appelt, J. C. Slootweg, K. Lammertsma, W. Uhl, *Angew. Chem. Int. Ed.* **2013**, *52*, 4256; *Angew. Chem.* **2013**, *125*, 4350; e) W. Uhl, E.-U. Werthwein, *Top. Curr. Chem.* **2012**, *334*, 101; f) W. Uhl, C. Appelt, J. Backs, H. Westenberg, A. Wollschläger, J. Tannert, *Organometallics* **2014**, *33*, 1212; g) M. Devillard, R. Declercq, E. Nicolas, A. W. Ehlers, J. Backs, N. Saffon-Merceron, G. Bouhadir, J. C. Slootweg, W. Uhl, D. Bourissou, *J. Am. Chem. Soc.* **2016**, *138*, 4917; h) L. Keweloh, H. Klöcker, E.-U. Werthwein, W. Uhl, *Angew. Chem. Int. Ed.* **2016**, *55*, 3212; *Angew. Chem.* **2016**, *128*, 3266.
- ⁵ See, for instance: a) A. M. Chapman, M. F. Haddow, D. F. Wass, *J. Am. Chem. Soc.* **2011**, *133*, 18463; b) D. F. Wass, A. M. Chapman, *Top. Curr. Chem.* **2013**, *334*, 261; c) A. Normand, P. Richard, C. Balan, C. G. Daniliuc, G. Kehr, G. Erker, P. Le Grendre, *Organometallics* **2015**, *34*, 2000; d) X. Xu, G. Kehr, C. G. Daniliuc, G. Erker, *J. Am. Chem. Soc.* **2015**, *137*, 4550; e) S. Arndt, M. Rudolph, A. S. K. Hashmi, *Gold. Bull.* **2017**, *50*, 267; f) J. Campos, *J. Am. Chem. Soc.* **2017**, *139*, 2944; g) N. Hidalgo, J. J. Moreno, M. Pérez-Jiménez, C. Maya, J. López-Serrano, J. Campos, *Chem. Eur. J.* **2020**, *26*, 5982.
- ⁶ Representative examples: a) L. Sesse, J. Hermeke, M. Oestreich, *J. Am. Chem. Soc.* **2016**, *138*, 6940; b) X. Ren, H. Du, *J. Am. Chem. Soc.* **2016**, *138*, 810; c) M. Shang, M. Cao, Q. Wang, M. Wasa, *Angew. Chem. Int. Ed.* **2017**, *56*, 13338; *Angew. Chem.* **2017**, *129*, 13523; d) W. Meng, X. Feng, H. Du, *Acc. Chem. Res.* **2018**, *51*, 191.
- ⁷ For a recent review, see: M. Hong, J. Chen, E. Y.-X. Chen, *Chem. Rev.* **2018**, *118*, 10551.
- ⁸ See, for instance: a) K. C. Szeto, W. Sahyoun, N. Merle, J. L. Castelbou, N. Popoff, F. Lefebvre, J. Raynaud, C. Godard, C. Claver, L. Delevoeye, R. M. Gauvin, M. Taoufik, *Catal. Sci. Technol.* **2016**, *6*, 882; b) J.-Y. Xing, J.-C. Buffet, N. H. Rees, P. Nørby, D. O'Hare, *Chem. Commun.* **2016**, *52*, 10478; c) M. Trunk, J. F. Teichert, A. Thomas, *J. Am. Chem. Soc.* **2017**, *139*, 3615; d) L. Wang, G. Kehr, C. G. Daniliuc, M. Brinkkötter, T. Weigand, A.-L. Wübker, H. Eckert, L. Liu, J. G. Brandenburg, S. Grimme, G. Erker, *Chem. Sci.* **2018**, *9*, 4859; e) Z. Niu, W. D. C. Bhagya Gunatilleke, Q. Sun, P. C. Lan, J. Perman, J.-G. Ma, Y. Cheng, B. Aguila, S. Ma, *Chem* **2018**, *4*, 2587; f) Z.-Q. Huang, L.-P. Liu, S. Qi, S. Zhang, Y. Qu, C. R. Chang, *ACS Catal.* **2018**, *8*, 546.
- ⁹ D. Mandal, R. Gupta, R. D. Young, *J. Am. Chem. Soc.* **2018**, *140*, 10682.
- ¹⁰ D. Mandal, R. Gupta, A. K. Jaiswal, R. D. Young, *J. Am. Chem. Soc.* **2020**, *142*, 2572.
- ¹¹ See also, R. Gupta, A. K. Jaiswal, D. Mandal, R. D. Young, *Synlett* **2020**, *31*, 933.
- ¹² For related selective activations mediated by FLPs, see: a) I. Mallov, A. J. Ruddy, H. Zhu, S. Grimme, D. W. Stephan, *Chem. Eur. J.* **2017**, *23*, 17692; b) P. Mehlmann, T. Witteler, L. F. B. Wilm, F. Dielmann, *Nat. Chem.* **2019**, *11*, 1139.
- ¹³ a) F. Jaroschik, *Chem. Eur. J.* **2018**, *24*, 14572; b) D. O'Hagan, *Chem. Soc. Rev.* **2008**, *37*, 308.

- ¹⁴ A. K. Jaiswal, P. K. Prasad, R. D. Young, *Chem. Eur. J.* **2019**, *25*, 6290.
- ¹⁵ For reviews, see: a) W.-J. van Zeist, F. M. Bickelhaupt, *Org. Biomol. Chem.* **2010**, *8*, 3118; b) I. Fernández, F. M. Bickelhaupt, *Chem. Soc. Rev.* **2014**, *43*, 4953; c) F. M. Bickelhaupt, K. N. Houk, *Angew. Chem. Int. Ed.* **2017**, *56*, 10070; *Angew. Chem.* **2017**, *129*, 10204; see also: d) I. Fernández, *Discovering the Future of Molecular Sciences*, (Ed.: B. Pignataro), Wiley-VCH, Weinheim, 2014, pp. 165–187.
- ¹⁶ For reviews on the EDA method, see: a) F. M. Bickelhaupt, E. J. Baerends, *Reviews in Computational Chemistry* (Eds.: K. B. Lipkowitz, D. B. Boyd), Wiley, New York, 2000, Vol. 15, pp. 1–86; b) M. von Hopffgarten, G. Frenking, *WIREs Comput. Mol. Sci.* **2012**, *2*, 43; c) G. Frenking, F. M. Bickelhaupt, *The Chemical Bond: Fundamental Aspects of Chemical Bonding*, (Eds.: G. Frenking, S. Shaik), Wiley-VCH, Weinheim, 2014, pp. 121–158.
- ¹⁷ Representative recent examples: a) T. A. Hamlin, I. Fernández, F. M. Bickelhaupt, *Angew. Chem. Int. Ed.* **2019**, *58*, 8922; *Angew. Chem.* **2019**, *131*, 9015; b) P. Vermeeren, T. A. Hamlin, I. Fernández, F. M. Bickelhaupt, *Angew. Chem. Int. Ed.* **2020**, *59*, 6201; *Angew. Chem.* **2020**, *132*, 6260; c) P. Vermeeren, F. Brinkhuis, T. A. Hamlin, F. M. Bickelhaupt, *Chem. Asian J.* **2020**, *15*, 1167; d) P. Vermeeren, T. A. Hamlin, I. Fernández, F. M. Bickelhaupt, *Chem. Sci.* **2020**, *11*, 8105; e) I. Fernández, *Chem. Sci.* **2020**, *11*, 3769, and references therein.
- ¹⁸ a) D. Yepes, P. Jaque, I. Fernández, *Chem. Eur. J.* **2016**, *22*, 18801; b) D. Yepes, P. Jaque, I. Fernández, *Chem. Eur. J.* **2018**, *24*, 8833; c) J. J. Cabrera-Trujillo, I. Fernández, *Chem. Eur. J.* **2018**, *24*, 17823; d) J. J. Cabrera-Trujillo, I. Fernández, *J. Phys. Chem. A* **2019**, *123*, 10095; e) J. J. Cabrera-Trujillo, I. Fernández, *Inorg. Chem.* **2019**, *58*, 7828; f) J. J. Cabrera-Trujillo, I. Fernández, *Dalton Trans.* **2020**, 49, 3129.
- ¹⁹ Gaussian 09, Revision D.01, M. J. Frisch, G. W. Trucks, H. B. Schlegel, G. E. Scuseria, M. A. Robb, J. R. Cheeseman, G. Scalmani, V. Barone, G. A. Petersson, H. Nakatsuji, X. Li, M. Caricato, A. Marenich, J. Bloino, B. G. Janesko, R. Gomperts, B. Mennucci, H. P. Hratchian, J. V. Ortiz, A. F. Izmaylov, J. L. Sonnenberg, D. Williams-Young, F. Ding, F. Lipparini, F. Egidi, J. Goings, B. Peng, A. Petrone, T. Henderson, D. Ranasinghe, V. G. Zakrzewski, J. Gao, N. Rega, G. Zheng, W. Liang, M. Hada, M. Ehara, K. Toyota, R. Fukuda, J. Hasegawa, M. Ishida, T. Nakajima, Y. Honda, O. Kitao, H. Nakai, T. Vreven, K. Throssell, J. A. Montgomery, Jr., J. E. Peralta, F. Ogliaro, M. Bearpark, J. J. Heyd, E. Brothers, K. N. Kudin, V. N. Staroverov, T. Keith, R. Kobayashi, J. Normand, K. Raghavachari, A. Rendell, J. C. Burant, S. S. Iyengar, J. Tomasi, M. Cossi, J. M. Millam, M. Klene, C. Adamo, R. Cammi, J. W. Ochterski, R. L. Martin, K. Morokuma, O. Farkas, J. B. Foresman, D. J. Fox, Gaussian, Inc., Wallingford, CT, **2016**.
- ²⁰ a) A. D. Becke, *J. Chem. Phys.* **1993**, *98*, 5648; b) C. Lee, W. Yan, R. G. Parr, *Phys. Rev. B* **1988**, *37*, 785; c) S. H. Vosko, L. Wilk, M. Nusair, *Can. J. Phys.* **1980**, *58*, 1200.
- ²¹ a) S. Grimme, J. Antony, S. Ehrlich, H. Krieg, *J. Chem. Phys.* **2010**, *132*, 154104. Grimme's dispersion correction was shown to provide a reasonable semiquantitative impression in combination with functionals like B3LYP, see: b) M. Bursch, E. Caldeweyherm, A. Hansen, H. Neugebauer, S. Ehlert, S. Grimme, *Acc. Chem. Res.* **2019**, *52*, 258; c) M. Bursch, L. Kunze, A. M. Vibhute, A. Hansen, K. M. Sureshan, P. G. Jones, S. Grimme, D. Werz, *Chem. Eur. J.* **2020**, <https://doi.org/10.1002/chem.202004525>.
- ²² F. Weigend, R. Ahlrichs, *Phys. Chem. Chem. Phys.* **2005**, *7*, 3297.
- ²³ a) S. Miertuš, E. Scrocco, J. Tomasi, *Chem. Phys.* **1981**, *55*, 117; b) J. L. Pascual-Ahuir, E. Silla, I. Tuñón, *J. Comput. Chem.* **1994**, *15*, 1127; c) V. Barone, M. Cossi, *J. Phys. Chem. A* **1998**, *102*, 1995.
- ²⁴ C. González, H. B. Schlegel, *J. Phys. Chem.* **1990**, *94*, 5523.
- ²⁵ NBO 6.0, E. D. Glendening, J. K. Badenhoop, A. E. Reed, J. E. Carpenter, J. A. Bohmann, C. M. Morales, C. R. Landis, F. Weinhold, Theoretical Chemistry Institute, University of Wisconsin, Madison, WI, 2013; <http://nbo6.chem.wisc.edu/>.

- ²⁶ AIMAll, version 19.02.13, T. A. Keith, <http://tkgristmill.com>.
- ²⁷ a) M. Mitoraj, A. Michalak, *J. Mol. Model.* **2007**, *13*, 347; b) M. P. Mitoraj, A. Michalak, T. Ziegler, *J. Chem. Theory Comput.* **2009**, *5*, 962.
- ²⁸ a) G. te Velde, F. M. Bickelhaupt, E. J. Baerends, C. Fonseca Guerra, S. J. A. van Gisbergen, J. G. Snijders, T. Ziegler, *J. Comput. Chem.* **2001**, *22*, 931; b) ADF2019, SCM, Theoretical Chemistry, Vrije Universiteit, Amsterdam, The Netherlands, <http://www.scm.com>.
- ²⁹ J. G. Snijders, P. Vernooijs, E. J. Baerends, *At. Data Nucl. Data Tables* **1981**, *26*, 483, tables.
- ³⁰ J. Krijn, E. J. Baerends, Fit Functions in the HFS-Method, Internal Report, in Dutch, Vrije Universiteit Amsterdam, The Netherlands, **1984**.
- ³¹ a) E. van Lenthe, E. J. Baerends, J. G. Snijders, *J. Chem. Phys.* **1993**, *99*, 4597; b) E. van Lenthe, E. J. Baerends, J. G. Snijders, *J. Chem. Phys.* **1994**, *101*, 9783; c) E. van Lenthe, A. Ehlers, E. J. Baerends, *J. Chem. Phys.* **1999**, *110*, 8943.
- ³² Although the profile depicted in Figure 8.1 involves the reaction of **1a** with the separate BCF and TPPY reactants, the process very likely proceeds through the so-called “encounter complex”, where the BCF and TPPY pair is bonded mainly by dispersion. This [BCF⋯TPPY] encounter complex lies -9.1 kcal mol⁻¹ below the separate BCF+TPPY.
- ³³ a) T. A. Rokob, A. Hamza, A. Stirling, T. Sojs, I. Pápai, *Angew. Chem. Int. Ed.* **2008**, *47*, 2435; *Angew. Chem.* **2008**, *120*, 2469; b) T. A. Rokob, I. Bakj, A. Stirling, A. Hamza, I. Pápai, *J. Am. Chem. Soc.* **2013**, *135*, 4425.
- ³⁴ E. R. Johnson, S. Keinan, P. Mori-Sánchez, J. Contreras-García, A. J. Cohen, W. Yang, *J. Am. Chem. Soc.* **2010**, *132*, 6498.
- ³⁵ Representative examples: a) A. Armstrong, R. A. Boto, P. Dingwall, J. Contreras-García, M. J. Harvey, N. J. Mason, H. S. Rzepa, *Chem. Sci.* **2014**, *5*, 2057; b) M. Breugst, E. Detmar, D. von der Heiden, *ACS Catal.* **2016**, *6*, 3203; c) D. Yepes, P. Pérez, P. Jaque, I. Fernández, *Org. Chem. Front.* **2017**, *4*, 1390; d) S. C. Schmid, I. A. Guzei, I. Fernández, J. M. Schomaker, *ACS Catal.* **2018**, *8*, 7907. See also: e) R. A. Boto, T. Woller, J. Contreras-García, I. Fernández, *Noncovalent Interactions in Catalysis*, (Eds.: K. T. Mahmudov, M. N. Kopylovich, M. F. C. Guedes da Silva, A. J. L. Pombeiro), RSC, Cambridge, 2019, chapter 29, pp. 628–643, and references therein.
- ³⁶ a) M. Yamashita, Y. Yamamoto, K.-Y. Akiba, D. Hashizume, F. Iwasaki, N. Takagi, S. Nagase, *J. Am. Chem. Soc.* **2005**, *127*, 4354; b) K.-Y. Akiba, Y. Moriyama, M. Mizozoe, H. Inohara, T. Nishii, Y. Yamamoto, M. Minoura, D. Hashizume, F. Iwasaki, N. Takagi, K. Ishimura, S. Nagase, *J. Am. Chem. Soc.* **2005**, *127*, 5893.
- ³⁷ For other confined systems, see also: a) T. R. Forbus, Jr., J. C. Martin, *J. Am. Chem. Soc.* **1979**, *101*, 5057; b) J. C. Martin, *Science* **1983**, *221*, 509.
- ³⁸ J. Z. Dávalos, R. Herrero, J.-L. M. Abboud, O. Mó, M. Yáñez, *Angew. Chem. Int. Ed.* **2007**, *46*, 381; *Angew. Chem.* **2007**, *119*, 385.
- ³⁹ A related example appeared also recently: A. Karim, N. Shulz, H. Andersson, B. Nekoueshahraki, A.-C. Carlsson, D. Sarabi, A. Valkonen, K. Rissanen, J. Gräfenstein, S. Keller, M. Ardélyi, *J. Am. Chem. Soc.* **2018**, *140*, 17571.
- ⁴⁰ a) I. Fernández, E. Uggerud, G. Frenking, *Chem. Eur. J.* **2007**, *13*, 8620; b) S. C. A. H. Pierrefixe, S. J. M. van Stralen, J. N. P. van Stralen, C. Fonseca Guerra, F. M. Bickelhaupt, *Angew. Chem. Int. Ed.* **2009**, *48*, 6469; *Angew. Chem.* **2009**, *121*, 6591.
- ⁴¹ a) E. Ihara, V. G. Young, R. F. Jordan, *J. Am. Chem. Soc.* **1998**, *120*, 8277; b) E. Y.-X. Chen, K. A. Abboud, *Organometallics* **2000**, *19*, 5541; c) H. M. Dietrich, J. W. Ziller, R. Anwender, W. J. Evans, *Organometallics* **2009**, *28*, 1173; d) A.-L. Schmitt, G. Schnee, R. Welter, S. Dagorne, *Chem. Commun.* **2010**, *46*, 2480; e) C. Stuhl, C. Maichie-Mössner, R. Anwender, *Chem. Eur. J.* **2018**, *24*, 14254.
- ⁴² C. Outeiral, M. A. Vincent, A. M. Pendás, P. L. A. Popelier, *Chem. Sci.* **2018**, *9*, 5517.
- ⁴³ C. Hansch, A. Leo, R. W. Taft, *Chem. Rev.* **1991**, *91*, 165.

⁴⁴ D. M. Lemal, *J. Org. Chem.* **2004**, *69*, 1.

⁴⁵ a) J. E. Leffler, *Science* **1953**, *117*, 340; b) G. S. Hammond, *J. Am. Chem. Soc.* **1955**, *77*, 334.

Supporting Information

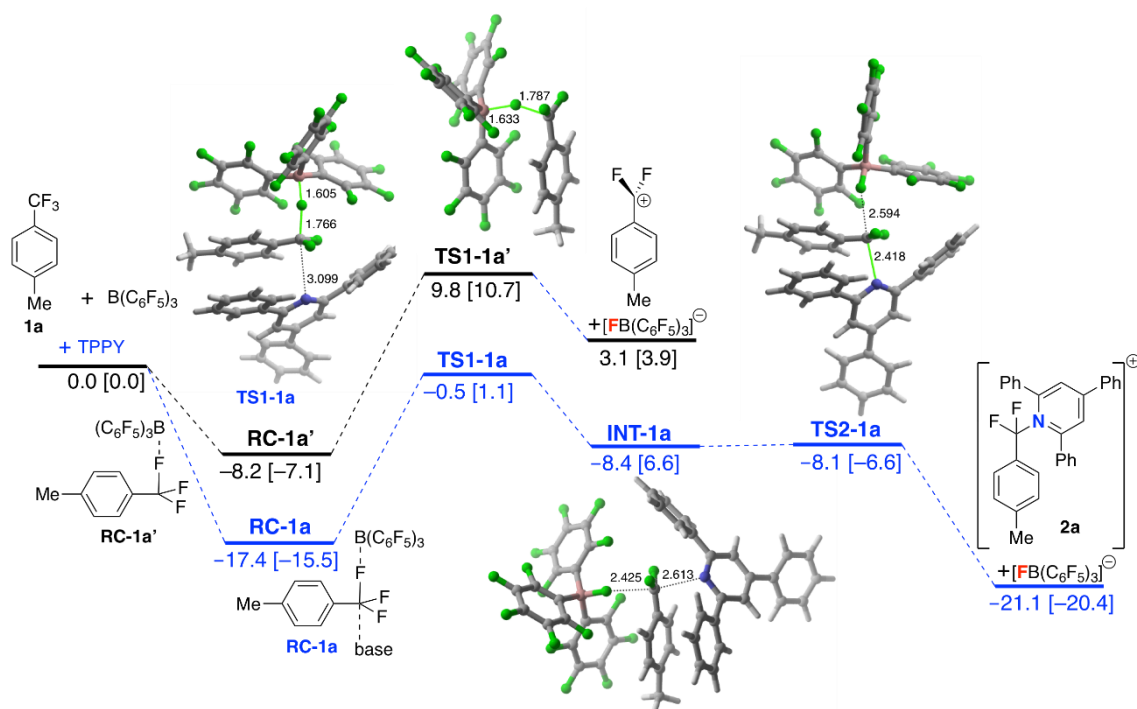


Figure 8.S1. Computed reaction profile for the BCF-mediated (black lines) and BCF/TPPY-mediated (blue lines) C-F activation reaction involving the trifluoromethyl system **1a**. Plain values refer to the relative energies computed at the PCM(DCM)-B3LYP-D3/def2-TZVPP//PCM(DCM)-B3LYP-D3/def2-SVP level, whereas values in brackets refer to relative energies computed at the PCM(DCM)-B3LYP-D3/def2-QZVPP//PCM(DCM)-B3LYP-D3/def2-SVP level.

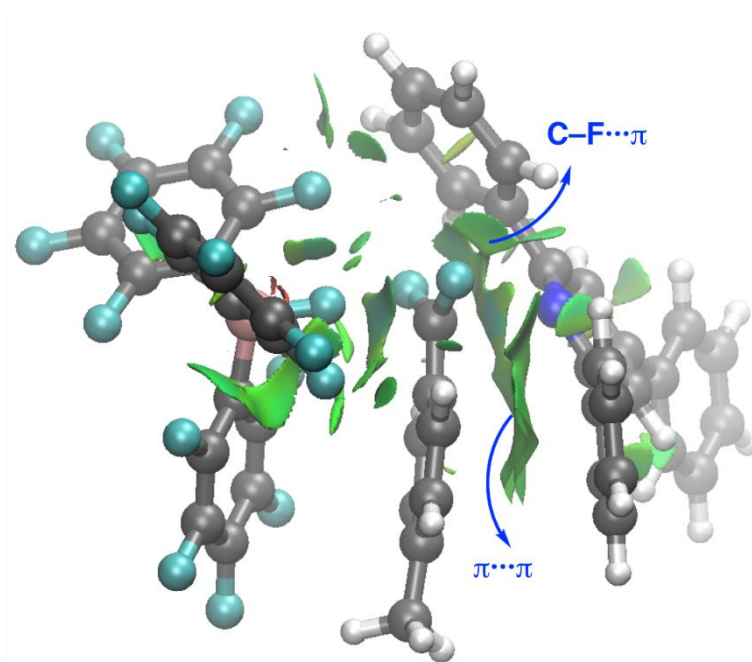


Figure 8.S2. Contour plots of the reduced density gradient isosurfaces (density cutoff of 0.03 a.u.) for **INT-1a**. The green surfaces indicate attractive non-covalent interactions.

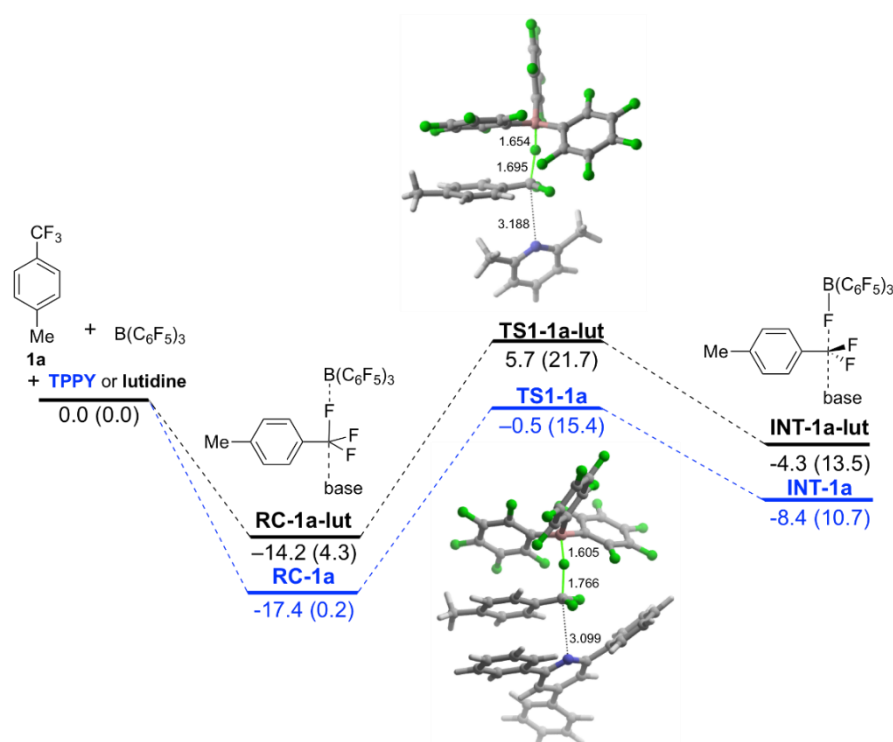


Figure 8.S3. Computed reaction profile for the processes involving **1a** and the BCF/TPPY FLP (blue lines) or BCF/lutidine FLP (black lines). Relative energies (computed at the PCM(DCM)-B3LYP-D3/def2-TZVPP//PCM(DCM)-B3LYP-D3/def2-SVP level) and bond lengths are given in kcal/mol and angstroms, respectively. Relative free energies (ΔG , 298 K) are given within parentheses and were computed at the PCM(DCM)-B3LYP-D3/def2-SVP level.

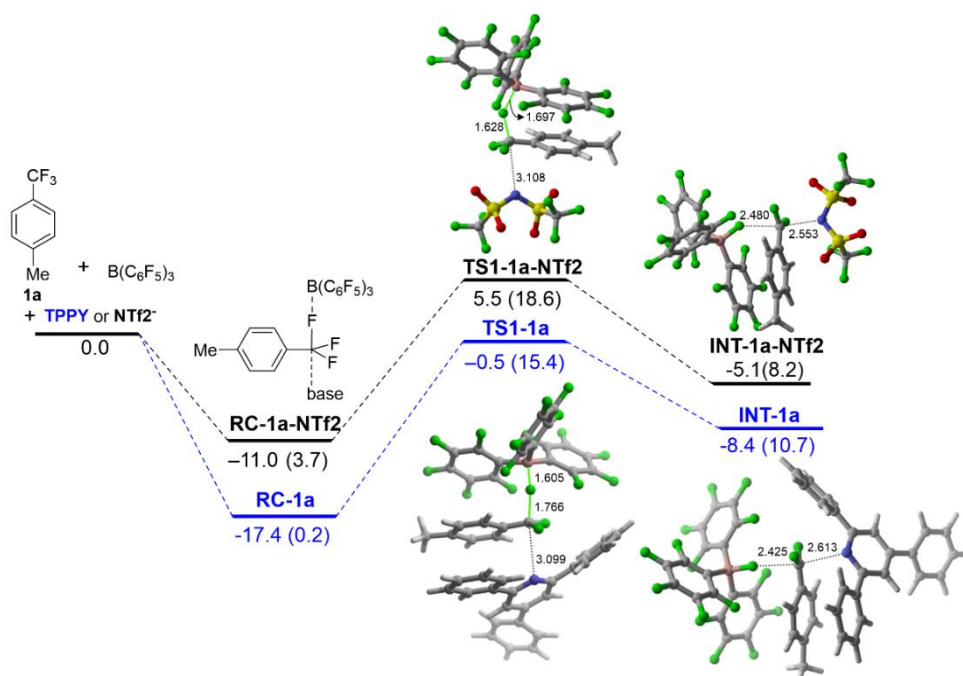


Figure 8.S4. Computed reaction profile for the processes involving **1a** and the BCF/TPPY FLP (blue lines) or BCF/NTf₂⁻ FLP (black lines). Relative energies (computed at the PCM(DCM)-B3LYP-D3/def2-TZVPP//PCM(DCM)-B3LYP-D3/def2-SVP level) and bond lengths are given in kcal/mol and angstroms, respectively. Relative free energies (ΔG , 298 K) are given within parentheses and were computed at the PCM(DCM)-B3LYP-D3/def2-SVP level.

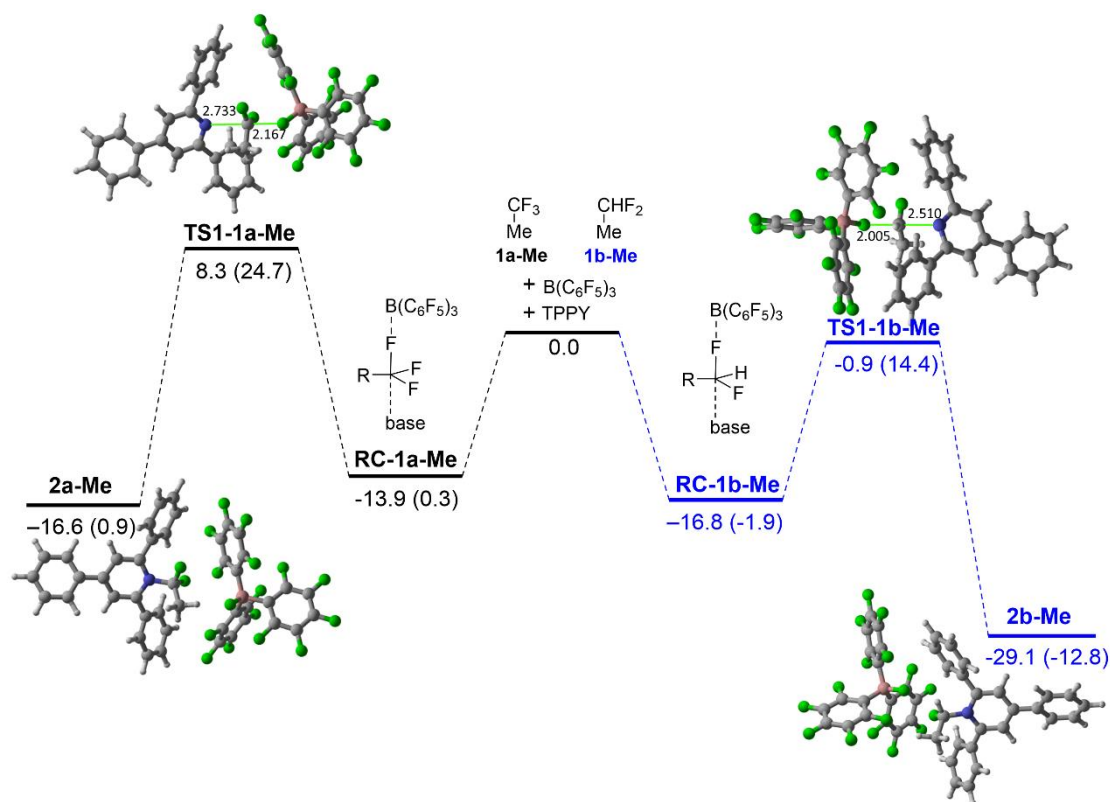


Figure 8.S5. Computed reaction profile for the C-F activation reaction involving non-aromatic substrates **1a-Me** (black lines) and **1b-Me** (blue lines). Relative energies (computed at the PCM(DCM)-B3LYP-D3/def2-TZVPP//PCM(DCM)-B3LYP-D3/def2-SVP level) and bond lengths are given in kcal/mol and angstroms, respectively. Relative free energies (ΔG , 298 K) are given within parentheses and were computed at the PCM(DCM)-B3LYP-D3/def2-SVP level.

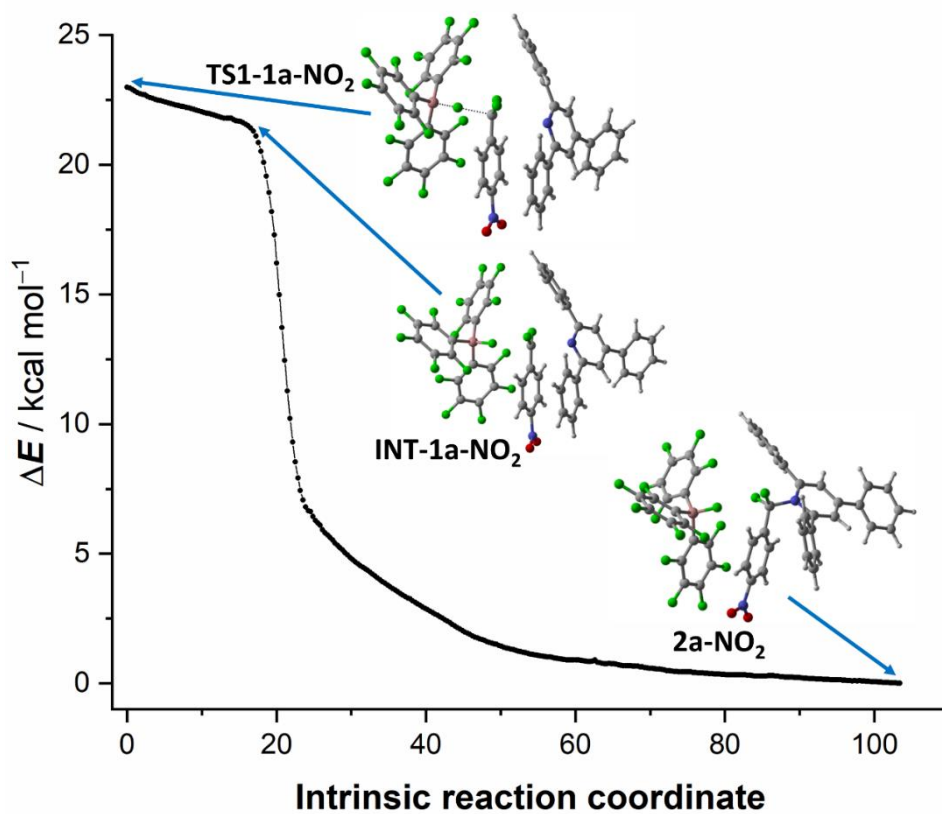


Figure 8.S6. Computed IRC for the process involving **TS1-1a-NO₂**.

IX. DISCUSSION

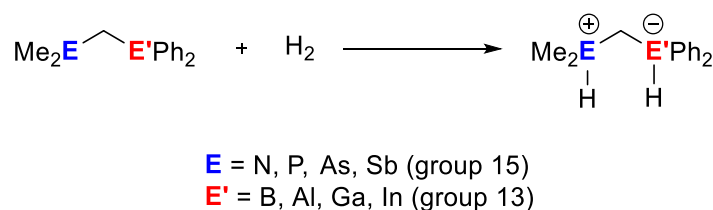
*“The numbers are meaningless, but
the trends are important.”*

Larry Burggraf

In this section, the most relevant aspects of the chapters discussed above will be discussed. In addition, a critical assessment of both the results and the initial objectives will be also presented.

9.1. Influence of the Lewis acid/base pairs on the reactivity of geminal E—CH₂—E' frustrated Lewis pairs.¹

First, we have explored the influence of the nature of the acid/basic partners on the reactivity of geminal FLPs composed of combinations of different Group 13 and Group 15 elements as acidic and basic atoms, respectively. We have selected this particular family of FLPs because, in comparison with intermolecular FLPs, the reactions involving intramolecular FLPs proceed with a lower entropy penalty due to the preorganization occurring in these systems.^{2,3} In addition, we have focused on the most representative reaction in the chemistry of FLPs, *i.e.* the dihydrogen activation reaction (Scheme 9.1). Besides understanding how the nature of the FLP antagonists impacts the reactivity, we aim at identifying the best combination of the Group 13/Group 15 elements leading to the most active system for the H₂ activation reaction.



Scheme 9.1. H₂ activation reaction mediated by geminal FLPs considered in this study.

Our Density Functional Theory (DFT) calculations for the reactions shown in Scheme 9.1, which involve up to 16 different combinations of LA/LB pairs, indicate that in all cases the process occurs in a concerted manner leading to the heterolytic splitting of the H₂ molecule. It is found that earlier transition states (TSs) are associated with lower activation barriers, thus satisfying the

¹ J. J. Cabrera-Trujillo, I. Fernández, *Chem. Eur. J.*, **2018**, *24*, 17823-17831.

² T. A. Rokob, A. Hamza, I. Pápai, *J. Am. Chem. Soc.*, **2009**, *131*, 10701-10710.

³ F. Bertini, V. Lyaskoosky, B. J. J. Timmer, F. J. J. de Kanter, M. Lutz, A. W. Ehlers, J. C. Slootweg, K. Lammertsma, *J. Am. Chem. Soc.*, **2012**, *134*, 201-204.

Hammond-Leffer postulate.⁴ Indeed, we found a very good linear relationship ($R^2 > 0.99$) when plotting the H \cdots H bond-breaking distances in the TSs versus the respective computed activation barriers. Similar linear correlations were also found when using the corresponding LA \cdots H bond-forming distances versus the respective activation energies. Therefore, these findings suggest that both the computed H \cdots H or the LA \cdots H distances in the respective TSs can be used as a reliable, quantitative measure of the barriers associated with the corresponding H₂ activation reactions mediated by these geminal FLPs.

Interestingly, the activation barrier for the considered H₂ activation reaction steadily increases when going down the Group 15 regardless of the nature of the acidic E' atom. This finding may be initially ascribed to the reduction of basicity when going down the Group 15 (*i.e.* nitrogen is much more basic than antimony). On the other hand, when having the same basic atom, we found that the activation barriers decrease when going down from boron to indium, with the remarkable exception of aluminum, which exhibits the lowest activation barriers in all the considered series. This means that the FLP composed of Al/N is the most active system of this family of geminal FLPs.

To gain a deeper insight into the physical factors that are responsible for the computed reactivity trend, we applied the activation strain model (ASM) of reactivity. First, we focused on the H₂ activation reactions involving the geminal Me₂E-CH₂-BPh₂ (E = N, P, As, Sb) FLPs. From the corresponding activation strain diagrams (ASDs, Figure 9.1), it becomes evident that the computed reactivity trend (*i.e.* activation barrier increases in the order B/N < B/P < B/As < B/Sb) directly originates from the strain energy (ΔE_{strain}) associated with the deformation of the reactants from their equilibrium geometries to the geometry they adopt in the corresponding transition states. The partitioning of the ΔE_{strain} term into contributions coming from both reactants (*i.e.*, H₂ and FLP) indicates that the strain associated with distorting the FLP reactant is the main contributor to the total ΔE_{strain} . At variance, the interaction energy between the deformed reactants is nearly identical in all cases, which suggests that the basicity of the Group 15 atom is not directly related to the observed reactivity trend.

⁴ (a) J. E. Leffler, *Science*, **1953**, *117*, 340-341; (b) G. S. J. Hammond, *J. Am. Chem. Soc.*, **1955**, *77*, 334-338.

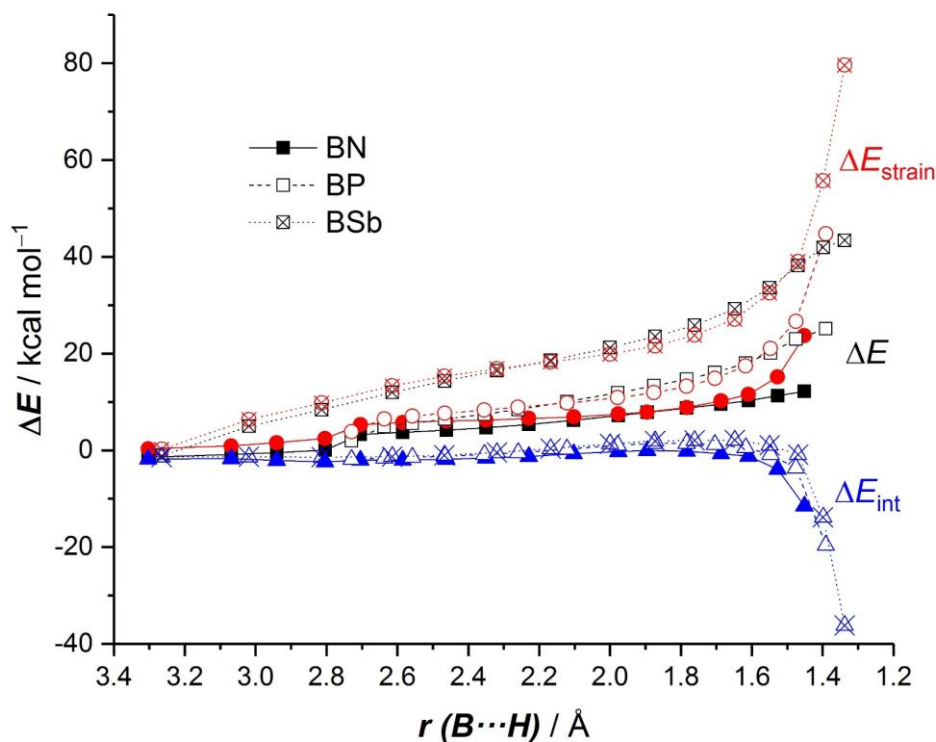


Figure 9.1. Comparative activation strain diagrams for the H_2 activation reaction involving the geminal FLPs B/N, B/P, and B/Sb.

We also applied the ASM approach to analyze the computed reactivity trends when the acidic atom is modified. Figure 9.2 graphically shows the evolution of the ASM terms for the processes involving the $\text{Me}_2\text{N}-\text{CH}_2-\text{E}'\text{Ph}_2$ FLPs ($\text{E}' = \text{B}, \text{Al}, \text{In}$). We found that the boron-based FLP required a much higher strain energy along the entire reaction coordinate as compared to the FLPs containing the heavier Group 13 acidic atoms. For this reason, the B/N-based FLP becomes the least reactive of this series. The ΔE_{strain} term is nearly identical for the systems containing Al and In and, therefore, this term is not responsible for the different reactivity computed for these two systems. At variance, the process involving the Al/N-based FLP benefits from a comparatively stronger interaction, which results in the lower barrier computed for this particular system. Therefore, the high reactivity of the Al-based FLPs can be ascribed to the combination of a lower ΔE_{strain} (in comparison with B-based FLPs), as well as a stronger interaction energy between the deformed reactants (in comparison with its heavier analogues) along the entire reaction coordinate.

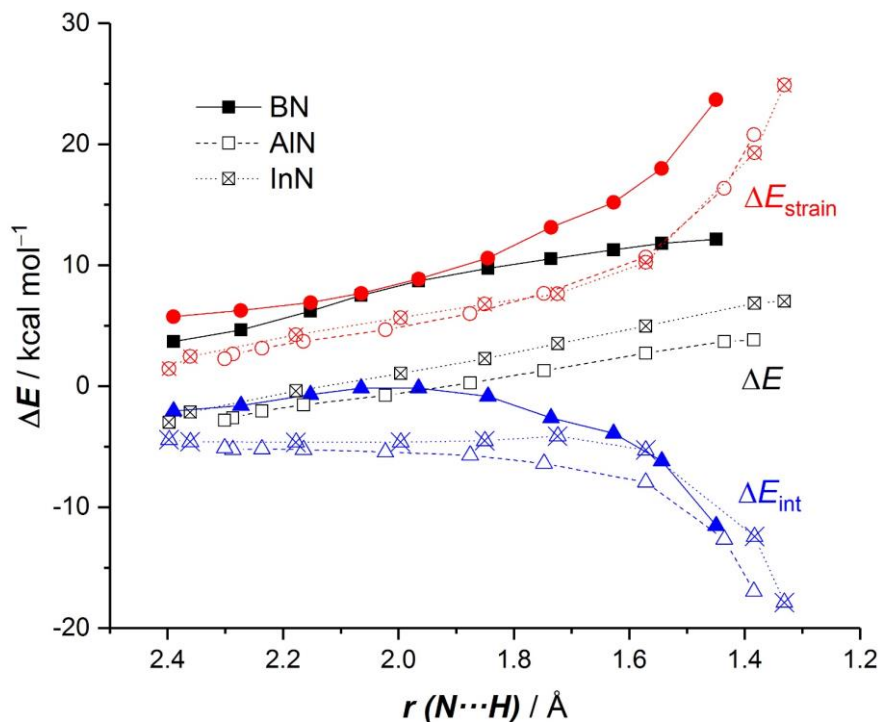


Figure 9.2. Comparative activation strain diagrams for the H₂ activation reaction involving the geminal FLPs B/N, Al/N, and In/N.

The origin of the stronger interaction between the reactants computed for the process involving the Al/N-based FLP was quantitatively analyzed with the help of the energy decomposition analysis (EDA) method. Figure 9.3 shows the evolution of the different EDA terms along the reaction coordinate for the H₂ activation reaction mediated by the geminal FLPs Me₂N-CH₂-E'Ph₂ (E' = B, Al, In). By comparing the processes involving the Al/N and In/N systems, we found that the Al/N FLP is more reactive exclusively due to a much stronger orbital interaction between the deformed reactants along the entire reaction coordinate. According to the natural orbital for chemical valence (NOCV) extension of the EDA method, the more stabilizing orbital interactions in the reaction involving the Al/N system derive from stronger cooperative electron donation from the nitrogen lone pair to the σ^* molecular orbital of the H₂ and the electron donation from the σ molecular orbital of the H₂ to the vacant p orbital of the acidic atom. The corresponding pairwise orbital interaction, which can be written as LP(N) \rightarrow $\sigma^*(\text{H}_2)$ and $\sigma(\text{H}_2) \rightarrow p_z(\text{Al or In})$, is ca. 8 kcal/mol higher for the Al/N system (computed at the same N...H bond-forming distance, see Figure 9.4). This finding is fully consistent with

the previous work on related geminal B/N FLPs reported by our research group⁵ and is also in line with the general *electron-transfer model* proposed by Pápai and co-workers where orbital interactions are key to promote FLP reactivity.⁶

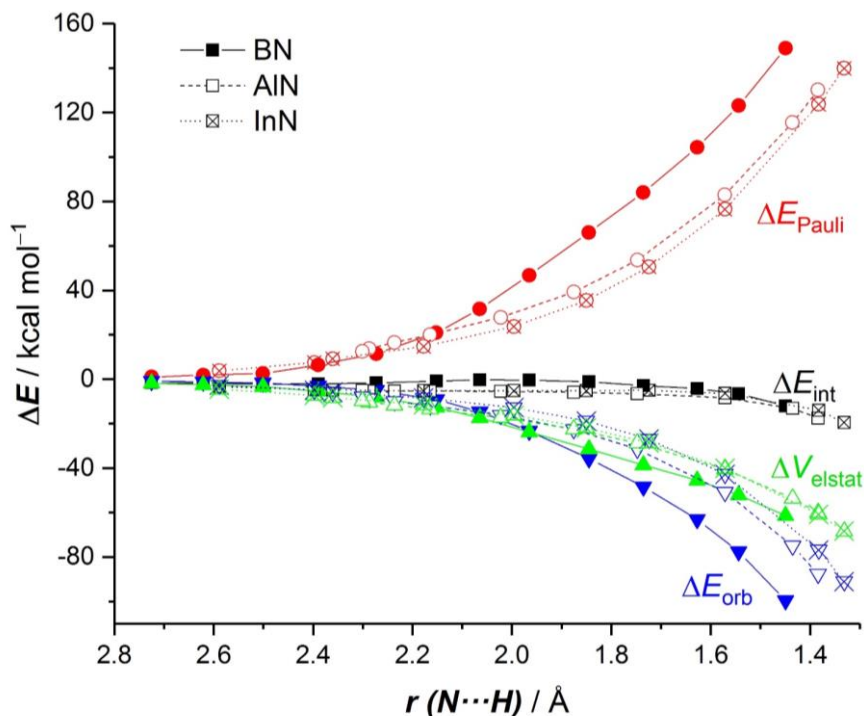


Figure 9.3. Comparative energy decomposition analysis for the H₂ activation reaction involving the geminal FLPs B/N, Al/N, and In/N.

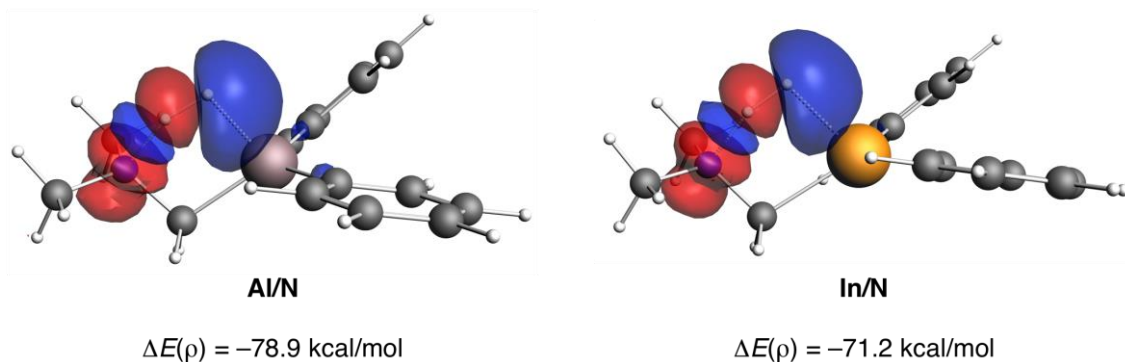


Figure 9.4. Plot of the deformation densities $\Delta\rho$ and their associated energies $\Delta E(\rho)$ of the main pairwise interaction between H₂ and the geminal FLPs Al/N (left) and the In/N (right). The electronic charge flows from red to blue.

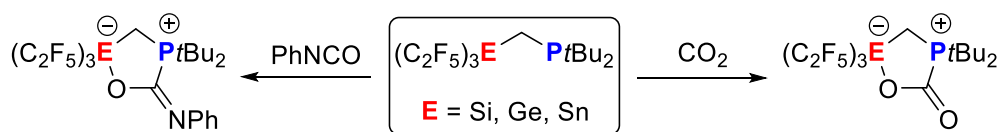
⁵ D. Yepes, P. Jaque, I. Fernández, *Chem. Eur. J.*, **2016**, *22*, 18801-18809.

⁶ T. A. Rokob, A. Hamza, A. Stirling, T. Sóos and I. Pápai, *Angew. Chem. Int. Ed.*, **2008**, *47*, 2435-2438.

Once the influence of the nature of the FLP antagonists on the reactivity has been analyzed and aiming at further reducing the barrier of the H₂ activation, we also explored the influence of the substituents directly attached to the acidic atom on the reactivity. To this end, we replaced the phenyl groups in the B/N and the Al/N geminal FLPs by highly electron-withdrawing groups (EWG), namely, C₆F₅ and Fxyl (3,5-(CF₃)₂C₆H₃). We found a clear reactivity trend in the order Ph < Fxyl < C₆F₅, which correlates with the electron-withdrawing ability of the substituents. Therefore, the geminal FLP Me₂N-CH₂-B(C₆F₅)₂ and particularly, its aluminum counterpart Me₂N-CH₂-Al(C₆F₅)₂, are predicted as the most promising (*i.e.*, active) candidates to perform facile dihydrogen activation reactions (*i.e.*, having relatively low activation barriers).

9.2. Understanding the reactivity of neutral geminal Group 14 element/phosphorus frustrated Lewis pairs.⁷

Directly related to the above study, we were interested in rationalizing the reactivity of the geminal FLPs (F₅C₂)₃E-CH₂-P(*t*Bu)₂, E = Si, Ge, Sn, recently prepared by Mitzel and co-workers,^{8,9,10} to understand the influence of the Group 14 element on their reactivity. We selected the CO₂ and phenyl isocyanate activation reactions (Scheme 9.2), rather than the archetypal H₂ activation, to compare our computational results with the available experimental data.



Scheme 9.2. Reactivity of Group 14 element containing geminal FLPs.

Our calculations indicate that in both reactions the corresponding activation barriers decrease when going down the Group 14 (Si > Ge > Sn), which resembles

⁷ J. J. Cabrera-Trujillo, I. Fernández, *J. Phys. Chem. A* **2019**, *123*, 10095-10101.

⁸ B. Waerder, M. Pieper, L. A. Körte, T. A. Kinder, A. Mix, B. Neumann, H.-G. Stammer, N. W. Mitzel, *Angew. Chem., Int. Ed.*, **2015**, *54*, 13416-13419.

⁹ T. A. Kinder, R. Pior, S. Blomeyer, B. Neumann, H.-G. Stammer, N. W. Mitzel, *Chem. Eur. J.*, **2019**, *25*, 5899-5903.

¹⁰ P. Holtkamp, F. Friedrich, E. Stratmann, A. Mix, B. Neumann, H.-G. Stammer, N. W. Mitzel, *Angew. Chem., Int. Ed.*, **2019**, *58*, 5114-5118.

the trend computed for their N/Group 13 analogues (see above). This finding is consistent with the experimental observation that the CO₂ activation mediated by the Si-based FLP occurs at room temperature,⁸ whereas the analogous reaction using the Sn-based FLP can be carried out at -70 °C.¹⁰

This reactivity trend is mainly the result of the much stronger interaction energy between the deformed reactants computed for the process involving the Sn/P FLP along the entire coordinate (Figure 9.5a). In addition, this system benefits from a less destabilizing strain energy as compared to the reaction involving the Si/P system. According to the EDA approach, the computed stronger interaction for the Sn/P system derives from both much stronger electrostatic and orbital attractions from the initial stages of the transformation up to the corresponding transition states (Figure 9.5b).

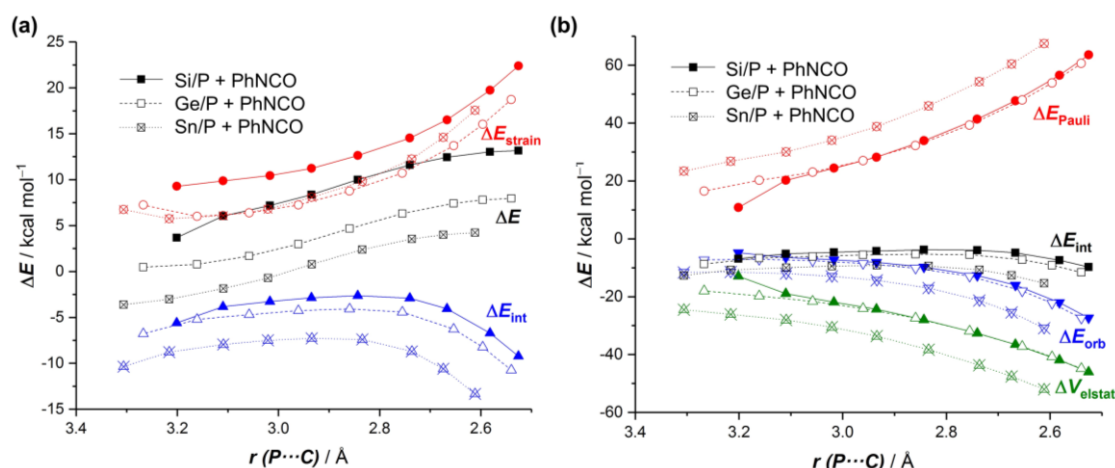
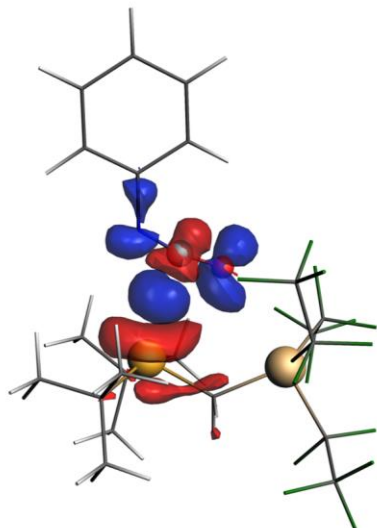


Figure 9.5. (a) Comparative activation strain diagrams and (b) comparative energy decomposition analysis for the phenyl isocyanate activation reaction involving the geminal FLPs (F₃C₂)₃E-CH₂-P(*t*Bu)₂, E = Si (solid line), Ge (dashed line), Sn (dotted line).

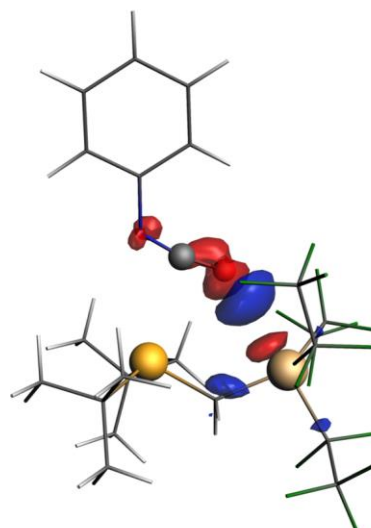
The nature of the molecular orbital interactions and their relative contribution to the total orbital interaction term, ΔE_{orb} , was further analyzed by means of the NOCV method. Two main orbital interactions are identified by this approach, namely the donation of electron density from the lone pair of the phosphorus to an antibonding π^* molecular orbital of the phenyl isocyanate located in the C=O moiety, LP(P)→ $\pi^*(\text{C}=\text{O})$, denoted as $\Delta E(\rho_1)$, and the charge transfer from the oxygen atom of the isocyanate to the E(C₂F₅) moiety, $\Delta E(\rho_2)$ (see Figure 9.6). Both orbital interactions are comparatively stronger in the Sn/P system than

in the less reactive Si/P, which is translated into the more stabilizing orbital interactions computed for the former system.

(a) Si/P + PhNCO

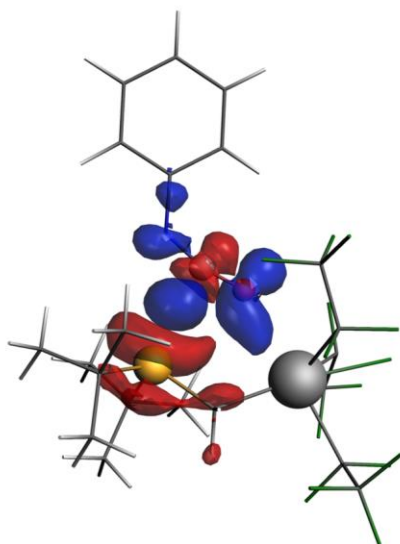


$$\Delta E(\rho_1) = -8.4 \text{ kcal/mol}$$

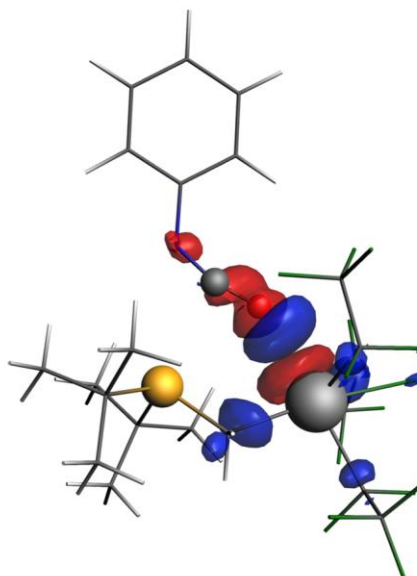


$$\Delta E(\rho_2) = -2.8 \text{ kcal/mol}$$

(b) Sn/P + PhNCO



$$\Delta E(\rho_1) = -12.6 \text{ kcal/mol}$$



$$\Delta E(\rho_2) = -5.1 \text{ kcal/mol}$$

Figure 9.6. Contour plots of NOCV deformation densities $\Delta\rho$ and their associated energies $\Delta E(\rho)$ for the main orbital interactions between PhNCO and geminal FLPs **Si/P** (a) and **Sn/P** (b). Computed at the same consistent P...C forming bond distance of 2.7 Å. Electronic charge flows from red to blue.

Interestingly, we found that the main pairwise orbital interaction ($\Delta E(\rho_1)$) is present even at the very early stages of the reaction. At variance, the second orbital interaction ($\Delta E(\rho_2)$) becomes relevant only in the TS region (Figure 9.7). Consequently, we propose that the synergistic action (derived from orbital interactions) of the LA and the LB in the considered transformations do not occur simultaneously, as proposed by Pápai,⁶ but asynchronously along the reaction coordinate, which agrees with previous results reported by our research group.⁵

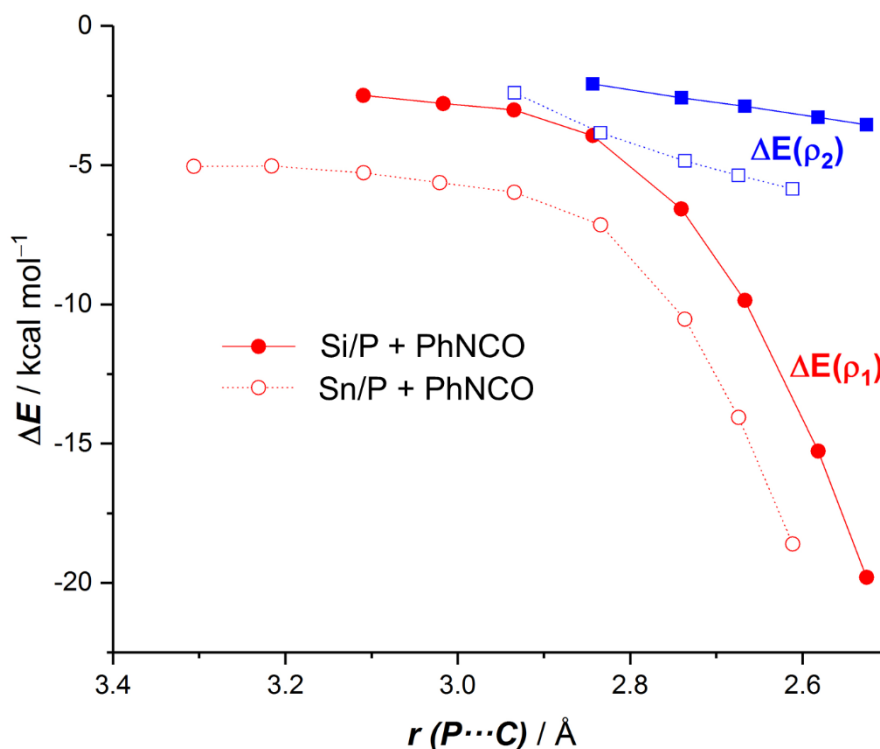


Figure 9.7. Evolution of the NOCV components for the PhNCO activation reactions mediated by FLP Si/P (solid lines) and Sn/P (dotted lines) along the reaction coordinate projected onto the forming P \cdots C bond distance.

9.3. Aromaticity can enhance the reactivity of P-donor/borole frustrated Lewis pairs.¹¹

Aimed at designing more active systems for the activation of small molecules, we merged the concepts of aromaticity and FLPs. Specifically, we explored the reactivity of geminal FLPs containing a borole fragment as acid functionality, whose 4π -antiaromaticity was previously demonstrated.¹² We envisioned that the

¹¹ J. J. Cabrera-Trujillo, I. Fernández, *Chem. Commun.*, **2019**, 55, 675-678

¹² H. Braunschweig, I. Fernández, G. Frenking, T. Kupfer, *Angew. Chem. Int. Ed.*, **2008**, 47, 1951-1954.

loss of antiaromaticity in the borole fragment during the activation reaction should result in a more favorable transformation, not only from a thermodynamic but also from a kinetic point of view. To check this hypothesis, we computationally compared different activation reactions involving the parent geminal FLP **9.1**, described by Lammertsma and co-workers,³ and **9.2**, the analogous system having a borole in its structure. For comparison, we also included the FLP counterpart **9.3**, having a 2π -aromatic borirene as acidic moiety (Figure 9.8).

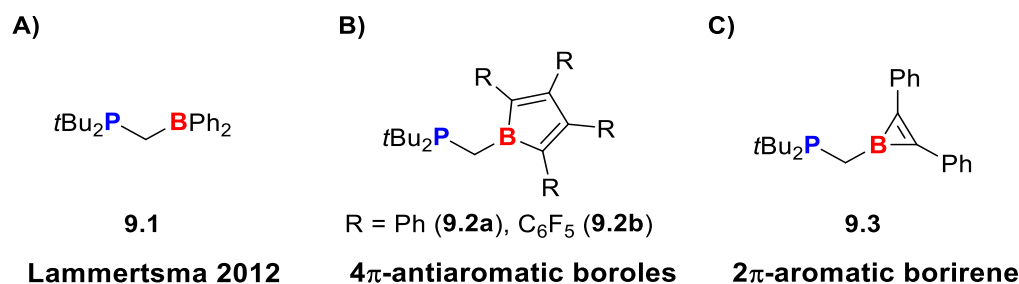


Figure 9.8. Geminal FLPs considered in this study.

Our calculations indicate that, regardless of the activation reaction (H_2 , CO_2 , CS_2 , $HC\equiv CH$, SiH_4 , and even CH_4), the processes mediated by FLPs **9.2a** and **9.2b**, containing a borole fragment, are both kinetically and thermodynamically favored over the analogous processes involving the parent FLP **9.1** and the aromatic **9.3**, which is in line with our initial expectations. We therefore predict that FLPs containing a 4π -antiaromatic borole fragment constitute really promising candidates to carry out facile small-molecule activation reactions, not only involving H_2 or CO_2 but also more challenging systems such as CH_4 .

The detailed analyses of the change of the aromaticity in the borole moiety along the reaction coordinate by means of the nucleus-independent chemical shift (NICS) values and the anisotropy of the induced current density (ACID) method, clearly confirm that a loss of antiaromaticity in the borole fragment occurs during the progress of the activation reaction. Thus, the ACID method confirms the paratropic nature of the induced current in the borole fragment in **9.2a** (Figure 9.9). In contrast, only a weakly paratropic current was found in the corresponding transition state **9.TS-2a**, associated with the heterolytic H_2 cleavage. This trend was further confirmed in the final adduct, where the attachment of the hydride to the boron atom provokes the interruption of the electronic circulation within the boron-heterocycle. These findings are supported by the computed NICS values,

which range from highly positive in **9.2a** (24.9 ppm) to nearly zero (1.3 ppm) in the final adduct (Figure 9.9).

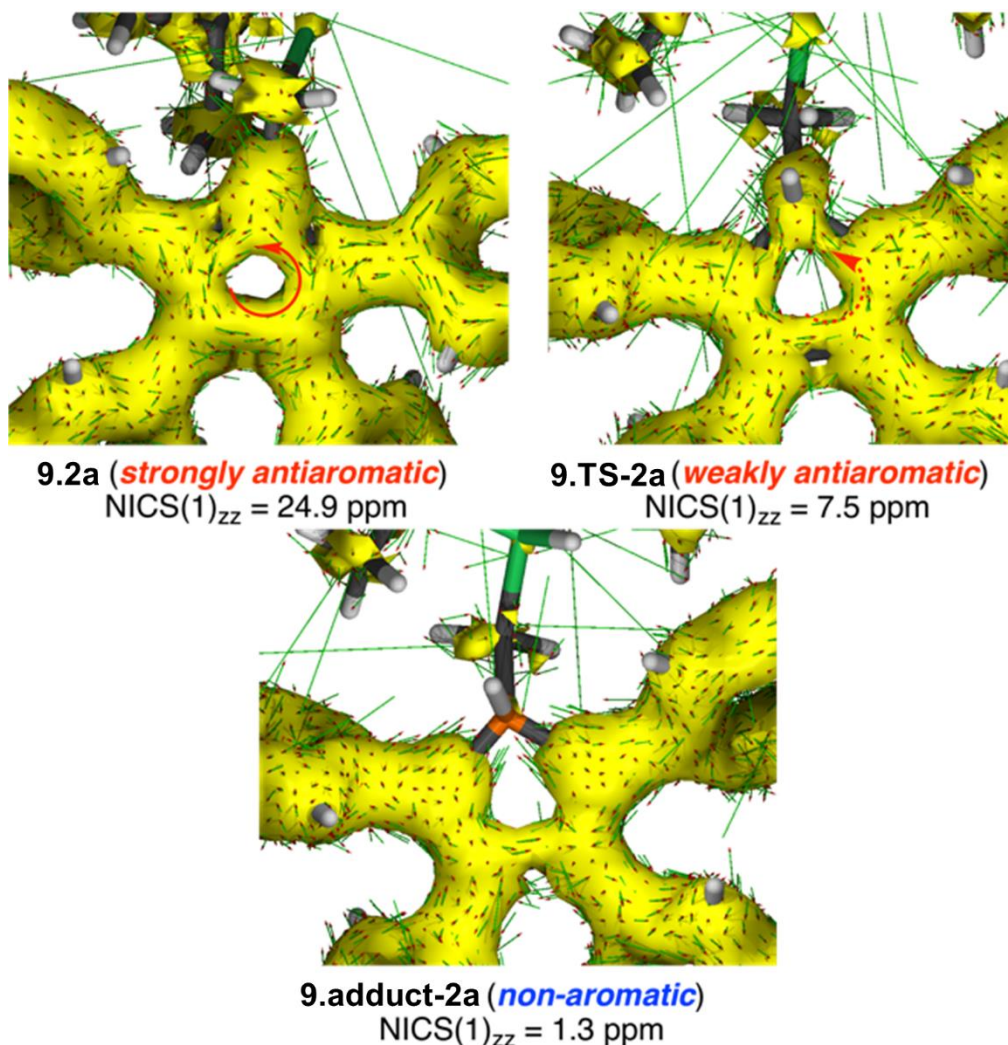


Figure 9.9. Computed ACID plots for the key points of the H₂ activation reaction mediated by FLP **9.2a** (isosurface value of 0.04).

These results therefore confirm that the reactivity of FLPs and (anti)aromaticity are related. Indeed, very good linear correlations ($R^2 > 0.98$) were found when plotting the NICS values versus the computed energy values (ΔE) along the entire reaction coordinate (from the initial reactant complex to the corresponding transition state) for the H₂ activation reaction involving the FLP **9.2a** (Figure 9.10). The main take-home message derived from this study is that the loss of antiaromaticity (or gain in aromaticity) can be used to significantly enhance the reactivity of FLPs. To the best of our knowledge, this is the first report merging the concepts of FLPs and aromaticity.

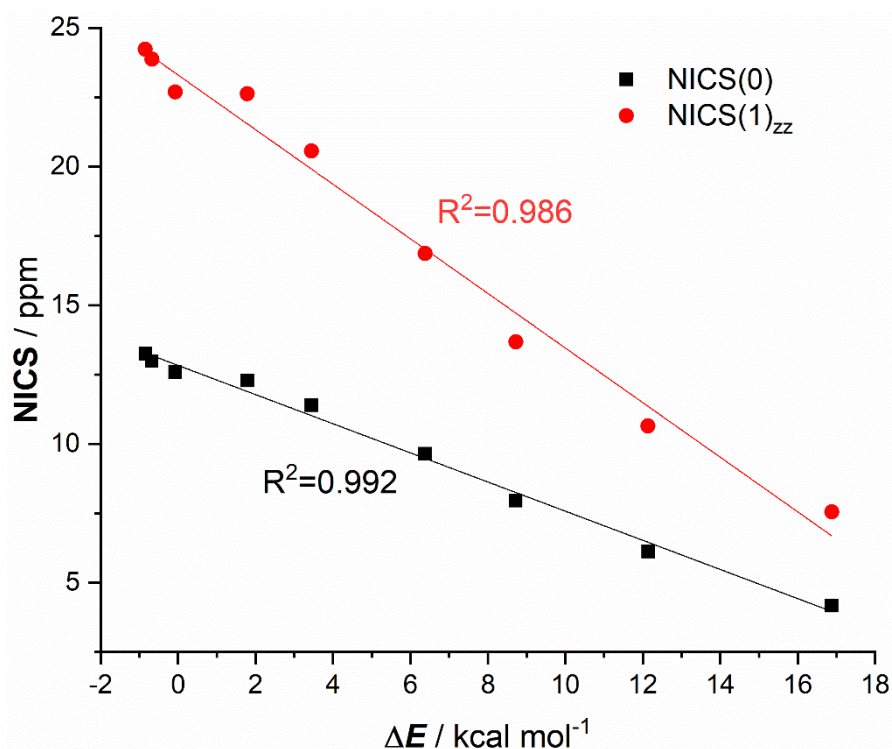


Figure 9.10. Plot of the NICS values vs the energy along the reaction coordinate (from the corresponding reactant complex to the TS) for the H₂ activation reaction mediated by FLP **9.2a**.

9.4. Carbenes and heavier ylidenes (EL₂) in frustrated Lewis pair chemistry: Influence of the nature of EL₂ on dihydrogen activation.¹³

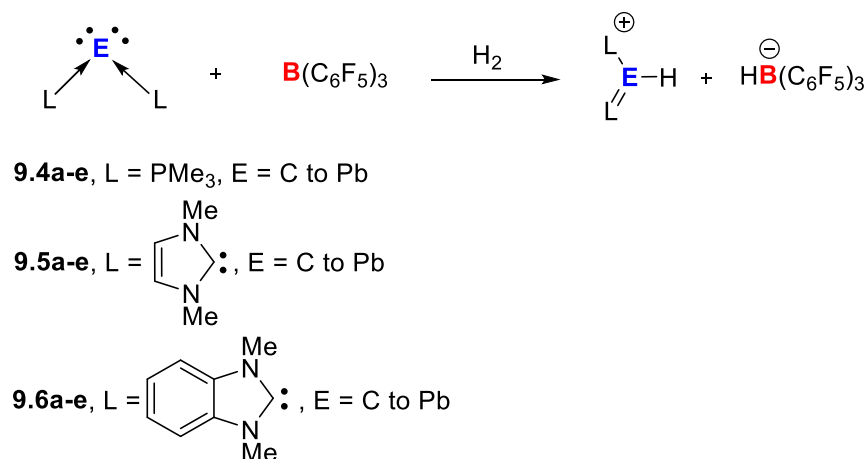
Carbon(0) species, also known as carbenes, are unconventional species containing a carbon atom that retains its four valence electrons as two lone pairs.¹⁴ Therefore, these species can be potentially used as a basic fragment in FLPs. Indeed, Alcarazo and co-workers confirmed that combinations of B(C₆F₅)₃ and carbodiphosphanes (a family of carbenes where the central carbon atom is flanked by two phosphines) do behave as highly active FLPs.¹⁵ Despite that, very little was known about the influence of the carbene on the reactivity of these intermolecular FLPs. For this reason, we carried out a comparative study on the reactivity of FLPs composed of BCF and not only carbodiphosphanes but also their heavier

¹³ J. J. Cabrera-Trujillo, I. Fernández, *Inorg. Chem.* **2019**, *58*, 7828-7836.

¹⁴ (a) R. Tonner, F. Öxler, B. Neumüller, W. Petz, G. Frenking, *Angew. Chem., Int. Ed.*, **2006**, *45*, 8038-8042; (b) R. Tonner, G. Frenking, *Angew. Chem., Int. Ed.*, **2007**, *46*, 8695-8698; (c) R. Tonner, G. Frenking, *Chem. Eur. J.*, **2008**, *14*, 3260-3272; (d) R. Tonner, G. Frenking, *Chem. Eur. J.*, **2008**, *14*, 3273-3289.

¹⁵ Alcarazo, M.; Gomez, C.; Holle, S.; Goddard, R. *Angew. Chem., Int. Ed.*, **2010**, *49*, 5788-5791.

analogues, known as ylidenes,¹⁶ to understand the impact of the nature of the LB. In addition, we also included carbodicarbenes in our study, a family of ylidenes where the central Group 14(0) element is flanked by two *N*-heterocyclic carbenes (see Scheme 9.3).



Scheme 9.3. H₂ activation reaction mediated by FLPs composed by carbenes/ylidenes and BCF.

By comparing the H₂ activation reaction mediated by the parent intermolecular FLP *t*Bu₃P/B(C₆F₅)₃ and the analogous transformation involving carbene C(PMe₃)₂ (**9.4a**), it becomes evident that the process involving the latter base is thermodynamically favored (also kinetically, albeit to a much lesser extent) over the process involving *t*Bu₃P (computed reaction energy difference of > 30 kcal/mol). This is consistent with the reported low temperature (-78 °C to room temperature) reported experimentally,¹⁵ and reflects the high proton affinity of carbenes.¹⁶

According to the EDA method, the process involving H₂ and [**9.4a**⋯B(C₆F₅)₃] benefits from a much more stabilizing orbital and electrostatic interactions between the deformed reactants along the entire reaction coordinate as compared to the parent process involving *t*Bu₃P. Despite that, the Pauli repulsion computed for this system is clearly more destabilizing and as consequence, the overall interaction energy between the deformed reactants is relatively similar along the transformation (Figure 9.11).

¹⁶ For a recent review, see: G. Frenking, R. Tonner, S. Klein, N. Takagi, T. Shimizu, A. Krapp, K. K. Pandey, P. Parameswaran, *Chem. Soc. Rev.*, **2014**, *43*, 5106-5139.

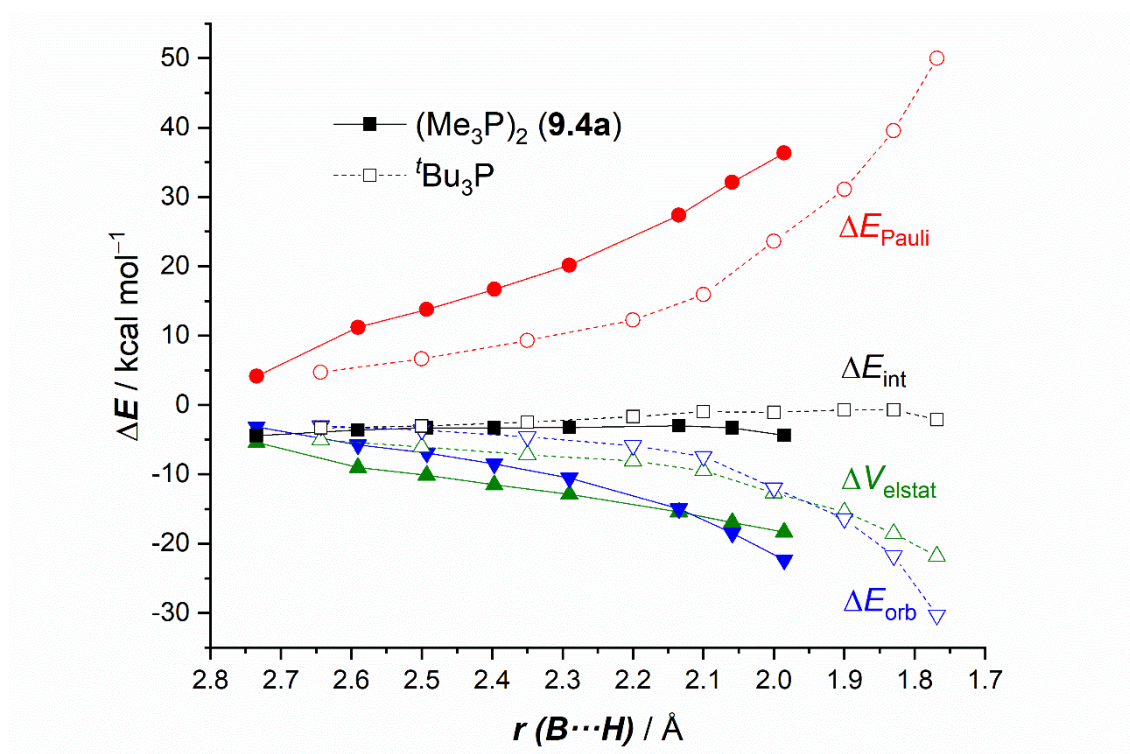


Figure 9.11. Comparative energy decomposition analysis of the H_2 activation reactions mediated by **9.4a** (solid lines) and $t\text{Bu}_3\text{P}$ (dashed lines) in the presence of $\text{B}(\text{C}_6\text{F}_5)_3$ along the reaction coordinate projected onto the forming $\text{B}\cdots\text{H}$ bond length.

The NOCV method has been particularly helpful to understand the differences in the cooperative action of the FLP antagonists when replacing the parent $t\text{Bu}_3\text{P}$ phosphine by the carbene $\text{C}(\text{PMe}_3)_2$. Figure 9.12 shows snapshots of the main pairwise orbital interactions at three key points along the reaction coordinate, namely, the reactant complex (RC), the transition state (TS), and a midpoint between them. As expected, the main orbital interaction is identified as the electron density transfer from the lone pair of the phosphine (or the carbene) to the antibonding σ^* molecular orbital of the H_2 coupled to the electron transfer from the σ molecular orbital of the H_2 to the vacant p orbital at the boron in the BCF. Whereas in the process involving the phosphine, the $\text{LP}(\text{P}) \rightarrow \sigma^*(\text{H}_2)$ orbital interaction takes place only in the TS region, the analogous $\text{LP}(\text{C}) \rightarrow \sigma^*(\text{H}_2)$ orbital interaction in the process involving the carbene **9.4a** is present even at the initial stages of the transformation. As a consequence, the associated deformation energy ($\Delta E(\rho_1)$) is comparatively higher in the latter system, which is finally translated into the stronger interaction energy along the reaction coordinate computed for the process involving the **9.4a**/BCF FLP. This finding therefore confirms the higher σ -donor ability of **9.4a** as compared to $t\text{Bu}_3\text{P}$.

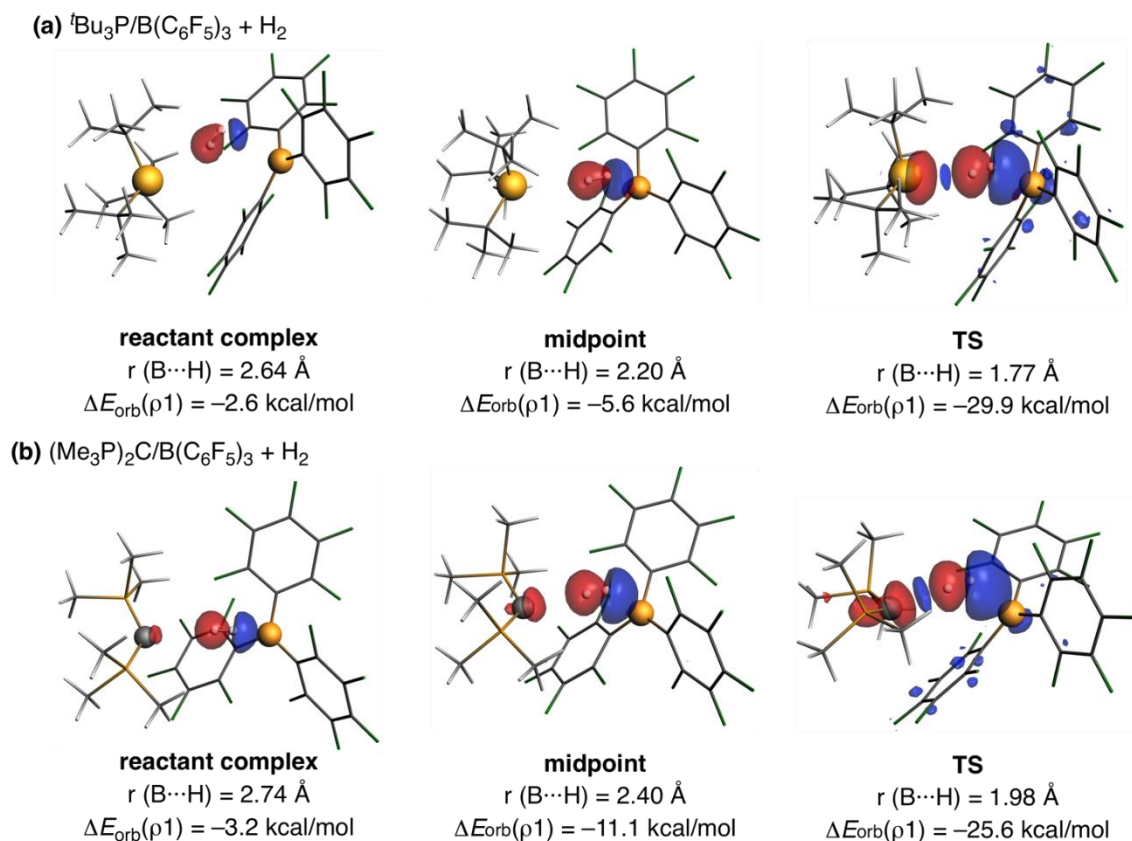


Figure 9.12. Contour plots of NOCV deformation densities $\Delta\rho$ and associated energies $\Delta E(\rho)$ (in kcal/mol) for the main orbital interactions between H_2 and (a) $[\text{tBu}_3\text{P}\cdots\text{B}(\text{C}_6\text{F}_5)_3]$ and (b) $[\mathbf{9.4a}\cdots\text{B}(\text{C}_6\text{F}_5)_3]$. Electronic charge flows from red to blue.

Regarding the reactivity trends observed when comparing the different ylidones shown in Scheme 9.3, we found that the activation energies steadily decrease when going down the Group 14 ($\text{C} > \text{Si} > \text{Ge} > \text{Sn} > \text{Pb}$) regardless of the ligand L attached to the central Group 14(0) element. This trend originates, according to the ASM-EDA(NOCV) method, mainly from stronger orbital interactions between the deformed reactants (mainly the key $\sigma(\text{H}_2) \rightarrow \text{p}_z(\text{B})$ and $\text{LP}(\text{E}) \rightarrow \sigma^*(\text{H}_2)$ interaction) in the heavier systems as compared to carbones. On the other hand, our calculations also show that when the central atom is carbon, the activation free energy ΔG^\ddagger decreases in the order $\mathbf{9.4a}$ ($18.7 \text{ kcal mol}^{-1}$) $>$ $\mathbf{9.6a}$ ($16.6 \text{ kcal mol}^{-1}$) $>$ $\mathbf{9.5a}$ ($15.5 \text{ kcal mol}^{-1}$). This reactivity trend is again fully consistent with the previously reported proton affinities for $\mathbf{9.5a}$ ($294.3 \text{ kcal mol}^{-1}$), $\mathbf{9.6a}$ ($284.7 \text{ kcal mol}^{-1}$), and $\mathbf{9.4a}$ ($278.4 \text{ kcal mol}^{-1}$).¹⁶ Therefore, our results indicate that the replacement of phosphine ligands by NHCs ligands facilitates the H_2 activation mediated by FLPs composed of carbones.

The analysis of the optimized geometries of the TSs for the processes involving ylidenes **9.4a-e**, **9.5a-e**, and **9.6a-e** indicates that earlier TSs are associated with lower activation energies, therefore satisfying the Hammond-Leffer postulate.⁴ Indeed, very good linear relationships were found when plotting the H···H bond-breaking distance in the respective TSs versus both the activation and the reaction energies (Figure 9.13). These findings suggest that this geometrical parameter can be used as a reliable quantitative measure of the energetics involved in the H₂ activation reactions mediated by ylidone-based FLPs.

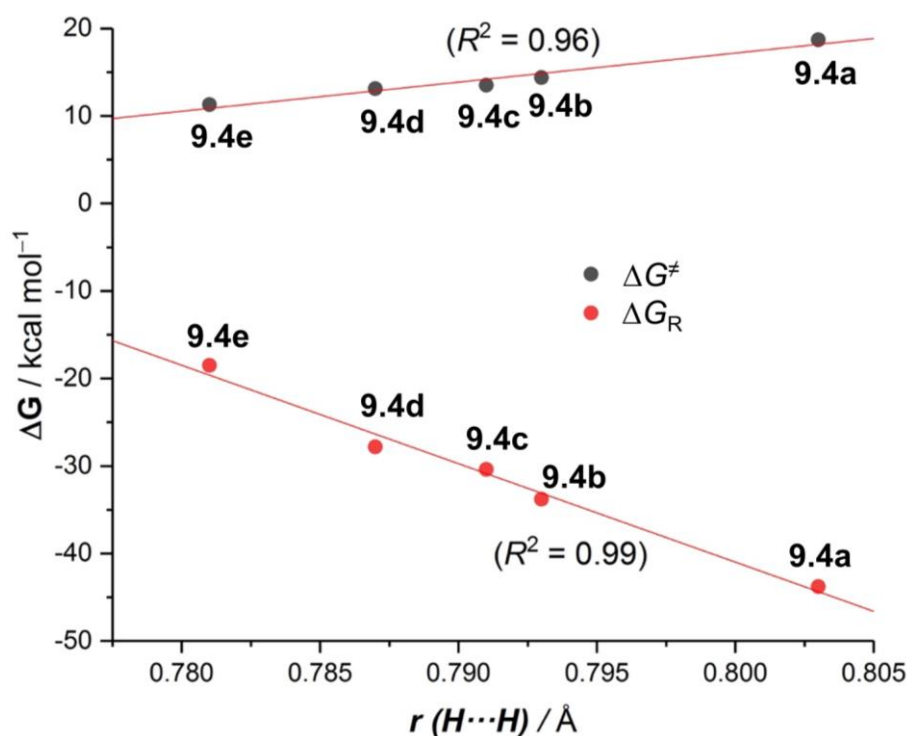


Figure 9.13. Plot of the computed activation barriers (ΔG^\ddagger , black circles) and reaction energies (ΔG_R , red circles) vs the breaking H···H distance in the corresponding TSs involved in the **9.4a-e** + B(C₆F₅)₃ + H₂ reaction.

9.5. Understanding the role of frustrated Lewis pairs as ligands in transition metal-catalyzed reactions.¹⁷

This study was inspired by the increasing number of reports which confirm the enhanced reactivity of transition metal complexes featuring an ambiphilic ligand in their structures. As FLPs can act as ambiphilic ligands, and indeed

¹⁷ J. J. Cabrera-Trujillo, I. Fernández, *Dalton Trans.* **2020**, 49, 3129-3137.

different intramolecular systems have been already used in transition metal chemistry,¹⁸ we decided to computationally explore the influence on the reactivity of transition metal complexes having FLPs as ligands. To this end, we first studied the so far poorly understood bonding situation of such complexes and then explored their reactivity in comparison with related complexes lacking these ambiphilic ligands. Thus, Au(I)-complexes featuring the FLPs **9.7–9.12** as ligands were considered (Figure 9.14). FLPs **9.7–9.9** were selected because they have been previously reported as ligands in transition metal chemistry.¹⁸ Geminal P/B FLP **9.10** was also included in our study because this particular system shows a remarkable reactivity towards the activation of small molecules.³ In addition, we also considered FLPs **9.11** and **9.12** bearing a 4π -antiaromatic borole fragment inspired by our study described previously.¹¹

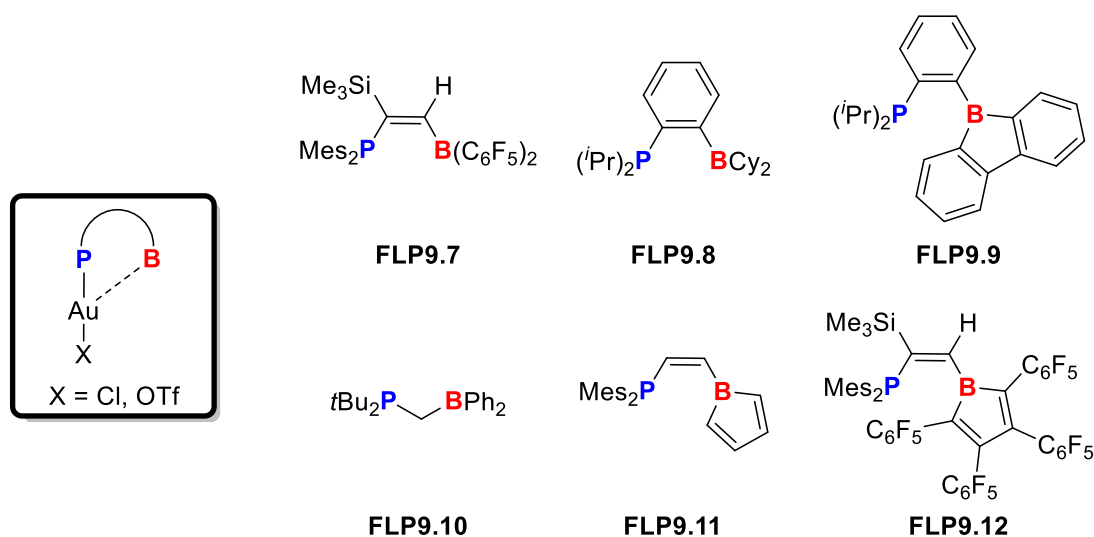


Figure 9.14. Ambiphilic FLP ligands considered in this study.

We first applied the EDA-NOCV method to quantitatively analyze the interaction between the ambiphilic FLP ligand and the transition metal fragment in FLP–AuX complexes (X = NTf₂, Cl). We also assessed the bonding situation in the parent Ph₃P–AuX complexes as a reference system lacking the B··Au interaction. The EDA-NOCV method confirmed that the interaction energy between the AuX fragment and the ligand is markedly stronger (*i.e.* more stabilizing) in the complexes bearing FLP ligands as compared to those having the

¹⁸ (a) S. Bontemps, G. Bouhadir, K. Miqueu, D. Bourissou, *J. Am. Chem. Soc.*, **2006**, *128*, 12056-12057; (b) A. Ueno, K. Watanabe, C. G. Daniliuc, G. Kehr, G. Erker, *Chem. Commun.*, **2019**, *55*, 4367-4370.

parent Ph_3P . This effect is a consequence of an enhancement of all the attractive EDA terms, namely, the electrostatic, orbital, and dispersion interactions. We found that in all the considered L–AuX complexes, the major contribution to the total interaction comes from the electrostatic term ($\Delta E_{\text{elstat}} \sim 58\text{--}65\%$), although the orbital interactions are also quite significant ($\Delta E_{\text{orb}} \sim 30\%$).

According to the NOCV method, the orbital term in the parent $\text{Ph}_3\text{P}\text{--AuNTf}_2$ system is dominated by three orbital interactions, namely the donation from the P-lone pair to the AuNTf₂ fragment (*i.e.* σ -type P \rightarrow Au dative bond) and two weak π -backdonations from the transition metal fragment to the PPh₃ ligand (Figure 9.15a). However, in the FLP–AuNTf₂ systems, there exists an additional orbital interaction that involves the donation of electron density from the transition metal fragment to the vacant p_z atomic orbital of the boron atom (denoted as ΔE_{orb2} in Figure 9.15b), which is much stronger than the corresponding π -backdonations. As a consequence, the electron density at the transition metal center is significantly reduced, thus enhancing its electrophilicity as compared to the parent $\text{Ph}_3\text{P}\text{--AuNTf}_2$ complex. Remarkably, we found that the ligands **FLP9.9**, **FLP9.11** and **FLP9.12** containing an antiaromatic, highly acidic borole moiety exhibit the strongest Au \cdots B interactions of all the considered complexes, which is reflected in significantly short Au \cdots B distances (ranging from 2.32 to 2.62 Å).

We hypothesized that the Au \cdots B interaction present in the considered complexes, which results in an increased electrophilicity of the gold center, should enhance the catalytic activity of these Au(I)-complexes. To check this, the hydroarylation reaction of phenylacetylene with mesitylene mediated by the corresponding active $[\text{Au}(\text{I})\text{--L}]^+$ catalysts was investigated (Scheme 9.4). Our DFT calculations confirmed that the rate-limiting initial nucleophilic addition reaction involving the FLP ligands does, with the exception of **FLP9.10**, proceed faster than the analogous reaction involving the parent PPh₃ ligand. Since the lower barriers were found for the processes involving the borole-containing FLPs, it becomes evident that there exists a direct correlation between the strength of the Au \cdots B interaction (which can be quantitatively estimated by means of the NOCV method) and the activity of the Au(I)-catalysts.

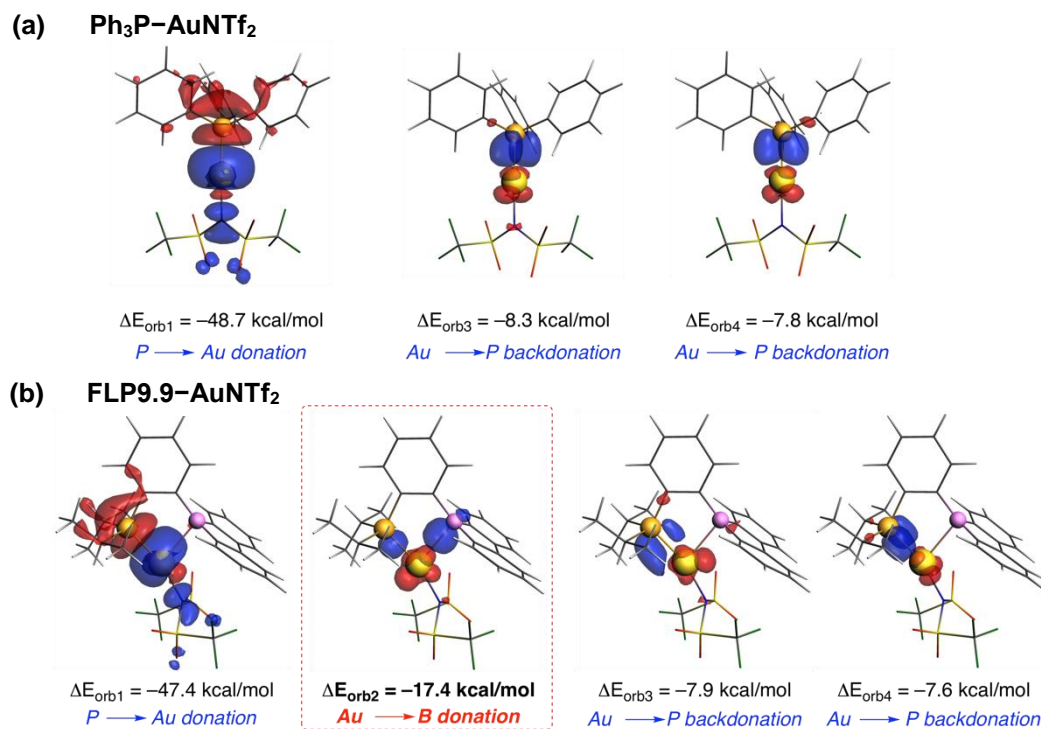
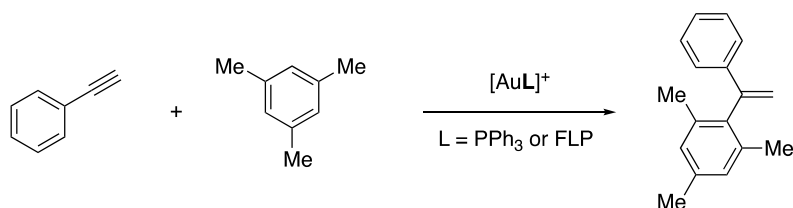


Figure 9.15. Plot of the deformation densities $\Delta\rho$ of the pairwise orbital interactions between AuNTf₂ and PPh₃ (a) or FLP **9.9** (b) ligands and associated stabilization energies $\Delta E(\rho)$. The code of the charge flow is red→blue.



Scheme 9.4. Hydroarylation reaction of phenylacetylene with mesitylene catalyzed by Au(I)-complexes considered in this study.

We applied the ASM method to quantitatively understand the reasons behind the computed higher activity of catalysts featuring a FLP as a ligand. Figure 9.16 compares the ASDs of the hydroarylation reactions involving mesitylene and the initially formed π -complexes $[\text{Ph}_3\text{P–Au–phenylacetylene}]^+$ or $[\text{FLP9.9}'\text{–Au–phenylacetylene}]^+$ (**FLP9.9'** ligand is modified **FLP9.9** where the isopropyl groups were replaced by phenyl groups to enable a direct comparison with the parent Ph₃P ligand). From the data in Figure 9.16, it is clear that the lower barrier computed for the process involving **FLP9.9'** exclusively derives from the stronger interaction between the deformed reactants along the entire reaction coordinate. Therefore, it can be concluded that the higher electrophilicity of the FLP-containing

Au(I)-complex strongly polarizes the reactive $[\text{FLP-Au-phenylacetylene}]^+$ complex facilitating the nucleophilic addition of mesitylene. This polarization is manifested in the charge of the reactive carbon atom of the $[\text{L-Au-phenylacetylene}]^+$ complex, which becomes increasingly more positive from the parent Ph_3P -system to that having the **FLP9.12** ligand, as well as in the energy of the LUMO, which becomes more a more stabilized with the increasing acceptor ability of the ligand (see Table 9.1).

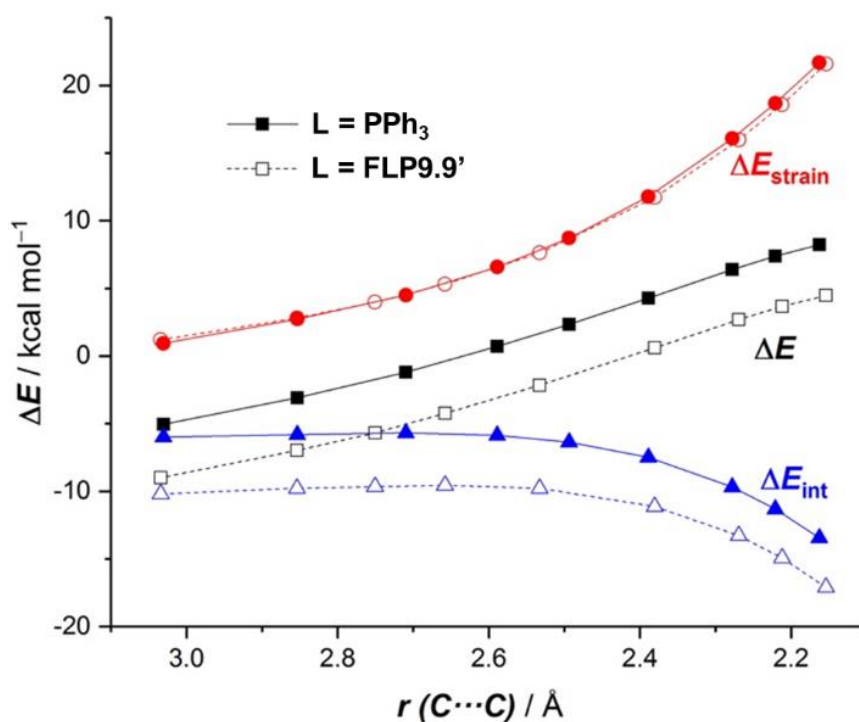
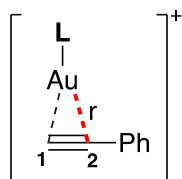


Figure 9.16. Comparative activation strain diagrams for the hydroarylation reactions involving mesitylene and the π -complexes $[\text{Ph}_3\text{P-Au-phenylacetylene}]^+$ (solid lines) or $[\text{FLP9.9'-Au-phenylacetylene}]^+$ (dashed lines) along the reaction coordinate projected onto the forming $\text{C}\cdots\text{C}$ bond.

Table 9.1. Main features (Au–C2 distance, natural charge at C2 and LUMO energy) of the initial π -complexes [L–Au–phenylacetylene]⁺ in kcal mol⁻¹.



| L | $r(\text{Au}-\text{C2})/\text{\AA}$ | $q(\text{C2})$ | $E_{\text{LUMO}}/\text{eV}$ | $r(\text{Au}\cdots\text{B})/\text{\AA}$ |
|------------------|-------------------------------------|----------------|-----------------------------|---|
| PPh ₃ | 2.348 | 0.050 | -3.66 | – |
| FLP9.7' | 2.440 | 0.062 | -3.80 | 3.079 |
| FLP9.9' | 2.397 | 0.052 | -3.73 | 2.818 |
| FLP9.10 | 2.425 | 0.058 | -3.51 | 3.457 |
| FLP9.11 | 2.467 | 0.071 | -4.07 | 2.430 |
| FLP9.12 | 2.544 | 0.093 | -4.59 | 2.371 |

Therefore, the catalytic activity of gold(I) complexes can be enhanced by increasing the acceptor ability of the boron atom of the ambiphilic FLP ligand. Highly acidic boron atoms are able to accept electron density from the transition metal, which results in (i) a significant shortening of the Au \cdots B distances and, more importantly, (ii) in an increase of the electrophilicity of the Au(I) center. As a consequence, reactions involving π -catalysis, such as the considered hydroarylation reaction, proceed faster than those reactions where the Au \cdots B interaction is not present. Once again, our calculations allowed us to predict that Au-complexes bearing a FLP ligand containing a 4π -antiaromatic borole as acid partner constitute promising candidates to achieve more efficient Au(I)-catalyzed reactions.

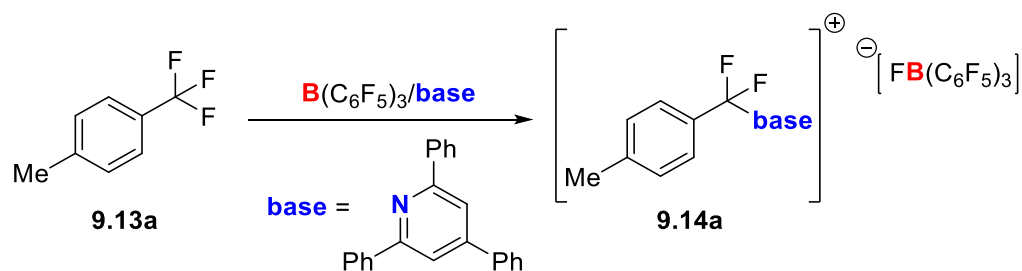
9.6. Understanding the C–F bond activation mediated by frustrated Lewis pairs: Crucial role of non-covalent interactions.¹⁹

Recently, Young and co-workers reported the selective activation of a single C–F bond in di- and trifluoride substrates mediated by FLPs.²⁰ This reaction proceeds under smooth reaction conditions, which is somewhat striking since C–F

¹⁹ J. J. Cabrera-Trujillo, I. Fernández, *Chem. Eur. J.*, **2021**, *27*, 3823-3831.

²⁰ (a) D. Mandal, R. Gupta, R. D. Young, *J. Am. Chem. Soc.*, **2018**, *140*, 10682-10686; (b) Mandal, R. Gupta, A. K. Jaiswal, R. D. Young, *J. Am. Chem. Soc.*, **2020**, *142*, 2572-2578.

bonds are the strongest single bonds between carbon and any other element across the periodic table. In addition, monoselective C–F bond activation reactions in di- and trifluoride substrates are really challenging because the resulting products are typically more reactive than the reactants. To overcome this difficulty, the Young group employed FLPs composed of neutral bases to form cationic products, which are less prone to a subsequent Lewis acid activation. Moreover, these cationic intermediates can be further functionalized by nucleophilic substitutions with a wide range of nucleophiles, therefore leading to valuable organofluoride compounds through a smooth procedure. Nevertheless, the cooperative action of the FLP antagonists in this synthetically useful reaction is essentially unknown. For this reason, we computationally explored the experimentally described C–F activation reaction involving *p*-Me-trifluoromethylbenzene (**9.13a**) mediated by the BCF/TPPY pair (TPPY=triphenylpyridine), which affords the experimentally isolated pyridinium salt **9.14a** (Scheme 9.5).^{20b}



Scheme 9.5. Monoselective C–F bond activation reaction mediated by FLPs explored in this study.

Two different reaction pathways were considered, namely (i) the non-cooperative pathway, where the Lewis acid solely activates the C–F bond and then the resulting cationic intermediate reacts with the Lewis base (*i.e.*, S_N1-type mechanism) or (ii) the cooperative path, where the C–F activation is mediated by the synergistic action of both the LA and the LB (*i.e.*, FLP mechanism). Our calculations (Figure 9.17) clearly indicate that the cooperative mechanism is favored along the entire reaction coordinate. Strikingly, this favored pathway proceeds through a hypervalent intermediate (**9.INT-13a** in Figure 9.17), whose geometry strongly resembles that of systems having pentacoordinate carbon atoms previously reported by Yamamoto, Akiba, and co-workers.²¹

²¹ (a) M. Yamashita, Y. Yamamoto, K.-Y. Akiba, D. Hashizume, F. Iwasaki, N. Takagi, S. Nagase, *J. Am. Chem. Soc.*, **2005**, *127*, 4354-4371; (b) K.-Y. Akiba, Y. Moriyama, M. Mizozoe, H. Inohara,

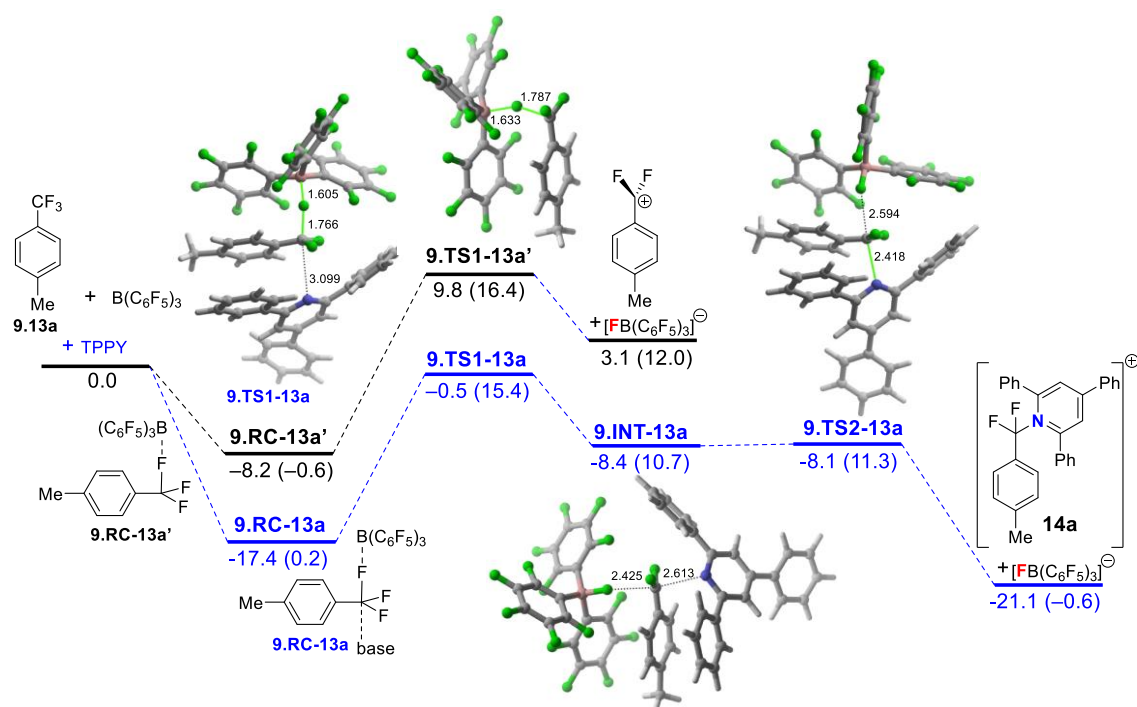


Figure 9.17. Computed reaction profile for the BCF-mediated (black lines) and BCF/TPPY-mediated (blue lines) C–F activation reaction involving the trifluoromethyl system **9.13a**. Relative energies and bond lengths are given in kcal mol⁻¹ and Å, respectively.

The ASM approach suggests that the FLP pathway (cooperative) not only exhibits a lower strain energy but also a more stabilizing interaction energy between the deformed reactants along the entire reaction coordinate. This stronger interaction does not derive from more stabilizing orbital interactions, which are actually rather similar to those in the non-cooperative pathway (Figure 9.18), but from stronger electrostatic attractions and particularly, from much more stabilizing dispersion interactions.

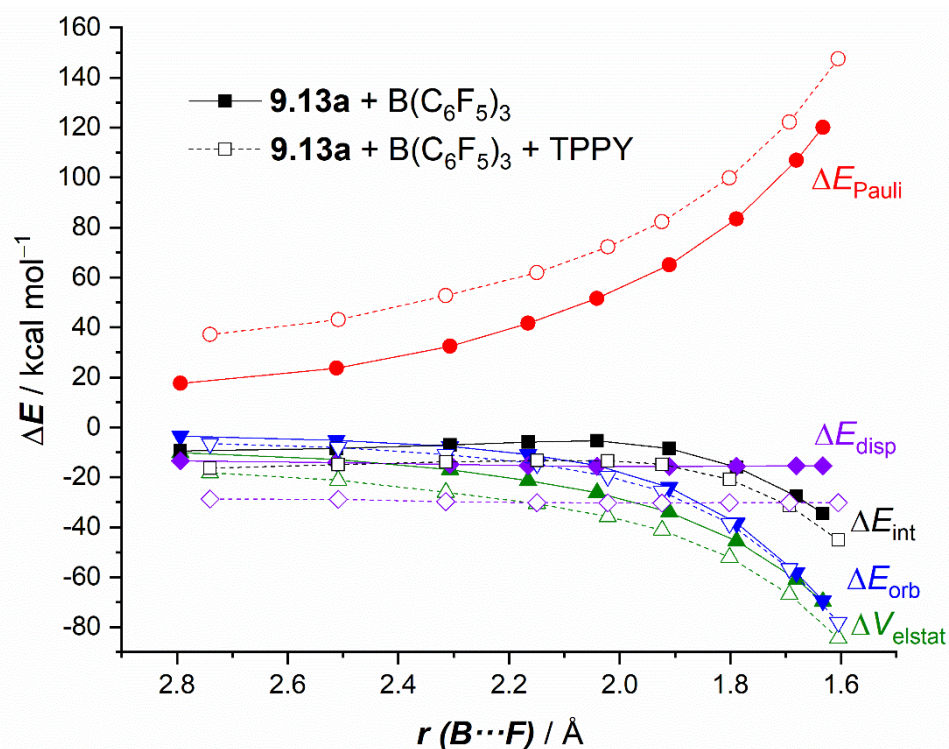


Figure 9.18. Comparative energy decomposition analyses for the non-cooperative (solid lines) and cooperative (dashed lines) C–F activation reactions involving **9.13a** along the reaction coordinate projected onto the forming B···F bond length.

We applied the NCIPLOT method²² to identify the non-covalent interactions responsible for the more stabilizing ΔE_{disp} term computed for the cooperative pathway. As depicted in Figure 9.19 for **9.TS1-13a**, there exist two significant non-covalent interactions between the TPPY base and substrate **9.13a**, namely, (i) $\pi \cdots \pi$ stacking between the aryl fragment of **9.13a** and a phenyl group of TPPY and (ii) two additional C–F··· π interactions involving the non-reactive fluorine atoms of **9.13a** and a different phenyl group of the base. The crucial role of these non-covalent interactions, which are also present in intermediate **9.INT-13a**, is further supported by comparing the analogous processes involving lutidine or NTf_2^- as bases, where these non-covalent interactions are not possible. Our results confirmed that these reactions become both kinetically and thermodynamically less favored than the reaction involving TPPY. This is in line with the experimentally reported lower conversions observed when the reactions are promoted by FLPs composed of lutidine or pyridine instead of TPPY as the base partner.^{20b}

²² E. R. Johnson, S. Keinan, P. Mori-Sánchez, J. Contreras-García, A. J. Cohen, W. Yang, *J. Am. Chem. Soc.*, **2010**, 132, 6498-6506.

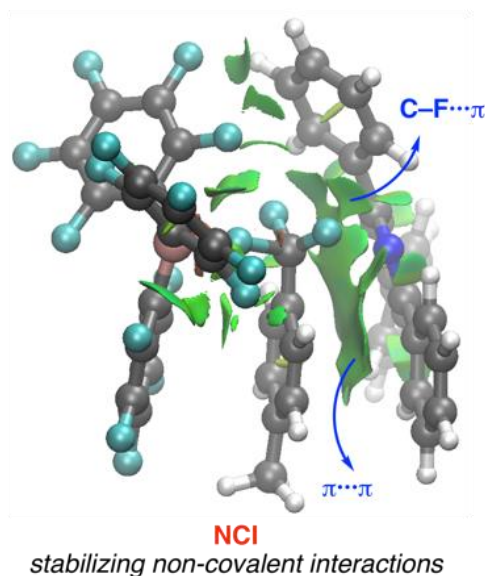


Figure 9.19. Contour plots of the reduced density gradient isosurfaces (density cutoff of 0.03 a.u.) for **9.TS1-13a**. The green surfaces indicate attractive non-covalent interactions.

The NOCV extension of the EDA method was applied to gain more quantitative insight into the cooperative action of the FLP antagonists in the C–F activation. Figure 9.20 shows that the main orbital interaction in the FLP mechanism is exclusively dominated by the $\sigma(\text{C–F}) \rightarrow p_z(\text{B})$ interaction with no measurable contribution of the Lewis base. This is exactly the same orbital interaction occurring in the absence of the Lewis base, and therefore it is not surprising that both processes exhibit nearly identical orbital interactions (see above). Once the transition state **9.TS1-13a** is reached, the Lewis base further approaches the electron-deficient carbon atom of the substrate and the $\text{LP}(\text{N}) \rightarrow p_z(\text{C})$ two-electron donation reinforces the $\sigma(\text{C–F}) \rightarrow p_z(\text{B})$ interaction (Figure 9.20). Therefore, our calculations indicate these key molecular orbital interactions do not occur in a concerted manner but at rather different stages of the transformation, which ultimately leads to the formation of a hypervalent intermediate featuring a 3-center 4-electron pentacoordinate carbon atom.

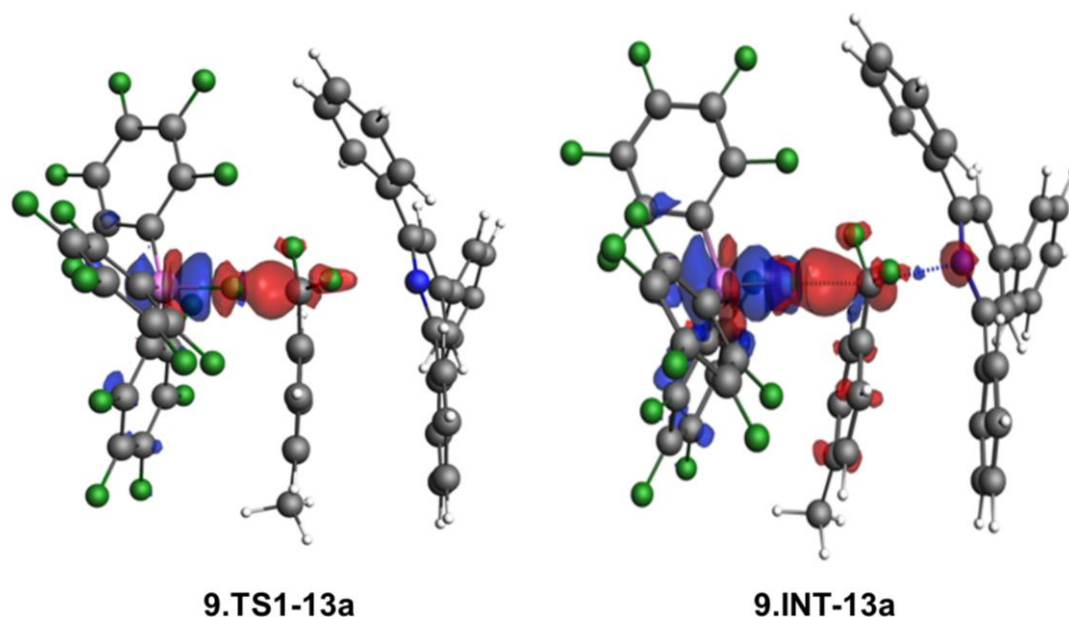


Figure 9.20. Plot of the deformation densities $\Delta\rho$ of the pairwise orbital interactions occurring in **9.TS1-13a** (left) and **9.INT-13a** (right). The color code of the charge flow is red→blue (isovalue of 0.0015 au).

According to the energy profile depicted above (Figure 9.17), the hypervalent intermediate **9.INT-13a** is highly reactive and for this reason, it could not be detected experimentally. However, we hypothesized that a further stabilization of the incipient positive charge of the trigonal carbon atom in **9.INT-13a** would increase the chances of isolating/detecting such species. To this end, we computed the analogous transformations where the methyl group placed in the *para* position of **9.13a** was replaced by good π -donor substituents (NMe_2 and OMe). Our calculations showed that both substituents not only stabilize the transition state associated with the C–F bond cleavage and the hypervalent intermediate, but also increase the barrier of the subsequent intramolecular $\text{S}_{\text{N}}2$ reaction. Therefore, we predict that systems having strong π -donor substituents in their structures constitute really promising candidates to, at least, detect under controlled experimental conditions these rare (and still elusive) hypervalent systems featuring a pentacoordinate carbon atom.

Therefore, our DFT calculations have been really helpful to unravel the hitherto unknown genuine features of the C–F activation reaction mediated by FLPs, namely (i) non-concerted cooperation between the FLP partners, (ii) the intermediacy of a hypervalent intermediate with a pentacoordinate carbon atom, and (iii) the critical role of non-covalent interactions in the transformation.

In a nutshell, we can conclude that the state-of-the-art computational methods used in this Thesis have been particularly useful to understand, in a quantitative manner, a part of the reactivity of FLPs. The insight gained in the different chapters was key towards the rational design of more active systems. We hope that the contents of this work will be useful not only to computational chemists interested in reactivity and bonding analysis but also to experimental chemists working on FLPs and main group chemistry.

X. CONCLUSIONS

“The reward of the young scientist is the emotional thrill of being the first person in the history of the world to see something or to understand something. Nothing can compare with that experience.”

Cecilia Payne-Gaposchkin

In this Ph.D. thesis, the main physical factors controlling the reactivity of selected FLPs have been computationally explored by means of state-of-the-art quantum chemical calculations. From the results obtained in this work, the following main conclusions can be drawn:

1. The activation barrier of the H_2 activation reaction mediated by $Me_2E-CH_2-E'Ph_2$ geminal FLPs steadily increases when going down in the Group 15 ($E = N < P < As < Sb$) regardless of the nature of the acidic E' (Group 13 element) atom. This reactivity trend derives from the much lower strain energy associated with the FLP having the lighter E atom, and not to the relative basicity. In contrast, the influence of the nature of the acidic atom (E') is opposite (*i.e.* the activation barrier decreases when going down in the Group 13), with the remarkable exception of $E' = Al$, which exhibits the lowest activation barrier of each series. This trend is ascribed not only to the required distortion energy but also to the stronger interaction between the deformed reactants for the processes involving the heavier E' atom. The particularly high reactivity of Al-based FLPs finds its origin in a rather low Pauli repulsion together with highly stabilizing $LP(E) \rightarrow \sigma^*(H_2)$ and $\sigma(H_2) \rightarrow p\pi(Al)$ orbital interactions. Consequently, the geminal N/Al-based FLP is identified as the most active system for the H_2 activation reaction. In addition, the activation barrier can be further reduced by replacing the phenyl groups attached to the acidic atom by strong electron-withdrawing groups such as C_6F_5 or $3,5-(CF_3)_2C_6H_3$.

2. The CO_2 and phenyl isocyanate activation reactions mediated by $(F_5C_2)_3E-CH_2-P(tBu)_2$ geminal FLPs ($E = Si, Ge, Sn$) becomes kinetically more favorable when going down in the Group 14 ($\Delta E^\ddagger = Si > Ge > Sn$). This reactivity trend mainly derives from the stronger interaction between the deformed reactants along the entire reaction coordinate computed for the processes involving the heavier systems. In addition, these reactions also benefit from a lower strain energy to deform the reactants. The more stabilizing interaction energy computed for the process involving the Sn-based FLP, as compared to that involving its lighter counterpart Si-FLP, is the result of the combination of more stabilizing electrostatic and orbital (mainly the $LP(P) \rightarrow \pi^*(C=O)$ interaction) attractions between the deformed reactants, particularly at the transition state region.

3. The role of aromaticity as a key factor enhancing the reactivity of geminal FLPs has been confirmed. It is predicted that geminal FLPs having a 4π -antiaromatic borole fragment as the Lewis acid partner constitute really promising candidates to achieve facile small molecule activations. These species exhibit a remarkable reactivity enhancement compared to more traditional FLPs as a consequence of the loss of antiaromaticity (or gain in aromaticity) in the borole moiety as the small-molecule activation reaction progresses.

4. Carbon(0)-species, also known as carbenes, can efficiently act as Lewis basic partners in FLPs. However, the corresponding systems exhibit significant differences in their mode of action when compared with more traditional FLPs having phosphines as bases. In this regard, the H_2 activation reaction mediated by C(0)-carbodiphosphorane/BCF-based FLPs proceed with a stronger interaction between the deformed reactants as a consequence of more stabilizing electrostatic and orbital interactions along the entire reaction coordinate. The stronger orbital interactions computed for the process involving carbenes-based FLPs originates from their highly σ -donor ability. This, at variance with phosphines, provokes that the key $LP(\text{carbene}) \rightarrow \sigma^*(H-H)$ orbital interaction is present along the entire process reinforcing the $\sigma(H-H) \rightarrow p_z(B)$ interaction. Furthermore, carbenes having NHCs in their structures (also known as carbodicarbenes) are more reactive than carbodiphosphoranes. Remarkably, the activation barrier of the heterolytic cleavage of H_2 steadily decreases by moving down in the Group 14 (i.e. from carbenes to heavier ylidenes), as a consequence of a less destabilizing Pauli repulsion and more stabilizing orbital interactions. Our calculations therefore predict that heavier ylidenes are really promising candidates to achieve facile H_2 activation reactions.

5. P/B FLPs as ambiphilic ligands in Au(I)-complexes are able to establish relatively strong $Au \cdots B$ interactions, whose strength is directly related to the acidity of the boron moiety. This interaction results from the donation of electron density from the transition metal atom to the vacant p_z atomic orbital of the boron atom, therefore enhancing the electrophilicity of the gold moiety as compared to the Ph_3P-AuX system. This effect enhances the reactivity of Au(I)-complexes in π -catalysis. For instance, in the particular gold(I)-catalyzed hydroarylation reaction considered in our study, the $Au \cdots B$ interaction makes the corresponding π -complex, initially formed upon coordination of the triple bond of

phenylacetylene to the active $[\text{Au-FLP}]^+$ catalyst, much more prone to undergo the key nucleophilic addition reaction, which is ultimately reflected in a faster reaction as compared to the analogous process involving the parent $[\text{Au-PPh}_3]^+$ catalyst. In line with our previous results (see above), catalysts having FLPs with a borole fragment as an acidic partner exhibit markedly strong $\text{Au}\cdots\text{B}$ interactions, which should result in a significant enhancement of their catalytic activity.

6. The activation of a single C–F bond in di- and trifluoromethyl groups mediated by FLPs exhibits a peculiar cooperative action between the FLP partners, which is markedly different from related FLP-mediated activation reactions. The process proceeds stepwise where the C–F activation occurs first followed by a $\text{S}_{\text{N}}2$ -like reaction involving the base. Therefore, only once the C–F bond is significantly activated by the Lewis acid, the $\text{LP}(\text{base})\rightarrow\text{p}_z(\text{C})$ orbital interaction takes place. Despite that, the Lewis base is not a mere spectator during the initial bond activation but also significantly contributes to the stabilization of the entire reaction coordinate by establishing non-covalent interactions ($\pi\cdots\pi$ and $\text{C-F}\cdots\pi$ interactions) with the substrate. As a result, the transformation involves the formation of a highly unusual hypervalent intermediate featuring a 3-center 4-electron pentacoordinate carbon atom, which might be isolated/detected through the stabilization of the positive charge on the pentacoordinate carbon by (i) π -donor substituents in the aryl group of the substrate and/or (ii) reducing the number of fluorine atoms attached to the reactive carbon atom.

XI. SUMMARY

*“Research is formalized curiosity. It is
poking and prying with a purpose.”*

Zora Neale Hurston

Understanding the reactivity of Frustrated Lewis Pairs

Frustrated Lewis Pairs (FLPs) have become highly versatile systems to carry out a wide range of different chemical transformations. Some outstanding examples include the activation of small molecules such as H₂, CO, CO₂, SO₂, N₂O, etc., transfer hydrogenations, hydroborations, hydroarylations, aminations, and even polymerization reactions. Despite that, in most cases the physical factors governing the reactivity of these species are poorly understood, which considerably hampers the rational design of new and more efficient FLPs.

The primary aim of this doctoral thesis is the rationalization of the reactivity of FLPs using state-of-the-art quantum-mechanical calculations. To this end, we have applied a methodology based on the combination of the so-called *Activation Strain Model* (ASM) of reactivity and the *Energy Decomposition Analysis* (EDA) methods. This approach is nowadays considered as a powerful tool to not only quantitatively understand those factors controlling the reactivity of different chemical systems but also to design new and more efficient transformations.

Specifically, we explored the influence of the nature of the acid/base pairs in geminal (Me₂E-CH₂-E'Ph₂) FLPs on the dihydrogen activation reaction. Two reactivity trends have been identified, namely (i) the activation barrier steadily increases when going down in the Group 15 (E = N < P < As < Sb) regardless of the nature of the acidic E' atom and (ii) the activation barrier decreases when going down in the Group 13, with the remarkable exception of E' = Al, which exhibits the lowest activation barrier of each series. Consequently, the geminal N/Al-based FLP has been identified as the most active system for the activation of H₂. In addition, we have confirmed that the activation barriers can be further reduced by replacing the phenyl groups attached to the acidic atom by highly electron-withdrawing groups such as C₆F₅ or 3,5-(CF₃)₂C₆H₃.

Closely related to the above study, we have also explored the influence of the nature of the Group 14 atoms (E = Si, Ge, Sn) on the reactivity of geminal (F₅C₂)₃E-CH₂-P(*t*Bu)₂ FLPs. In this case, we selected the experimentally described activation reactions of CO₂ and phenyl isocyanate. It is found that the reactivity of these species becomes kinetically more favorable when going down in the Group 14 (Si < Ge < Sn). According to the ASM/EDA methodology, this

reactivity trend mainly derives from the stronger interaction between the reactants computed for the processes involving the heavier systems.

Aiming at designing highly active FLPs, we have merged the concepts of FLP and aromaticity for the first time. We found that geminal FLPs featuring a 4π -antiaromatic borole fragment as the acid partner exhibit a remarkable reactivity enhancement compared to more traditional FLPs. This can be ascribed to the progressive loss of antiaromaticity (gain of aromaticity) in the borole moiety as the small-molecule activation reaction progresses. Our study therefore establishes a pioneering concept in FLP chemistry: the role of aromaticity as a key factor enhancing the reactivity, which might be useful to guide future experimental developments.

Besides intramolecular FLPs, we have also explored the reactivity of intermolecular systems. Namely, we studied the role of carbon(0)-species (CL_2 , L = phosphines or carbenes) and its heavier analogues known as “ylidones” (EL_2 , E = Si, Ge, Sn, Pb) as basic functionalities in FLP chemistry. We have found that the H_2 activation reaction mediated by a carbodiphosphorane/ $B(C_6F_5)_3$ FLP proceeds with a stronger interaction between the deformed reactants compared to more traditional intermolecular FLPs composed of phosphines. This is mainly ascribed to the stronger orbital interactions between the reagents as a consequence of the higher σ -donor ability of carbenes compared to phosphines. In addition, our calculations predict that heavier Group 14 ylidones are even more active than carbenes to promote the heterolytic splitting of H_2 .

The role of FLPs as ambiphilic ligands in gold(I)-catalyzed reactions has been also considered in this work. The EDA method revealed that P/B-based FLP ligands in gold(I)-complexes establish a relatively strong $Au\cdots B$ interaction, which is directly related to the acidity of the boron fragment. As a consequence, the electron density at the gold atom is significantly reduced, thus enhancing its electrophilicity compared to the more traditional gold(I)-complexes featuring a Ph_3P ligand. The impact of such electrophilicity enhancement on the catalytic activity of gold(I)-complexes has been further evaluated by modeling a representative π -catalysis reaction, namely, the hydroarylation reaction of phenylacetylene with mesitylene. In line with our previous results, catalysts having

FLPs with a borole fragment as the acidic partner exhibit markedly strong Au...B interactions, which is translated in an enhanced catalytic activity.

Finally, we computationally studied the so far poorly understood cooperative action of the FLP antagonists in the activation of a single C–F bond activation in polyfluoride substrates. Our calculations revealed the occurrence of crucial non-covalent interactions established between the Lewis base and the substrate which leads to the formation of an unusual hypervalent intermediate featuring a 3-center 4-electron pentacoordinate carbon atom. Although this is a fleeting intermediate, we predict that its isolation/detection might be feasible when using substrates having electron-donor groups in their structures or a lower number of fluorine atoms attached to the reactive carbon atom.

We do believe that the insight derived from the present doctoral thesis has contributed significantly to our current understanding of the reactivity of FLPs. In our opinion, the results presented herein are expected to promote further theoretical and experimental studies in the growing and prosperous chemistry of these fascinating systems.

XII. RESUMEN

“Dila -dijo don Quijote- y sé breve en tus razonamientos, que ninguno hay gustoso si es largo.”

Miguel de Cervantes

Entendiendo la reactividad de Pares de Lewis Frustrados

Los pares de Lewis frustrados (FLPs, de sus siglas en inglés) se han convertido en sistemas muy versátiles para llevar a cabo una amplia gama de transformaciones químicas. Entre ellas, podemos destacar la activación de pequeñas moléculas como H_2 , CO , CO_2 , SO_2 , N_2O , etc., reacciones de hidrogenación, hidrobtoración, hidroarilación, aminación, e incluso reacciones de polimerización. A pesar de ello, en la mayoría de los casos los factores físicos que gobiernan la reactividad de estas especies no se conocen en detalle, lo que dificulta considerablemente el diseño racional de nuevos y más eficientes FLPs.

El objetivo principal de esta tesis doctoral es la racionalización de la reactividad de los FLPs utilizando cálculos computacionales. Para ello, hemos aplicado una metodología basada en la combinación de los métodos denominados *Activation Strain Model (ASM) of reactivity* y *Energy Decomposition Analysis (EDA)*. Dicha aproximación se considera hoy en día una herramienta muy útil no sólo para comprender cuantitativamente los factores que controlan la reactividad de diferentes sistemas químicos, sino también para el diseño de transformaciones nuevas y más eficientes.

De manera más específica, hemos explorado la influencia de la naturaleza de los pares ácido/base en FLPs geminales ($Me_2E-CH_2-E'Ph_2$) en la reacción de activación de dihidrógeno. Se han identificado dos tendencias de reactividad, a saber: (i) la barrera de activación aumenta al descender en el Grupo 15 ($E = N < P < As < Sb$) independientemente de la naturaleza del átomo ácido E' y (ii) la barrera de activación disminuye al descender en el Grupo 13, con la notable excepción de $E' = Al$, que exhibe la barrera de activación más baja de cada serie. En consecuencia, hemos identificado al FLP geminal formado por N/Al como el sistema más activo para la activación de H_2 . Además, las barreras de activación se pueden reducir aún más si los grupos fenilo unidos al átomo ácido son reemplazados por grupos altamente aceptores de electrones como C_6F_5 ó $3,5-(CF_3)_2C_6H_3$.

Estrechamente relacionado con el estudio anterior, también hemos explorado la influencia de la naturaleza de los átomos del Grupo 14 ($E = Si, Ge, Sn$) en la reactividad de los FLPs geminales ($(F_3C)_3E-CH_2-P(tBu)_2$). En este caso, se seleccionaron las reacciones de activación de CO_2 e isocianato de fenilo, descritas

experimentalmente. Se ha descubierto que la reactividad de estas especies se vuelve cinéticamente más favorable al descender en el Grupo 14 (Si < Ge < Sn). Según la metodología ASM/EDA, esta tendencia de reactividad deriva principalmente de una mayor interacción entre los reactivos a lo largo de toda la coordenada de reacción para los procesos que involucran los sistemas más pesados.

Con el objetivo de diseñar FLPs altamente activos, hemos fusionado por primera vez los conceptos de FLP y aromaticidad. Así, hemos encontrado que aquellos FLPs geminales que presentan un fragmento de borol 4π -antiaromático como ácido de Lewis exhiben una mayor reactividad que FLPs más tradicionales. Esto se debe principalmente a la pérdida progresiva de antiaromaticidad (o ganancia de aromaticidad) en el borol a medida que avanza la reacción de activación. Por tanto, nuestro estudio confirma el papel de la aromaticidad como factor clave para mejorar la reactividad, lo que podría ser de gran utilidad para futuros estudios experimentales.

Además de los FLPs intramoleculares, también hemos explorado la reactividad de sistemas intermoleculares. Concretamente, hemos estudiado el papel de especies de carbono(0) (CL_2 , L = fosfinas o carbenos) y sus análogos más pesados (EL_2 , E = Si, Ge, Sn, Pb) como funcionalidades básicas en la química de FLPs. Hemos descubierto que la reacción de activación de H_2 mediada por el sistema carbodifosforano/ $B(C_6F_5)_3$ ocurre con una mayor interacción entre los reactivos que otros FLPs intermoleculares más tradicionales compuestos por fosfinas. Esto se debe principalmente a unas interacciones orbitales entre los reactivos más estabilizantes como consecuencia de la mayor capacidad de donación σ de $C(0)L_2$ en comparación con las fosfinas. Además, nuestros cálculos predicen que los correspondientes sistemas con átomos del Grupo 14 más pesados que el carbono son incluso más activos que aquellos basados en CL_2 para promover la ruptura heterolítica de H_2 .

En este trabajo también se ha considerado el papel de los FLPs como ligandos ambifílicos en reacciones catalizadas por Au(I). El método EDA reveló que en aquellos complejos con ligandos FLP basados en P/B, se establece una interacción $Au\cdots B$ relativamente fuerte, que está directamente relacionada con la acidez del fragmento de boro. Como resultado, la densidad electrónica en el átomo de oro se reduce significativamente, aumentando así su electrofilia en comparación con

complejos de Au(I) más tradicionales que contienen un ligando Ph₃P. Adicionalmente, se ha evaluado el impacto de dicho aumento de la electrofilia en la actividad catalítica de dichos complejos en la reacción de hidroarilación de fenilacetileno con mesitileno. En consonancia con nuestros resultados anteriores, aquellos catalizadores con FLPs que tienen un fragmento borol como ácido de Lewis exhiben una interacción Au...B considerablemente fuerte, lo que se traduce en una elevada actividad catalítica.

Por último, hemos estudiado computacionalmente la acción cooperativa de las funcionalidades ácido/base en la activación selectiva de un único enlace C–F en sustratos polifluorados mediada por FLPs. Nuestros cálculos revelaron la presencia de interacciones no covalentes entre la base de Lewis y el sustrato que conducen a la formación de un intermedio hipervalente que contiene un átomo de carbono pentacoordinado. Aunque este intermedio es altamente reactivo, predecimos que su aislamiento/detección podría ser factible si se utilizan sustratos con grupos dadores de electrones en sus estructuras o con un número menor de átomos de flúor unidos al átomo de carbono reactivo.

Creemos firmemente que los resultados derivados de la presente tesis doctoral han contribuido significativamente a la comprensión actual de la reactividad de los FLPs. En nuestra opinión, es muy probable que dichos resultados motiven nuevos estudios tanto teóricos como experimentales sobre la rica y creciente reactividad de estos fascinantes sistemas.

XIII. ANNEXES

Frustrated Lewis Pairs

Influence of the Lewis Acid/Base Pairs on the Reactivity of Geminal E-CH₂-E' Frustrated Lewis Pairs**Jorge Juan Cabrera-Trujillo and Israel Fernández*^[a]

Abstract: The influence of the nature of the acid/base pairs on the reactivity of geminal frustrated Lewis pairs (FLPs) (Me₂E-CH₂-E'Ph₂) has been computationally explored within the density functional theory framework. To this end, the dihydrogen-activation reaction, one of the most representative processes in the chemistry of FLPs, has been selected. It is found that the activation barrier of this transformation as well as the geometry of the corresponding transition states strongly depend on the nature of the E/E' atoms (E = Group 15 element, E' = Group 13 element) in the sense that

lower barriers are associated with earlier transition states. Our calculations identify the geminal N/Al FLP as the most active system for the activation of dihydrogen. Moreover, the barrier height can be further reduced by replacing the phenyl group attached to the acidic atom by C₆F₅ or 3,5-(CF₃)₂C₆H₃ (FxyI) groups. The physical factors controlling the computed reactivity trends are quantitatively described in detail by means of the activation strain model of reactivity combined with the energy decomposition analysis method.

Introduction

The chemistry of frustrated Lewis pairs (FLPs) has arguably experienced a tremendous development since the seminal report by Stephan and co-workers in 2006.^[1] These species are characterized by having coordinatively unsaturated Lewis acidic and basic atoms in either single molecules or bimolecular systems where steric hindrance hampers the formation of a classical donor–acceptor dative bond between them. Owing to this peculiar bonding situation, FLPs exhibit a unique reactivity, which allows, among other processes, the activation of different species (e.g., H₂, CO, CO₂, N₂O, etc.) in stoichiometric and catalytic reactions.^[2]

Among the different FLPs described so far, geminal FLPs, that is, systems where the Lewis acidic and basic atoms are separated by a carbon atom, should be especially highlighted (Scheme 1). Indeed, geminal P/Al^[3] and P/B^[4,5] Lewis pairs have attracted considerable interest quite recently due to their remarkable activity in the activation of small molecules. In addition, other geminal FLPs based on N/B,^[6] N/Al,^[7] P/X^[8] (X = Group 14 element), and even P/Ga^[9] have been prepared in order to tune the Lewis acidity/basicity of the FLP antagonists and consequently, to modify the activity of the system. Despite

that, the influence of the nature of the Lewis pairs on the reactivity of the FLP is so far not fully understood, which is of crucial importance for further development of FLPs.

To gain a deeper, quantitative insight into the relationship between the nature of the active sites of geminal FLPs and their reactivity, we explore herein the dihydrogen activation, one of the most important and representative reactions in FLP chemistry,^[2,10] mediated by geminal Me₂E-CH₂-E'Ph₂ (E = Group 15 element, E' = Group 13 element) FLPs (Scheme 2). In these systems, which are strongly related to the *t*Bu₂P-CH₂-BPh₂ FLP experimentally described by Lammertsma and co-workers,^[5a] both the acidic and basic atoms will be modified to identify the E/E' combination leading to the most active geminal FLP (i.e., which exhibits the lowest activation barrier for the considered dihydrogen activation).

The computed reactivity trends will be analyzed in detail by means of the activation strain model (ASM)^[11] of reactivity in combination with the energy decomposition analysis (EDA) method.^[12] This methodology has been particularly helpful very recently to understand the factors controlling both the H₂ activation and the subsequent dihydrogen release into multiple bonds mediated by geminal B/N FLPs.^[13,14] Indeed, by means of this state-of-the-art approach we have proposed an orbital-controlled mechanism, complementary to the traditional mechanisms suggested by Pápai et al.^[15] and Grimme et al.,^[16] where the degree of charge-transfer cooperativity between the key donor–acceptor orbital interactions, that is, LP(N)→σ*(H₂) and σ(H₂)→p_π(B), along the reaction coordinate constitutes a suitable indicator of the reaction barrier.^[13] In addition, a cooperative concerted, yet asynchronous, double hydrogen transfer mechanism was also found for the subsequent hydrogenation of multiple bonds.^[14]

[a] J. J. Cabrera-Trujillo, Prof. Dr. I. Fernández
Departamento de Química Orgánica I and
Centro de Innovación en Química Avanzada (ORFEO-CINQA)
Facultad de Ciencias Químicas
Universidad Complutense de Madrid, 28040-Madrid (Spain)
E-mail: israel@quim.ucm.es

[**] E = Group 15 element; E' = Group 13 element.

Supporting information and the ORCID identification number(s) for the author(s) of this article can be found under:
<https://doi.org/10.1002/chem.201804198>.

Understanding the Reactivity of Neutral Geminal Group 14 Element/Phosphorus Frustrated Lewis Pairs

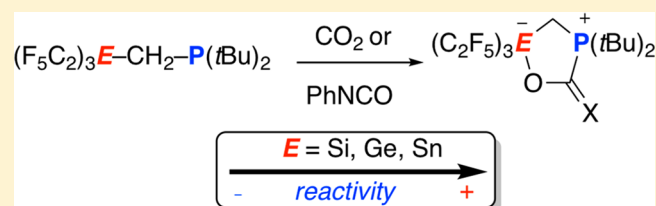
Published as part of *The Journal of Physical Chemistry virtual special issue "Paul Geerlings Festschrift"*.

Jorge Juan Cabrera-Trujillo and Israel Fernández*[✉]

Departamento de Química Orgánica I and Centro de Innovación en Química Avanzada (ORFEO–CINQA), Facultad de Ciencias Químicas, Universidad Complutense de Madrid, 28040-Madrid, Spain

Supporting Information

ABSTRACT: The influence of the nature of the group 14 elements (E = Si, Ge, Sn) on the reactivity of $(F_5C_2)_3E-CH_2-P(tBu)_2$ geminal frustrated Lewis pairs (FLPs) has been computationally explored by means of density functional theory calculations. To this end, the experimentally described activation reactions of CO_2 and phenyl isocyanate have been investigated and compared to the analogous processes involving the corresponding B/P geminal FLP. It is found that the reactivity of these species is kinetically enhanced when going down the group 14 (Si < Ge < Sn). This trend of reactivity is quantitatively analyzed in detail by means of the activation strain model of reactivity in combination with the energy decomposition analysis method, which identify the interaction energy between the deformed reactants as the main factor controlling the reactivity of these group 14 containing geminal FLPs.



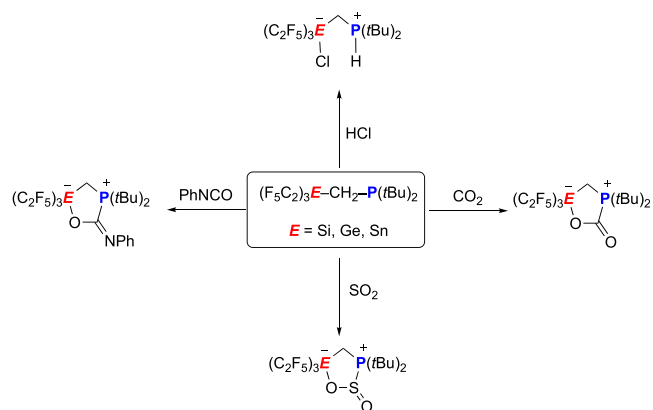
INTRODUCTION

Since the seminal report by Stephan and co-workers in 2006 of a metal-free molecule that was able to reversibly activate dihydrogen,¹ the chemistry of the so-called frustrated Lewis pairs (FLPs) has experienced an impressive development.^{2–7} These species are typically composed of a simple combination of a sterically encumbered Lewis acid and Lewis base, where the severe steric demands hamper the formation of a classical donor–acceptor bond. This particular bonding situation leads to a unique reactivity which allows the relatively facile activation of small molecules (such as H_2 , CO , CO_2 , N_2O , SO_2 , ...) or the metal-free hydrogenation of polar multiple bonds, among other processes.²

Aiming at enhancing the activity of these systems, a good number of different FLPs have been prepared. Among them, geminal FLPs, i.e., systems where the donor/acceptor atoms are separated by a carbon atom, should be especially highlighted because their preorganized molecular structure results in a significant enhancement of the reactivity as compared to their corresponding intermolecular FLP counterparts.^{8–14} Although most of these geminal FLPs are typically based on the combination of B/N and B/P pairs, other systems including heavier group 13 elements^{15,16} or transition metal fragments^{17–21} in their structures have been prepared to tune the Lewis acidity/basicity of the FLP antagonists. In this sense, Mitzel and co-workers have recently prepared a series of group 14 element containing neutral geminal FLPs, i.e., $(F_5C_2)_3E-CH_2-P(tBu)_2$, E = Si,²² Ge,²³ Sn,²⁴ which have been proven to readily activate small molecules such as CO_2 , SO_2 , CS_2 , HCl ,

or phenyl isocyanate (Scheme 1), therefore resembling the reactivity of more traditional B/P FLPs.

Scheme 1. Reactivity of Group 14 Element Containing Geminal FLPs Described by Mitzel and Co-workers^{22–24}



Despite this evident similarity, very little is known about the actual influence of the nature of the group 14 element on the reactivity of these novel geminal FLPs. For this reason, herein we decided to computationally explore the reactivity of these species to gain detailed quantitative insight into the impact of the nature of the group 14 element on the reactivity. To this

Received: September 9, 2019

Revised: October 14, 2019

Published: November 5, 2019



Aromaticity can enhance the reactivity of P-donor/borole frustrated Lewis pairs†

Jorge Juan Cabrera-Trujillo  and Israel Fernández *

Cite this: *Chem. Commun.*, 2019, 55, 675

Received 10th December 2018,
Accepted 12th December 2018

DOI: 10.1039/c8cc09777a

rsc.li/chemcomm

Geminal frustrated Lewis pairs (FLPs) having a borole fragment as the Lewis acid partner constitute really promising candidates to achieve facile small molecule activation reactions. The predicted enhanced reactivity of these species, as compared to more traditional FLPs, finds its origin in the loss of the antiaromatic character of the borole moiety along the reaction coordinate.

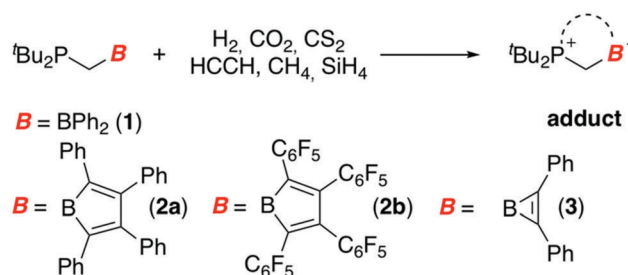
Frustrated Lewis pairs (FLPs) are species typically composed of a pair of a sterically encumbered Lewis acid and Lewis base, which prevents the formation of a classical donor–acceptor bond between both centers.¹ Due to this particular bonding situation, these compounds exhibit a unique reactivity as a result of the cooperative action of the FLP antagonists. Thus, FLPs have emerged as potential metal-free catalysts able to, among other processes, activate small molecules (H₂, CO, CO₂, SO₂, N₂O, *etc.*).¹ Owing to this rich reactivity, in most cases restricted to transition metals, the chemistry of FLPs has attracted much attention since the seminal report by Stephan and co-workers in 2006.²

Much progress has been made, particularly in recent years, to produce more active systems. Among them, intramolecular FLPs (where the Lewis pairs are part of the same molecule)³ and systems having transition-metal fragments in their structures⁴ should be specially highlighted. Despite that, the vast majority of FLPs are still based on the combination of B/N or B/P pairs, with the boron center typically attached to electron-withdrawing substituents. Aiming at developing more active FLPs, herein we shall introduce a novel concept in FLP chemistry: aromaticity as the key factor enhancing the reactivity of FLPs.

To this end, we focused on a particular FLP, the geminal ^tBu₂P–CH₂–BPh₂ (**1**) system, synthesized by Slootweg, Lammertsma and co-workers,⁵ whose preorganized structure results in a

remarkable reactivity for small molecule activations without the need for strongly electron-withdrawing substituents attached to the boron center. We computationally⁶ replaced the BPh₂ moiety by the sterically hindered tetraphenyl-borole fragment (**2a**, Scheme 1), whose antiaromatic nature was confirmed previously by Braunschweig, some of us and co-workers.⁷ Our initial hypothesis follows: the gain of aromaticity in the borole moiety during the activation of a small molecule (H₂, CO₂, CS₂, HC≡CH, SiH₄ and CH₄ in our calculations, Scheme 1) should result in a gain of stability in both the corresponding transition state, therefore leading to a lower barrier transformation, and in the final zwitterionic adduct, therefore making the process thermodynamically more favourable.

In agreement with previous results involving the dihydrogen activation mediated by the parent FLP **1**⁵ and related geminal systems,⁸ our calculations confirm that the heterolytic H₂-splitting occurs in a concerted manner *via* a five-membered transition state (**TS-1**) and through the formation of an initial van der Waals reactant complex (**RC-1**) which lies *ca.* 2 kcal mol⁻¹ above the separate reactants (this energy difference becomes higher when including thermal free energy corrections, see Fig. 1). Although the computed reaction profile for the process involving the 4π-electrons borole-containing FLP **2a** is rather similar, the dihydrogen activation becomes both kinetically and thermodynamically (ΔΔ*E*[‡] = 5.5 kcal mol⁻¹ and ΔΔ*E*_R = 12.5 kcal mol⁻¹, respect to the separated reactants) more favoured than the



Scheme 1 FLP-mediated small molecule activation reactions considered herein.

Departamento de Química Orgánica I and Centro de Innovación en Química Avanzada (ORFEO-CINQA), Facultad de Ciencias Químicas, Universidad Complutense de Madrid, 28040-Madrid, Spain. E-mail: Israel@quim.ucm.es

† Electronic supplementary information (ESI) available: Computational details, Fig. S1 and S2, and Cartesian coordinates for all species discussed in the text. See DOI: 10.1039/c8cc09777a

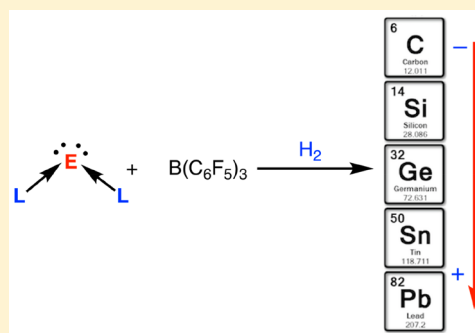
Carbones and Heavier Ylidones (EL₂) in Frustrated Lewis Pair Chemistry: Influence of the Nature of EL₂ on Dihydrogen Activation

Jorge Juan Cabrera-Trujillo and Israel Fernández*[✉]

Departamento de Química Orgánica I and Centro de Innovación en Química Avanzada, Facultad de Ciencias Químicas, Universidad Complutense de Madrid, Madrid 28040, Spain

Supporting Information

ABSTRACT: The role of carbones (CL₂; L = phosphines vs carbenes) as Lewis bases in dihydrogen (H₂) activation reactions in the presence of the Lewis acid B(C₆F₅)₃ has been computationally explored by means of density functional theory calculations. To this end, the interaction between H₂ and the [carbone⋯B(C₆F₅)₃] pair along the reaction coordinate has been quantitatively analyzed in detail and compared to the parent [^tBu₃P⋯B(C₆F₅)₃] frustrated Lewis pair. In addition, the influence on the reactivity of both the nature of the central E atom and the surrounding ligands in ylidones (EL₂) has also been considered. It is found that the activation barrier of the H₂ activation reaction as well as the geometry of the corresponding transition states strongly depends on the nature of both E and L in the sense that lower barriers are systematically associated with earlier transition states. Our calculations identify heavier EL₂ as the most active systems to achieve facile H₂ activation reactions.

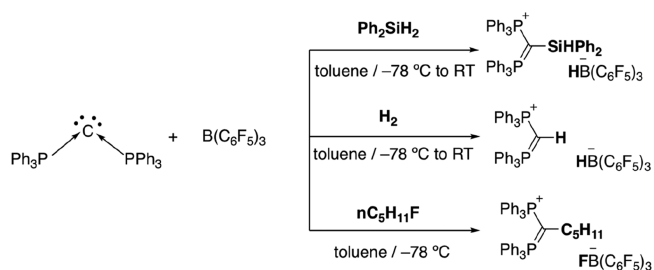


INTRODUCTION

The term “carbone” was coined by Frenking and co-workers to refer to a family of divalent carbon(0) compounds CL₂ whose central carbon atom retains all four valence electrons as two lone pairs and where bonding to the adjacent σ -donor ligands (L) occurs mainly through donor–acceptor interactions (i.e., L \rightarrow C⁰ \leftarrow L).^{1,2} Since the report by Ramirez and co-workers in 1961 on the first and most representative member of this family of compounds, the parent hexaphenylcarbodiphosphorane [C(PPh₃)₂],³ a good number of carbon(0) species have been prepared and fully characterized.⁴ In addition, this family of compounds has also been expanded to systems having heavier group 14 elements in their structures [also known as ylidones (EL₂)].^{2a,5} Because of their peculiar bonding situation, these species not only are potential donor ligands in main-group compounds or transition-metal complexes but also exhibit a rich and varied reactivity.^{2,4–6} For instance, carbodicarbenes [carbones where L = carbene or N-heterocyclic carbene (NHC)] have attracted considerable attention because of their captodative behavior in catalysis.⁷

In this regard, Alcarazo and co-workers recently found that the parent carbone, C(PPh₃)₂, can be used as a carbon-based Lewis base in combination with the Lewis acid B(C₆F₅)₃ to form a highly active frustrated Lewis pair (FLP) able to activate not only H–H bonds but also C–O, C–H, Si–H, and C–F bonds (Scheme 1).⁸ This behavior therefore strongly resembles that found for typical FLPs based mainly on P-based Lewis bases [for instance, ^tBu₃P/B(C₆F₅)₃ or Mes₃P/B(C₆F₅)₃].⁹ Despite this evident similarity, very little is known about the actual role of carbone in the bond activation

Scheme 1. Activation Reactions Mediated by Hexaphenylcarbodiphosphorane and B(C₆F₅)₃ Described by Alcarazo and Co-workers⁸



process compared to analogous transformations involving either intermolecular or intramolecular P/B FLP systems.¹⁰

Recently, we combined state-of-the-art computational methods known as the activation strain model (ASM) of reactivity¹¹ and energy decomposition analysis (EDA)¹² to gain more quantitative insight into the factors controlling the dihydrogen (H₂) activation reactions promoted by strongly related intramolecular geminal FLPs.¹³ This approach allowed us to propose an orbital-controlled mechanism, complementary to the widely accepted mechanisms suggested independently by Pápai and co-workers¹⁴ and Grimme and co-workers,¹⁵ where the degree of cooperativity between the key donor–acceptor orbital interactions, i.e., LP(Lewis base) \rightarrow σ^* (H₂) and σ (H₂) \rightarrow p_z(Lewis acid), along the reaction coordinate that can be used as an indicator of the reaction

Received: February 20, 2019

Published: May 24, 2019



Cite this: *Dalton Trans.*, 2020, **49**, 3129

Received 18th December 2019,
Accepted 2nd February 2020

DOI: 10.1039/c9dt04806e

rs.c.li/dalton

Understanding the role of frustrated Lewis pairs as ligands in transition metal-catalyzed reactions†

Jorge Juan Cabrera-Trujillo and Israel Fernández *

The role of frustrated Lewis pairs (FLPs) as ligands in gold(I) catalyzed-reactions has been computationally investigated by using state-of-the-art density functional theory calculations. To this end, the nature of (P, B)-FLP-transition metal interactions in different gold(I)-complexes has been first explored in detail with the help of the energy decomposition analysis method, which allowed us to accurately quantify the so far poorly understood Au...B interactions present in these species. The impact of such interactions on the catalytic activity of gold(I)-complexes has been then evaluated by performing the Au(I)-catalyzed hydroarylation reaction of phenylacetylene with mesitylene. With the help of the activation strain model of reactivity, the factors governing the higher activity of Au(I)-complexes having a FLP as a ligand as compared to that of the parent PPh₃ system have also been quantitatively identified.

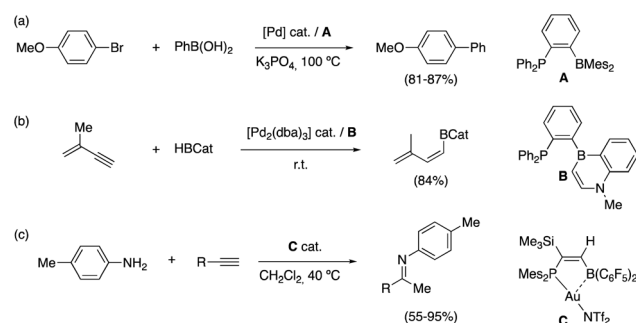
Introduction

Since the seminal work by Stephan and co-workers in 2006 on reversible dihydrogen activation mediated by a system having a Lewis acid and a Lewis base in its structure,¹ the so-called frustrated Lewis pairs (FLPs) have emerged as powerful species to activate small molecules under metal-free conditions in both stoichiometric and catalytic reactions.² These species are typically composed of a pair of sterically encumbered Lewis acidic and Lewis basic centers, in either single molecules or bimolecular systems, which severely hampers the formation of a classical donor-acceptor bond between them. This peculiar bonding situation is responsible for the unique and rich reactivity of these compounds, which in many instances was traditionally restricted to transition metals.²

FLPs have also been used as ambiphilic ligands in transition metal chemistry.^{3,4} Interestingly, the presence of a Lewis acid moiety nearby transition metals can significantly influence their reactivity. For instance, Bourissou and co-workers reported that, in comparison with PPh₃ as a ligand, FLP **A** improved the efficiency of the Pd-catalyzed Suzuki-Miyaura coupling of *p*-bromoanisole with PhB(OH)₂ (Scheme 1a).⁵ Similarly, Liu and co-workers used related FLP **B** in the Pd-catalyzed hydroboration of enynes (Scheme 1b).⁶ As compared to the analogous process involving *o*-naphthalenyl phosphine,

FLP **B** not only improves the activity of the catalyst but also provides a markedly different selectivity as a *trans*-hydroboration product is almost exclusively formed. In contrast, a 1,4-hydroboration reaction product is formed in the analogous reaction involving a phosphine lacking the Lewis acidic fragment.

Related intramolecular FLPs have also been used as ligands in gold(I)-catalyzed transformations such as, among others, the intramolecular cyclization reactions of propargylamides⁷ or, quite recently, the intra- and intermolecular hydroamination reactions of alkynes (Scheme 1c).⁸ Based on X-ray diffraction studies, it is assumed that the interaction between the strong Lewis acid moiety and the transition metal in either the FLP AuX (X = Cl, NTf) complex or the active catalytic species FLP(Au)⁺ significantly enhances the electrophilic properties of the catalyst, which ultimately results in an enhancement of its catalytic activity. Despite that, very little is known about the



Scheme 1 Representative examples of transition metal-catalyzed reactions using FLPs as ligands.

Departamento de Química Orgánica I and Centro de Innovación en Química Avanzada (ORFEO-CINQA), Facultad de Ciencias Químicas, Universidad Complutense de Madrid, 28040 Madrid, Spain. E-mail: israel@quim.ucm.es

† Electronic supplementary information (ESI) available: Table S1 and Fig. S1, Cartesian coordinates (in Å) and total energies of all the stationary points discussed in the text. See DOI: 10.1039/C9DT04806E

■ Frustrated Lewis Pairs

Understanding the C–F Bond Activation Mediated by Frustrated Lewis Pairs: Crucial Role of Non-covalent Interactions

Jorge Juan Cabrera-Trujillo and Israel Fernández*^[a]

Abstract: The activation of a single C–F bond in di- and trifluoromethyl groups by frustrated Lewis pairs (FLPs) has been computationally explored by means of Density Functional Theory calculations. It is found that in this activation reaction the FLP partners exhibit a peculiar cooperative action, which is markedly different from related FLP-mediated processes, and where non-covalent interactions established between the Lewis base and the substrate play a decisive role. In addition, the process proceeds through the in-

termediacy of a hypervalent species featuring a pentacoordinate carbon atom, which is rare in the chemistry of FLPs. The physical factors controlling this process as well as the bonding situation of these hypervalent intermediates have been quantitatively analyzed in detail by using state-of-the-art computational methods to not only rationalize the mechanism of the transformation but also to guide experimentalists towards the realization of these so far elusive hypervalent systems.


Introduction

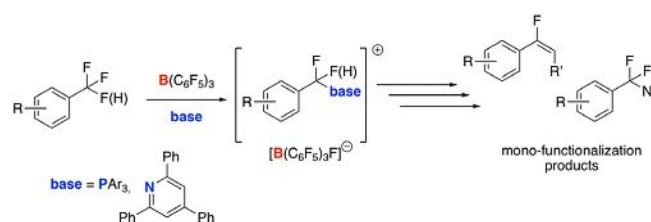
The discovery in 2006 by Stephan and co-workers that combinations of sterically encumbered Lewis acids and bases can activate dihydrogen^[1] constituted the starting point of the so-called Frustrated Lewis Pairs (FLPs) chemistry. Owing to the cooperative action of the FLP antagonists, where the formation of a donor–acceptor bond between them is precluded, these species exhibit a unique and rich reactivity, which in most cases is restricted to transition-metal complexes.^[2,3] Since the seminal work by Stephan, impressive progress in this field has been made. As a result, a good number of highly active FLPs have been developed including, among others, intramolecular species^[4] or systems having transition-metal fragments in their structures.^[5] In addition, the number of applications of FLPs has broadened significantly, particularly in recent years. Indeed, FLPs have been not only successfully applied to activate different small molecules (H₂, CO, CO₂, N₂O, SO₂, etc.) but also have been used in asymmetric syntheses^[6] and polymerization reactions.^[7] More recently, the concept of FLPs has been even applied towards the development of heterogeneous catalysts and new materials,^[8] which clearly illustrates the current growing interest in this area of main group chemistry.

In this regard, FLPs were recently applied by Young and co-workers to activate a single C–F bond in di- and trifluoromethyl groups (Scheme 1).^[9–11,12] The use of FLPs in this reaction constitutes an elegant solution to the longstanding problem of multiple C–F functionalizations typically observed in Lewis acid-catalyzed reactions, which derives from the lower reactivity of the polyfluoride starting materials with respect to their substituted products.^[13] In contrast, the resulting phosphonium or pyridinium salts formed in this novel FLP-mediated process are “deactivated” intermediates that can be further functionalized by nucleophilic substitutions or electrophilic transfer reactions, therefore leading to a wide variety of products with potential applications in medicinal chemistry or materials science.^[9–11]

Despite the evident synthetic potential of this transformation, which can be even performed catalytically in the Lewis acid by the addition of TMSNTf₂ as a fluoride sequestering agent,^[10,14] very little is known about the actual role of the FLP in the process. For this reason, we decided to gain a detailed understanding of the unknown cooperative action of the FLP partners in the transformation. The physical factors controlling this novel and synthetically useful FLP-mediated C–F activation reaction will be quantitatively analyzed by the combination of

[a] J. J. Cabrera-Trujillo, Prof. Dr. I. Fernández
 Departamento de Química Orgánica I and
 Centro de Innovación en Química Avanzada (ORFEO-CINQA)
 Facultad de Ciencias Químicas
 Universidad Complutense de Madrid
 28040 Madrid (Spain)
 E-mail: Israel@quim.ucm.es

 Supporting information and the ORCID identification numbers for the authors of this article can be found under:
<https://doi.org/10.1002/chem.202004733>



Scheme 1. Mono-selective functionalization of C–F bonds in di- and trifluoromethyl groups described by Young and co-workers (see refs. [9]–[11]).

